Characterization of the structure and adsorption capacity of activated carbons produced from South African coals

Botha, Francois Daniel

Award date:
1992

Awarding institution:
University of Bath

CHARACTERIZATION OF THE STRUCTURE AND ADSORPTION CAPACITY OF ACTIVATED CARBONS PRODUCED FROM SOUTH AFRICAN COALS

submitted by

François Daniël Botha

for the degree of Ph.D

of the University of Bath

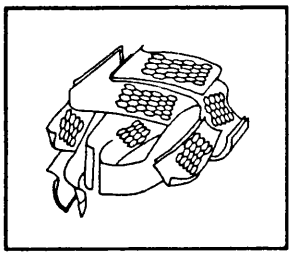

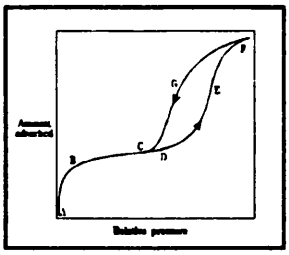

July 1992

ProQuest LLC
789 East Eisenhower Parkway
P.O. Box 1346
Ann Arbor, MI 48106-1346

INDEX

ABSTRACT

Two high mineral matter content South African coals were used as precursors for the production of activated carbon. *Bosjesspruit* is a predominantly inertinite rich coal with a mineral matter content of 24 wt. %, while the *Waterberg* coal is high in vitrinite and has a mineral matter content of 60 wt. %. A high mineral matter content in the coal precursor transforms to ash during the activation process, can act as a catalyst for the activation reaction, leads to reduced mechanical strength in the carbons and may also block entrances to the pores.

Column flotation proved to be a successful cleaning method to reduce the mineral matter content of the coals. The mineral matter content of Bosjesspruit coal was reduced to 12 wt. %, and it was found that the vitrinite and exinite macerals were removed in the tailings, leading to a coal product with a 89 vol. % inertinite content. The mineral matter content of the Waterberg coal was reduced to 11 wt. %, but the product yield for the coal was low at 22 wt. %. No selective flotation of macerals were observed for this coal.

Activation of the carbonized chars using steam and CO_2 as activating agents led to predominantly microporous carbons, with mesopores constituting less than 10 % of the total surface area. The porosity in the activated carbons was found to be affected by the nature of the precursor, the activating agent used and the ash in the final product. Steam activation proved to be successful in both carbons to maximize the development of micro - and mesoporosity for sample burn-offs less than 40 wt. %. For burn-offs higher than 40 wt. % in the Bosjesspruit column cleaned (BCC)

carbons, steam activation led to a higher degree of mesoporosity due to the burn-out of existing micropores, while CO_2 activation maximized microporosity at these burn-offs. For burn-offs higher than 40 wt. % in the Waterberg column cleaned (WCC) carbons, CO_2 activation led to higher mesopores; a sample having 18 % mesoporosity was obtained at 950 °C for 4 h activation time.

Some of the ash in the carbons could be removed by washing the carbons with a 0.5M HCl solution. The ash was found to be concentrated mainly in the mesopores, blocking access to the micropores. Single parameter estimates of the micropore width showed that the acid washing led to an increase in micropore width, with the WCC carbons exhibiting narrower micropores than the BCC carbons. The porosities of the carbons approached those found for two commercial activated carbons, but the prepared carbons showed a high degree of macroporosity due to the high mineral matter content of the coal precursors.

The Q_s value gives the amount of gold cyanide that is adsorbed onto the carbons after 60 minutes of contact time with the solution. The powdered activated carbons showed fast initial kinetics and high Q_s values when compared to the granular activated carbons. The Q_s values of the carbons appeared to be influenced more by the transport pore network than by the total adsorptive capacity of the carbon, e.g. as measured by the total BET surface area. The adsorption of $Au(CN)_2^-$ is enhanced by a well-developed meso - macropore system, although a substantial microporosity is also necessary to act as a sink for the adsorbed species. The adsorption process was found to be additionally influenced by other factors, e.g. the nature of the precursor and the chemical composition of the activated carbon. The WCC carbons prepared from the vitrinite rich coal precursor showed higher Q_s values than the BCC carbons, which were prepared from the inertinite rich coal. Evidence was found for

a possible reaction between $Au(CN)_2^-$ and the sulphur species in the carbons, with the pyritic form of sulphur showing a high affinity for gold cyanide.

ACKNOWLEDGMENTS

The author would like to express his gratitude to :

- Sastech Research and Development whose financial support made this research possible

- The Center for Applied Energy Research, University of Kentucky, for additional financial support and the use of their facilities

- My supervisor, Prof Brian McEnaney, and Dr Tim Mays for guidance, encouragement and suggestions

- All the personnel from the University of Bath and the University of Kentucky Center for Applied Energy Research for help with the experimental equipment and for valuable discussions

- God who deserves all honour and glory

DEDICATION

In honor of my mother, Muriël and loving memory of my father Piet Botha

Thanks to my special American friend, Vicki Bell

TABLE OF CONTENTS

Chapter 8
Concluding remarks and future research

LIST OF FIGURES

Chapter 1
Introduction

Chapter 2
Literature survey

Chapter 3
Experimental methods

Chapter 4

Results and discussion : Beneficiation and carbonization

Chapter 5

Results and discussion : Physical activation

Chapter 6
Results and discussion : Chemical activation

Chapter 7
Results and discussion : Gold cyanide adsorption

Chapter 8
General discussion, summary and conclusions

LIST OF TABLES

Chapter 5
Results and discussion : Physical activation

Chapter 6
Results and discussion : Chemical activation

Chapter 7
Results and discussion : Gold cyanide adsorption

NOMENCLATURE

[Au]	concentration of gold in the bulk solution
$[Au]_c$	concentration of gold on the carbon surface
A	adsorption potential
a_m	cross-sectional area of the adsorbate molecule
C	constant in the BET equation
C_f	% combustible material in the froth
C_t	% combustible material in the tailings
c'	100 - % ash in froth product
d	distance between two parallel plates in the parallel plate model
d'	average carbon particle diameter
d_m	micropore width accessible to molecular probes
E	energy parameter in the DR equation
E_o	characteristic energy, relating to the structure of the adsorbent
f	100 - % ash in original coal feed
k	observed rate constant
k_f	film transfer coefficient
L	Avogadro's constant
M	mass of activated carbon
p	applied pressure
p_{Hg}	pressure of mercury in the liquid phase
p_o	vapour saturation pressure of the adsorbate
p/p_o	relative pressure
Q	amount of gold adsorbed onto activated carbon
Q_s	amount of gold adsorbed onto activated carbon after 60 minutes of contact with the solution
R	universal gas constant
R_c	% combustible recovery of froth floated product
R_g	average Guinier gyration radius
r_p	radius of a cylindrical pore
S	surface area

S_{BET}	apparent BET surface area
S'_{BET}	mesopore surface area
S_{Hg}	surface area estimated by mercury porosimetry
S_{macro}	macropore surface area
S_{micro}	micropore surface area
S_{ref}	surface area of the reference material used in the α_s method
T	temperature
t	time
t	100 - % ash in tailings
V	amount of adsorbate adsorbed
V'	volume of solution used in gold adsorption tests
$V_{0.4}$	amount of adsorbate adsorbed onto the reference material at a relative pressure of 0.4 in the α_s method
V_m	amount of gas adsorbed in the monolayer
V_{macro}	macropore volume
V_{me}	amount of adsorbate adsorbed in the mesopores
V_o	micropore volume
V_{ref}	amount of adsorbate adsorbed onto the reference material in the α_s method
W_f	% weight recovery in the froth
W_t	% weight recovery in the tailings
x_o	micropore half width

α_s	normalizing factor in the α_s method
β	affinity coefficient from the slope of the DR equation
γ	surface tension of liquid adsorbate
γ_i	interfacial surface energy between mercury and adsorbent pore wall
γ_s	mercury solid-vapour surface energy
η	constant in the α_s method, equation 2.4
θ	contact angle between solid and liquid
ρ	density of carbon particles
ξ	constant in the DR equation, equation 2.11
ψ	shape factor of carbon particles

CHAPTER 1

INTRODUCTION

1.1. Overview

The Sasol company in South Africa uses the Fischer-Tropsch process whereby coal is converted into liquid fuels. During the mining and crushing of the coal, coal fines are generated which are usually discarded. These coal fines, and the vast coal reserves of the Sasol collieries, have prompted Sasol to fund a research project through its research arm Sastech to investigate the possibility of producing activated carbon from coal. The results of that project are presented in this thesis. Sasol is interested in producing an activated carbon that can be used for gold adsorption by the gold mining industry. The activated carbon that is in use by the gold mines in South Africa is produced from a coconut shell precursor and is currently imported. South African coals however, have a high mineral matter content that is detrimental in the activation process because it leads to reduced mechanical strength in the final product.

1.2. Flow diagram of activated carbon project

Due to the many facets of the project, the experimental objectives and procedures need to be explained in more detail. For this purpose a flow diagram of the project is given in Figure 1.1, page 2.

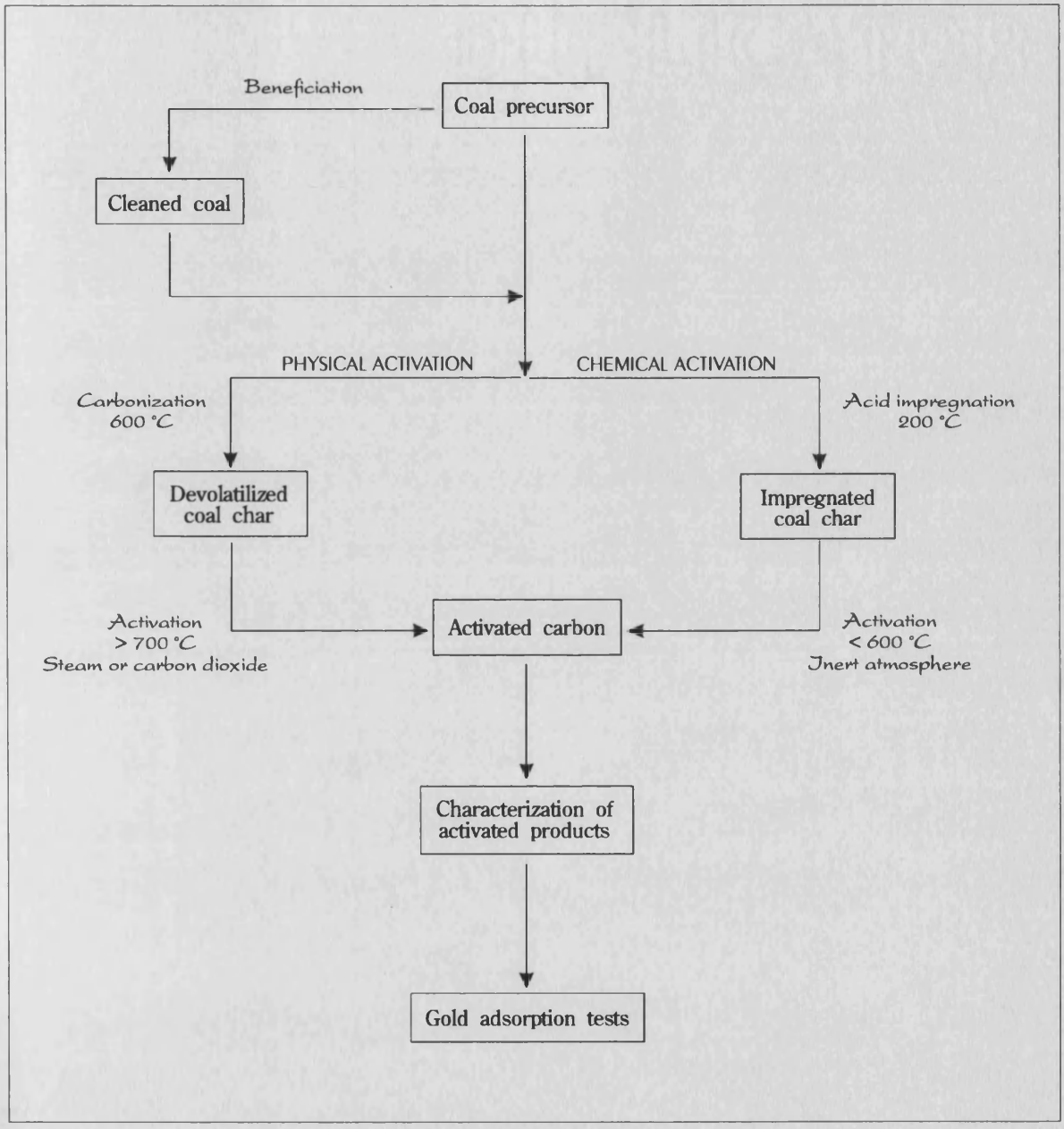

Figure 1.1 : Flow diagram of the activated carbon project.

First, the mineral matter content of the coal is reduced in the beneficiation step before being converted to activated carbon using either a physical or a chemical activation route. In the physical activation route the coal is carbonized in an inert atmosphere; this ensures removal of the volatiles in the coal. The carbonized chars are then activated at temperatures above 700 °C using steam or CO_2 as the activating gas. In the chemical activation route the coal carbonization step is replaced by impregnating the coal with the activating chemical; H_3PO_4 acid was used during this project. Activation of the impregnated char is accomplished at lower temperatures compared to the physical activation route (< 600 °C). In this research the pore structure of the carbons is extensively characterized before using selected samples in the gold adsorption tests.

1.3. Objectives of this study

The objectives of this study are threefold :

- ⌘ Reduction of the mineral matter content of the coal precursors using an industrially feasible method.
- ⌘ Production of activated carbons from the cleaned coals, and the subsequent characterization of the activated products.
- ⌘ Selection of carbons with the highest surface area to test their ability to adsorb gold from cyanide solutions.

1.4. Coals used in this study

Activated carbon will be produced from two bituminous South African coals. *Bosjesspruit* is an inertinite rich coal from the Secunda area with a mineral matter content of 24 %, and *Waterberg* coal, from the Grootegeluk mine near Ellisras, is high in vitrinite, but has a mineral matter content of 60 %. The analysis of the coals is given

in Table 1.1. Although low in sulphur, all the coals have a high mineral matter content which make them unsuitable for direct activation.

Table 1.1 : Analysis of South African coal samples

	Bosjesspruit coal	Waterberg coal
PROXIMATE ANALYSIS		
(% as determined)		
Moisture	5.9	1.4
Volatile content	21.7	18.9
Fixed carbon	51.4	19.7
Ash	22	60
ULTIMATE ANALYSIS		
(% dry, ash free)		
Carbon	82.2	71.6
Hydrogen	3.9	6.0
Nitrogen	2.2	2.5
Sulphur	1.3	2.2
Oxygen (by difference)	10.4	17.7
PETROGRAPHY (%)		
Vitrinite	40	67
Exinite	2	3
Inertinite	58	30
Fusinite	5	9
Semifusinite	52	19
[1] Other	1	2

1 The remaining inertinite macerals consists mainly of macrinite, micrinite and resinite.

Although there are many collieries in South Africa which produces coal with a lower mineral matter content (and thus a better precursor), the chosen coals for this project are from collieries either owned by Sasol (i.e. Bosjesspruit) or are of interest to the company (i.e. Waterberg). Activated carbon will be produced from the following precursors :

- ⌘ Bosjesspruit run-of-mine coal, hereafter called BROM coal
- ⌘ Bosjesspruit cleaned coal, hereafter called BCC coal
- ⌘ Waterberg cleaned coal, hereafter called WCC coal

1.5. Commercial activated carbons used in this study

The porosity and adsorption characteristics of the active carbons prepared from the coals during this study are compared to three commercially-available activated carbons used in industry. The porosity information for each of the carbons is given in Table 1.2.

Table 1.2 : Information on commercially available active carbons.

Sample	Precursor	BET N_2 surface area m^2/g	Notional micropore surface area m^2/g	Micropore volume cm^3/g	Mesopore surface area m^2/g	Macropore volume cm^3/g	Ash in product %
G210	Coconut shell	1190	1175	0.44	15	0.28	1
Supra	Peat	940	855	0.32	85	0.46	4
207A	Coal	1060	1025	0.38	35	0.21	10

Pica G210 AS is a coconut shell based carbon with a high microporosity and is used extensively worldwide in the gold mining industry for adsorbing gold from cyanide solutions. Norit Supra ROW is a peat based active carbon with a high meso- and macroporosity and finds specific use in the water purification industry. Sutcliffe Speakman 207 A is a typical bituminous coal-based active carbon which can be used for a variety of applications. The carbons will hereafter be referred to as G210, Supra and 207A respectively.

1.6. Structure of the thesis

The structure of this thesis will follow the procedures outlined in Figure 1.1, page 2. Chapter 2 is a survey of the current literature pertaining to the project. The procedures used during the different experimental methods are outlined in Chapter 3.

The results and general discussions are given in Chapters 4 - 7. In Chapter 4 the results of the coal cleaning and the carbonization of the coal precursors are discussed. The production of activated carbons by physical activation using steam and CO_2 are given in Chapter 5, together with a discussion on the pore structure of the carbons. Chapter 6 gives the results for the production of activated carbons by chemical activation, using H_3PO_4 acid as the activating agent. The carbons with the highest prepared surface area were subjected to the gold adsorption tests, and the results from these experiments are given in Chapter 7.

Finally, the major findings of the research are summarized in Chapter 8, which also includes recommendations for future research.

CHAPTER 2

LITERATURE SURVEY

Summary

This survey starts by discussing the structure, applications and manufacture of activated carbon. Coal structure and its major organic and inorganic constituents will be reviewed, as well as the mineral matter content of coal, and its removal from the coal structure. This is followed by a broad perspective of the carbonization and activation processes used to produce activated carbon. The techniques available for characterization of the activated carbon will then be highlighted. Finally, the chemistry of gold cyanidation and the application of active carbon towards the recovery of gold from cyanide solutions will be discussed. As a large number of seperate topics are to be covered in this chapter, it is presented as a broad survey which links the background literature of the various components of the project. To keep this survey within reasonable bounds, much of the detail in each section has been omitted.

2.1. ACTIVATED CARBON

2.1.1. Definition of activated carbon

Activated carbon is a collective name for a wide range of carbonaceous materials with a high degree of porosity and an extended intraparticulate surface area. The active carbons can be in either granular or powdered form; the granular active

carbons usually have smaller pore diameters and are more abrasive resistant. The nature of the active carbon will depend on the carbon precursor and the activation conditions, and will affect the final applications of the carbon.

2.1.2. Main applications of activated carbon

The history of activated carbon can be traced back to the Egyptians who used carbonized wood as early as 1500 B.C. for medicinal purposes and also as purifying agents. In 1900 active carbons replaced bone char as a refining agent in the sugar industry, and during World War 1 activated carbon was used extensively in gas masks to adsorb poisonous gases. [Bansal *et al.* 1988]

Modern activated carbons are excellent adsorbents and have found applications in almost every aspect of modern life. The main applications are listed in Table 2.1.

Table 2.1 : Major activated carbon applications.

Application	Type of industry	Examples of substances adsorbed
Air purification	Rubber and paint	Waste gases
	Nuclear	Radioactive vapours, iodine, noble gases
	Chemical	Various hydrocarbons
Water purification	Municipal waterworks	Organic chemicals, toxic substances, humic acids
Metal recovery	Mining	Gold, silver copper
Decolourizing	Food and beverage	Surface active agents, phenol, aldehydes
Antidote, activated carbon filters	Medicine	Bacterial toxins, nicotine
Gas masks	Defense	Toxic gases
Catalyst	Chemistry and engineering	Synthesis of various compounds

A study in 1987 showed that 70 % of granular active carbons were used in liquid phase applications, against more than 90 % of powdered active carbons. Stricter environmental laws have spurred a new boom for activated carbon, and it is estimated that actived carbon demand will rise by 7 % each year until the middle 1990s. [Anon. 1990]

2.1.3. Manufacture of activated carbon

The manufacture of activated carbon involves two steps : the carbonization of the carbonaceous precursor and the subsequent activation of the carbonized product. All carbonaceous materials can be converted into activated carbon; the most widely used materials in industry are wood, coal, peat and coconut shells. The properties of the final product will depend on the starting material, as well as the manufacturing conditions.

In the carbonization step the starting material is heated in an inert atmosphere and most of the non-carbon elements are driven off as volatile gaseous products. A fixed carbon mass consisting mostly of carbon is formed; this mass, called char, has a low surface area and a rudimentary pore structure. In the activation step, the pore structure of the char is enhanced by oxidizing the char with an activating agent, thus removing any disorganized carbon and developing a carbon product with a randomly distributed pore structure and a high surface area.

2.1.4. Structure of activated carbon

Figure 2.1, page 10, gives a schematic representation of the microstructure of activated carbon. The activated carbon structure consists mainly of carbon atoms which are grouped into stacks of flat, aromatic sheets or planes, cross-linked in a random manner by aliphatic bridging groups. The width of the layer sheets varies,

but is typically about 5 nm. The arrangement of these sheets is irregular and leaves free interstices between the sheets, which gives rise to a porous structure. [Bailey & Maggs 1971; Bansal *et al.* 1988; Doying 1965; McEnaney 1988; Peters 1966] The pores are classified into three groups depending on their average width : [Sing *et al.* 1985]

micropores - width less than 2 nm

mesopores - width between 2 and 50 nm

macropores - width greater than 50 nm

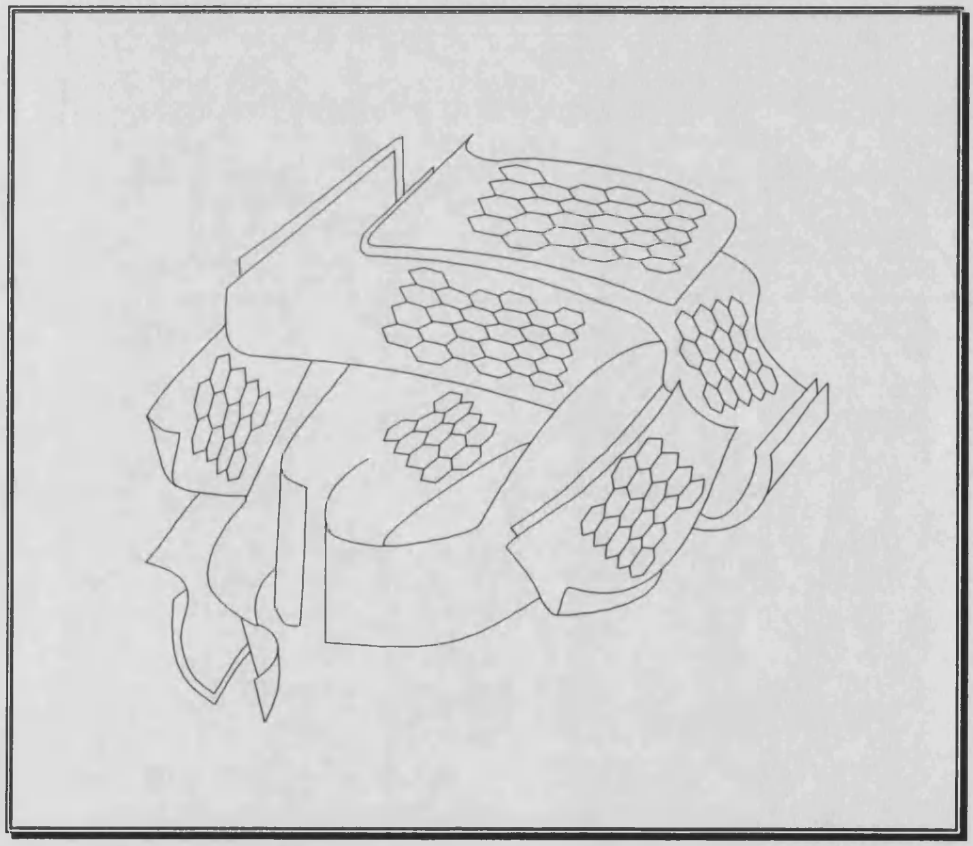

Figure 2.1 : Schematic representation of the microstructure of carbons.
(After Bansal *et al.* 1988)

In a microporous carbon produced by steam activating an anthracite coal, Fryer [1981] found the average interlayer spacing to be 0.7 nm. Oberlin and her co-workers [1980] found that in microporous carbons the layer planes occur singly or in stacks of up to four; the interlayer plane separation varied between 0.34 and 0.8 nm. Figure 2.2 illustrates how the pore volume distribution of the final carbon can vary according to the rank of the precursor coal.

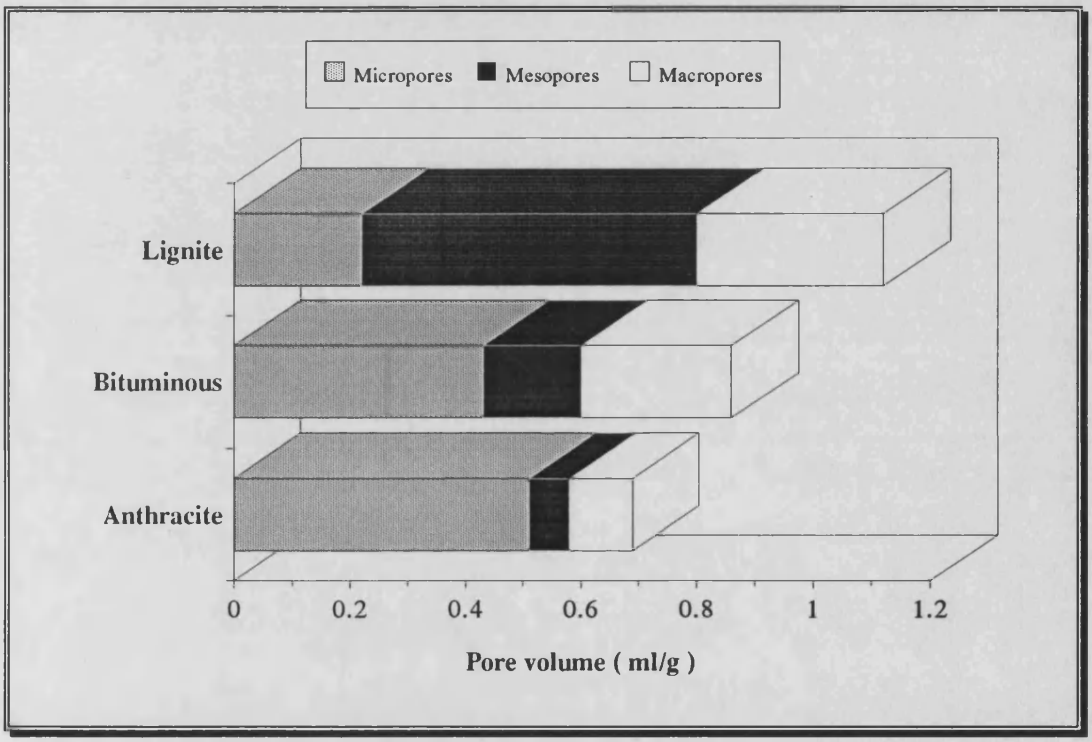

Figure 2.2 : Influence of coal rank on the pore volumes of activated carbons
(Data from Wilson 1981)

2.2. COAL STRUCTURE

2.2.1. Introduction

Coal is fundamentally composed of the fossilised remains of plant debris which have undergone physical and chemical alteration through geological time. [Falcon & Snyman 1986; Tsai 1982; Van Krevelen & Schuyer 1957] This alteration with time is called coalification. The level to which a coal has coalified determines the coal rank, and the amount of mineral matter determines the grade of the coal. Coal consists of three physical entities, namely the pore structure, the macerals or the organic components, and the minerals or inorganic components. The maceral composition and coal rank play an important part in the reactivity of the coal, and it is also well known that certain minerals can act as catalysts during coal liquefaction and gasification. [Tsai 1982]

2.2.2. Rank classification

Coal is ranked, in increasing order, as lignite, subbituminous coal, bituminous coal and anthracite. The classification is based on ASTM standards (ASTM D 388), and involves the evolution of the parent material towards a pure carbon structure. With an increase in the rank of the coal, the carbon contents increases and the hydrogen and oxygen contents decreases. [Tsai 1982]

2.2.3. Macerals

2.2.3.1. Introduction

Microscopically coal is composed of a number of organic constituents, ranging in size from 1 - 50 μm in diameter, called macerals. The macerals originate from different plant structures and are therefore grouped together according to their morphology, size, shape, colour and reflectance. The three main maceral groups are vitrinite, exinite and inertinite, and their origins are given in Table 2.2, page 13.

The coals from the southern hemisphere or Gondwana province are usually rich in inertinite, in contrast to northern hemisphere coals which have a high vitrinite content. This difference in maceral composition can be ascribed to the difference in vegetation which occurs in the two hemispheres. [Falcon & Snyman 1986]

Table 2.2 : Petrographic classification of coal.

Maceral Group	Maceral	Origin
Vitrinite	Telinite	Well preserved, distinct cell walls in large pieces
	Collinite	Well preserved cell walls and cell fillings, forming homogeneous, structureless layers
	Vitrodetrinite	Fragmentary detrital pieces
Exinite	Algenite	Waxy walls of algae
	Cutinite	Waxy coatings of leaves
	Resinite	Resinous secretions of cells
	Sporonite	Waxy coatings of spores and pollen
Inertinite	Fusinite	Well preserved cell walls which have undergone extreme oxidation
	Semifusinite	Well to semi-preserved cell walls which have undergone partial oxidation
	Macrinite	Particles of ~ 10 μm; no recognisable plant cell structure
	Micrinite	Particles commonly~ 1 μm; no recognisable plant cell structure
	Sclerotinite	Round to oval bodies, size 20-300 μm, or interlaced tissues of fungal origin

2.2.3.2. Chemical composition

Various studies have been conducted on bituminous coal macerals and their chemical composition. Exinite is the most volatile and has the highest H/C ratio, from 0.6 to 1.2. Inertinite is the least volatile, and has a low H/C ratio (0.47 - 0.65). Vitrinite has medium volatility and H/C ratio (0.6 - 0.8) when compared to the other

macerals. Chemically, both exinite and vitrinite consists of hydro-aromatic structures and when heated in an inert atmosphere, both soften and devolatilize to form a porous char. Inertinite, as its name suggests, is unreactive and undergoes little change during heating, forming a dense char which is usually difficult to ignite. [Given *et al.* 1960; Kessler 1973; Van Krevelen & Schuyer 1957; Tsai 1982]

2.2.3.3. Physical structure

The specific gravity of the maceral groups increases in the order exinite (s.g. 1.0 - 1.3), vitrinite (s.g. 1.3 - 1.45), and inertinite (s.g. > 1.5). The macerals can easily be separated into concentrated fractions on the basis of their difference in specific gravities. Vitrinite is the most brittle of the macerals, due to the prescence of shrinkage cracks and fissures. Exinite is characterized by its high tensile strength and increases the strength of coal bands. With the exception of fusinite, which is brittle, the inertinite group of macerals exhibits a high mechanical strength, especially when occuring in thick layers. [Falcon & Snyman 1986]

Density gradient centrifugation has been used to prepare small quantities of very pure maceral groups. [Dyrkacz & Horwitz 1982; Dyrkacz *et al.* 1984] This has allowed extensive investigations into maceral structure and maceral behaviour during carbonization. [Falcon & Snyman 1986; Jones *et al.* 1985; Landais *et al.* 1989; Pandolfo *et al.* 1988; Winans *et al.* 1986] Vitrinite behaviour during carbonization depends on the rank of vitrinite, sometimes degasifying and becoming soft before hardening into coke. Inertinite shows little reaction between 300 - 500 °C for all levels of rank, but transitional macerals between vitrinite and inertinite may show limited softening and subsequent agglomeration of the particles. Studies showed that vitrinite has a microporous structure of uniform distribution, while inertinite has a high mesopore content with a large portion of the pores being less than 10 nm in

diameter. Exinite has the least porous structure, consisting of irregular, tubular macropores. [Harris & Yust 1976]

2.2.4. Minerals

Minerals are the inorganic constituents found in coal; the most abundant in South African coals are clays, carbonates, sulphides, quartz and glauconite. [Falcon & Snyman 1986] The minerals can occur in coal in two forms. *Intrinsic* minerals are inorganic materials that were present in the original plant tissues, trapped in the coal in the form of organo-metallic complexes and mineral grains. The *extrinsic* minerals were introduced from external sources and can further be divided into two classes. The *syngenic* minerals were deposited by water and wind or were precipitated in situ, while the *epigenic* minerals were deposited by percolating waters into fissures and cracks long after the initial peat has accumulated. Some minerals can easily be liberated by grinding and beneficiation processes; but the minerals inherent to the coal structure may prove difficult or impossible to remove.

The first step in producing activated carbon from coal is to prepare a clean coal precursor. This is the subject of the next section.

2.3. COAL BENEFICIATION

Beneficiation of coal is generally performed using gravity-based processes, such as jigs, cyclones, tables, spirals, etc. However, coal finer than 0.5 mm does not respond to gravity-based processes. For this size fraction, surface chemistry-based processes such as froth flotation and oil agglomeration are most effective. [Aplan 1976, Leja 1982] Both these processes use the difference in physical and chemical

surface properties of coal and minerals to produce low ash products. The three types of surfaces most commonly encountered are :

- ⌘ hydrophobic surfaces - usually not wettable by water
- ⌘ polar hydrophilic surfaces
- ⌘ heteropolar surfaces

Coal is an example of a heteropolar surface, since it contains a hydrophobic carbon structure and hydrophilic mineral matter. It is important however that coal oxidation be kept to a minimum since oxygen-containing functional groups renders the coal surface hydrophilic and thus inhibits cleaning. [Van Nierop 1986]

2.3.1. Oil Agglomeration

In this process oil is added to fine coal particles suspended in water and vigorously mixed. The oil coates the hydrophobic particles (mostly coal) selectively and combines to form agglomerates, wheras the hydrophilic (mineral matter) particles remains in the suspension. The agglomerated coal is separated from the mineral matter by using a fine size screen. [Du Plessis 1985; Reinecke 1987]

Major disadvantages of this technique are high oil consumption and the coal must be ground to a very small size in order to liberate the minerals - this is especially true in the case of South African coals with their inherent mineral matter content. This also leads to an increase in the amount of oil required for agglomeration; in some cases an oil concentration of 50 % is needed for the agglomerates to form [Sun 1954; Van Nierop 1988]

2.3.1. Froth Flotation

Froth flotation is widely recognized as the most effective method to separate fine coal from minerals [Allum *et al.* 1954] In the froth flotation technique, a small amount of reagents (fuel oil or kerosene and a frother, usually a low-carbon alcohol) are added to the coal slurry and mixed thoroughly. Air is then sparged into the slurry, and the hydrophobic coal attaches to the air bubbles. The mineral particles, being hydrophilic, stay in suspension. [Wills 1981]. Flotation of fine ($< 75\ \mu m$) particles using conventional techniques is not effective due to excess of the agitation of the slurry, resulting in entrainment of the mineral matter.

Column flotation overcomes the problems encountered in the conventional cell. A schematic diagram of a column flotation cell is shown in Figure 2.3.

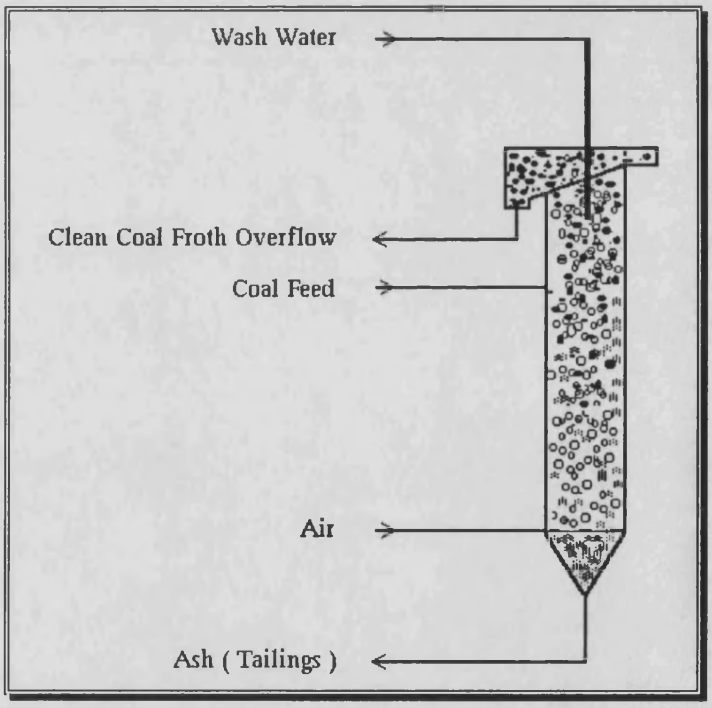

Figure 2.3 : Schematic diagram of a flotation column.

The cell is about six meters high and the diameter varies from ~ 5 cm for the laboratory cell to ~ 3 meters for a commercial size cell. The coal slurry, conditioned with the reagents, enters the column at about two-thirds distance from the bottom of the cell and air bubbles are sparged from the bottom of the cell using special devices. The counter-current flow of bubbles and coal particles provide effective attachment of the fine coal to the bubbles, whereas the mineral matter travels to the bottom of the column, where it is removed as tailings. The bubble-loaded coal reaches the froth zone at ~ 1.2 m from the top of the column where a gentle spray of wash water removes the entrained impurities. According to Hyde [1987] up to 99% of the entrained mineral matter can be removed by the froth washing process.

The advantages of column flotation when compared to batch flotation are threefold :

- ⌘ Smaller coal particles can effectively be recovered in the column
- ⌘ Entrained mineral matter is removed during the washing of the froth
- ⌘ The recovery and grade of the cleaned coal is much higher than for conventional flotation

2.3.2. Factors influencing the flotation behaviour of coal

The factors that influences the flotation behaviour of coal are summarized below :

2.3.2.1. Coal rank

In general, the higher the rank of the coal, the easier it is to float. This is due to the decrease in oxygen content and an increase in carbon content for higher rank coals. A high mineral matter content in the coal will also influence the natural hydrophobicity of the coal; minerals render the coal hydrophilic. [Aplan 1976]

2.3.2.2. Petrographic constituents

The three major maceral groups have different surface properties (section 2.2.3.2) which will influence the floatability of a coal. Sarkar *et al.* [1984], in a conventional batch flotation study of a medium rank vitrinite rich coal fraction, observed that vitrinite floated first. They recovered 94% of the vitrinite within 120 seconds, but the extent of recovery decreased for higher density fractions due to an increase in mineral matter. Beafore *et al.* [1979] however, found that the recovery of inertinite in their experiments was the highest, followed by vitrinite and exinite. It is thus possible to have maceral enrichment when floating coal; the relative ratios of the macerals and the amount of mineral matter present will influence the separation.

2.3.2.3. Surface functional groups and oxidation

In the presence of oxygen-containing functional groups, water adsorbs onto the surface of the coal and forms a hydrated layer on the coal surface that hinders flotation. [Bujnowska 1985] Various researchers have found a decrease in the floatability of coal as the amount of carbolic and phenolic groups present on the surface increases [Fuerstenau 1982; Fullard 1986; Van Nierop 1986]

When oxidation of the coal surface occurs, the amount of surface functional groups increase with a subsequent decrease in floatability. [Beafore *et al.* 1979; Sun 1954; Zimmerman 1964] This is represented graphically in Figure 2.4, page 20.

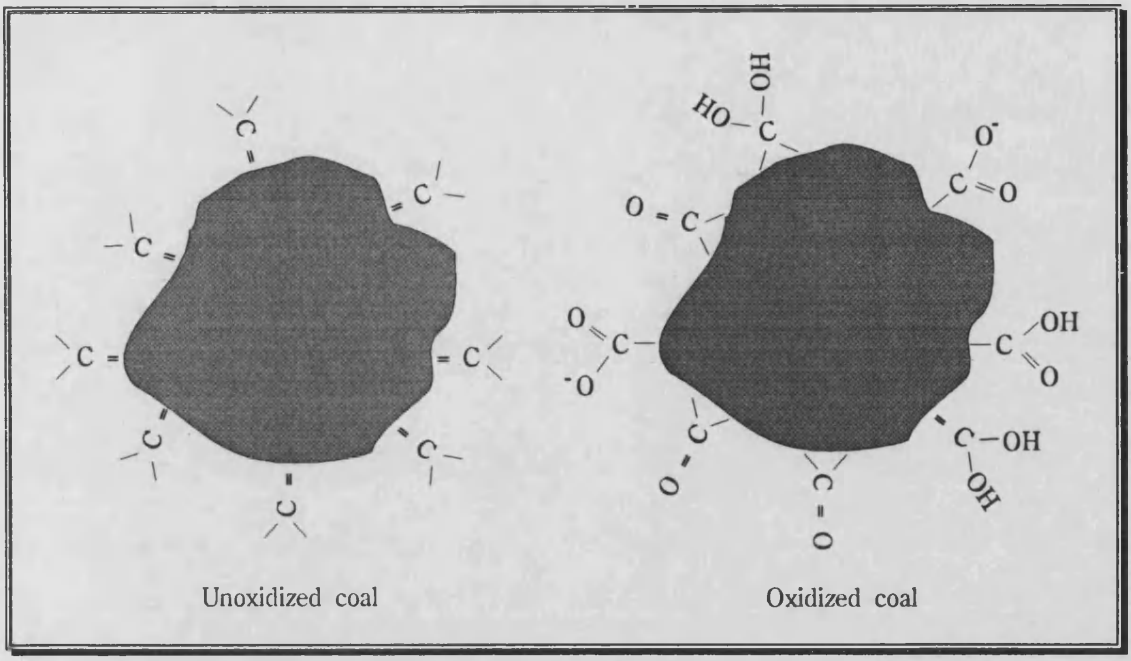

Figure 2.4 : Schematic diagram of the changes that occur on the coal surface due to oxidation. (After Beafore *et al.* 1979)

2.3.2.4. Particle size

The flotation rate of coal as a function of particle size is represented graphically in Figure 2.5, page 21. Larger particles often need more than one air bubble to float. The flotation behaviour of larger particles is also a function of coal rank; larger particles of a low rank coal will be more difficult to float than similar size particles of a high rank coal due to the low degree of hydrophobicity of the low rank coal. In the column cell coal sizes lower than 5 μm can be effectivly floated. [Sun *et al.* 1950; Wheeler *et al.* 1986]

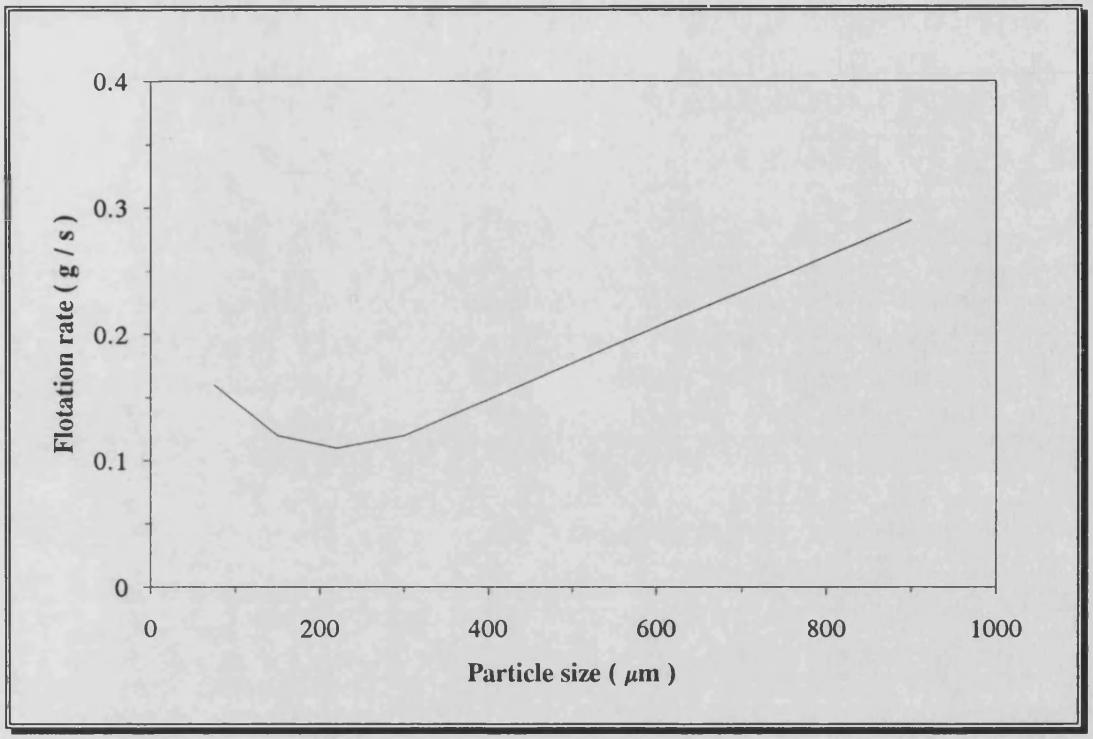

Figure 2.5 : Influence of particle size on the flotation rate of coal.
(Data from Elasivich *et al.* 1969)

2.3.2.5. Two-stage flotation

Higher coal selectivity is possible when the floated coal fraction is subjected to a second flotation. According to Reinecke [1987b] the frother adsorbs onto the coal surface during the first flotation with a subsequent decrease in the frother concentration in the solution. This is called negative conditioning of the coal surface because it prevents the air bubbles from adhering to the hydrophobic parts of the coal particles, and is schematically represented in Figure 2.6, page 22. Particles with a high mineral matter content however are influenced even more by negative conditioning and will not float during a second flotation process. The particles with a low mineral matter content still have a hydrophobic surface to which the bubble can adhere, and will be recovered in the froth.

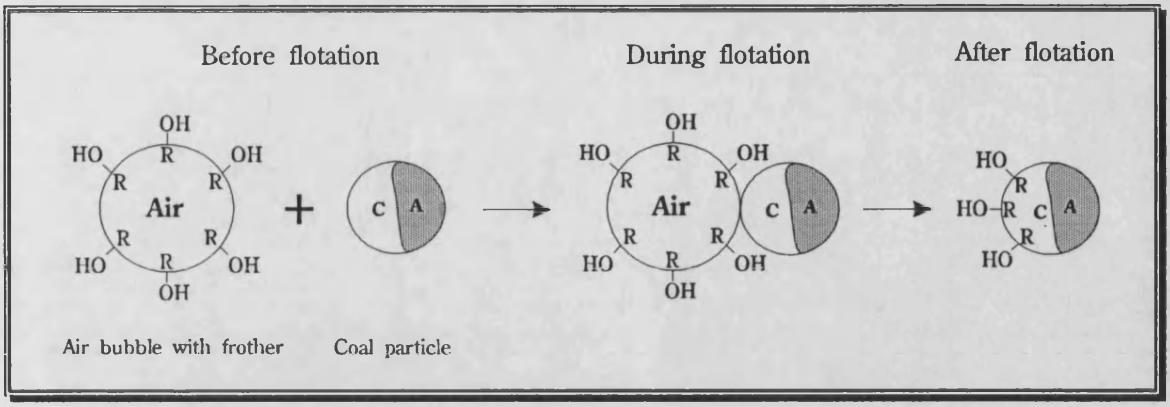

Coal particle that will *not* float in second flotation due to an insufficient hydrophobic surface

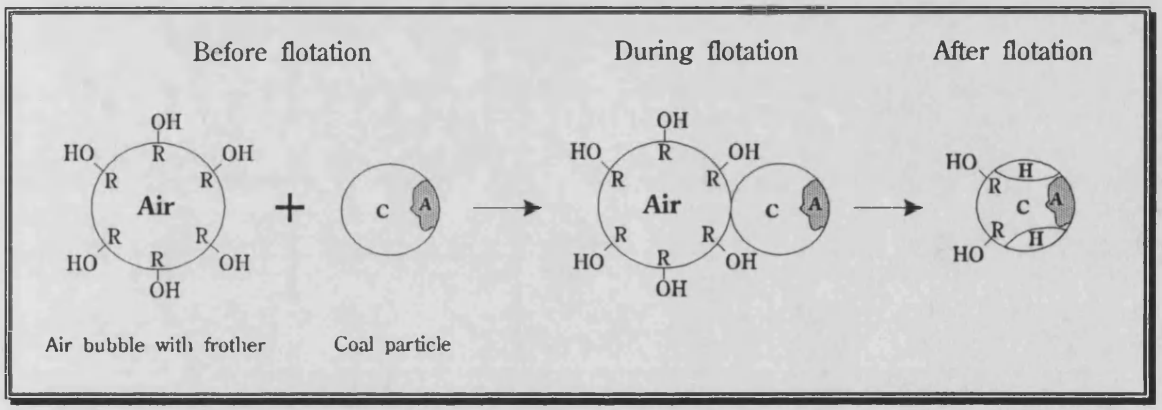

Coal particle that will float during a second flotation due to a sufficient hydrophobic surface for air bubble to adhere to.

Figure 2.6 : Schematic diagram showing the adsorption of frother onto coal particles with a low and high mineral matter content respectively.
(R-OH = frother, C = coal, A = ash, H = hydrophobic surface)

Although conventional flotation is widely used, the implementation of column flotation in the coal industry unfortunately has, until recently, received little attention. No information could be found regarding research on the column flotation of the two selected South African coals. In this study an attempt was made to float the two South African coals in a 50 mm diameter, 6.5 m high column.

2.4. COAL CARBONIZATION

2.4.1. Introduction

After the cleaning process the next step in the preparation of activated carbon is the carbonization of the cleaned coal. The carbonization process is outlined in this section.

Carbonization or pyrolysis can be defined as the thermal decomposition of a carbonaceous material in an inert atmosphere, eliminating non-carbon species as gaseous products and producing a solid, carbon mass (called char) with a rudimentary pore structure. The volatile products consists mostly of combustible gases (e.g. CH_4, H_2, CO, and higher hydrocarbons), CO_2, H_2O and tar vapours. [Bansal *et al.* 1988; Tsai 1982] The char produced will depend on the nature of the original coal as well as on the carbonization conditions. [Solomon & Hamblen 1985]

Two stages can be identified during low temperature carbonization. Upon heating at 350-400 °C the coal particles soften and become fluid-like, and forms an unstable intermediate phase called metaplast, followed by swelling when the particles fuse together and contributes to the resistance to the flow of volatile matter. This behaviour of bituminous coals is called the plastic properties of coal. The metaplast stage is followed by the shrinkage of the produced char at temperatures > 500 °C, during which stage recondensation reactions take place and a semi-coke is formed.

The plastic properties will thus affect the pore structure of the final char. For this reason it has been suggested that the coal be oxidized first to reduce the plastic properties before carbonizing the coal. [Tsai 1982] The oxidation is usually performed at temperatures below 200 °C, and serves to form chemical cross-linkages in the coal structure that inhibits swelling.

2.4.2. Factors influencing the structure of the final char

Coal carbonization can be classified into low temperature carbonization, where the final coking temperature is below 700 °C, and high temperature carbonization, where the final coking temperature exceeds 900 °C. In producing active carbon the carbonization temperature usually does not exceed 800 °C. The various parameters that influence the quality and structure of the final char are :

- the heating rate
- the final heat treatment temperature (HTT)
- the soak time at the final temperature
- the rank of the parent coal

[Bansal *et al.* 1988]

2.4.3. Carbonization scheme

Although the precise chemical structure of coal varies with coal rank, researchers have proposed that two general types of chemical reactions occur during coal carbonization. [Mastral *et al.* 1990; Loison *et al.* 1989] These reactions occur simultaneously, and an example of such reactions are given in Figure 2.7, page 25. The reactions can be summarized as follows :

- The *cracking reactions* involves the rupture of carbon-carbon bonds and the formation of two radicals. The radicals are stabilised by hydrogen, which is formed during the second type of reaction.

⌘ In the *condensation or aromatization reactions* formation occurs of aromatic groups, either by dehydrogenation and/or by recombination of aromatic groups and fragments. The result is the formation of aromatic C-C bonds and ultimately a solid carbon residue.

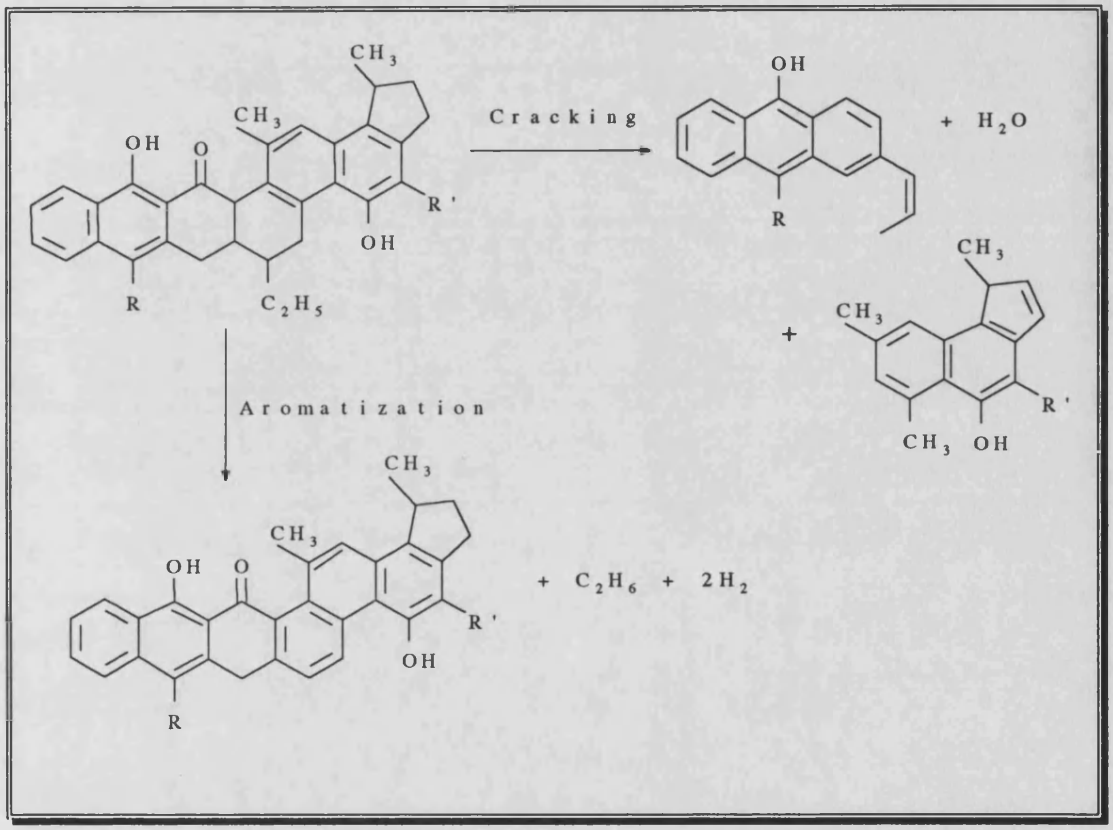

Figure 2.7 : Schematic diagram of the two main types of carbonization reactions found in coal. (After Loison *et al.* 1989)

The carbonized char consists mainly of a carbon skeleton with an undeveloped pore structure. The next step in the production of activated carbon is the activation of the carbonized chars.

2.5. ACTIVATION OF COAL CHARS

2.5.1. Introduction

During the activation step the porosity of the carbonized char is enhanced by creating new pores and enlarging the diameters of the existing pores. This is accomplished by selective removal of disorganized carbon by the activating agent. Dubinin and Zaverina [1949] first showed that a microporous carbon is produced when the extent of carbon burnoff is less than 50 %, and that meso - and macroporosity in the active carbon are developed when the burnoff is greater than 75 %.

2.5.2. Methods of activation

There are two methods of activation. *Physical activation* is the most widely used method and involves a gasification reaction of the carbonized char with steam, CO_2, air or combinations of these gases at temperatures between 800 - 1100 °C. The result is a porous char with a well developed pore structure, called activated carbon.

During *chemical activation* the carbon precursor is first impregnated by a chemical compound; the chemicals most often used are phosphoric acid and zinc chloride, many others have been identified through the years. [Smizek & Cerny 1970] The impregnation step replaces the carbonization step of physical activation. Activation is accomplished at lower temperatures than physical activation, usually between 400 - 600 °C, and leads to products with better developed porosity than the carbons obtained by physical activation. Kadlec *et al.* [1970] observed that the shape of the pores in activated carbons were different when activated by chemical or physical methods. They found bottle shaped pores in the case of chemical activation, while the pores were found to be cone shaped for physical activation. The bottle shaped pores may be formed by the gases released during the thermal decomposition of the carbonaceous material which creates hollows in the plastic matter at the

activation temperature of 500 °C. Chemical activation is primarily used to produce activated carbon from cellulosic raw materials, e.g. wood, and is not used commercially for the activation of bituminous and sub-bituminous coals. Chapter 6 in this thesis will discuss the results of the chemical activation of the South African coals.

2.5.3. Mechanism of activation

Although the exact mechanism of activation is not known, it can be visualised as a reaction between the activating agent and the carbon atoms on the edge and/or the atoms situated at dislocations and defect positions in the aromatic sheets. These carbon atoms have a high potential energy and can easily react to form oxidized surface compounds. [Bansal *et al.* 1988] These compounds are removed as gaseous oxides, exposing new carbon atoms for further reactions with the activating agents. The gasification reactions for physical activation has been proposed as a two step model :

$$CO_2 + * \rightarrow CO + O*$$

$$C + O* \rightarrow CO + *$$

and

$$H_2O* \rightarrow H_2 + O*$$

$$C + O* \rightarrow CO + *$$

where the asterisk represents a catalytically active center. [Salinas-Martinez *et al.* 1990] The water gas shift reaction also occurs when steam is used as activating agent, and occurs on the solid surface rather than in the gas phase : [Tsai 1982]

$$CO + H_2O \rightarrow CO_2 + H_2$$

Hydrogen and CO both retard the rate of activation when CO_2 is used as activating gas; Rand and Marsh [1971] however observed that the presence of CO produces a more uniform gasification rate. Activation with CO_2 requires higher activation temperatures because of the less energetic reaction, but develops mainly microporosity over a wide range of burnoffs. [Bansal *et al.* 1988] This is illustrated by the results of Tomków *et al.* [1977] in Figure 2.8 which shows the development of pore volumes at different activation levels for brown coal chars activated by steam and CO_2 activation respectively.

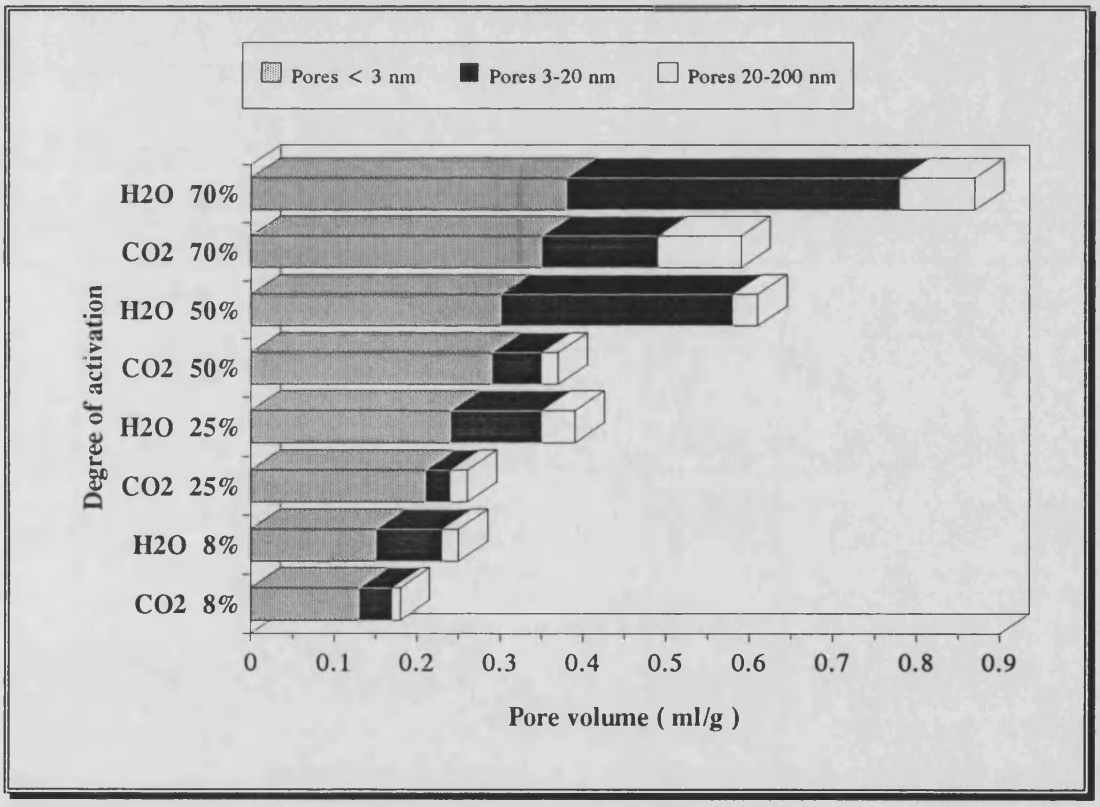

Figure 2.8 : Pore volumes for activated carbons prepared from brown coal chars for different levels of activation. (Data from Tomków *et al.* 1977)

In summarizing, the main factors affecting the final carbon product during the activation step is the nature of the activating agent, the activation temperature and the residence time of the char in the furnace. The next section focuses on characterizing the activated carbon product.

2.6. CHARACTERIZATION OF ACTIVATED CARBON

2.6.1. Introduction

In characterizing activated carbons, two properties of importance should be obtained : the available surface area of the solid onto which adsorption can take place, and information on the pore structure i.e. the extent of micro-, meso- and macroporosity.

2.6.2. Adsorption in activated carbon

Physical adsorption of gases in microporous active carbons follows the theory of Dubinin. [1965, 1966, 1975] First, the gases are strongly adsorbed in the micropores by a process called volume filling, because of the enhancement of adsorption potential due to the overlap of the force fields of the opposite pore walls. The adsorption then shifts to the meso- and macropores, forming multilayers and exhibiting capillary condensation. Microporous carbons also show molecular sieve action by preferential adsorption of small molecules. There is also shape selectivity by the preferential adsorption of flat molecules; this can be expected due to the slit shapes of the micropores. The meso and macropores act mainly as transport pores, although liquid retention may occur in these pores. [Barton *et al.* 1974; McEnaney 1988; Stoeckli 1990]

Expand

The heteroelements hydrogen and oxygen can also be incorporated into the carbon structure during activation, and these elements are located at the edge of the carbon

planes. It has been shown that functional groups, especially those containing oxygen, can have a marked influence on adsorption. [Cookson 1978; Faust & Aly 1983; Mattson *et al.* 1969] Constrictions can also occur in the microporous network and render certain areas inaccessible for adsorption. The constrictions can be due to functional groups [Boehm & Voll 1970, 1971] and by carbon deposits formed by thermal cracking of the volatile components during the carbonization step. These constrictions leads to activated diffusion effects at low adsorption temperatures, where the adsorbate (e.g. N_2 at 77 K) has insufficient kinetic energy to fully penetrate into the micropores.

2.6.3. Adsorption isotherms

The adsorption of a gas by a solid has been extensively used to yield information on the surface area and pore structure. This method entails the construction of an adsorption isotherm, which gives the relationship between the amount of gas adsorbed and the relative pressure of the gas at a constant temperature. In practise a large number of gases have been used as adsorbates, e.g. N_2, Ar, Xe, Kr, CO_2, H_2O and light hydrocarbons. The most common adsorbate used is nitrogen at is boiling point, 77 K. [Bansal *et al.* 1988; Gregg & Sing 1982; Lee *et al.* 1987; Mahle & Friday 1989; Rodríguez-Reinoso *et al.* 1989] Brunauer *et al.* [1940] classified the adsorption isotherms into five categories, known as the BDDT - classification. The typical types of isotherms usually found are shown in Figure 2.9, page 31.

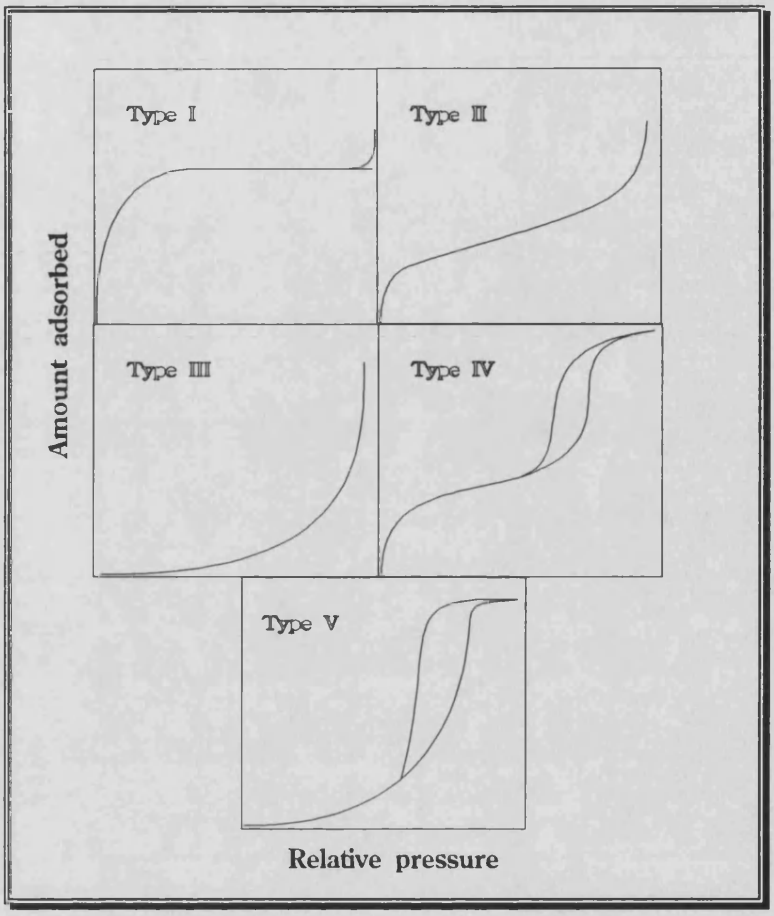

Figure 2.9 : The five main types of adsorption isotherms according to the BDDT-classification. (After Brunauer *et al.* 1940)

The Type I isotherm is found for microporous activated carbons, while the Type IV isotherm is found for carbons having both micro - and mesopores.

2.6.4. Capillary condensation

A characteristic of the Type IV isotherm in the BDDT - classification is the hysteresis loop at higher relative pressures, and a more detailed example of the isotherm is given in Figure 2.10.

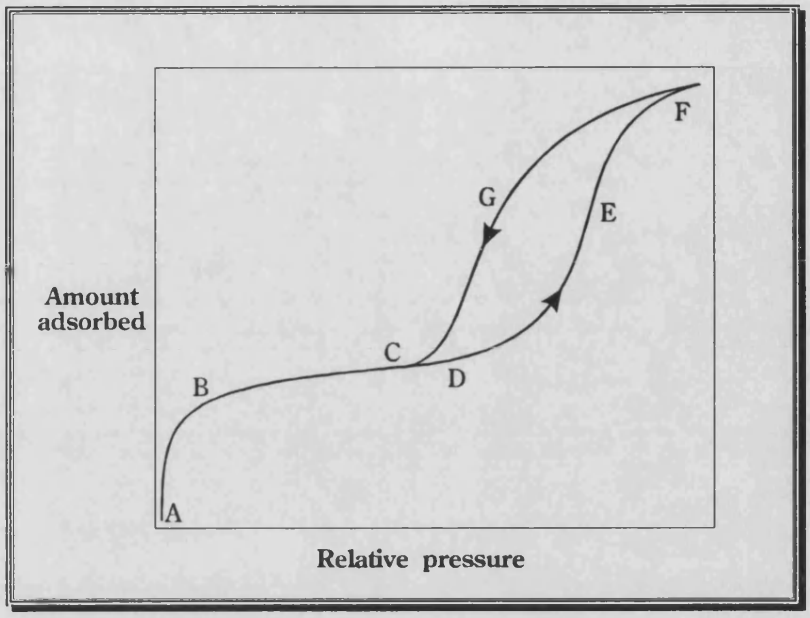

Figure 2.10 : A typical Type IV isotherm.

In the low pressure region the isotherm shows the initial uptake of adsorbate following the curve ABC in Figure 2.10. At a certain point the isotherm begins to deviate upwards, following the path DEF until the saturation vapour pressure is reached at point F. Many Type IV isotherms may show little variation near the saturation point F with a plateau reached at this point. The hysteresis loop implies that at any given relative pressure on the desorption branch FGC, the amount adsorbed is always greater than along the adsorption branch DEF. The reason for the occurance of a hysteresis loop was first explained by Zsigmondy [1911] in his capillary condensation theory. The model proposed by Zsigmondy assumed that along the adsorption branch ABC, adsorption is restricted to the walls of the pores, until at point D capillary condensation occurs in the finest pores. As the pressure is increased, wider pores are filled with liquid adsorbate until at the saturation vapour pressure F all the pores are full of condensate. Hysteresis occurs on desorption because the mechanism of emptying the pore is now capillary evaporation, instead of multilayer formation as was the case during the adsorption stage. Evaporation in a

pore will continue at the same pressure at which it started until the pore is empty; thus at any given relative pressure during desorption, the amount still adsorbed onto the solid will be more than the corresponding value during adsorption, giving rise to the hysteresis loop.

The different types of hysteresis loops were first classified by de Boer in 1958. A revision of the classification was proposed by Gregg and Sing in 1982, and is given in Figure 2.11. Type B hysteresis has been found for adsorbents having slit-shaped pores or plate-like particles. [Gregg and Sing 1982]

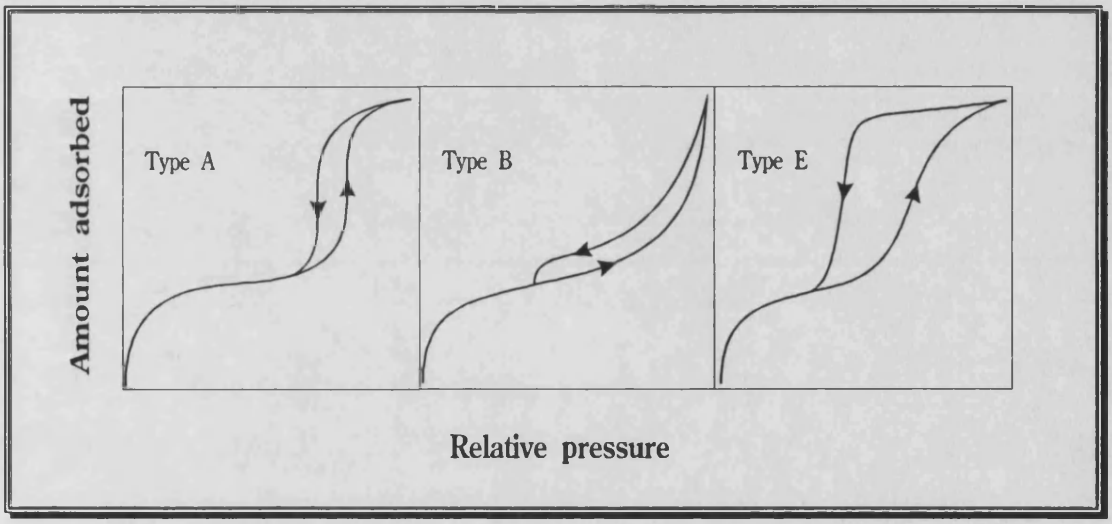

Figure 2.11 : Types of hysteresis loop. (Gregg and Sing revised classification 1982)

2.6.5. The BET - model

2.6.5.1. Estimation of surface area by the BET model

The best known and most widely used quantitative interpretation of the Type II isotherm was proposed by Brunauer, Emmett and Teller, also called the BET equation. [Brunauer *et al.* 1938] The equation is developed from a kinetic model of

the adsorption process by Langmuir, where the surface of the solid is seen as an array of adsorption sites. The mathematical form of the BET equation is :

$$\frac{V}{V_m} = \frac{C\,(p/p_o)}{[\,1 - p/p_o\,][\,1 + (C-1)\,(p/p_o)\,]} \qquad 2.1$$

where V = amount adsorbed

V_m = the monolayer capacity

C = BET constant

p_o = vapour saturation pressure of the adsorbate

p/p_o = relative pressure

From the isotherm a value of the monolayer capacity of the solid is calculated, which can in turn be used to calculate the surface area of the solid. The monolayer capacity is defined as the amount of adsorbate that can be accommodated in a single layer - the monolayer - on the surface of 1 gram of the solid. Using the value of the monolayer capacity Vm calculated from equation 1, the surface area A (in m^2/g) of the solid can then be expressed as :

$$S_{BET} = [(V_m)(a_m)(L) \times 10^{-20}] / 22412 \qquad 2.2$$

where V_m = the monolayer capacity adsorbed in cm^3/g STP / g

a_m = the average area occupied by a molecule of adsorbate ($Å^2$)

L = Avogadro's constant

2.6.5.2. Application of the BET equation to experimental data

In the experimental stage, the amount of gas adsorbed is measured as a function of the pressure of the system at constant temperature. From equation 2.1 the BET equation can be written as :

$$\frac{p}{V(p_o - p)} = \frac{1}{V_m C} + \frac{(C-1)}{V_m C}(p/p_o) \qquad 2.3$$

A plot of $p/(V(p_o-p))$ versus p/p_o should yield a straight line with slope $s = (C-1)/(V_mC)$ and an intercept of $i = 1/(V_mC)$. By solving these two simultaneous equations the values of C and V_m can be obtained. Substituting the value of V_m in equation 2.2 gives the BET surface area in m^2/g. The linear portion of the BET equation has been shown to lie in the range of relative pressures 0.05 to 0.35, and only data points in this range should be used for the calculation of V_m and C. [Gregg & Sing 1982]

2.6.5.3. Criticisms of the BET model

Through the years the BET model has been criticized for producing unrealistic high values for the surface area for microporous carbons and for giving no indication of the pore volume of the solid. These criticisms can be summarized as follows :

- The model assumes all sites an the surface are energetically identical - experiments where the heats of adsorption is calculated as a function of the amount adsorbed shows considerable heterogeneity of the carbon surface.

- The model focuses on the adsorbent-adsorbate interactions and neglects the interactions between the adsorbate molecules in the monolayer.

⌘ The BET equation takes no account of enhanced adsorption (volume filling) in micropores due to superposition of the force fields from opposite pore walls.

Despite these criticisms, the BET surface area is still widely used and is an important characteristic to quote when dealing with activated carbons, although Stoeckli and Ballerini [1991] recently suggested that the micropore volume may be a more realistic value to quote when dealing with adsorbent carbons.

2.6.6. The α_s - method

2.6.6.1. Estimation of the micropore volume

From the studies of physical adsorption onto solids it is clear that each adsorbent-adsorbate system will have its own isotherm. The need arose to compare the isotherms, and express the adsorption in normalised terms. This led to the idea of the standard isotherm, the most widely used is the α_s - method, first developed by Sing. [1970]

In the α_s - method, the monolayer capacity V_m of the BET equation is replaced by a normalizing factor, which gives the amount adsorbed at a fixed relative pressure - in the α_s - method this pressure is taken at $p/p_o = 0.4$. The normalized adsorption is given by $\alpha_s = V_{ref}/V_{0.4}$, and is obtained from the isotherm of a reference solid, where V_{ref} is the amount adsorbed onto the surface of the reference solid at a given p/p_o , and $V_{0.4}$ is the amount adsorbed onto the reference material at a relative pressure of 0.4. The choice of a suitable reference material has been the subject of debate. [Carrott *et al.* 1986; Rodriguez-Reinoso *et al.* 1987,1989] It was shown by Rodriguez-Reinoso *et al.* however that both the reference materials under discussion

can be used in the pressure range p/p_o = 0.1 - 0.8 to give identical values of the micropore volume.

The final form of the equation of the α_s - method, as applied to microporous solids, is given as :

$$V = V_o + \eta\alpha_s \qquad 2.4$$

where V = total amount adsorbed at pressure p/p_o

V_o = maximum amount adsorbed in the micropores

η = $[(V_{me})(V_{0.4})]/V_{ref}$, a constant

V_{me} = maximum amount adsorbed in the mesopores

A plot of the amount adsorbed V versus α_s should yield a straight line with slope η and an intercept of V_o. The linear range is usually extrapolated from the high end of the α_s range above α = 1.0, which corresponds to p/p_o = 0.4. The micropore volume can thus be determined directly from the intercept of the plot.

2.6.6.2. Calculation of the mesopore and micropore surface area

The α_s - method can also be used to calculate the mesoporous surface area, S'_{BET} of the carbons. The surface area, from equation 2.1, can be expressed in general as :

$$S = k.V \qquad 2.5$$

where k is a constant indicative of the adsorbate used and V is the amount adsorbed. The slope of the α_s - plot, from equation 2.4, page 37, is :

$$\eta = [(V_{me})(V_{0.4})]/V_{ref} \qquad 2.6$$

In substituting V_{me} and V_{ref} using equation 2.5, equation 2.6 can be written as

$$\eta = (S'_{BET})(V_{0.4}) / S_{ref} \qquad 2.7$$

Substituting the values for the reference material into equation 2.7 and rearranging gives :

$$S'_{BET} = 2.75\,\eta \quad (m^2/g) \qquad 2.8$$

The *notional* microporous area is then given by subtracting the mesoporous surface area S'_{BET} from the BET surface area, i.e.

$$S_{micro} = S_{BET} \text{ (equation 2.1)} - S'_{BET} \text{ (equation 2.8)} \qquad 2.9$$

2.6.7. The Dubinin-Radushkevich (DR) equation

2.6.7.1. Estimation of the micropore volume

Dubinin and Radushkevich [1947] put forward an equation to estimate the micropore volume from the low and medium-pressure parts of the adsorption isotherm. The equation is based on the Polanyi theory of adsorption potentials, and assumes that the degree of the filling of the micropores is a function of the adsorption potential. The mathematical form of the DR - equation is :

$$V = V_o\, e^{-(A/E)^2} \qquad 2.10$$

where V = amount adsorbed (ml / g)

V_o = liquid micropore volume (ml / g)

A = adsorption potential

$= RT \ln(p_o / p)$

E = Energy parameter

Substituting the adsorption potential $RT \ln(p_o/p)$ for A in equation 2.10, the DR - equation can be rewritten as

$$\ln V = \ln V_o - \xi \ln^2(p_o / p) \qquad 2.11$$

with ξ a constant. A plot of ln V against $\ln^2(p_o/p)$ should yield a straight line with an intercept equal to the logarithmic value of the micropore volume.

2.6.7.2. Estimation of the characteristic energy

The slope of the linear plot in equation 2.11 is :

$$-\xi = (RT/E)^2 \qquad 2.12$$

Dubinin showed that the energy parameter E is a function of a characteristic energy E_o, relating to the structure of the adsorbent, and an affinity coefficient β, which is constant for a given adsorbate. For nitrogen at 77 K the value of β is 0.34 [Dubinin 1988], so that equation 2.12 can be written for nitrogen adsorption as :

$$-E_o = \frac{RT}{\beta \xi^{0.5}} \qquad 2.13$$

$$= 1.89 \xi^{-0.5} \quad kJ / mol$$

Since the adsorption energy will increase when the micropore size decreases, due to the overlapping fields of the opposite pore walls and the interaction between the molecules, the energy value can be used as an indicator during the activation process to follow the development of microporosity in a sample. There are a few models available to calculate physical values of the micropore width from the characteristic energy; this is discussed in the next section.

2.6.8. Calculation of micropore sizes from the characteristic energy

The characteristic energy E_o can be used to calculate a single parameter estimate of the micropore width. The simplest model assumes that the pores can be modelled by parallel plates. If the surface area of a plate is S, and the distance between the plates is d, then the surface area and volume between the plates are given by $S_{micro} = 2S$ and $V_{micro} = V_o = Sd$ respectively. The pore width is then given by :

$$d = V_o / S$$

$$= 2V_o / S_{micro} \qquad 2.14$$

A value for the micropore width can thus be calculated from the micropore surface area S_{micro} (equation 2.9) and the micropore volume V_o, either calculated from the α_s - method (equation 2.4) or the DR - equation (equation 2.11).

McEnaney [1987] showed that the data obtained from small-angle scattering of X-rays (SAXS) and microprobe experiments may be correlated with E_o by a two-constant, semilogarithmic equation :

$$d_m\,(\,nm\,) = 4.691\, e^{(\,-\,0.0666 E_o\,)} \qquad 2.15$$

where d_m is the micropore width accessible to molecular probes.

A comparison between E_o and the average Guinier gyration (inertia) radius R_g of the micropores and SAXS data led Dubinin and Stoeckli [1980] to propose the relationship :

$$E_o R_g = 14.8 \pm 0.6 \qquad kJ{\cdot}nm/mol \qquad 2.16$$

The relationship between the gyration radius and the micropore half-width x_o (= d/2) is suggested by Dubinin [1988] as :

$$R_g\,(\,nm\,) = 0.055 + 1.1\, x_o \qquad 2.17$$

$$= 0.055 + 0.55\ d$$

It must be emphasized that these calculations of micropore width are approximate. The models used for the calculation of d are oversimplified, and the error for the overall relationship between d and E_0 for $0.45 < d < 2$ nm was calculated by Stoeckli [1990] to be in the order of 10 - 15 %.

2.6.9. The mean-field density theory

In the calculation of the molecular cross sectional area a_m to be used in the BET - equation, a liquid-like state for the adsorbate is assumed. Similar assumptions are made in the α_s - method and the DR - equation when calculating the liquid micropore volume from the amount of gas adsorbed. In modelling the adsorption of N_2 in slit shaped pores using the statistical mechanical approach known as the mean-field density theory, Seaton, Walton and Quirke [1989] showed that the density of nitrogen is a function of the pore width, approaching the liquid state only in the larger mesopores (> 20 nm), as is shown in Figure 2.12. For the micropore range the density of nitrogen in the pores is less than the liquid density, thus introducing an error in the calculation of S_{BET} and V_o if the liquid density value is used.

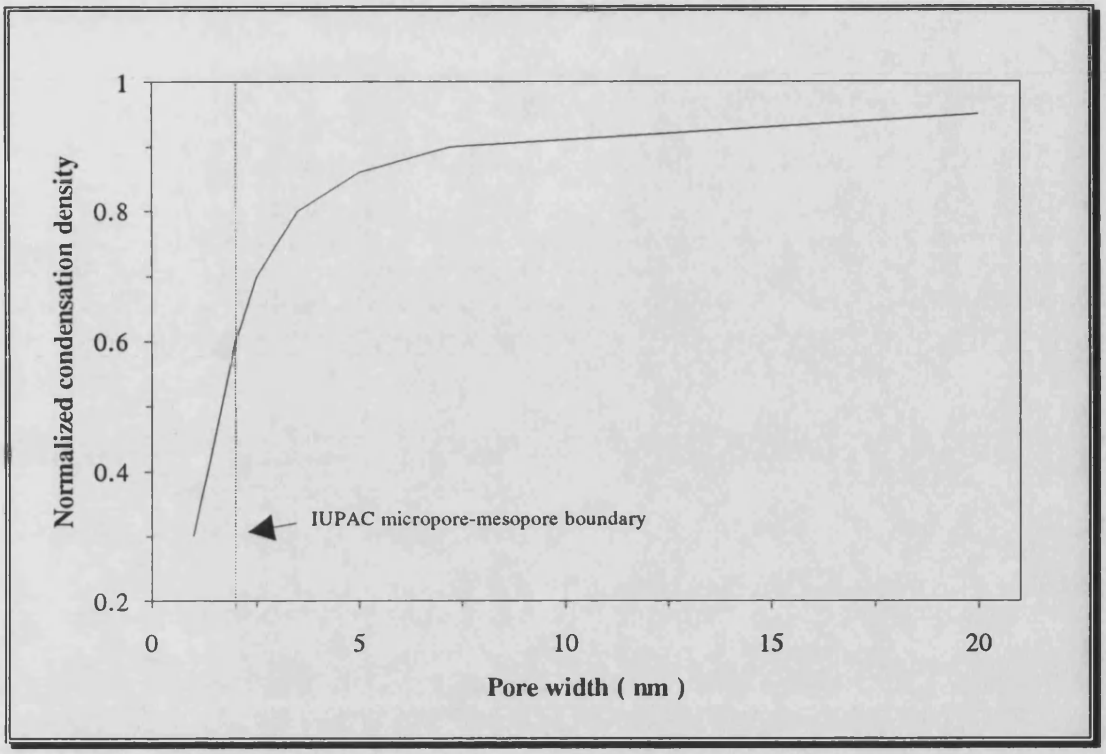

Figure 2.12 : Condensation density of N_2 at 77 K in model slit-shaped pores.
(Data from Seaton *et al.* 1989)

2.6.10. Mercury porosimetry

2.6.10.1. Estimation of the macro- and mesopore volume

Mercury porosimetry is a technique developed by Ritter and Drake in 1945 after Washburn [1921] suggested that mercury can be used to measure pore sizes, and consists of measuring the volume of mercury penetrating into an evacuated solid as a function of the applied hydrostatic pressure. The technique is used to estimated the pore volume of the macro- and mesopore range in solids. Mercury is a non-wetting liquid, and under a pressure p fills a cylindrical pore of radius r_p by the Washburn equation

$$r_p = - (2\gamma \cos \theta) / p \qquad 2.18$$

where θ = contact angle between the solid and the mercury

γ = surface tension of liquid adsorbate

p = applied pressure

The values recommended for use at room temperature is γ = 480 mN/m and θ = 140° [Ritter and Drake 1945], although the choice of the contact angle can vary between 135 - 150°. [Bansal *et al.* 1988] The pressure p is given by $p = p_{Hg} - p_g$, the difference between the pressure of mercury in the liquid phase and the gas phase. At any value of the applied pressure p_i, the value of v_i gives the amount of mercury in all pores having a radius equal to or greater than r_p^i, and is termed the cumulative pore volume. A plot of cumulative pore volume versus log r_p gives the pore volume distribution graph for mesoporosity. Experimentally the volume intruded into the sample is measured as a function of pressure. The macropore volume V_{macro} is the volume of mercury intruded into the sample at a pressure of 4250 psig, which correlates to a pore radius of 25 nm. Subtracting this value from the total intruded volume gives the volume of mercury intruded into the mesopore range. The technical limit of mercury porosimetry is about 3.5 nm, and excludes the contribution of the finer mesopores and micropores. Cormack and his co-workers [1980] showed that the practical limit for their study of Hg intrusion into a series of alumina gels was 4 nm. When used in conjunction with gas adsorption techniques however, porosimetry can give an estimation of the complete pore distribution of the solid.

2.6.10.2. Estimation of surface areas

Rootare and Prenzlow applied the mercury intrusion technique to determine a surface area S from the Washburn equation (equation 2.18), assuming that the pore is of a constant cross-section. The work required to force a volume of mercury dv into the pore of a solid at a pressure p can be related to the decrease in the surface energy at the pore wall :

$$pdv = -(\gamma_s - \gamma_i)\, dS \qquad 2.19$$

Where γ_s is the solid-vapour surface energy of the pore wall and γ_i is the interfacial surface energy between the pore wall and the mercury. The relationship between the surface energies and the surface tension of the mercury γ is given by the Young and Dupré equation $(\gamma_s - \gamma_i) = \gamma\cos\theta$. Substituting this into equation 2.19 and integrating leads to

$$S_{Hg} = -\frac{1}{\gamma\cos\theta}\int_0^{p_{max}} p(v)dv \qquad 2.20$$

where S_{Hg} gives the surface area up to a pressure p. It is assumed that γ and θ stays constant over the range of p, and, using the Washburn equation 2.18, the pressure p is transformed to a pore radius r by assuming a cylindrical pore model. A graph of surface area *vs* pore radius can thus be constructed from the intrusion data.

2.6.10.3. Criticisms of the Washburn equation

Various criticisms can be raised against the technique of mercury porosimetry. These are summarized below :

- Although the values of Ritter and Drake [1945] are widely used for γ and θ, these values have been a subject of debate for many years.

- Various researchers have shown that at higher pressures mercury had damaged the pore structure, possibly by fracturing the pore walls and thus giving access to pores not generally accessible, or by compacting the structure leading to the closure of previously opened pores. [Dickinson and Shore 1968; Pinote *et al.* 1968, Milburn *et al.* 1988] In a study of mercury intrusion into carbon black compounds Milburn *et al.* found evidence of

disintegration of the carbon particles at pressures as low as 2500 psia, corresponding to a pore radius of 43 nm.

⌘ The model of non-intersecting cylindrical pores ignores any three dimensional pore network effects. This is especially true since hysteresis in porosimetry can be explained by aperture-cavity effects. This is explored in more detail in Chapter 5.

2.6.11. Summary of characterization methods used in this study

In this study only a selected few of the methods described are used for characterizing the pore structure of the activated carbons. These methods are summarized in Table 2.3.

Table 2.3 : Summary of the characterization methods used in this study.

Method used	Calculated parameters	Information gained
Gas adsorption (N_2 at 77 K)		
BET equation (2.1)	S_{BET}	Total surface area
α_s - method (2.4, 2.8, 2.9)	S_{micro} , S'_{BET} , V_o	Micropore - and mesopore surface area, micropore volume
DR - equation (2.12)	E_o	Characteristic energy
DS - equation (2.17)	d	Estimated micropore width
Mercury porosimetry		
Washburn equation (2.18)	V_{macro} , V_{meso}	Macropore - and mesopore volume
Rootare and Prenzlow equation (2.20)	S_{macro} , S'_{BET}	Macropore - and mesopore surface area

Once the samples have been extensively characterized by gas adsorption and mercury porosimetry, the samples which show high surface areas and well developed porosity are subjected to the gold adsorption tests. The adsorption of gold cyanide onto activated carbon is the subject of the next section.

2.7. GOLD ADSORPTION

2.7.1. Introduction

It was as early as 1880 that Davis patented a process for the recovery of gold by adsorption onto wood charcoal, and a few years later Johnson [1894] patented a process for gold adsorption onto wood charcoal from cyanide leach solutions. The processes were not viable then because the charcoal did not have the pore structure and high surface areas of modern activated carbons, and the only method known to elute the gold from the charcoal was to burn the charcoal to ash. The ash was in many cases much more than the gold, which made the recovery of the gold difficult.

Zadra and his co-workers started renewed interest in the recovery of gold by carbon when they developed the carbon-in-pulp (CIP) process in the early 1950^{s}. [Zadra 1950; Zadra *et al.* 1952] In this process, activated carbon granules are added directly to a cyanide pulp and stirred countercurrent to it. The carbon is recovered by filtration, and the gold is recovered from the carbon by a subsequent stripping using a hot, caustic sodium cyanide solution. The gold is electrowon from the solution by depositing it onto steel wool.

The first commercial plant to use this technology was the Homestake Mining Company in the U.S.A. in 1973, and since then the CIP method has received widespread application in South Africa, with modifications especially in the stripping process. [Hall 1974; Davidson & Duncanson 1977] Most of the larger mines now

use CIP plants after successful pilot-plant studies were conducted during the early 1980s. [McDougall & Hancock 1981]

2.7.2. Factors influencing adsorption of gold onto granular activated carbon

There are various factors that have an influence on the kinetics and adsorption of gold onto activated carbon. [Dixon *et al.* 1978; McDougall *et al.* 1980; Tsuchida & Muir 1986, 1986b] These are summarized below :

2.7.2.1. Nature of the activated carbon

Most charcoal will adsorb gold but the carbon most suited to gold adsorption has a high BET surface area and a high micropore volume, and should be abrasive resistant for use in the CIP - process. For this reason active carbons prepared from coconut shells are especially effective for gold adsorption.

2.7.2.2. Size of the activated carbon

The size used by industry in the CIP process is in the range 1.2 - 3.4 mm (6 x 16 mesh), with 0.8 mm the minimum size to ensure successful screening . A smaller particle size enhances gold uptake especially in the early stages of adsorption.

2.7.2.3. Effect of ionic strength

The adsorption of gold is enhanced by the presence of electrolytes in the solution, especially $CaCl_2$. The effect of the cations is in the order $Ca^{2+} > K^+ > Na^+$.

2.7.2.4. Other anions in solution

Complex cyanides also adsorb onto the carbon, and thus lowers the gold loading. The effect of these anions is in the order $Au(CN)_2^- > Ag(CN)_2^- > Cu(CN)_3^- > CN^-$

2.7.2.5. Effect of pH

Adsorption is virtually independent of the pH value in the range 6 to 12, but increases strongly at pH values below 5. In the acid medium however, toxic HCN gas may be liberated, and therefore the CIP plants operate at a pH value above 9.

2.7.2.6. Effect of temperature

The equilibrium adsorption isotherms at temperatures between 20 - 80 °C show that gold loading decreases at higher temperatures. The CIP plants and adsorption experiments are conducted at 20 - 25 °C. This observation has led to the development of high temperature stripping techniques, since the solubility of $KAu(CN)_2$ in hot water is about fourteen times larger than in cold water.

2.7.2.7. Influence of oxygen

The importance of oxygen in the adsorption process has been shown by various researchers [Dixon *et al.* 1976; Tshuchida and Muir 1986; Van der Merwe and Van Deventer 1988]. Dixon *et al.* found a decrease in gold loading when maintaining a nitrogen atmosphere during the adsorption process, while Van der Merwe and Van Deventer found a decreased loading of gold and silver when the level of oxygen in the solution fell below 8 mg/l. Tshuchida and Muir found a decrease in gold loadings for a decrease in surface functional groups on the surface of the carbon. Typical C-O functionalities supposed to be involved in the adsorption reaction include lactones, carboxylic acids, quinones and chromene groups. The role of oxygen containing functional groups in the adsorption of $Au(CN)_2^-$ was first proposed by Garten and Weiss in 1957. They proposed an electrostatic attraction between the negatively charged $Au(CN)_2^-$ anion and a positively charged carbonium site, as given in equation 2.21 :

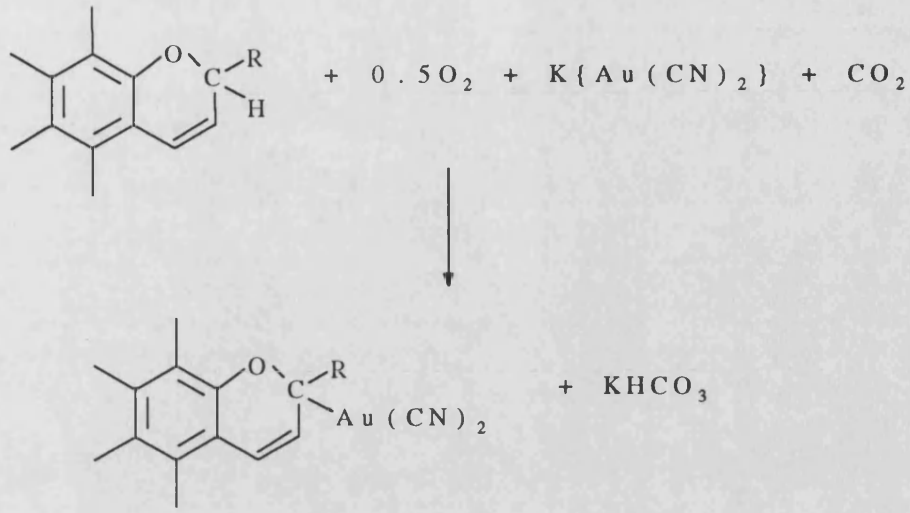

2.21

Tsuchida and Muir proposed the related benzpyrene group as a more logical structure since it is found in many natural products :

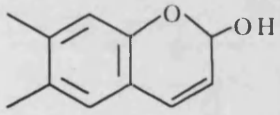

Substituted benzpyrene

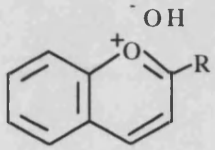

Resonance stabilized tautomer with fully aromatic ring structures

2.7.3. Model for adsorption of gold cyanide onto carbon

The adsorption of gold cyanide onto activated carbon can be seen as two processes that occur simultaneously, i.e. adsorption on active surface sites of the carbon and diffusion of gold cyanide through the pores. The following scheme has been suggested by Fuerstenau *et al.* [1987] for the various stages of the adsorption reaction :

- *Initial stage* - fast - Adsorption of gold cyanide onto the external active surface sites of the carbon. The rate of this reaction is controlled by the diffusion of gold cyanide to the surface of the carbon and to the macropores.

- *Intermediate stage* - slow - As the available surface sites decrease, the reaction rate is controlled by the diffusion of gold cyanide through the pores, where first the macropores and then the micropores are filled with gold.

- *Final stage* - very slow - During this stage, which approaches equilibrium, the rate of the reaction is controlled by diffusion of the gold cyanide through the micropores.

From the above model the carbon can be partitioned into two regions; a fast adsorbing macro-mesopore region and a slow adsorbing micropore region. The model also assumes that :

- gold cyanide entering the macropores from the solution first has to diffuse through an external boundary layer
- transport in the macropore region is by a surface diffusion mechanism
- the adsorption reaction itself is not rate controlling

[Fuerstenau *et al.* 1987; Van Deventer 1983]

2.7.4. Mechanism of gold adsorption

The mechanism of gold adsorption onto carbon is a subject of great debate. A few mechanisms have been proposed through the years, namely :

- the adsorption of the gold cyanide ($Au(CN)_2^-$) ion without any chemical change

- the adsorption of the $Au(CN)_2^-$ ion with subsequent decomposition of $Au(CN)_2^-$ to AuCN

- adsorption of the $Au(CN)_2^-$ ion with subsequent reduction of gold(I) to either metallic gold (gold(0)) or an intermediate state between gold(0) and gold(I)

- the dual mechanism, where gold is adsorbed by an ion-exchange interaction followed by decomposition to AuCN.

[Davidson 1974; Dixon *et al.* 1978; McDougall *et al.* 1980; Tsuchida & Muir 1986, 1986b]

After analyzing most of the experimental results available, McDougall and Fleming [1987] came to the conclusion that gold is adsorbed as the $Au(CN)_2^-$ ion without chemical change. They suggested the formation of ion pairs of the type $M^{n+}[Au(CN)_2^-]_n$, where M^{n+} = Na^+, K^+, Ca^{2+}, Mg^{2+}, etc. at high pH values. This mechanism has recently been confirmed during further research by Adams and Fleming in 1989. Cook *et al.* [1989] in a XPS study on Norit R2020 active carbon, found that gold was present as a combination of $KAu(CN)_2$ and AuCN, with the

latter species dominating at higher gold loadings. Van der Merwe and Van Deventer [1988] also suggested the formation of insoluble AuCN, and proposed that the nature of the carbon may influence the type of species deposited.

The gold adsorption theories discussed above all assume that oxygen surface structures, which are located randomly on the edges of the graphitic planes, play an important role in the adsorption process. Jones *et al.* [1989] argued that there are insufficient oxygen functionalities on activated carbons to match experimentally measured gold capacities found on the carbons. They suggested that the gold is also adsorbed onto the basal planes of the carbons via a weak carbon to gold π - donor complex, as is shown in Figure 2.13.

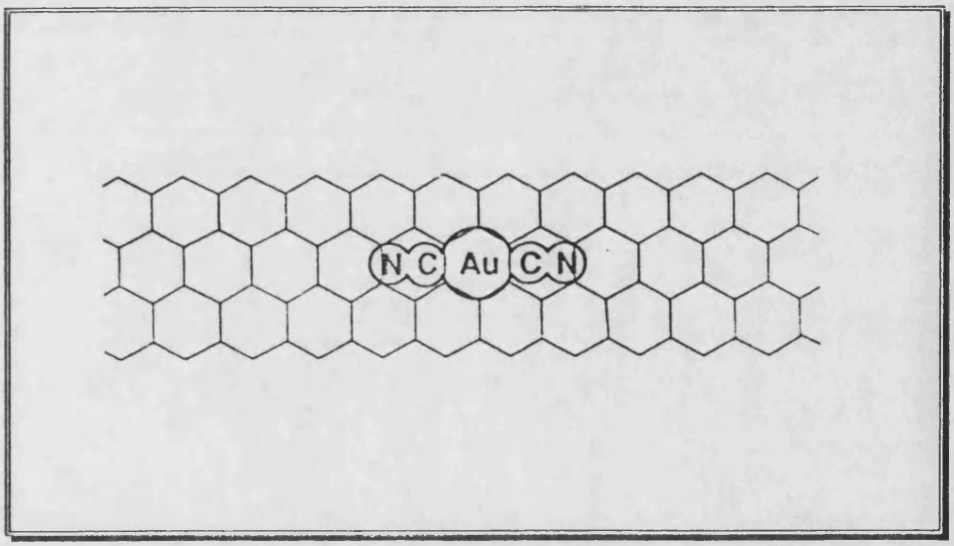

Figure 2.13 : Adsorption of gold cyanide onto the graphitic planes of activated carbon. (From Jones *et al.* [1989]. C, N and Au atoms have been scaled in relation to the graphitic ring size.)

Jones *et al.* [1989] support this theory by their observed XPS results for the N-1s peak, which consisted of a single peak with the same electron binding energy. Because the peak was unsplit, these researchers argued that the terminal N atoms in

the linear $(N\equiv C\text{-}Au\text{-}C\equiv N)^-$ ionic structure experience the same chemical environment on the surface of the carbons. The geometry match of a graphitic plane and the planar $Au(CN)_2^-$ and $Ag(CN)_2^-$ ions would also explain why these ions are preferentially adsorbed over the non-linear $Cu(CN)_4^{3-}$ ions.

Jones and his co-workers also discarded the ion-pair mechanism as suggested by McDougall and Fleming [1987], since the ion-pair geometry would remove the symmetry they observed for the N - interaction. They suggest that the cations M^{n+} may co-adsorb at the carbon-solution interface, but they do not suggest why an increase in gold loading is observed for an increase in ionic strength, as discussed in section 2.7.2.3.

2.7.5. Kinetics of gold cyanide adsorption

Various researchers have proposed a first order rate equation for modeling the adsorption of gold cyanide onto activated carbon. [Fuerstenau *et al.* 1987; McDougall *et al.* 1980; Van Deventer 1983] The rate of adsorption can be written from the liquid phase material balance as :

$$-\frac{d[Au]}{dt} = k\{[Au] - [Au]_c\} \qquad 2.22$$

where $[Au]$ = gold concentration in the bulk solution, (mg / l)

$[Au]_c$ = gold concentration on the carbon surface (mg / l)

k = observed rate constant

For a reaction controlled by film diffusion $[Au]_c$ is negligible, so that integration of equation 2.22 yields :

$$\ln[Au] = \ln[Au]_o - kt \qquad 2.23$$

where [Au] = gold concentration in the bulk solution at time t, (mg / l)

$[Au]_o$ = initial concentration of gold in the solution, (mg / l)

t = duration of adsorption, (min)

Equation 2.23 is the rate expression used commonly in batch reactor kinetic studies. The observed rate constant k is related to the film transfer coefficient k_f by the equation :

$$k = \frac{6M\psi k_f}{d'\rho V'} \qquad 2.24$$

where k_f = film transfer coefficient

M = mass of active carbon

ψ = shape factor of particles, spherical = 1

d' = average particle diameter

ρ = density of carbon particles

V' = volume of solution

[Fuerstenau *et al.* 1987]

The rate constant k is calculated from the slope of a plot of ln[Au] *vs* t (equation 2.23) for the adsorption of the gold cyanide during the first 20 minutes of the reaction. An additional value Q_S, which gave the amount of gold loaded per gram of carbon after 60 minutes of adsorption, was also calculated for each of the carbons.

CHAPTER 3

EXPERIMENTAL PROCEDURES

3.1. Coal Beneficiation

3.1.1. Conventional batch flotation

Conventional batch flotation was conducted in a 1.5 liter cell for both coals to estimate working parameters for the column. The flotations were carried out using two frothing agents - methyl-isobutyl carbinol (MIBC) and 2-ethyl hexanol, known commercially as Aerofroth 88. A hydrocarbon oil (fuel oil # 2) was used as a collector. Duration of the flotations were 4 minutes at a rotating speed of 1200 RPM. After filtering and drying both the froth and the filtrate (tailings), the weight of each fraction was recorded and the mineral matter content was determined by the standard ASTM method. (ASTM D 3174)

The *combustible recovery* is defined as the total amount of combustible material corrected for mineral matter content, and can be calculated from the material balance as

$$R_c = \frac{C_f * W_f}{(C_f * W_f) + (C_t * W_t)} \qquad 3.1$$

where R_c = % combustible recovery of the product

C_f = % combustible material in froth

W_f = % weight recovery of froth

C_t = % combustible material in tailings

W_t = % weight recovery of tailings

[Wills 1979]

The combustible recovery and mineral matter of the products were calculated for different collector dosages while keeping the frother dosage constant. Once the optimum collector dosage was found, the frother dosage was varied for both frothers under investigation. The mineral content of the coal product was reduced even further by subjecting the cleaned coal to a second flotation step.

3.1.2. Column flotation

The column used in this study had a diameter of 25 mm, was 6.5 m high and made of translucent plastic. The column was fitted with an air sparger at the bottom. The frother and collector were mixed separately before being pumped together with the coal slurry to enter the column about 2 m from the top. The froth collecting plate opened into a bucket which collected the froth; the plate was periodically washed with water to prevent buildup of the froth. The height of the froth in the column was kept at 1 m by varying the tailings overflow. A sample of froth and tailings was taken after stabilization of the experiments; these samples were filtered, dried and submitted for proximate, ultimate and petrographic analysis. (ASTM methods D 3172 - 3179 and ASTM D 2799).

The frother and collector dosages determined from the batch flotations were used in the column flotation of both coals. The influence of the wash water flowrate on the recovery and mineral matter content of the froth was investigated, and samples from

the froth and tailings were taken during the run. The combustible recovery was estimated for each flotation by using the formula :

$$R_c = \frac{c * (f - t')}{f * (c - t')} \qquad 3.2$$

where R_c = % combustible recovery of the product

c = 100 - % ash in froth

f = 100 - % ash in original coal feed

t' = 100 - % ash in tailings

[Wills 1979]

3.2. Coal carbonization

A schematic diagram of the experimental setup for the carbonization of the coal is given in Figure 3.1.

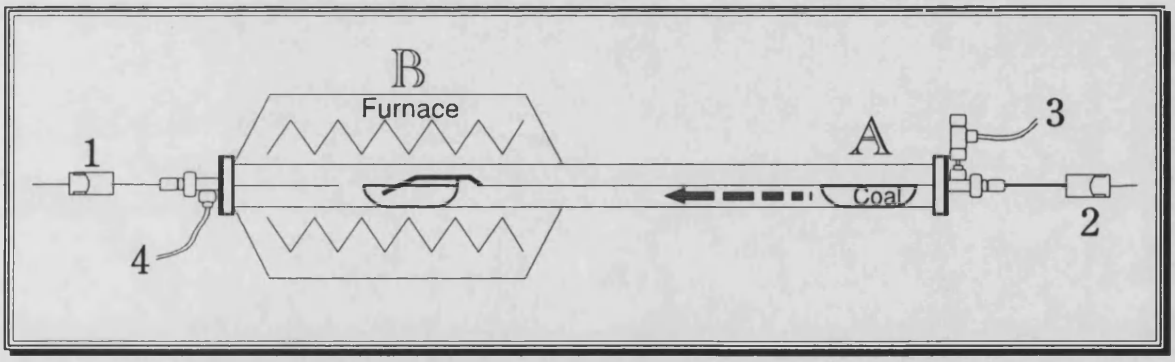

Figure 3.1 : Schematic diagram of the experimental apparatus for coal carbonization and activation.

1 = thermocouple to measure furnace temperature
2 = thermocouple to measure sample temperature
3 = gas inlet (steam outlet during steam activation)
4 = gas outlet (steam inlet during steam activation)

The reactor vessel is made of stainless steel and has an extension A (Figure 3.1) which is used as a loading bay for the sample. The coal was placed in the sample boat (made of quartz glass) and the vessel sealed with a flange at A. The reactor tube was then purged with nitrogen gas at a flowrate of 100 cm^3/min while the furnace was heated to the desired temperature. Once the furnace had reached the set temperature, the sample was pushed into the furnace to position B. The furnace temperature was determined by the main thermocouple which measured the reaction temperature ~ 3 mm above the coal sample. After the experimental time had elapsed, the sample holder was pulled to position A again while the furnace was kept at the set temperature. The sample cooled rapidly to under 100 °C (10 - 15 minutes) while under a nitrogen flow. All the samples were carbonized at a final heat treatment temperature (HTT) of 600 °C in a flow of pure N_2. The heating rate of the sample was 200 °C/min and the sample was kept at this temperature for a soak time of 40 minutes. The Waterberg (WCC) samples were pre-oxidized at 150 °C for 12 h to prevent caking of the coal.

3.3. Activation of coal chars

3.3.1. Physical activation

The experimental apparatus used for the carbonization experiments was also used for the activation of the carbonized chars. For each sample 15 g of the coal was spread out in the sample boat. In this study CO_2 and steam were used as activating gases, following the same experimental and procedure discussed above (section 3.2). The CO_2 flowrate was kept constant at 100 cm^3/min. The flange at the exit end of the vessel was modified to also allow steam to be used as activating gas.

Steam was generated by pumping the water (flowrate 5 cm^3/min) through a 1/16" stainless steel tube running above the sample. The steam was thus heated before being allowed to react with the sample. The weight of the sample was recorded both before and after an experiment to calculate the burn-off value. Samples with high surface areas were subjected to an acid wash (2 g carbon / 200 ml 0.5 M HCl) for two hours to removed some of the ash formed during the activation process. The activation temperature range investigated was 750 - 800 °C for steam activation and 850 - 950 °C for CO_2 activation. Samples were activated up to 50 % burn-off values, and for experimental purposes the maximum activation time was not to exceed 5 h.

3.3.2. Chemical activation

The coal was mixed with a 50 % w/v H_3PO_4 acid solution in the ratio 3:5. The mixture was then impregnated at 200 °C under a flow of 100 cm^3/min N_2 for 30 minutes before being removed to the cool end of the reactor tube. The reactor was then heated to the desired activation temperatures (450, 550 and 650 °C) before the sample was reintroduced and activation started while keeping the flow of N_2 constant at 100 cm^3/min. The samples were washed with boiling water to a pH=7 before submitted for further analysis.

All the samples were washed thoroughly with distilled water and dried at 150 °C for 12 h before being submitted to further analysis. Standard ASTM methods were performed on the samples to determine the proximate and ultimate analysis (ASTM D 3172 - 3179) and the petrographic composition. (ASTM D 2799).

3.4. Gas adsorption

The activated samples were submitted to nitrogen adsorption at 77 K using a Quantachrome Autosorb-6 automated analyzer. The samples were first outgassed overnight at a vacuum of 10^{-2} torr at an outgassing temperature of 200 °C. A sorption isotherm, providing 40 adsorption and 40 desorption points was then constructed and the surface areas and pore volumes calculated from the data. The supplied software for calculating the different parameters was found to be inadequate and the additional calculations were performed by importing the adsorption data to a spreadsheet. The accuracy of the surface areas calculated from the adsorption data using the BET - and α_s - methods are given for selected samples in Table 3.1. On average the BET surface areas vary by 5 % per sample; the mesopore surface areas however showed an average difference of 9 % per sample. The calculated 5 % divergence in this study compares favourably with the error on the BET equation of 10 % as suggested by Gregg and Sing [1982]. The graphs of BET surface areas *vs* burn-off in the following chapters will include error bars of 5 % on the data.

Table 3.1 : Accuracy of surface areas obtained from nitrogen adsorption.

Sample	BET surface area			Mesopore surface area α_s method		
	Sample 1	Sample 2	% difference	Sample 1	Sample 2	% difference
BROM, A6	480	460	4	19	17	11
BCC, A69	580	540	7	23	21	9
WCC, A105	710	740	4	30	32	7

3.5. Mercury porosimetry

Specific volumes and surface areas of the meso- and macropore region were investigated by the mercury porosimetry technique using a Quantachrome Autoscan-60 porosimeter. The sample was first evacuated in the filling chamber to a vacuum of 20 - 30 torr before being allowed to take up mercury to atmospheric pressure. A typical run provided 750 adsorption and 750 desorption points in the pressure range 0 - 60 kpsig. The macropore volume and surface area were calculated from the amount of mercury intruded at a pressure of 4250 psig; this value correlates to a pore diameter of 50 nm, which is the IUPAC defined minimum diameter of macropores. [Sing *et al.* 1985] Subtracting these values from the total pore volume and surface area gave the mesopore parameters. The accuracy of the porosimetry data was calculated to diverge with up 5 % per sample.

3.6. Gold adsorption

All tests were conducted by following the experimental outlines given by Anglo American Research Laboratories in South Africa in their reference CA/75. This reference is included in full in Appendix 1. The tests were applied as suggested for the granular activated carbons, but the experiments had to be adapted for powdered carbon studies, and the modifications are discussed below where appropriate. All powdered carbons were sieved to the fraction of 75 - 150 μm, and conditioned with 5 ml of a borate buffer solution at pH=10 before being used in the tests. For the powdered carbon kinetic tests 0.2 g of carbon was contacted with 1 liter of a 50 ppm solution of gold cyanide, and stirred for 60 minutes. A 5 ml aliquot of the solution was taken through a Whatman filter paper at different time intervals during the one hour adsorption time, and these aliquot solutions were analyzed for gold by atomic absorption spectrophotometry as suggested by Robinson [1966]. The filter paper prevented the fine carbon to be removed from the solution during the taking

of an aliquot sample. No $CaCl_2$ was added to the solution for the powdered carbon studies as the uptake of gold was then found to be too fast to monitor with the current experimental procedures.

CHAPTER 4

RESULTS AND DISCUSSION
Beneficiation and carbonization

Summary

The first step in producing activated carbon is the preparation of the coal chars. The first section of this Chapter gives the results of the cleaning of the coal by froth flotation to produce a low mineral matter precursor for the project. Conventional batch flotation studies were conducted to establish the parameters for the successful operation of the column flotation unit. The cleaned coal is subjected to carbonization in an inert atmosphere to produce the coal chars. The carbonization behaviour of the coals were simulated by thermogravimetric experiments, and these results are compared to the actual carbonization results found for the coals in the carbonization furnace.

4.1. COAL BENEFICIATION

4.1.1. Conventional batch flotation

The conventional batch flotation experiments were used to establish reagent parameters for the column flotation unit since no flotation data was available for the column flotation of the coals used in this study. In the first test, a fixed frother

concentration of 0.22 kg frother per ton coal was used while varying the fuel oil concentration. These experiments established :

- ⌘ the frother that would maximize the coal yield while minimizing the mineral matter content of the coal. Aerofroth 88 (AF88, 2-ethyl hexanol, American Cyanimid Corporation) and MIBC (methyl isobutyl carbinol) were used as frothing agents.

- ⌘ the optimum fuel oil concentration to be used with the selected frother.

In the second series of tests the optimum fuel oil concentration was then used to obtain the frother concentration that would maximize the yield while minimizing the mineral matter content of the coal.

4.1.1.1. Determination of the fuel oil concentration

The results of the experiments to obtain the most efficient frother are shown graphically in Figure 4.1 and Figure 4.2 for the Bosjesspruit and Waterberg coals respectively. A higher combustible recovery for both coals can be obtained using the alcohol based frother AF88, and is probably due to a better interaction between the coal particles and the alcohol frother-coated air bubbles. This interaction is related to the surface chemistry of the coal. The combustible recovery was found to increase with an increase in fuel oil dosages. At higher fuel oil dosages more coal particles are coated by the oil, thereby increasing the hydrophobicity of the coal, and leads to better interaction between the coal particles and the air bubbles.

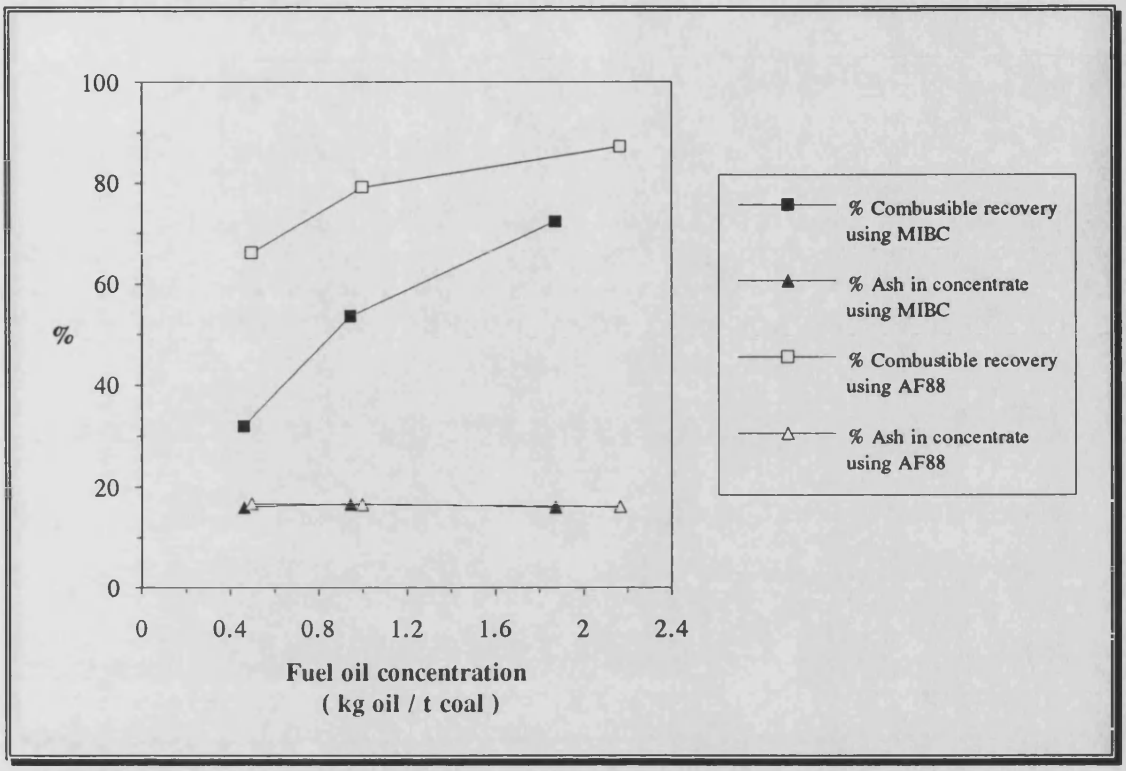

Figure 4.1 : Influence of fuel oil concentration on the flotation parameters of Bosjesspruit coal. (Frother concentration of 0.22 kg / t coal.)

For the Bosjesspruit coal the mineral matter content of the product could be reduced from 24 % to 16 %, while the mineral matter of the Waterberg coal could only be reduced from 61 % to 41 %. The mineral matter content showed little dependence on the fuel oil concentration for the Bosjesspruit coal, and stayed virtually constant over the fuel oil concentration range investigated. The mineral matter content of the floated coal was the same for both frothers, but higher combustible recoveries were obtained using AF88 frothing agent. The Waterberg coal showed a lower mineral matter content in the product using MIBC as the frothing agent; the combustible recovery of this frother however was 20 % lower than that obtained with the AF88 frother. These results showed that most of the mineral matter was inherent to the coal structure and would be difficult to remove.

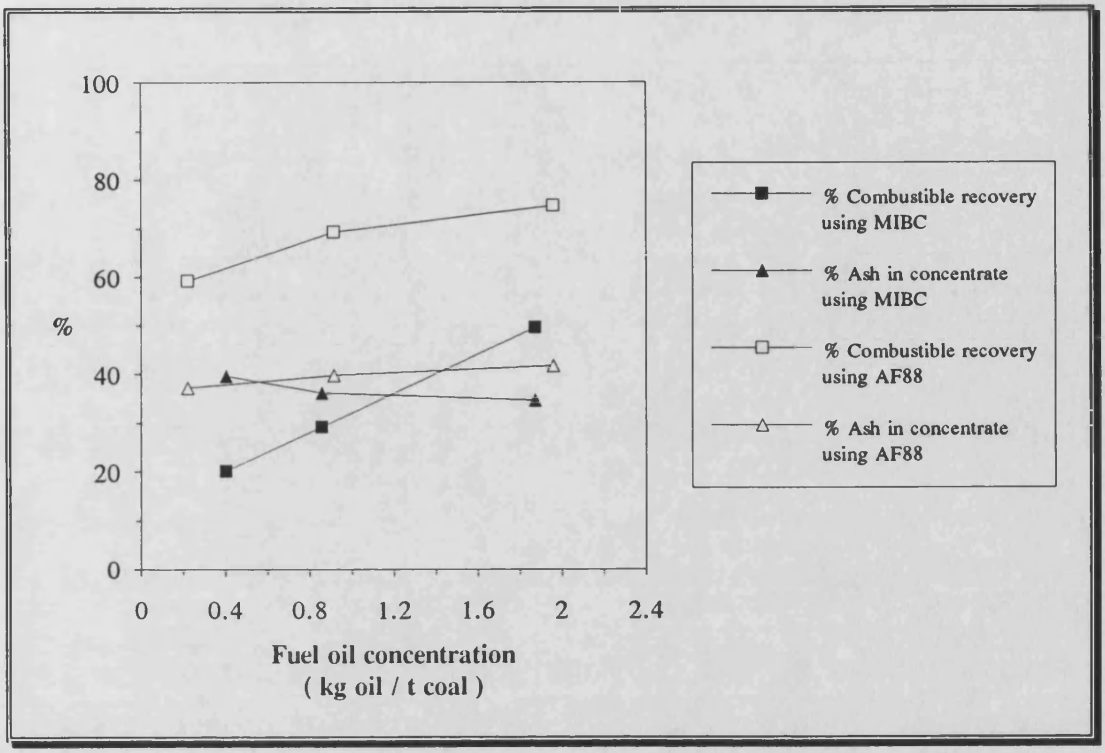

Figure 4.2 : Influence of fuel oil concentration on the flotation parameters of Waterberg coal. (Frother concentration of 0.22 kg / t coal.)

A maximum combustible recovery of 85 % could be obtained for the Bosjesspruit coal when using 0.22 kg / t coal of AF88 and 2 kg fuel oil per ton coal, resulting in a product containing 16 % mineral matter. The combustible recovery for the Waterberg coal using the same parameters was 75 % with a product having a mineral matter content of 41 %.

4.1.1.2. Determination of the frother concentration

The optimum frother concentration using a fuel oil dosage of 2 kg oil per ton coal was subsequently determined by varying the frother concentration in each experiment. The influence of varying AF88 frother concentrations on the flotation parameters of the two coals are shown in Figure 4.3, page 67.

For the Bosjesspruit coal an optimum combustible recovery of 86 % could be obtained for a frother concentration of 0.27 kg per ton coal. The floated coal product had a mineral matter content of 16 %. The optimum combustible recovery of the Waterberg coal of 75 % was obtained at a concentration of 0.25 kg frother per ton coal, resulting in a product with a mineral matter content of 42 %. Higher concentrations of frother AF88 led to lower recoveries and a marginal increase in the mineral matter content of the product for both coals.

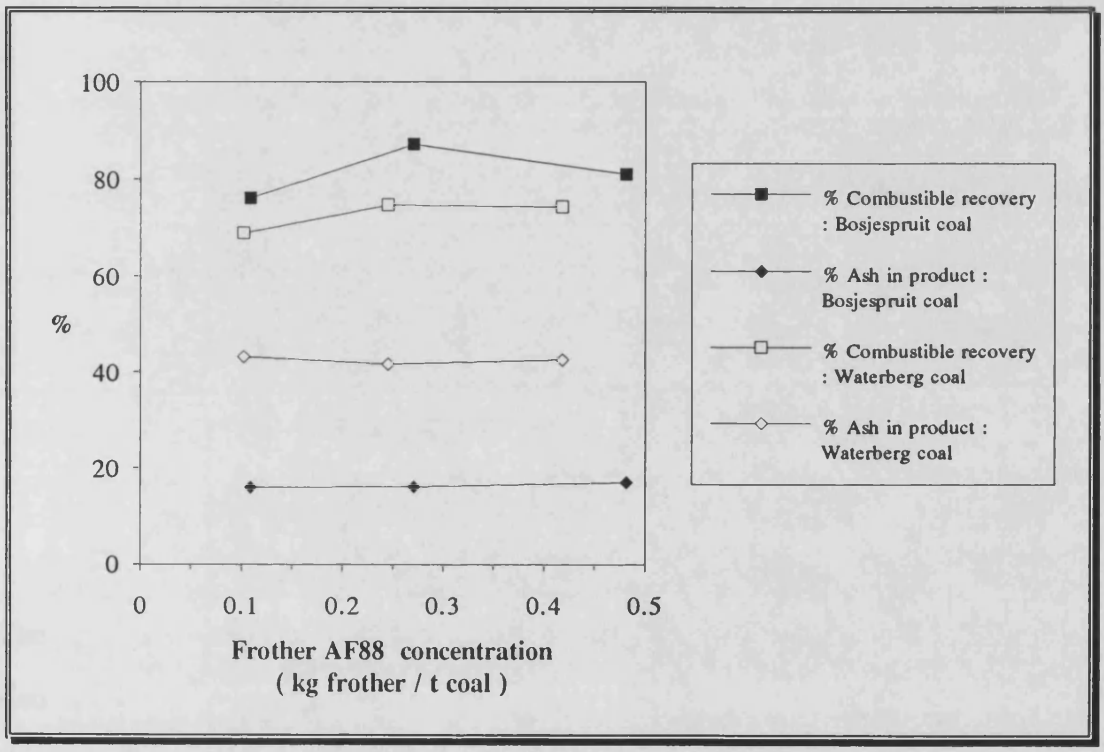

Figure 4.3 : Influence of frother concentration on the flotation parameters of batch floated coal. (Fuel oil concentration : 2 kg / t coal)

4.1.2. Column flotation

4.1.2.1. Product recovery for Bosjesspruit coal

Bosjesspruit coal was used in the initial experiments to establish process parameters for the column. The first test was to establish whether the fuel oil and frother concentrations of 2 kg / ton and 0.25 kg AF88 / ton respectively, as determined by the conventional batch flotation studies, would lead to acceptable results in the column. The parameters used in operating the laboratory column are summarized in Table 4.1.

Table 4.1 : Operating parameters for the laboratory column flotation unit.

Coal particle size	< 150 μm
Solid concentration	5 % (5 g coal / 100 ml water)
Fuel oil concentration	2 kg oil / t coal
Frother concentration	0.25 kg AF88 / t coal
Solid slurry feed rate	1 l / min
Frother - fuel oil feed rate	50 cm^3 / min
Airflow through sparger	1 l / min

The influence of the wash water flowrate on the recovery of the coal product was also investigated; these results are shown graphically in Figure 4.4. The results showed that 400 ml/min is the best washwater flowrate to use, leading to optimum product yield and low mineral matter products.

An experiment using only half of the reagents were also conducted (i.e. 1 kg/t fuel oil and 0.12 kg/t frother). An overall combustible recovery of 84 % was obtained in this test, while the floated coal product had a 15 % mineral matter content. Actual product yield was calculated to be 79 %. These tests showed that considerable

savings can be obtained in the consumption of the chemicals used in operating the column for only a 10 % decrease in the combustible recovery of the product.

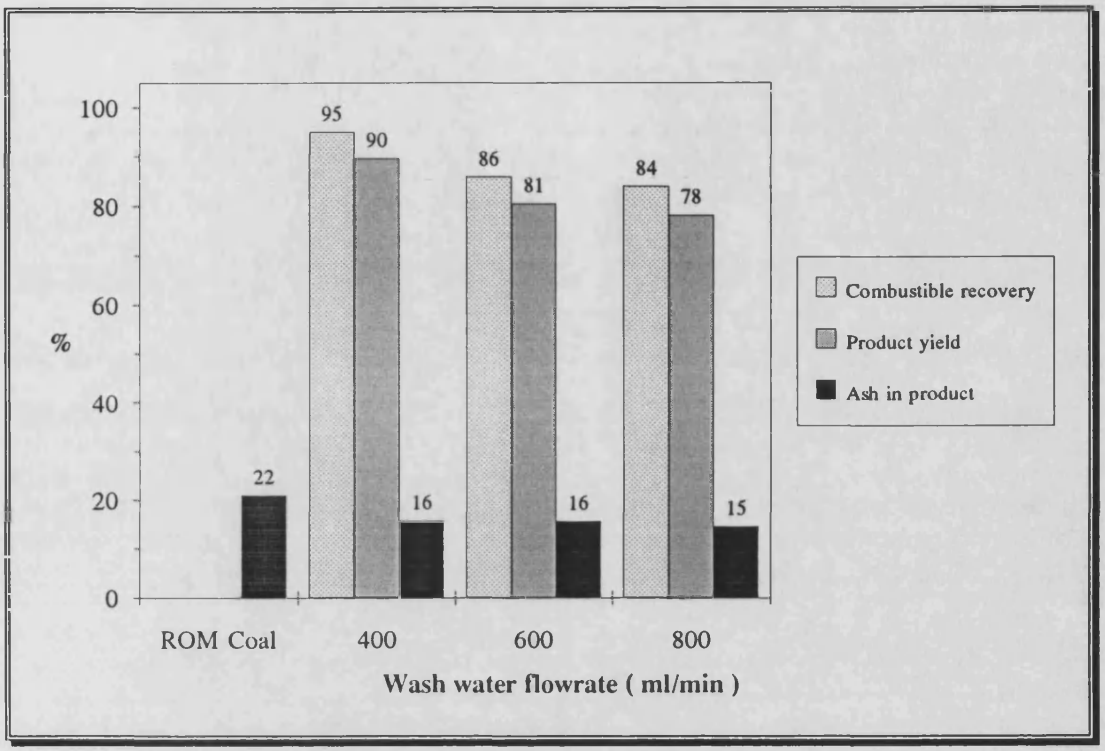

Figure 4.4 : Influence of wash water flowrate on column floated Bosjesspruit coal.

4.1.2.2. Product recovery for Waterberg coal

Column flotation studies of the Waterberg coal were conducted using the same parameters as is listed in Table 4.1. For this coal, a combustible recovery of only 44 % (product yield 23 %) was obtained using a wash water flowrate of 400 ml/min. The mineral matter content of the floated coal decreased from 60 % to 22 %. The low recovery was suspected to be due to insufficient interaction between the froth bubbles and the coal particles. Two reasons for the lack of these interactions may be low air flowrates and insufficient coal particles in the froth. The latter seems especially true because the high mineral matter content of the coal may produce insufficient coal rich particles to stabilize the froth. The experiment was repeated by

increasing the solid slurry concentration to 10 % and the air flowrate to 2 l/min. The combustible recovery increased to 68 % and a coal product with a mineral matter of 26 % was obtained.

4.1.2.3. Results of two-stage column flotation experiments

The froth obtained from the column after the first flotation was subjected to a second flotation in order to try and reduce the mineral matter of the coal even further. Lower mineral matter products can be obtained using a second flotation step due to the negative conditioning of the coal surface after the first flotation step, as explained in section 2.3.4.5. The first flotation is also known as the rougher stage, while the second flotation is known as the cleaner stage. The results of the second flotation are given in Table 4.2.

Table 4.2 : Results of negative conditioning on column floated coals

	Bosjesspruit coal		Waterberg coal	
	First flotation (Rougher)	Second flotation (Cleaner)	First flotation (Rougher)	Second flotation (Cleaner)
Combustible recovery	84	79	68	50
Product yield	79	76	37	22
Ash in product	15	12	26	11

An additional decrease in the mineral matter content of 3 % was obtained for the Bosjesspruit coal while the overall combustible recovery decreased from 84 % to 79 %. The overall yield of coal after two column flotation steps was 76 %. The results obtained for the Waterberg coal was the most pronounced. The second flotation step produced a coal with a mineral matter content of 11 %, but the combustible recovery dropped to 50 %. The product yield was calculated to be only 22 % after

the second flotation step. Although the two floated coal products had similar mineral matter contents, the product yield obtained for Bosjesspruit coal was almost 3.5 times higher than for the Waterberg coal. The second flotation step for the Waterberg coal seemed to be especially effective in removal of additional mineral rich particles.

Optical microscopy showed that the particle size of the tailings was larger than that of the froth, and was dominated by a particle size of < 40 μm. Clays and carbonates appeared to be important minerals in the tailings.

4.1.2.4. Fate of sulphur in the column floated coal

The sulphur contents of the run-of-mine (ROM) and the two-stage floated coal are compared in Table 4.3.

Table 4.3 : Sulphur content of the ROM and floated coals.

[1]Sulphur form	Bosjesspruit coal			Waterberg coal		
	ROM	After second flotation	% Removed	ROM	After second flotation	% Removed
Pyritic	0.46	0.22	52	1.31	0.12	91
Sulphate	0.05	0.03	40	0.1	0.01	90
Organic	0.52	0.32	38	0.82	0.78	5
Total	0.98	0.54	45	2.23	0.91	59

1 Sulphur analysis is on a dry, ash free basis.

The results show that mostly inorganic sulphur is removed using the column flotation process; the sulphur content of the floated Bosjesspruit coal was 45 % less than the parent ROM coal while the sulphur content of the cleaned Waterberg coal decreased by 59 %. The pyritic sulphur was the easiest to remove, since it is mainly

associated with the mineral matter. According to Hower *et al.* [1984] the flotation behaviour of pyrite will be influenced by the size and association of the sulphides, with the retention of ultra fine pyrite particles in the cleaned coal. Since almost twice the amount of pyritic sulphur could be removed from the Waterberg coal when compared to the Bosjesspruit coal, it can be concluded that the pyrite in the Bosjesspruit coal is smaller in size and is dispersed within the coal matrix which makes it difficult to remove.

4.1.2.5. Petrographic analysis of the column floated coals

The influence of column flotation on the petrographic composition of the floated coal product is shown in Table 4.4.

Table 4.4 : Petrography analysis of column floated coals.

Petrography (%)	Bosjesspruit coal			Waterberg coal		
	Parent coal	First flotation	Second flotation	Parent coal	First flotation	Second flotation
Vitrinite	40	15	10	67	70	73
Exinite	2	1	1	3	2	1
Inertinite	58	84	89	30	28	26
Fusinite	5	21	17	9	11	9
Semifusinite	52	63	72	19	17	17
[1]Other	1	0	0	2	0	0

1 The remaining inertinite macerals consists mainly of macrinite, micrinite and resinite.

The inertinite rich Bosjesspruit coal showed a progressive removal of vitrinite-rich coal particles in each of the flotation steps. The vitrinite content decreased by 75 % and the resulting final product had an inertinite content of 89 %. The inertinite macerals consisted mainly of semifusinite. The Waterberg coal, which has a high vitrinite content in the parent coal, showed marginal removal of inertinite macerals

during the flotation process. The coal product obtained after the second flotation step showed a similar petrographic composition as the parent coal. For both the coals the macrinite, micrinite and resinite macerals were all removed in the first flotation step, while the exinite macerals decreased in each flotation step.

The results of the selective flotation of macerals by the froth flotation technique is contradictory. Derbyshire *et al.* [1991] used the same laboratory column employed in this study to clean two Illinois - basin coals. The parent coals were high in vitrinite, and the researchers found little change in the vitrinite and inertinite contents of the cleaned coal, although liptinite was selectively removed in the cleaning process. In a study of the flotation behaviour of bituminous Western Kentucky coals using single stage bench scale flotation, maceral selectivity was also observed by Hower *et al.* in 1984. They suggested that the separation between vitrinite and inertinite using froth flotation is rank dependent, with vitrinite being concentrated in the froth for higher rank coals. A high volatile C parent coal produced a product high in the inertinite macerals of fusinite and semifusinite - this is similar to the analysis that was obtained for the Bosjesspruit coal. In contrast they found a product with a higher vitrinite content when floating a high volatile A bituminous coal. The redistribution of macerals during froth flotation is also heavily dependent on the associated mineral matter. The interaction between the vitrinite and the mineral matter in the two South African coals are obviously different since vitrinite selectivity was observed for the Waterberg coal instead of the inertinite enrichment observed for the Bosjesspruit coal. In the Bosjesspruit coal the vitrinite macerals could be intimately dispersed along with the mineral matter in the coal structure, which ensures that the vitrinite is removed along with the mineral matter.

4.2. COAL CARBONIZATION

4.2.1. Thermogravimetric simulation of the carbonization process

The carbonization behaviour of the different coal precursors in the carbonization furnace was simulated by thermogravimetric (TG) experiments. The coals were heated at a rate of 200 °C per minute up to a temperature of 600 °C. Once this final heat treatment temperature (HTT) was reached, the sample was maintained at this temperature for 40 minutes. The thermograms for the three coal precursors are given in Figure 4.5.

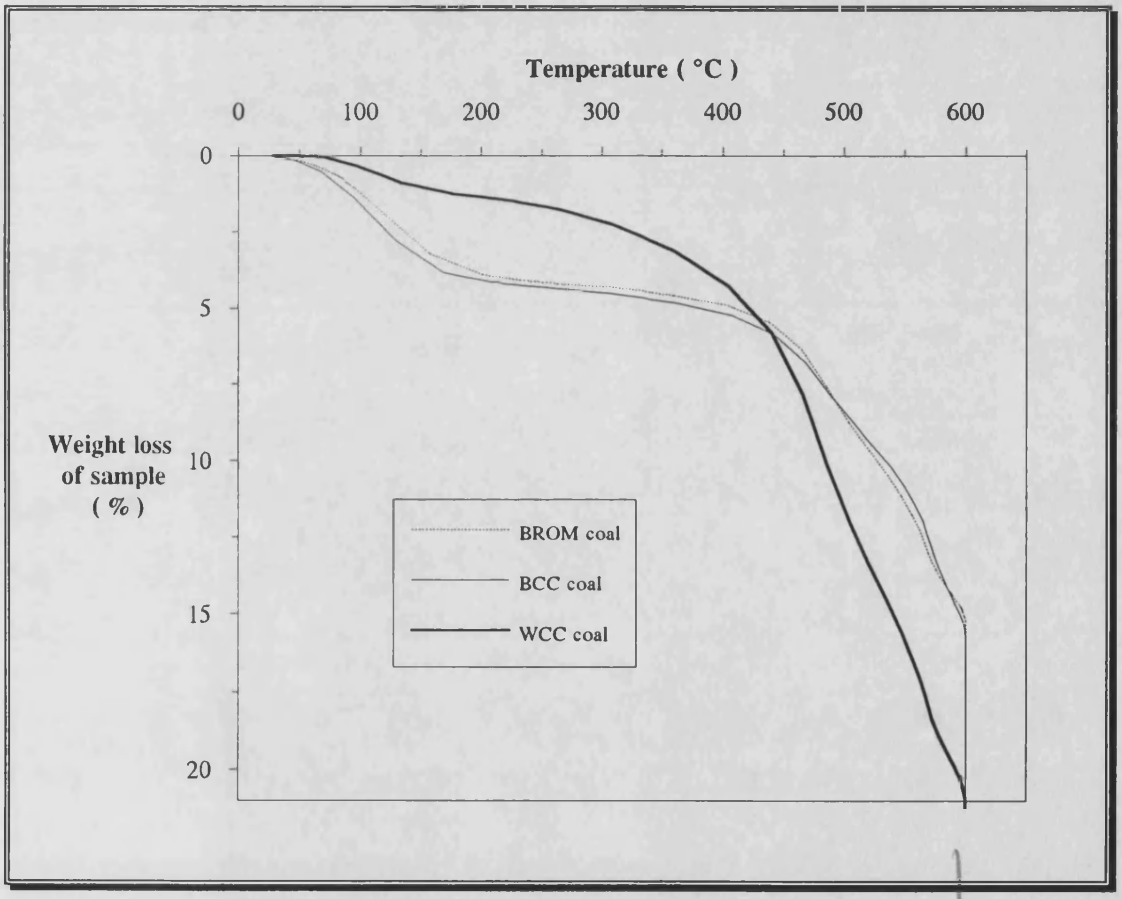

Figure 4.5 : Thermograms of the simulated carbonization process of the coal precursors

From Figure 4.5 it can be seen that the carbonization behaviour of the BROM and BCC coals are similar. The initial weight loss of all the samples up to 200 °C is due to the release of water. Little weight loss is observed for the temperature range 200 - 400 °C, shown by the decrease in the slope of the TG curve. For both coals the major weight loss of the sample occurs above 400 °C, which is due to the evolution of the volatile matter in the coal. The rate of evolution of these species showed a slight decrease at 550 °C, evident by a small deviation in the curve. The samples showed a weight loss of about 15 % at the HTT of 600 °C. The final weight loss of the BROM coal after the soak time of 40 minutes at 600 °C was 19 % compared to the BCC coal which showed a weight loss of 25 %. It is possible that the removal of the mineral matter during the beneficiation process promotes the removal of volatile matter from the coal.

Table 4.5 compares the weight loss of the samples from the TG results to the moisture and volatile matter content of the coals obtained from proximate analysis. A good agreement was found between the weight loss of the coal at 200 °C and the moisture content as determined by proximate analysis. The combination of moisture and volatile content from the proximate analysis was higher than the TG sample weight loss after the final soak time of 40 minutes at 600 °C. This may be mainly due to the higher temperature (950 °C) used in proximate analysis.

Table 4.5 : Comparison between the TG simulated weight loss values and proximate analysis of the carbonized chars.

Coal precursor	Weight loss from thermogram, %		Proximate analysis data, % as received		
	Water [1]	Total [2]	Moisture	Volatiles	Moisture + volatiles
BROM	4	19	6	22	28
BCC	4	25	4	23	27
WCC	2	27	3	33	36

1 Calculated from the thermogram at 200 °C

2 Calculated after 40 minutes soak time at 600 °C

The thermogram for the WCC coal showed that this precursor behaves differently during the carbonization process. The weight loss of the sample was only 2 % at 200 °C which correlates well with the moisture content for the coal obtained from proximate analysis. Contrary to the Bosjesspruit coals, the WCC sample showed a gradual weight loss in the range 200-400 °C. The release of volatile matter started at around 400 °C which is 50 °C less than for the Bosjesspruit samples. The rate of evolution was also faster in the WCC coal; a weight loss of 21 % was recorded at 600 °C, compared to the weight loss of 16 % for the Bosjesspruit coals.

4.2.2. Comparison between TG experiments and actual furnace carbonizations

Table 4.6 shows the comparison between the weight loss of the samples as predicted by TG and the actual weight loss obtained from furnace experiments. The values for the BROM chars were the same, but the TG values overestimated the weight loss for the column cleaned coals. The discrepancies in these values may be ascribed to the sample size, which is much larger in the furnace experiments, leading to heat transfer gradients in the sample.

Table 4.6 : Comparison between the TG simulated and actual weight loss values of the carbonized chars.

Coal precursor	Average weight loss predicted by TG (%)	Actual average weight loss from furnace (%)
BROM	19	19
BCC	25	18
WCC	27	24

4.2.3. Development of BET surface area in the carbonized chars

Table 4.7 shows the BET surface areas obtained from the adsorption of nitrogen at 77 K onto the carbonized chars.

Table 4.7 : BET surface areas (m^2/g) of carbonized chars.

Coal precursor	S_{BET} before carbonization	S_{BET} after carbonization
BROM	☹	67
BCC	☹	☹
WCC	☹	43

☹ S_{BET} too low to measure accurately by nitrogen adsorption data (< 15 m^2/g)

S_{BET} for the parent coals and BCC char after carbonization was less than 15 m^2/g, which is below the reliability limit of detection of the automated adsorption apparatus. The results show that little accessible porosity was developed for the BCC char during the carbonization process. S_{BET} values of 67 and 43 m^2/g were found for the BROM and WCC coals respectively, showing that the devolatilization of the coals created a small degree of open porosity in the carbon structure.

CHAPTER 5

RESULTS AND DISCUSSION
Physical activation

Summary

This chapter gives the results for the physical activation of the carbonized chars using steam and CO_2 as activating agents. Examples of the graphs obtained from the different analysis techniques employed to characterize the porosity of the samples are shown before the porosity values of the samples obtained from the N_2 adsorption data and mercury intrusion results are discussed in detail. Selected samples from each of the coal precursors were subjected to a mild acid wash to remove the ash in the carbon before the porosity of these carbons were compared to the commercially-available carbons.

5.1. Introduction

This section will begin by showing various graphs obtained from the data of the different analysis techniques before discussing the results in more detail. Although the graphs are given for either a specific series of carbons or certain activation conditions, they are representative of the results found for the other carbons prepared at different conditions and coal precursors. Individual carbons which showed variations from these graphs will be referred to under the appropriate sections when discussing the results in detail.

5.2. Representative sorption isotherms and α_s - plots

The typical isotherms found for the sorption of N_2 at 77 K onto the activated carbons prepared from the BCC coal are shown in Figure 5.1.

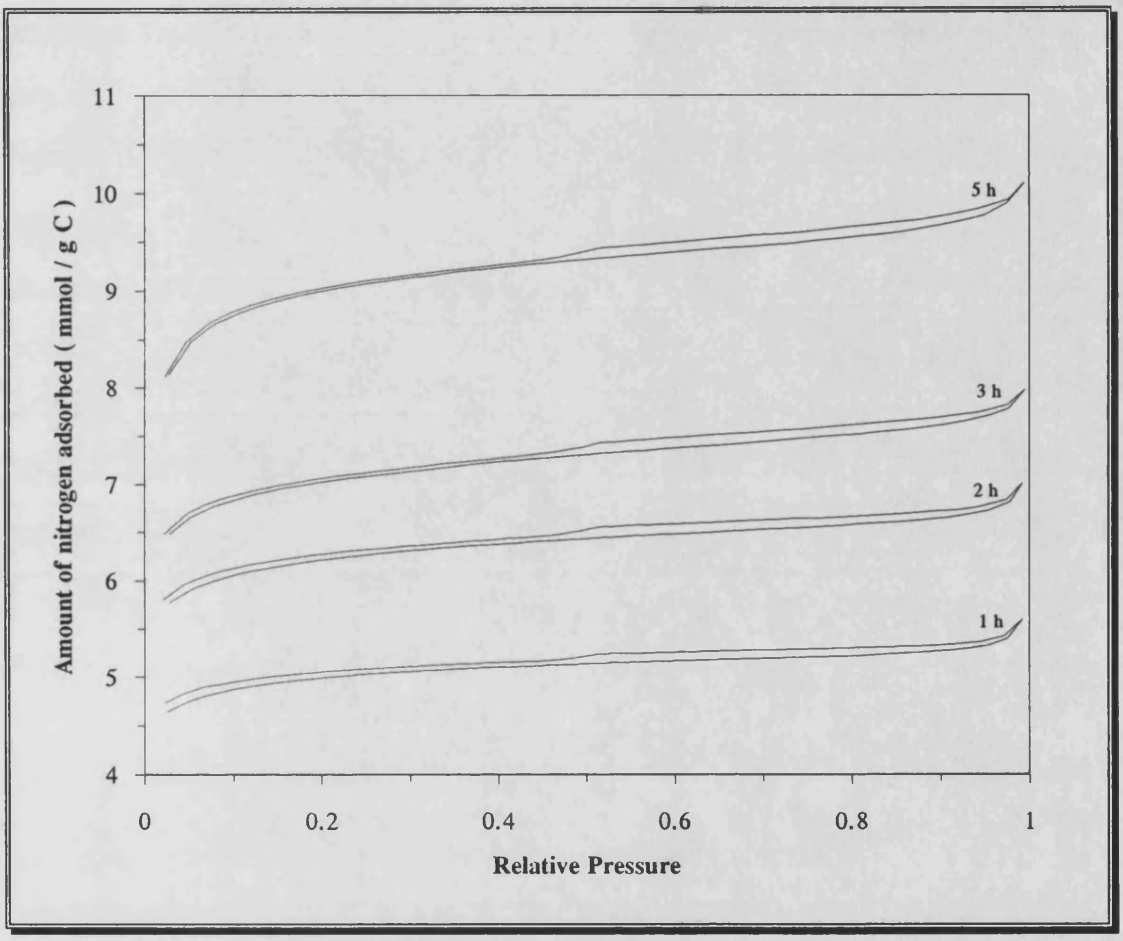

Figure 5.1 : Nitrogen sorption isotherms at 77 K for activated carbons prepared from BCC coal.

(CO_2 activation at 875 °C for various activation times.)

Useful qualitative information can be obtained from a visual inspection of the isotherms. The shape of the isotherms for the moderately activated carbons are close to Type I in the BDDT classification [Brunauer *et al.* 1940], showing that the

carbons are predominantly microporous. As the relative pressure approaches 1.0, the adsorption of nitrogen in the gaseous phase has shifted to the process of capillary condensation with the pores being filled by liquid adsorbate, and accounts for the upswing in the isotherm curve at p/p_o ~ 1.0. Open-loop hysteresis at low relative pressures was found for the moderately-activated carbons and is indicative of activated diffusion of N_2 through apertures in the microporous network whose size is similar to that of the nitrogen molecule. The progressive reduction in low pressure hysteresis with increasing activation also points to a widening of the microporous apertures. [Gregg and Sing 1982] The high pressure hysteresis is similar to Type B in the IUPAC classification [Sing *et al.* 1985], which is usually found for capillary condensation in slit-shaped pores. The steep fall and closure of the desorption branch of the isotherm at a relative pressure of ~ 0.45 was first explained by Schofield in 1948. He suggested that the relative pressure at which loop closure occurs is due to tensile strength effects of the adsorbate, and this point shows the critical value where the adsorbate undergoes a phase transition from a liquid-like state to a gaseous-like state.

The extent of adsorption increases with activation, reflecting increases in both microporosity (shown by an increase in the uptake of N_2 at low relative pressures) and mesoporosity (shown by the increase in the slope of the isotherm at higher relative pressures). The same trends are observed for the corresponding α_s - plots, given in Figure 5.2. The development of surface area as interpreted from the qualitative observations of the isotherm shape is confirmed by the physical values calculated from the isotherms, which are given in Table 5.1.

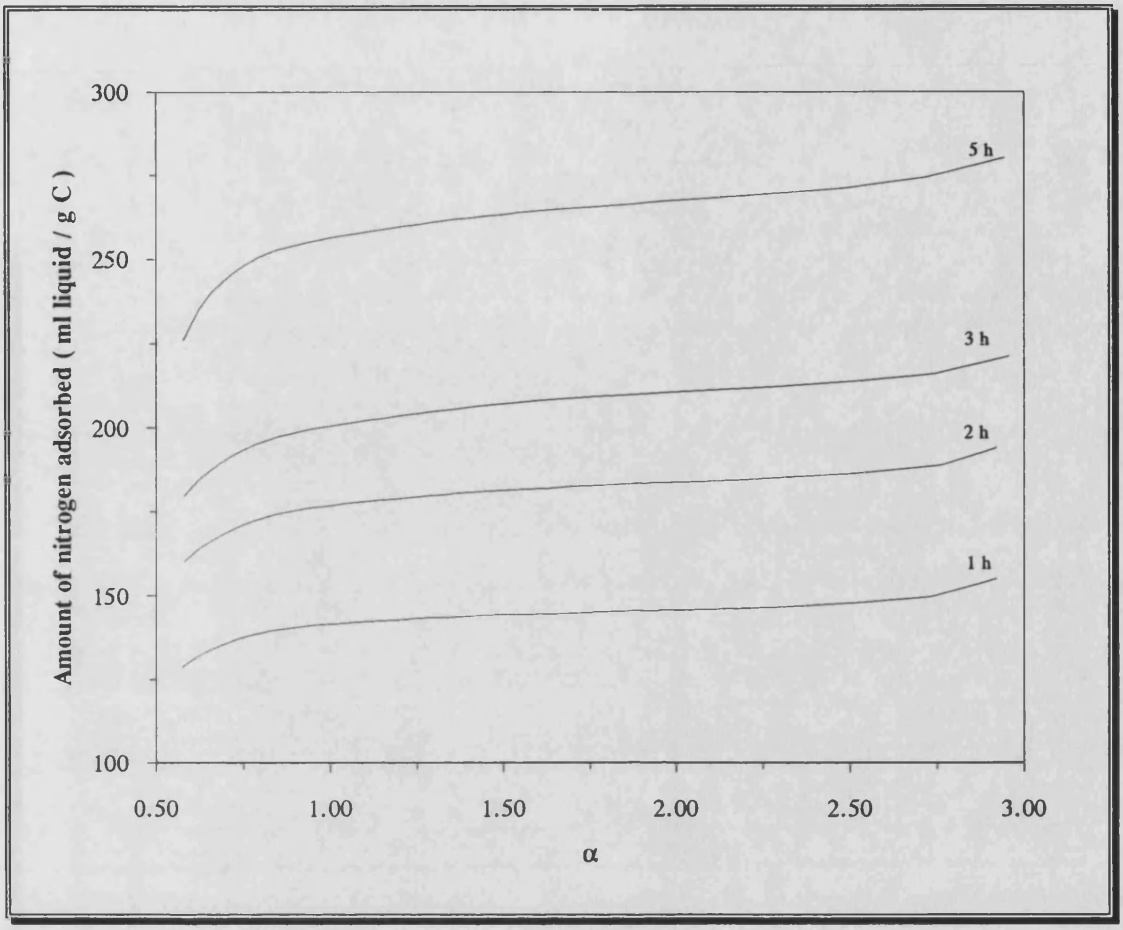

Figure 5.2 : α_s - plots for activated carbons prepared from BCC coal. (CO_2 activation at 875 °C for various activation times.)

Table 5.1 : Pore structure analysis for BCC carbons prepared by CO_2 activation at 875 °C.

Activation time h	Sample burn-off %	BET surface area m^2/g	Micropore volume[1] cm^3/g	Mesopore surface area[1] m^2/g
1	21	380	0.14	7
2	31	470	0.17	12
3	38	530	0.19	17
5	50	680	0.25	18

1 Calculated from the α_s - plot, Figure 5.2

5.3. Representative Dubinin - Raduskevich (DR) plots

The Dubinin - Raduskevich (DR) plots for the carbons prepared from BCC chars at 875 °C by steam activation are given in Figure 5.3.

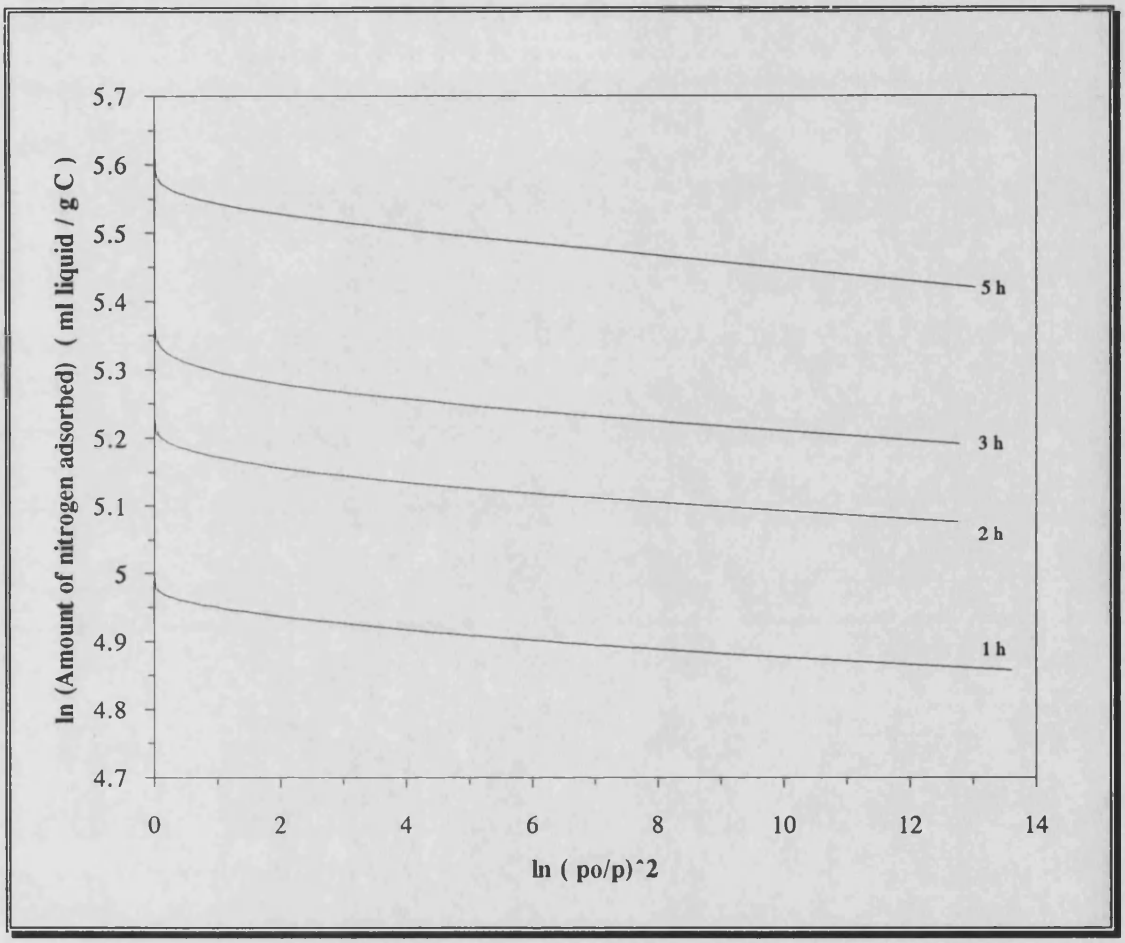

Figure 5.3 : DR - plots for activated carbons prepared from BCC coal (CO_2 activation at 875 °C for various activation times.)

The DR - plots gave good linearity for values of $\ln^2(p_o / p) > 1$, but displayed an upward turn as the saturation pressure is approached. This upturn is found due to the multilayer adsorption and capillary condensation in the mesopores. [Gregg and Sing 1982] In calculating the micropore volume in cases where the DR- plot displays an

upward swing, the linear portion of the plot must be extrapolated to ensure exclusion of the mesopore contribution at low $\ln^2(p_o / p)$ values.

5.4. Representative mercury porosimetry graphs

Mercury porosimetry graphs for the range 0 - 60 kpsig are given in Figure 5.4 for the series of BCC carbons steam activated at 775 °C. In this figure, the pressure has been converted to a pore radius assuming a cylindrical pore model.

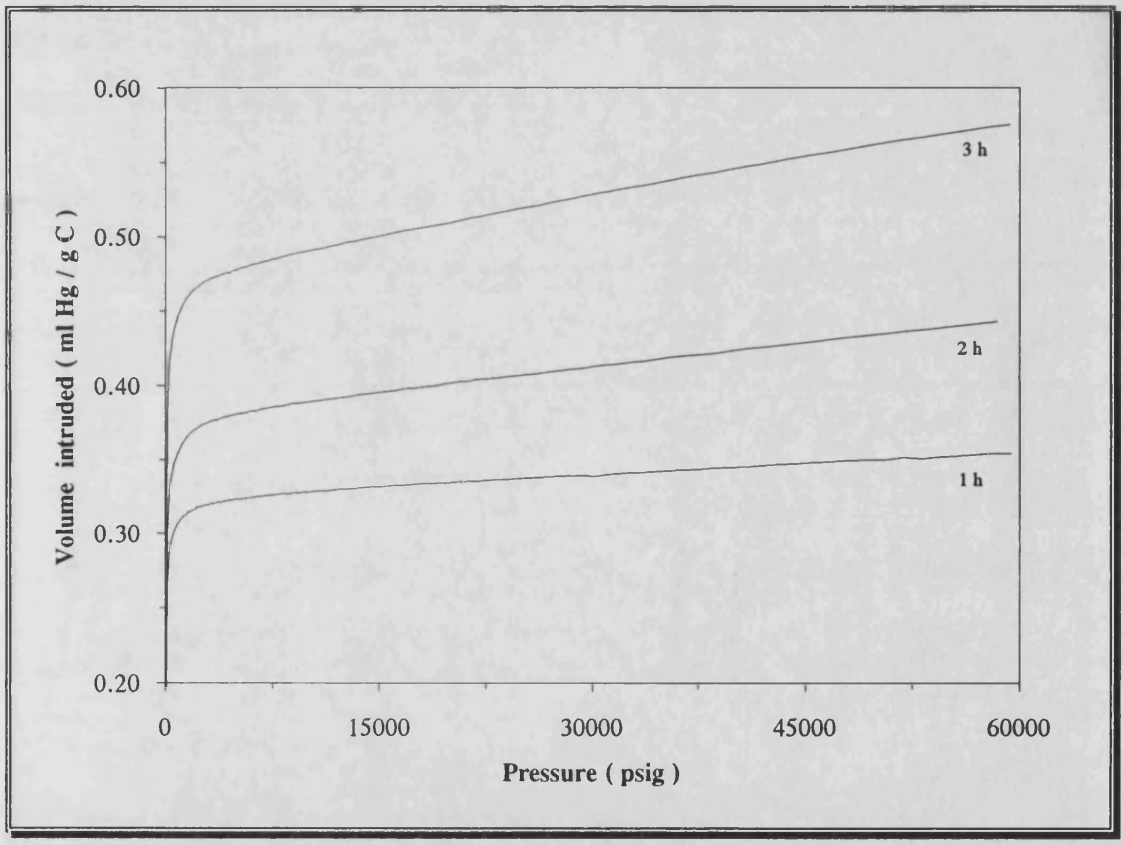

Figure 5.4 : Mercury intrusion graphs for activated carbons prepared from BROM coal.
(Steam activation at 775 °C for various activation times.)

The amount of mercury that could be intruded into the sample increased with an increase in activation, showing the development of meso- and macro-porosities. For

1 hour activation time the slope of the graph above ~ 7000 psig was small. Since a pressure of 7000 psig translates to a pore radius of 15 nm assuming cylindrical pores, the small value of the slope shows that the majority of the porosity were concentrated in the macropore region (r > 25 nm). The slope of the plot increased with activation, which shows that the mercury could intrude into a larger range of pores, showing the development of mesoporosity as well as macroporosity.

Evidence was found that the mercury intrusion at high pressures damaged some samples; an example is given in Figure 5.5. In this figure the pressure has been converted to a pore radius (higher pressures correlates to smaller pores).

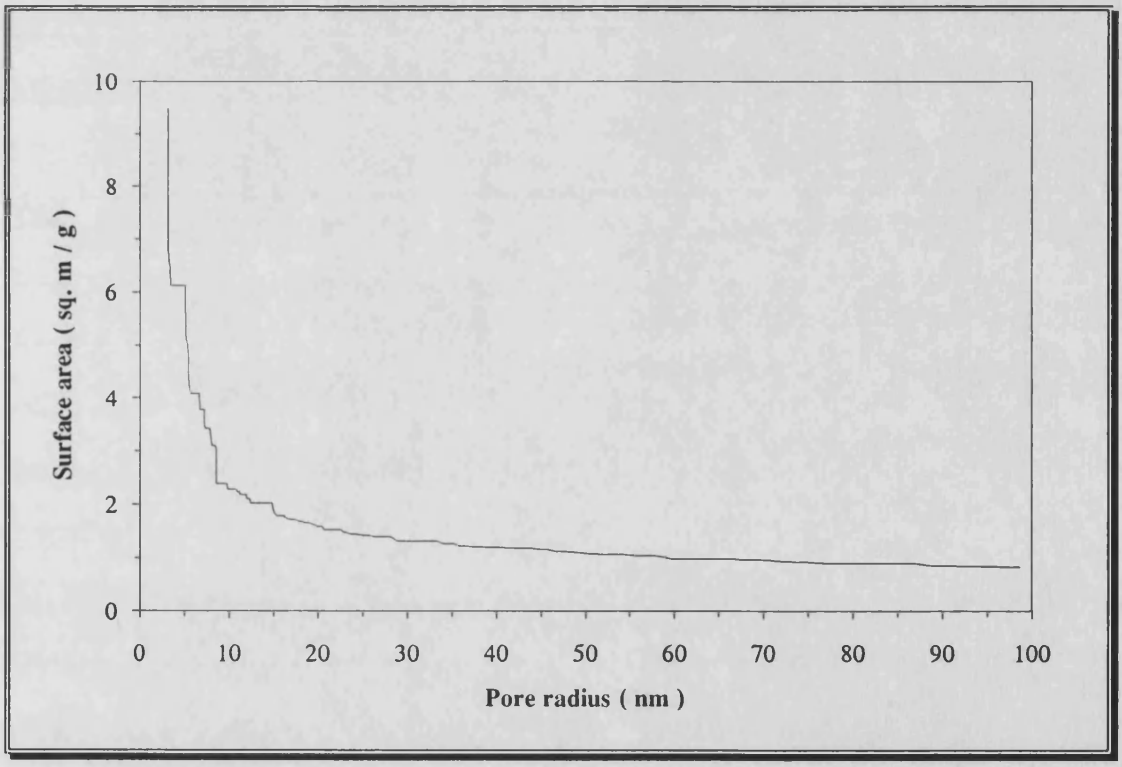

Figure 5.5 : Mercury intrusion graph showing pore damage to the sample at high pressures.

(WCC carbon A97, CO_2 activation at 875 °C for 3 h activation time.)

Intrusion at high pressures can expand existing pore walls or may damage them to such an extent that they collapse, giving access to previously closed pores. The first evidence of damage in the sample shown in Figure 5.5 occurs for a pore radius of ~ 15 nm, but the most extensive damage occurs at pore radii less than 10 nm, corresponding to a pressure of 10 650 psig. In a study of mercury porosimetry in carbon black compacts Milburn *et al.* [1988] found disintegration of carbon particles at pressures as low as 2500 psig (r = 43 nm). For practical purposes the graphs were analyzed only for pressures up to 50 000 psig (corresponding to r = 2 nm) to ensure that the calculated values from porosimetry excluded any mercury intruded due to the damage of the pore structure above 50 000 psig. In cases where pore damage was noted, the mesoporosity values were obtained from the nitrogen adsorption data, and the porosimetry data was used only to calculate the degree of macroporosity. Pore damage was observed especially for the WCC carbons,

The mercury intrusion-extrusion graphs for all the samples showed extensive hysteresis; an example is shown in Figure 5.6, page 86. Hysteresis can be linked to the shape of the pore and pore network effects. Emptying a pore filled with mercury can occur at a lower pressure than the filling of the pore due to constrictions in the pore, for example a narrow pore entrance. Two examples of such pores are given in Figure 5.7. Hysteresis also shows that the assumption of the cylindrical pore model for porosimetry should be approached with caution, since restrictions in cylindrical pores are limited and the graph will show little hysteresis. Hysteresis is also to be expected if the sample showed pore damage during the intrusion step, and as a result of pore network effects. [Androutsopoulos and Mann 1979]

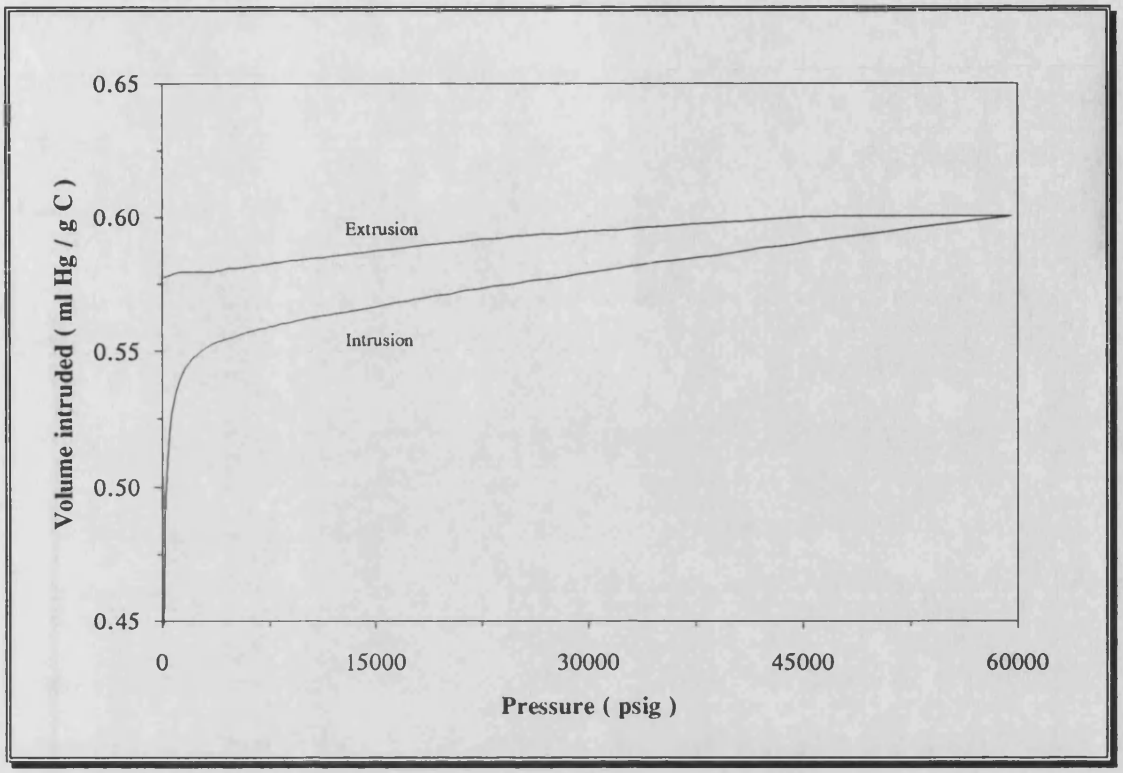

Figure 5.6 : Occurrence of hysteresis in mercury porosimetry for an activated carbon prepared from WCC coal.
(CO_2 activation at 875 °C for a 4 h activation time.)

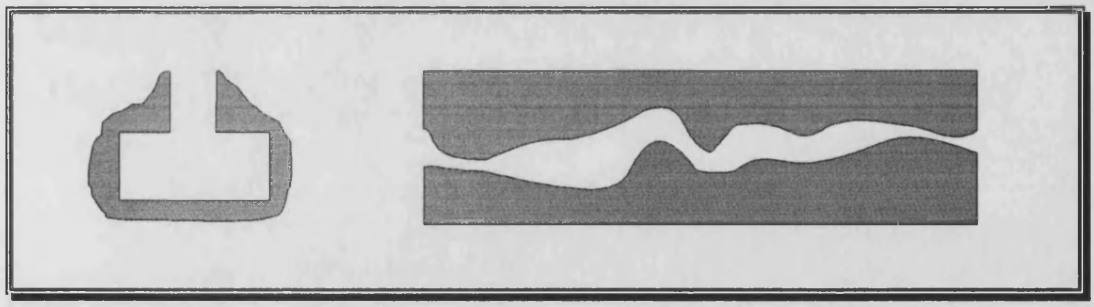

Figure 5.7 : Examples of mesopores which can give rise to adsorption hysteresis.

5.5. Activation of Bosjesspruit run-of-mine (BROM) chars

5.5.1. CO_2 Activation of BROM chars

The development of BET surface area with burn-off at the different temperatures is compared in Figure 5.8.

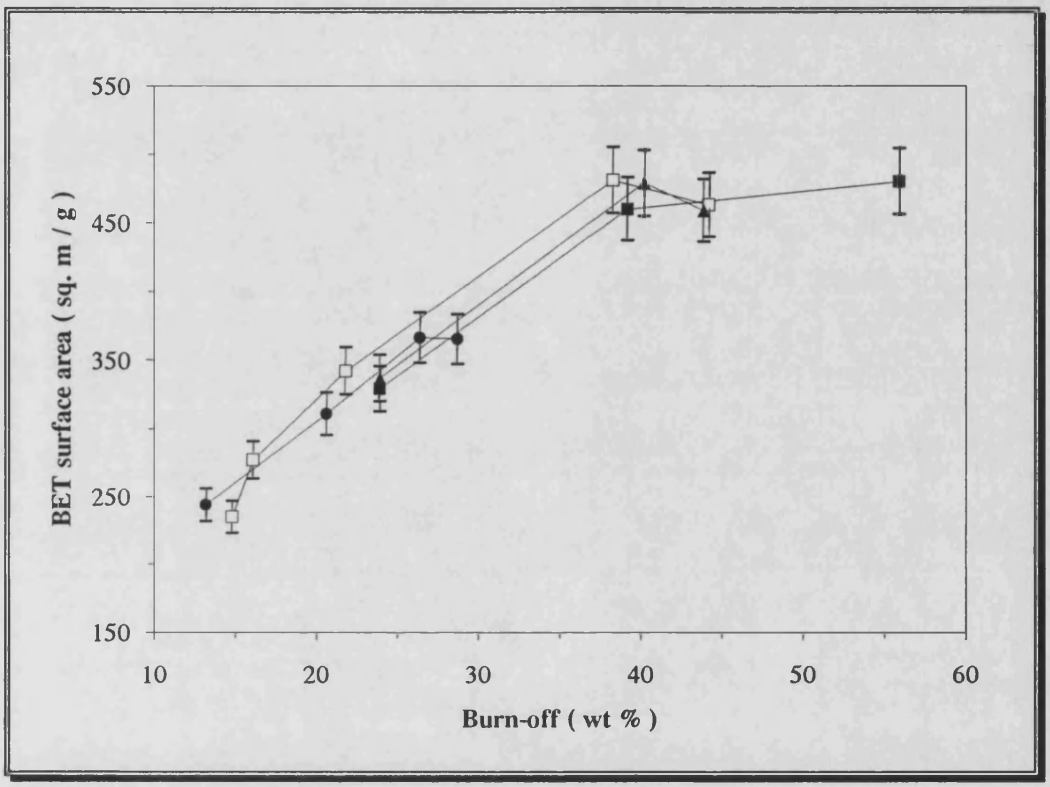

Figure 5.8 : Development of BET surface area in CO_2 activated BROM chars.
(Activation temperatures : ● 850 °C □ 875 °C ▲ 900 °C ■ 950 °C)

From Figure 5.8 it can be seen that the surface area in the carbons was increased with burn-offs up to 40 % at each of the activation temperatures. There is evidence that the S_{BET} values reached a maximum value of ~ 480 m^2/g at a burn-off value of ~ 40 %, since no increase in S_{BET} was found for burn-offs higher than 40 % when taking the 5 % variance of S_{BET} into account. For any given burn-off (< than 40 %) there is also a marginal shift to higher surface areas when using lower

activation temperatures, which suggests that the activation process is more efficient at lower temperatures. The porosity values calculated from the nitrogen adsorption data for each of the samples are shown in Table 5.2.

Table 5.2 : Pore structure analysis from N_2 adsorption data for CO_2 activated BROM carbons.

Sample no.	Activation conditions								
	Temp °C	Time h	Burn-off %	BET N_2 surface area, S_{BET} m^2/g	Notional micropore surface area, S_{micro} m^2/g	Micropore volume, V_o cm^3/g	Mesopore surface area, S'_{BET} m^2/g	Charac-teristic energy E_o kJ/mol	Ash %
A11	850	1	13	240	235	0.09	5	13.5	30
A12		2	21	310	306	0.11	4	16.3	32
A51		3	26	370	364	0.13	6	15.1	34
A52		4	29	360	354	0.13	6	15.0	34
A1	875	1	16	280	275	0.1	5	13.5	31
A2		2	22	340	333	0.13	7	13.2	34
A25		4	38	480	462	0.17	18	10.0	32
A47		5	44	460	444	0.17	16	10.4	44
A5	900	1	24	340	333	0.12	7	13.6	33
A6		2	40	480	461	0.17	19	9.9	42
A46		3	44	460	442	0.17	18	8.9	43
A9	950	0.5	24	330	318	0.12	12	10.1	34
A8		1	39	460	433	0.16	27	8.0	41
A7		2	56	480	451	0.17	29	7.8	56

Analogous to the BET surface area the micropore volume and mesopore surface area reached a maximum value. The micropore volume reached a value of 0.17 cm^3/g for the higher activation temperatures at 40 % burn-off; this burn-off value was

independent of the activation temperature. Little mesopore surface area was developed at 850 °C and it was independent of activation time. S'_{BET} for activation temperatures of 875 and 900 °C reached a maximum value of ~ 19 m^2/g before declining. S'_{BET} for an activation temperatures of 950 °C showed a progressive increase and a value of 29 m^2/g was obtained for 56 % burn-off in sample A7. Overall the mesopores constituted less than 6 % of the total surface area, showing that the samples are predominantly microporous. A good agreement was found between mesoporosity calculated from the N_2 data and the values calculated from mercury porosimetry, as is shown in Table 5.3.

Table 5.3 : Pore structure analysis from mercury porosimetry data for CO_2 activated BROM carbons.

Sample no.	Activation conditions		Mercury porosimetry data (50 kpsig max)				N_2 data
	Temp °C	Time h	Macropore volume V_{macro} cm^3/g	Mesopore volume V_{meso} cm^3/g	Macropore surface area S_{macro} m^2/g	Mesopore surface area S'_{BET} m^2/g	Mesopore surface area S'_{BET} m^2/g
A11	850	1	0.16	0	1	4	5
A12		2	0.27	0.02	1	8	4
A51		3	0.26	0.01	1	8	6
A52		4	0.23	0.01	1	6	6
A1	875	1	0.29	0.01	1	7	5
A2		2	0.31	0.02	1	9	7
A25		4	0.44	0.04	1	19	18
A47		5	0.44	0.03	1	17	16
A5	900	1	0.29	0.01	1	10	7
A6		2	0.40	0.03	1	16	19
A46		3	0.47	0.02	1	15	18
A9	950	0.5	0.30	0.02	1	11	12
A8		1	0.44	0.04	1	21	27
A7		2	0.52	0.04	2	24	29

The porosimetry results showed that the macropore volume for the 850 °C carbons went through a maximum, which did not follow burn-off, and for the 875 °C carbons the macropore volume reached a maximum value after 4 hours activation. For the higher activation temperatures, the macropore volume of the samples increased progressively with burn-off, due to the enlargement of the pores. All the samples contained a negligible macropore surface area.

5.5.2. Characteristic energy of CO_2 activated BROM carbons

The values of the characteristic energy E_o of the carbons, calculated from the DR - equation (see section 2.6.7.2), are shown in Figure 5.9.

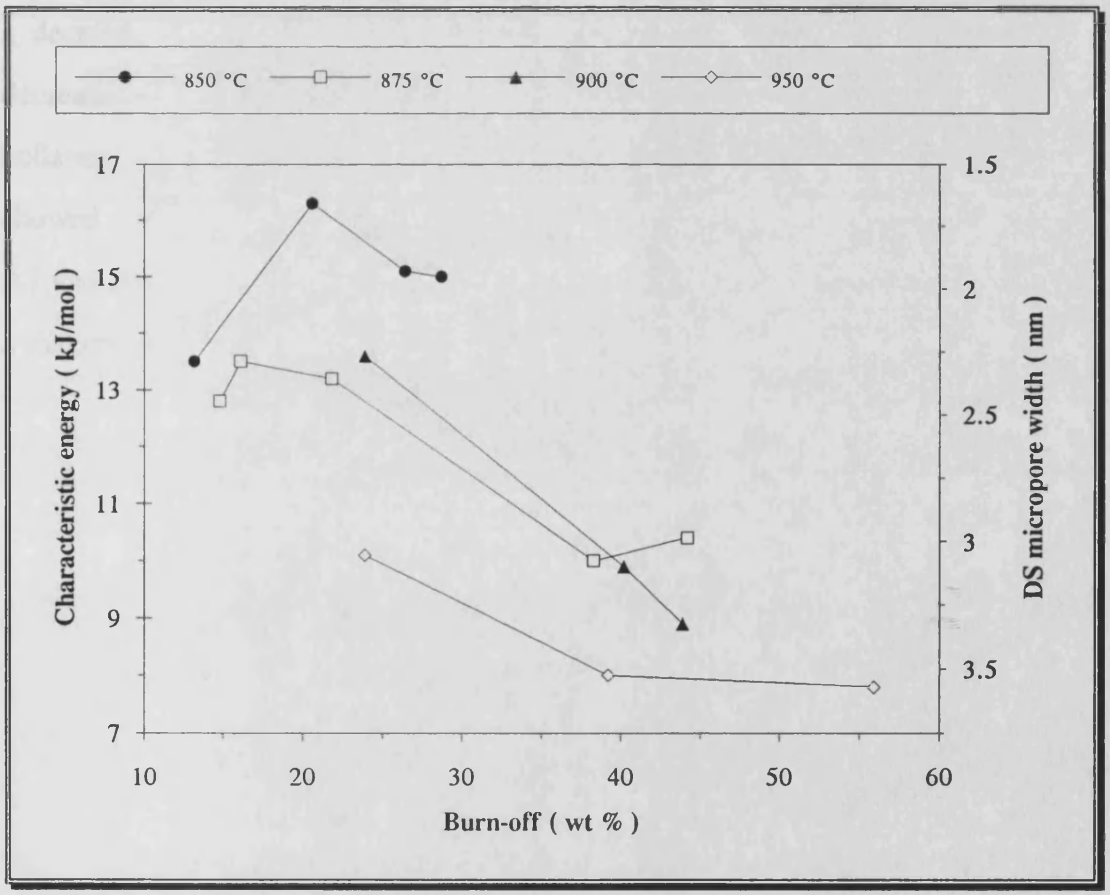

Figure 5.9 : Characteristic energy plots for CO_2 activated BROM carbons.

The characteristic energy is a measure of the adsorption potential between the adsorbate molecules and adjacent pore walls, and can be linked to the average micropore width (see section 2.6.8). A reference axis showing the values of the Dubinin-Stoeckli average micropore widths calculated from the E_o values, using equation 2.17, is included in Figure 5.9.

The values of E_o shifted towards lower energies as the activation temperature increased, showing that a higher activation temperature produces larger pores for similar burn-off values. The lower E_o values at burn-offs below 15 % can be attributed to limited activation, as is reflected in the S_{BET} values from Table 5.2 on page 88. The increase in E_o after 40 % burn-off at 875 °C shows that there has been a decrease in the pore width of the sample. Combining this observation with the decrease in S_{BET} and S'_{BET} for the sample (A47), confirms that the pore structure collapsed partially, due to the longer activation time. At 950 °C the E_o values showed little increase for a burn-off above 40 %. Since the S_{BET} values of samples A7 and A8 were similar; this confirms that the development of porosity has reached a maximum of ~ 480 m^2/g, with little increase in pore diameter.

5.5.3. Steam activation of BROM chars

The development of BET surface area for the steam activated BROM chars is shown in Figure 5.10, while the porosity values calculated from the N_2 adsorption data are given in Table 5.4, page 93.

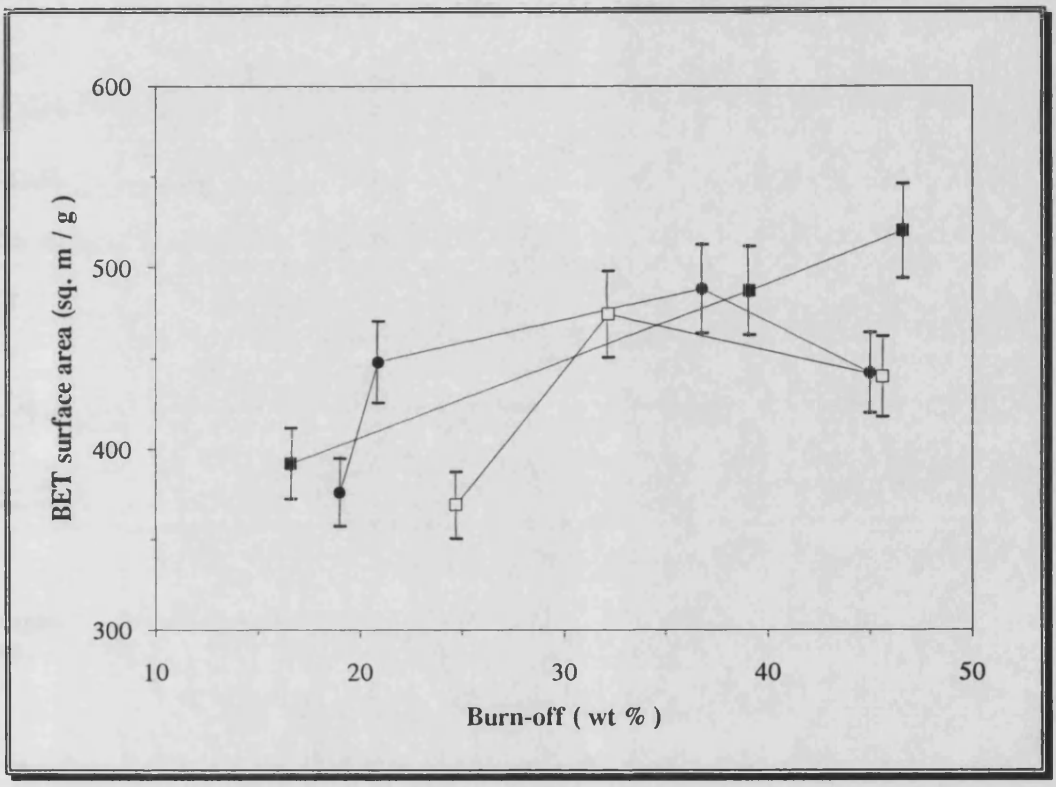

Why no trend

Figure 5.10 : Development of BET surface area for steam activated BROM chars.
(Activation temperatures : ● 750 °C ■ 775 °C □ 800 °C)

The development of surface area went through a maximum value of ~ 490 m^2/g at activation temperatures of 750 °C and 800 °C respectively. These values are close to the maximum S_{BET} value of 480 m^2/g obtained for the CO_2 activation of the same chars. The maximum S_{BET} at 750 °C and 800 °C was obtained for burn-off values of 35 % and 32 % respectively (Table 5.5); both these values are lower than the burn-off value of 40 % found for the CO_2 activated chars that displayed similar surface

areas. This shows that activation of the BROM chars is more efficient using steam as the activating agent. An increase in the mesopore surface area was observed over the burn-off range at an activation temperature of 800 °C, although the marginal decrease in S_{BET} would suggest that the creation of mesopores are by the enlarging of existing micropores. At the intermediate activation temperature of 775 °C used in this study there was a steady increase in surface area, and when the 5 % error on S_{BET} is taken into account, the surface area of 520 m^2/g is similar to the surface area of 490 m^2/g found at activation temperature of 750 and 800 °C. These observations support the view that the development of surface area using steam as activating agent reaches at maximum at a burn-off value of about 40 %, similar to the results found for the activation of the BROM chars using CO_2 as activating agent.

Table 5.4 : Pore structure analysis from N_2 adsorption data for steam activated BROM carbons.

Sample no.	Activation conditions		Burn-off	BET N_2 surface area, S_{BET}	Notional micropore surface area, S_{micro}	Micropore volume, V_o	Mesopore surface area, S'_{BET}	Characteristic energy E_o	Ash
	Temp °C	Time h	%	m^2/g	m^2/g	cm^3/g	m^2/g	kJ/mol	%
A58	750	3	21	450	437	0.17	13	10.7	36
A59		4	37	490	473	0.19	17	9.4	41
A63		5	45	440	421	0.17	19	8.2	38
A55	775	1	17	390	381	0.15	9	11.9	33
A56		2	39	490	466	0.19	24	8.8	40
A57		3	47	520	480	0.20	40	8.1	46
A62	800	1	25	370	356	0.14	14	11.3	32
A61		2	32	470	442	0.18	28	9.6	39
A60		3	46	440	389	0.16	51	8.4	43

why are these different

From these results it appears that the development of surface area using steam in BROM chars is especially sensitive to the activation temperature. The micropore volumes V_o at 750 and 800 °C followed the trend observed for S_{BET} and went through a maximum value of ~ 0.19 cm^3/g. The maximum V_o obtained was 0.20 cm^3/g at 775 °C for a burn-off of 47 %.

The mercury intrusion data for the steam activated BROM chars are given in Table 5.5.

Table 5.5 : Pore structure analysis from mercury porosimetry data for steam activated BROM carbons

Sample no.	Activation conditions		Mercury porosimetry data (50 kpsig max)				N_2 data
	Temp °C	Time h	Macropore volume V_{macro} cm^3/g	Mesopore volume V_{meso} cm^3/g	Macropore surface area S_{macro} m^2/g	Mesopore surface area S'_{BET} m^2/g	Mesopore surface area S'_{BET} m^2/g
A58	750	3	0.32	0.03	1	20	13
A59		4	0.34	0.04	2	19	17
A63		5	0.28	0.18	1	28	19
A55	775	1	0.32	0.03	1	14	9
A56		2	0.38	0.04	2	28	24
A57		3	0.48	0.07	2	44	40
A62	800	1	0.26	0.03	1	18	14
A61		2	0.33	0.06	1	25	28
A60		3	0.37	0.07	2	38	51

Good agreement was found for the mesopore surface areas calculated from porosimetry and the adsorption data. Sample A60 was the only sample where the difference was substantial, this shows that most of the extra pore surface area

calculated from the adsorption data is due to pores having a radius less than 2.1 nm, which is the limit of porosimetry at 50 000 psig. The samples showed negligible macropore surface area, but an increase in the macropore volume for increased activation, due to the burn-out of existing pores.

5.5.4. Characteristic energy of steam activated BROM carbons

The characteristic energy values for the steam activated BROM chars are given in Figure 5.11.

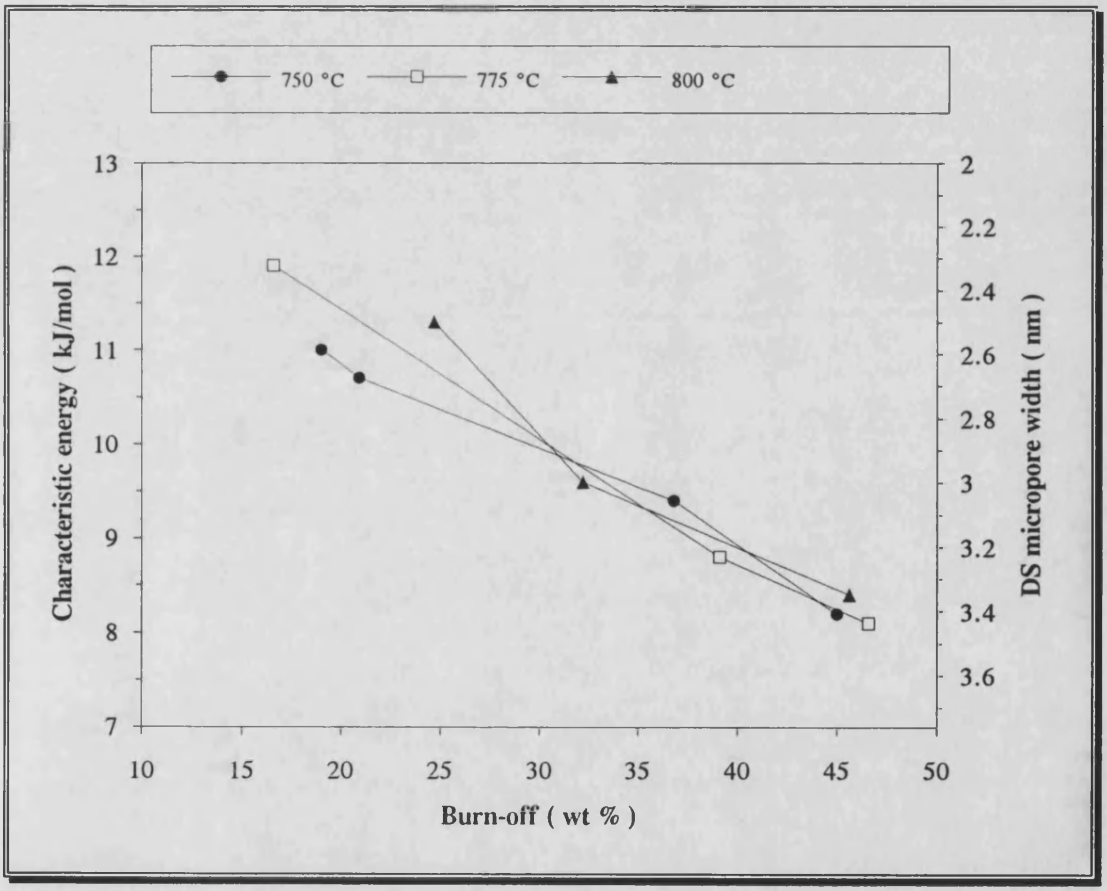

Figure 5.11 : Characteristic energy plots for steam activated BROM chars.

The plots show a progressive decrease in characteristic energy for all activation temperatures, showing that the pore radius increased with increased activation. At similar sample burn-offs below 30 %, the E_o values decreased in the following order

for activation temperatures : 800 > 775 > 750 °C. This means that for a given burn-off the samples prepared at the higher activation temperatures have pores of smaller radii than the samples produced at the lower temperatures. It appears that steam activation of the BROM chars at higher temperatures produces smaller pores in the early stages of activation than activation at lower temperatures. For a given burn-off above 30 % the E_o values for the various activation temperatures showed little variance from each other, indicating that the pores in the samples produced at each of the different temperatures have similar radii. This is in contrast to the E_o values produced by the CO_2 activation of the same chars, which, at constant burn-off, showed a progressive shift to lower E_o values (and thus larger pore diameters; cf. Figure 5.9 page 90).

5.5.5. Comparison between CO_2 and steam activation of BROM chars

The pore structure of the carbons prepared from the BROM chars by CO_2 and steam activation is influenced by the activation method and temperature. This is more clearly illustrated in Figures 5.12 and 5.13. Figure 5.12 on page 97 shows the development of microporosity in the carbons; for lower burn-off values steam activation produced a higher micropore surface area, but for burn-off values between 25 - 40 % the microporosity values were similar for both activating agents. At 45 % burn-off CO_2 activation produced a marginally higher degree of microporosity.

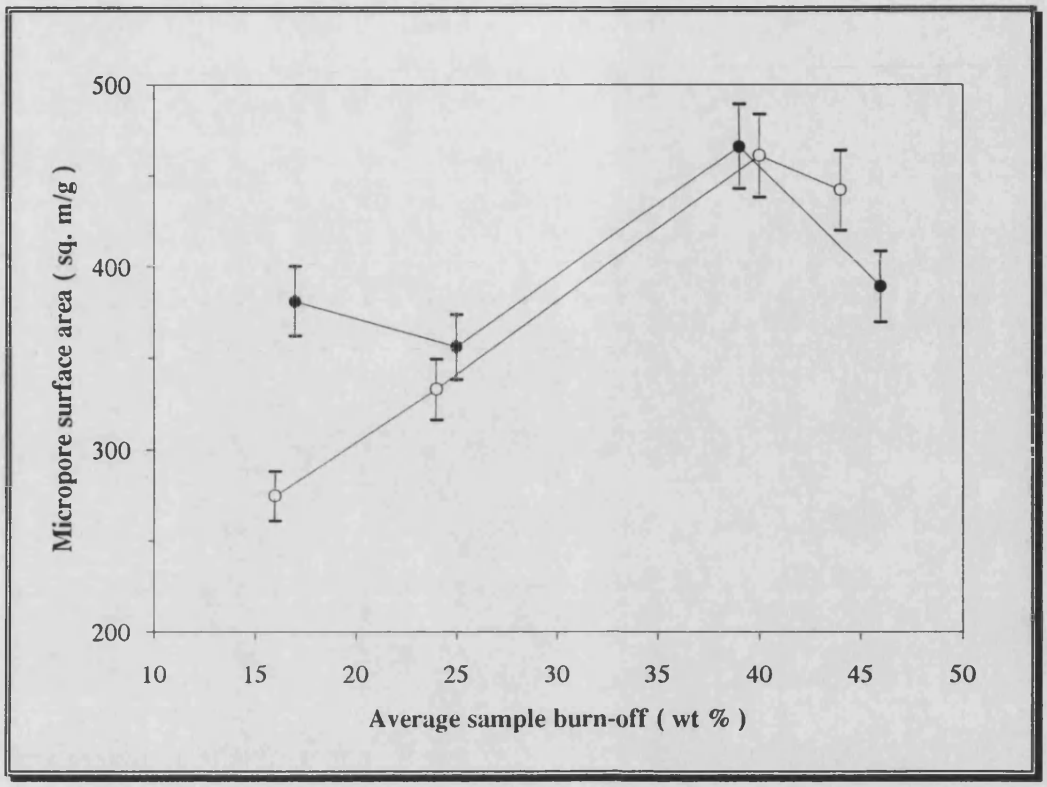

Figure 5.12 : Development of micropore surface area in BROM activated carbons.
(o CO_2 activation • Steam activation)

Figure 5.13 shows the development of mesopore surface area S'_{BET} for different burn-off values; higher mesopore surface areas are obtained when using steam as the activating agent. The difference is especially pronounced at 45 % burn-off; however the higher S'_{BET} value is created at the expense of micropore surface area due to the burn-out of these pores. Finally, for burn-off values lower than 40 % in BROM carbons, steam activation will produce the maximum values of both meso - and microporosity.

The highest S_{BET} value of 520 m^2/g was obtained from steam activation at 775 °C. When allowing for the experimental variance for the BET equation of 5 %, this value is similar to the maximum S_{BET} of 480 m^2/g obtained for the CO_2 activated

carbons. Thus it would seem that the maximum surface area that can be produced from BROM chars for both activating agents at the conditions studied is in the range of 480 - 520 m^2/g.

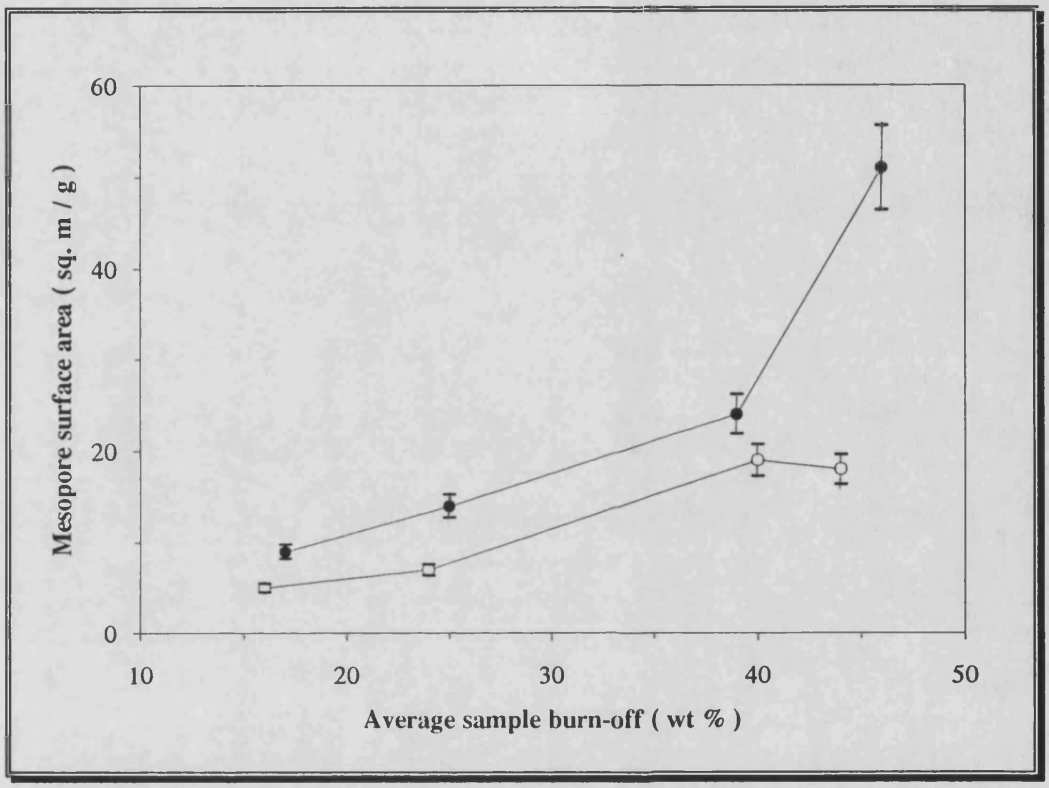

Figure 5.13 : Development of mesopore surface area in BROM activated carbons.
(o CO_2 activation ● Steam activation)

The maximum values of surface area and micropore volume may be associated with the development of high ash content. The ash contents of the activated carbons increased progressively with burn-off, reaching a maximum value of 56 % as is shown in Table 5.2. Possibly with the growth of an ash layer on the external surface of the carbon granules there is a transition from internal development of pores to burn-off from the external surface of the carbon particle. This is reflected in the results for samples A6 and A8, (Table 5.2, page 88) where higher burn-off of sample A8 developed some mesoporosity, but no additional micropore surface area.

Similarly, higher burn-off of sample A7 produced little surface area when compared to sample A8. The growth of this ash layer may be analogous to the shrinking core model for combustion of char particles. [Loison *et al.* 1989]

5.5.6. Influence of acid washing on BROM activated carbons

The samples with the highest surface area was subjected to a mild acid wash (see section 3.3.1) to remove some of the ash in the activated product. The results are given in Table 5.6, page 100, with the acid washed samples identified by the -HCL suffix in the sample number. Assuming that the ash content of the carbon makes a negligible contribution to S_{BET} , the value of S_{BET} was corrected for ash content to give the theoretical maximum surface area S_{MAX} that can be obtained if the sample had no ash content. S_{MAX} is obtained from the simple formula $S_{MAX} = S_{BET} / (1 - 0.01x)$ where x is the ash content (wt %) of the sample. These values are included in Table 5.6.

From Table 5.6 it can be seen that the acid washing proved to be very successful in reducing the ash content and increasing the porosity of the activated carbons. In sample A46 the ash content of the carbons was reduced by 58 % while the surface area increased by 54 %. These results show that the ash accumulates in the meso - and micropores and can be removed by the acid wash. This allows access to especially the micropores with a subsequent widening of the pores, shown by the decrease of the characteristic energy values. Analysis using the α_s - method showed that the ash content reduction produced similar proportional increases in both microporosity and mesoporosity in samples A25HCl and to a lesser degree in sample A46HCl (Table 5.6). This suggests that the mineral matter in these carbons blocked access to the micropores and mesopores to similar extents. In the other samples the

mesoporosity benefited the most from the acid wash, with sample A52HCl showing the biggest gain in mesoporosity.

Table 5.6 : Influence of acid washing on BROM activated carbons.

Sample no.	Ash in product	Parameters from N_2 adsorption					Parameters from mercury porosimetry	
		BET surface area, S_{BET} m^2/g	BET surface area ash free, S_{MAX} m^2/g	Micro-pore volume, V_o cm^3/g	Mesopore surface area S'_{BET} m^2/g	Charac-teristic energy E_o kJ/mol	Macropore volume, V_{macro} cm^3/g	Mesopore volume V_{meso} cm^3/g
	%							
A52	34	370	550	0.13	6	15.0	0.23	0.01
A52HCl	20	460	570	0.17	11	10.0	0.13	0.03
% Difference	*- 41*	*+ 25*		*+ 31*	*+ 83*	*- 33*	*- 43*	*+ 200*
A25	32	480	710	0.17	18	10.0	0.44	0.04
A25HCl	23	620	800	0.23	24	7.9	0.36	0.06
% Difference	*- 28*	*+ 29*		*+ 35*	*+ 33*	*- 21*	*- 18*	*+ 50*
A47	44	460	820	0.17	16	10.4	0.44	0.06
A47HCl	27	660	900	0.25	28	7.7	0.28	0.05
% Difference	*- 39*	*+ 42*		*+ 47*	*+ 75*	*- 26*	*- 36*	*- 17*
A46	43	460	810	0.17	18	8.9	0.02	0.47
A46HCl	18	710	860	0.25	39	8.8	0.04	0.73
% Difference	*- 58*	*+ 54*		*+ 47*	*+ 61*	*- 1*	*+ 100*	*+55*
A57	46	520	970	0.20	40	8.1	0.07	0.48
A57HCl	28	760	1040	0.30	59	5.8	0.11	0.25
% Difference	*- 39*	*+ 45*		*+ 50*	*+ 48*	*- 28*	*+ 57*	*- 48*

Sample A25, A46, A47 and A52 prepared by CO_2 activation
Sample A57 prepared by steam activation

Some of the activated carbons showed a decrease in macropore volume, this may be due to the collapsing of the macropore network when the ash is removed during the acid wash. However, the collapsing of the macropores did not influence the meso-

and microporosity, since an increase in both types of porosity were observed. Although sample A46 and A47 showed similar ash contents, the ash in sample A46 was more readily removed. Since sample A46 showed the highest burn-off of 56 %, most of this ash may be in the outer boundaries of the carbon. This confirms the model proposed earlier for an ash layer forming on the surface of the carbon at high burn-off values.

The higher surface areas of the samples due to acid washing approached the corresponding S_{MAX} value calculated in Table 5.6. The surface area of 710 m^2/g found for sample A46HCl was only 22 % less than the S_{MAX} value of 860 m^2/g. The discrepancy between the values of S_{MAX} and S_{BET} may be due to the inherent mineral matter content of the carbon.

5.5.7. Summary of the activation results for BROM chars

The main findings for the activation of the BROM chars are summarized below :

⌘ The maximum BET surface area that can be obtained from either steam or CO_2 activation is in the range 480 - 520 m^2/g, with a maximum micropore volume in the range 0.17 - 0.19 cm^3/g.

⌘ The carbons are predominantly microporous with the mesopores constituting less than 10 % of the total surface area.

⌘ For burn-off values less than 40 %, steam activation will produce the maximum values of both meso- and microporosity. For burn-off values higher than 40 %, CO_2 activation will produce predominantly microporous carbons, while steam activation will produce higher mesoporosity by burn-out of micropores.

⌘ The carbons show a high ash content, varying in the range 30 - 60 %. The ash is concentrated in the macro- and mesopores and blocks access to the micropores.

⌘ Some of the ash can be successfully removed by washing the carbons with a 0.5M HCl solution, leading to big increases in both meso- and microporosity, and an increase in micropore width.

5.6. Activation of Bosjesspruit column cleaned (BCC) chars

5.6.1. CO_2 activation

Figure 5.14 shows the development of surface area *vs* burn-off for the CO_2 activation of the BCC chars.

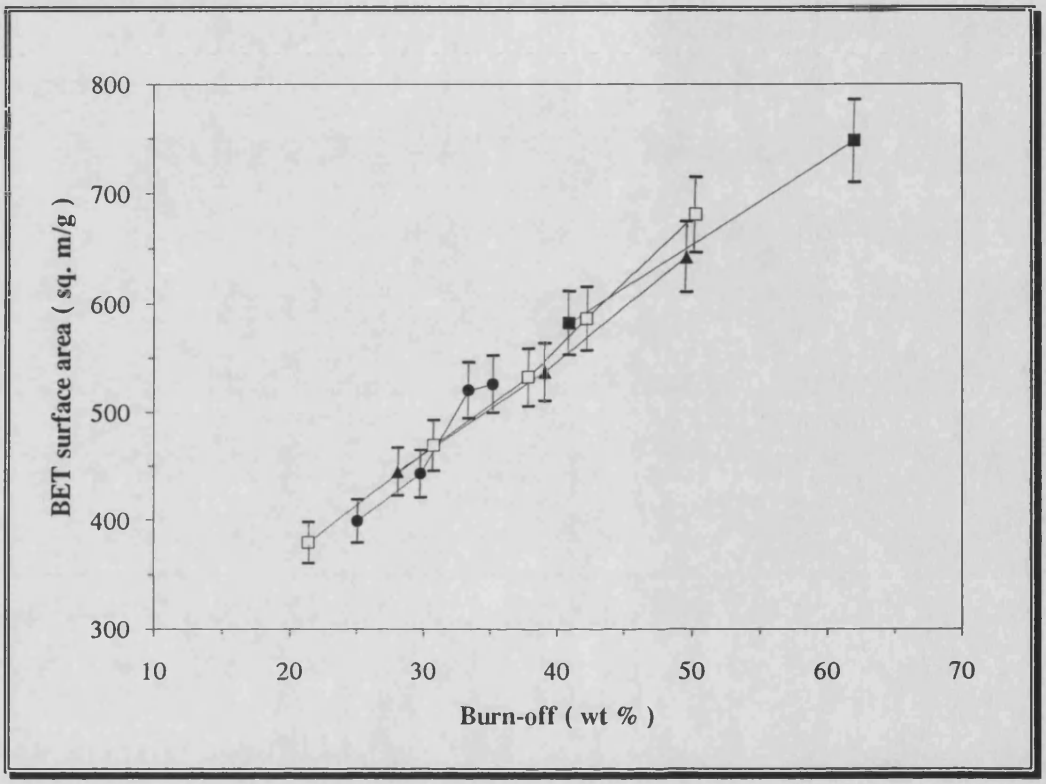

Figure 5.14 : Development of BET surface area for the CO_2 activation of BCC chars.

(Activation temperatures : ● 850 °C □ 875 °C ▲ 900 °C ■ 950 °C)

The porosity values calculated from the N_2 adsorption data are given in Table 5.7, page 104. The most obvious difference between the graphs of surface area *vs* burn-off for the BROM activated carbons in Figure 5.8, page 86, and the BCC carbons shown above is that the surface area in the BCC chars is little affected by the activation temperature. The activation process reached a plateau for 4 h activation time at 850 °C; a longer activation time produced little additional porosity while

little additional sample burn-off was obtained. Little variance in surface area was obtained for burn-off values up to 50 % at 875, 900 and 950 °C activation temperatures (Figure 5.14). Assuming that the activation temperature has a negligible influence on the development of surface area, a relationship between S_{BET} and burn-off x can be represented by a linear equation :

$$S_{BET} = 175.5 + 9.6\,x$$

(CO_2 activation of BCC chars, activation temperature in the range 850 - 950 °C)

Table 5.7 : Pore structure analysis from N_2 adsorption data for CO_2 activated BCC carbons.

Sample no.	Activation conditions								
	Temp °C	Time h	Burn-off %	BET N_2 surface area, S_{BET} m^2/g	Notional micropore surface area, S_{micro} m^2/g	Micropore volume, V_o cm^3/g	Mesopore surface area, S'_{BET} m^2/g	Charac-teristic energy E_o kJ/mol	Ash %
A48	850	2	25	400	393	0.15	7	15.1	19
A45		3	30	440	433	0.16	7	14.8	20
A49		4	33	520	510	0.19	10	14.3	22
A50		5	35	530	520	0.19	10	14.3	22
A37	875	1	21	380	373	0.14	7	15.1	19
A41		2	31	470	458	0.17	12	13.5	21
A35		3	38	530	513	0.19	17	12.5	24
A36		4	42	590	572	0.21	18	11.6	25
A42		5	50	680	662	0.25	18	11.3	27
A40	900	1	28	450	438	0.16	12	11.7	20
A39		2	39	540	521	0.19	19	10.4	23
A38		3	50	640	616	0.23	24	10.0	30
A43	950	1	41	580	554	0.21	26	8.8	24
A44		2	62	750	713	0.26	37	8.2	36

A maximum surface area of 680 m^2/g was obtained at 50 % burn-off for 5 h activation at 875 °C; this carbon had an ash content of 27 % (sample A42). BROM carbons prepared under similar conditions had lower surface areas and higher ash contents. The removal of the mineral matter from the coal precursor by column cleaning thus helped to produce better activated carbons. The development of mesopore surface area reached a plateau after 38 % burn-off, but the microporosity increased to reach a value of 0.25 cm^3/g at 50 % burn-off. Although the maximum S_{BET} at 900 °C (sample A38) was slightly lower than the S_{BET} at 875 °C (sample A42), this value is still within the error allowed for the BET equation, and the two S_{BET} values can thus be assumed to be similar. Sample A38 showed a lower degree of microporosity, but higher mesopore surface area. The higher S'_{BET} is thus created by the enlarging of existing micropores. The reaction at 950 °C (sample A43) produced a carbon with a 40 % burn-off within 1 h activation time. Although this sample had similar microporosity to the samples prepared with similar burn-offs at the lower temperatures (samples A36 and A39), sample A43 showed higher mesopore surface area than the other samples. Activation at higher temperatures can thus be used to produce higher mesoporous carbons.

The macro- and mesoporosity parameters from mercury porosimetry data are given in Table 5.8, page 106. The values for mesopore surface area were in excellent agreement with the corresponding values obtained from the α_s - method using the N_2 data. Although the macropore surface area was slightly higher than the values obtained for the BROM carbons, it was still negligible when compared to the total S_{BET} . Except for sample A50, all samples showed progressive increases in macropore volume with increased activation due to the enlargement of the pore system by burn-out of existing pores. The values are much higher for the BCC

carbons, showing that the mineral matter in the BROM carbons prohibited the formation of excessive macroporosity.

Table 5.8 : Pore structure analysis from mercury porosimetry data for CO_2 activated BCC carbons.

Sample no.	Activation conditions		Mercury porosimetry data (50 kpsig max)				N_2 data
	Temp °C	Time h	Macropore volume V_{macro} cm^3/g	Mesopore volume V_{meso} cm^3/g	Macropore surface area S_{macro} m^2/g	Mesopore surface area S'_{BET} m^2/g	Mesopore surface area S'_{BET} m^2/g
A48	850	2	0.72	0.02	2	10	7
A45		3	0.71	0.02	2	10	7
A49		4	0.76	0.03	2	13	10
A50		5	0.65	0.05	2	13	10
A37	875	1	0.71	0.02	2	9	7
A41		2	0.72	0.02	2	13	12
A35		3	0.79	0.02	2	15	17
A36		4	0.81	0.03	2	16	18
A42		5	0.87	0.05	3	23	18
A40	900	1	0.73	0.02	2	11	12
A39		2	0.77	0.04	2	17	19
A38		3	0.91	0.04	3	22	24
A43	950	1	0.80	0.06	2	33	26
A44		2	0.99	0.11	4	40	37

5.6.2. Characteristic energy of CO_2 activated BCC carbons

The characteristic energy values for the CO_2 - activated BCC carbons are shown in Figure 5.15. The plots were similar to those obtained for the CO_2 activation of the BROM chars, showing a progressive decrease in E_o values for an increase in burn-off. The diameter of the pores developed during the activation process is clearly

dependent on the activation temperature, with higher temperatures leading to larger pores for a given burn-off.

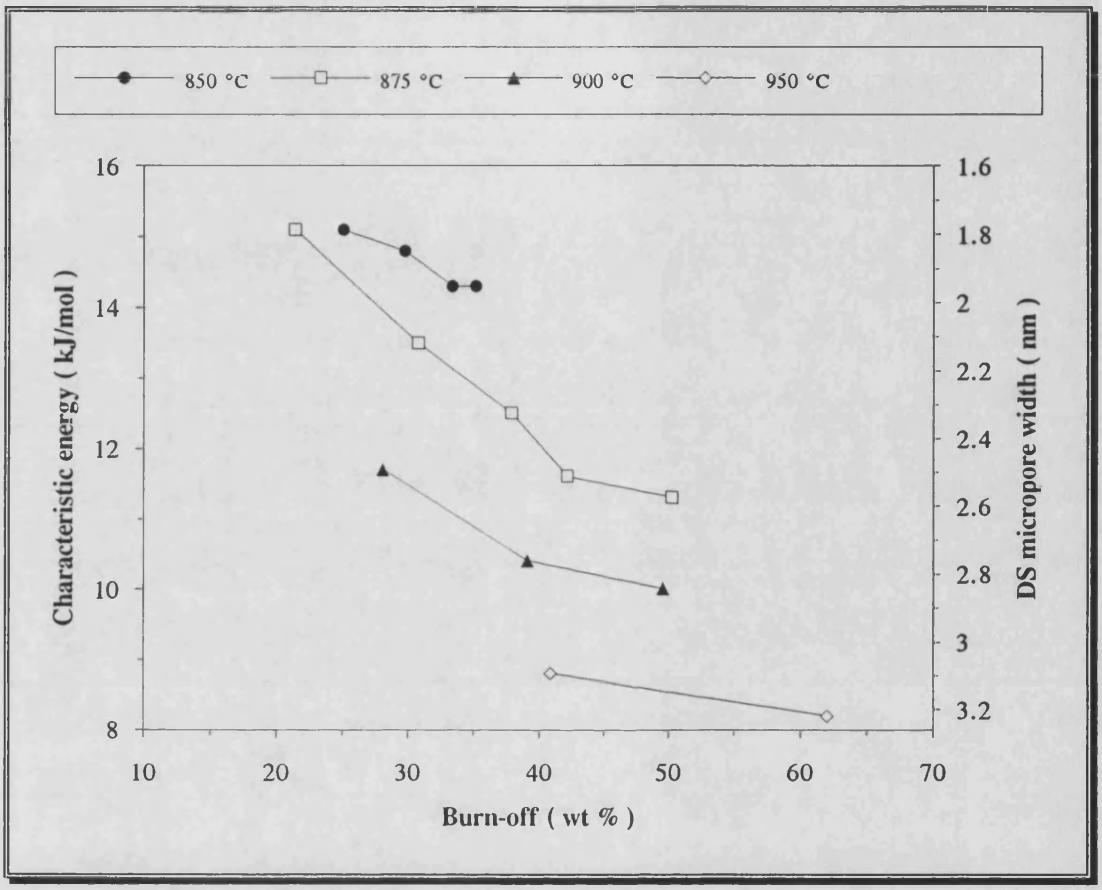

Figure 5.15 : Characteristic energy plots for CO_2 activated BCC carbons.

In comparing the E_o values of the CO_2 activated BROM and BCC carbons, it was found that the BCC carbons gave consistently higher E_o values for a given burn-off, showing that the pores for the BCC samples were smaller than those produced for the BROM carbons under the same experimental conditions. Thus the reduced mineral matter contents of the BCC coal precursor not only produced carbons with a higher surface area, but the pore dimensions in these carbons were found to be smaller than for the carbons produced from the run-of-mine coal.

5.6.3. Steam activation of BCC carbons

Figure 5.16 shows the development of surface area for different extents of burn-off for the steam activation of the BCC carbons. The surface area of the carbons were little affected by the changes in the activation temperatures chosen for activation, similar to the results found for the carbons activated by CO_2. A maximum S_{BET} of 600 m^2/g was obtained at 800 °C (sample A71); this occurred at a sample burn-off of ~ 44 %, as shown in Figure 5.16. This value is similar to the maximum S_{BET} of 580 m^2/g obtained for sample A69, which suggests that this is the maximum surface area that can be obtained under the conditions investigated. Additional porosity values are given in Table 5.9, page 109.

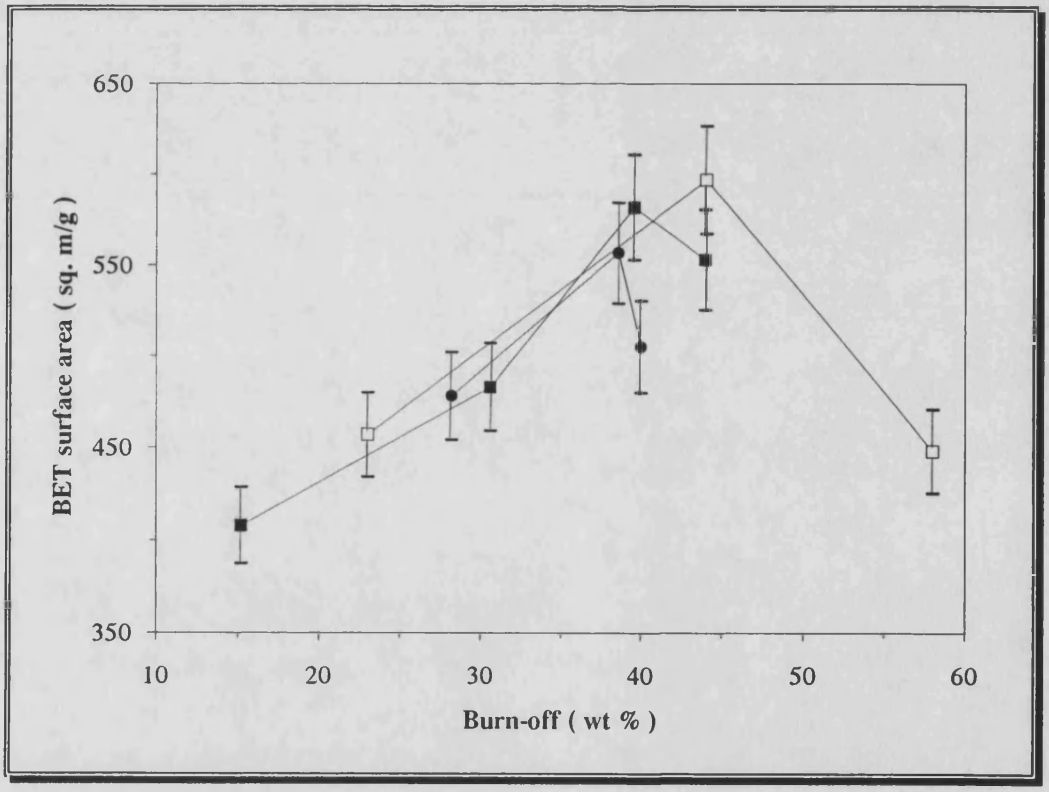

Figure 5.16 : Development of BET surface area for steam activated BCC carbons.
(Activation temperatures : ● 750 °C ■ 775 °C □ 800 °C)

Table 5.9 : Pore structure analysis for steam activated BCC carbons from N_2 adsorption data.

Sample no.	Activation conditions								
	Temp °C	Time h	Burn-off %	BET N_2 surface area, S_{BET} m^2/g	Notional micropore surface area, S_{micro} m^2/g	Micropore volume, V_o cm^3/g	Mesopore surface area, S'_{BET} m^2/g	Energy E_o kJ/mol	Ash %
A64	750	2	28	480	472	0.18	8	13.8	19
A65		4	39	560	546	0.22	14	9.4	22
A66		5	40	500	486	0.20	14	8.8	22
A67	775	1	15	410	402	0.15	8	13.7	19
A68		2	31	480	468	0.18	12	11.6	19
A69		3	40	580	557	0.23	23	8.0	24
A34		4	44	550	507	0.21	43	6.3	49
A70	800	1	23	460	449	0.17	11	10.3	20
A71		2	44	600	581	0.23	19	8.7	23
A58		3	58	450	439	0.17	11	10.8	39

The development of micropore volume followed the trend of S_{BET} and reached a maximum value of 0.23 cm^3/g. This value was obtained at activation temperatures of both 775 and 800 °C, and supports the observation that the surface area reaches a maximum value at 40 - 45 % burn-off. The ash contents of the carbons increased progressively with burn-off, Table 5.9. The ash contents for the carbons up to 40 % burn-off varies between 19 - 24 %, which is similar to the values obtained for the BCC carbons. The decrease in surface area of sample A34 can be attributed to the high ash content of 49 %, which shows that the reaction at these conditions leads to excessive activation of the char.

The development of mesoporosity reached a plateau at 750 °C, but increased progressively at 775 °C. For sample A34 a higher mesopore surface area was developed at the expense of microporosity, since the micropore surface area decreased in this sample. Sample A58, produced at 800 °C for 3 h activation time showed a decrease in mesopore surface area, which may be due to the collapsing of the pore structure due to excessive activation conditions.

The mercury intrusion data for the steam activated BCC chars is given in Table 5.10.

Table 5.10 : Pore structure analysis from mercury porosimetry data for steam activated BCC carbons.

Sample no.	Activation conditions		Mercury porosimetry data (50 kpsig max)				40 kpsig	N_2 data
	Temp °C	Time h	Macropore volume V_{macro} cm^3/g	Mesopore volume V_{meso} cm^3/g	Macropore surface area S_{macro} m^2/g	Mesopore surface area S'_{BET} m^2/g	Mesopore surface area S'_{BET} m^2/g	Mesopore surface area S'_{BET} m^2/g
A64	750	3	0.70	0.03	2	18	10	8
A65		4	0.78	0.04	3	25	16	14
A66		5	0.76	0.05	3	27	18	14
A67	775	1	0.70	0.02	2	12	8	8
A68		2	0.68	0.02	2	13	9	12
A69		3	0.80	0.04	3	28	18	23
A34		4	0.42	0.11	2	52	38	43
A70	800	1	0.70	0.02	2	16	10	11
A71		2	0.77	0.03	3	23	15	19
A58		3	0.32	0.04	1	19	14	11

Porosimetry at 50 kpsig overestimated the mesopore surface area when compared to the surface area obtained from N_2 data, probably due to damage to the carbon structure by the intrusion of mercury into the pores. A better agreement was found

when the values were recalculated at 40 kpsig. This shows that the pore structure in the steam activated BCC carbons is more fragile than the CO_2 activated carbons, since a very good agreement was found for the porosimetry and N_2 data at 50 kpsig for the CO_2 activated carbons.

The mesopore volumes also showed an increase with burn-off, reaching a value of 0.11 cm^3/g for sample A34, activated at 775 °C for 4 h. The porosimetry results shows that high degrees of meso- and macro-porosity were obtained before pore structure collapsed. Similar results were observed for sample A58.

The macropore volumes of the samples were in the same range as those obtained for the CO_2 activation of the chars, reaching a maximum value of 0.80 cm^3/g for sample A69. The degree of macro - and meso-porosity in sample A71 however is lower than for sample A69, even though sample A71 was produced at a higher activation temperature; this may be due to the shorter residence time in the furnace of sample A71. The macropore surface areas of all the samples were similar to the values obtained for the CO_2 activation of the chars, and these are negligible when compared to the total S_{BET}.

5.6.4. Characteristic energy of the steam activated BCC carbons

The characteristic energy values for the steam activated BCC carbons are given in Figure 5.17, page 112. The plots show the characteristic trend observed for the CO_2 activated chars, i.e. a progressive decrease in E_o with an increase in activation temperature, showing the formation of pores with larger diameters. The plots differ from those found for the BROM steam-activated carbons (Figure 5.11, page 95) in that the plots are not insensitive to activation temperature. This supports the view that for the BROM carbons the formation of a high ash content inhibits the activation process at higher temperatures.

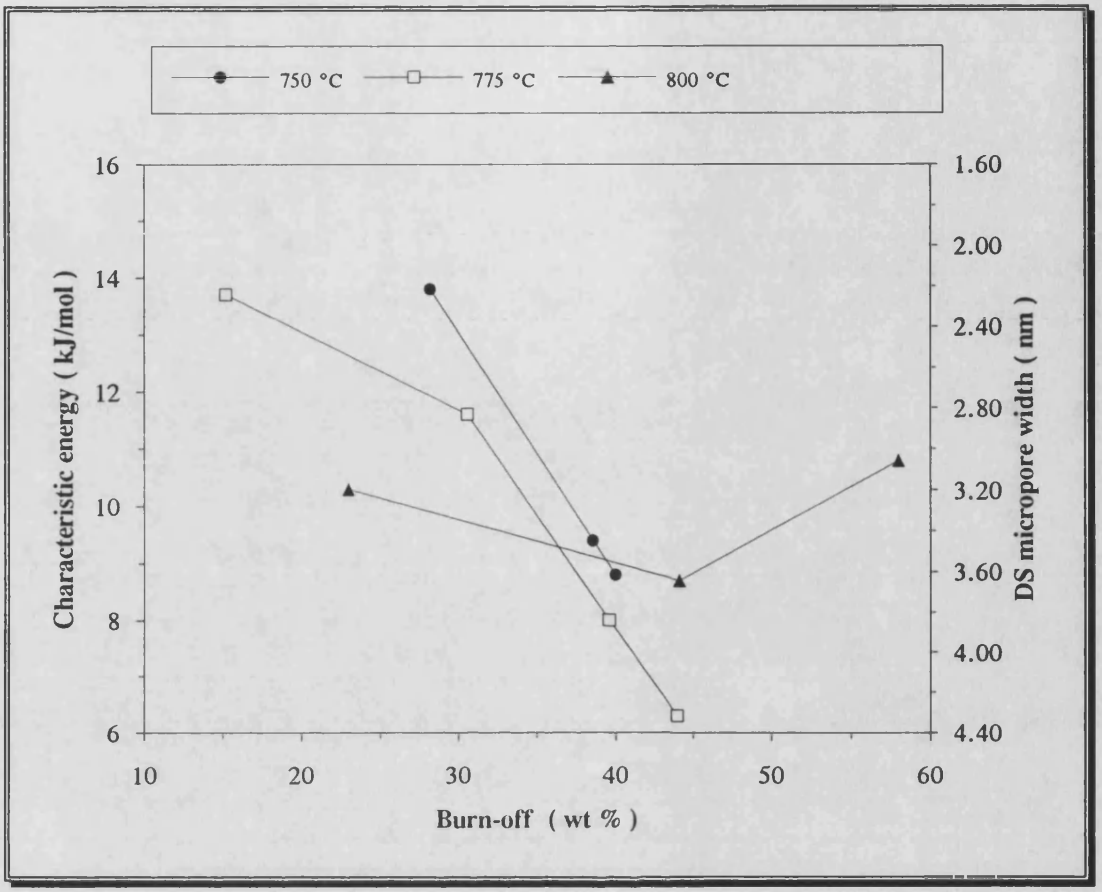

Figure 5.17 : Characteristic energy plots for steam activated BCC carbons.

The E_o values found at 800 °C shows that there is a decrease in pore diameter for sample burn-offs larger than 40 %. This is probably due to a partial collapsing of the pores at this high activation temperature, which was facilitated by the removal of the ash from the precursor since this trend was not observed for the BROM steam activated carbons.

5.6.5. Comparison between CO_2 and steam activation of BCC chars

The porosity values of the different BCC carbons, prepared by the two activation methods, are compared for similar burn-off values in Figures 5.18 and 5.19.

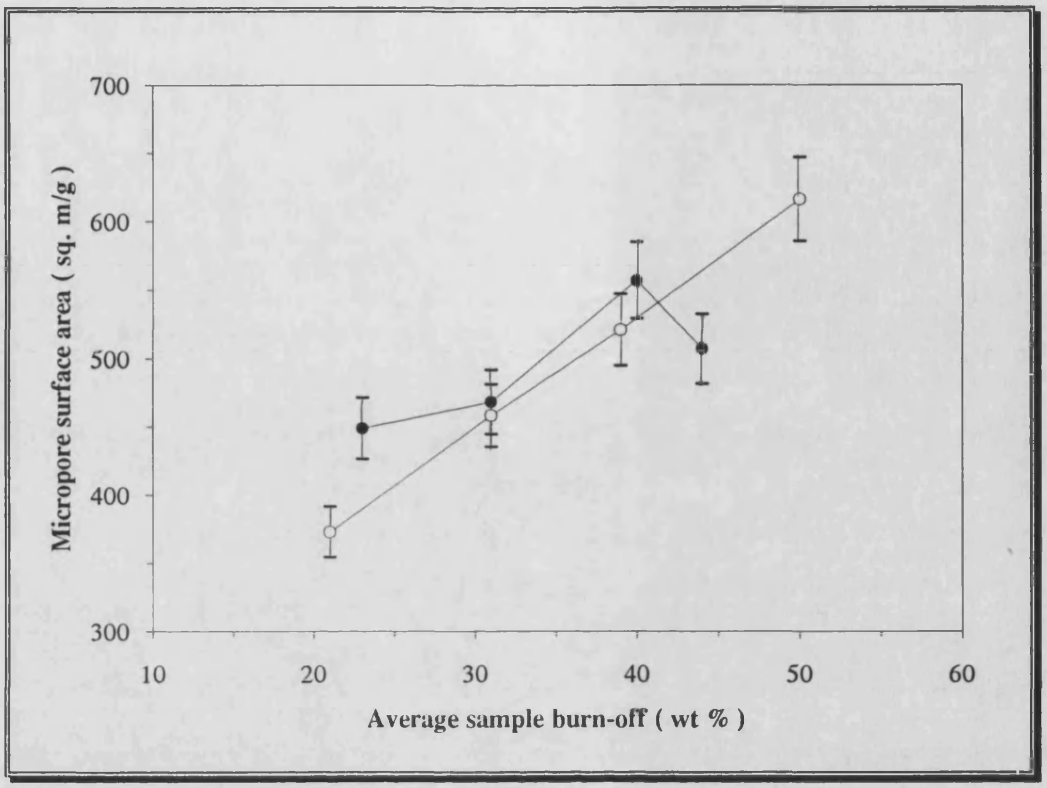

Figure 5.18 : Development of micropore surface area in BCC activated carbons (o CO_2 activation • Steam activation)

In Figure 5.18 the microporosity of the carbons are compared for burn-off values ranging from 20 - 50 %. The CO_2 - activated carbons showed an increase in micropore surface area through a range of burn-offs up to ~ 50 %, reaching a maximum value of 660 m^2/g. (sample A42). The surface area for the steam activated carbons showed a similar increase in surface area with burn-offs up to 40 %, developing marginal higher micropore surface areas than the carbons prepared by CO_2 activation. For an average burn-off value higher than ~ 40 %, the CO_2 - activated carbons gave higher surface areas than the steam-activated carbons.

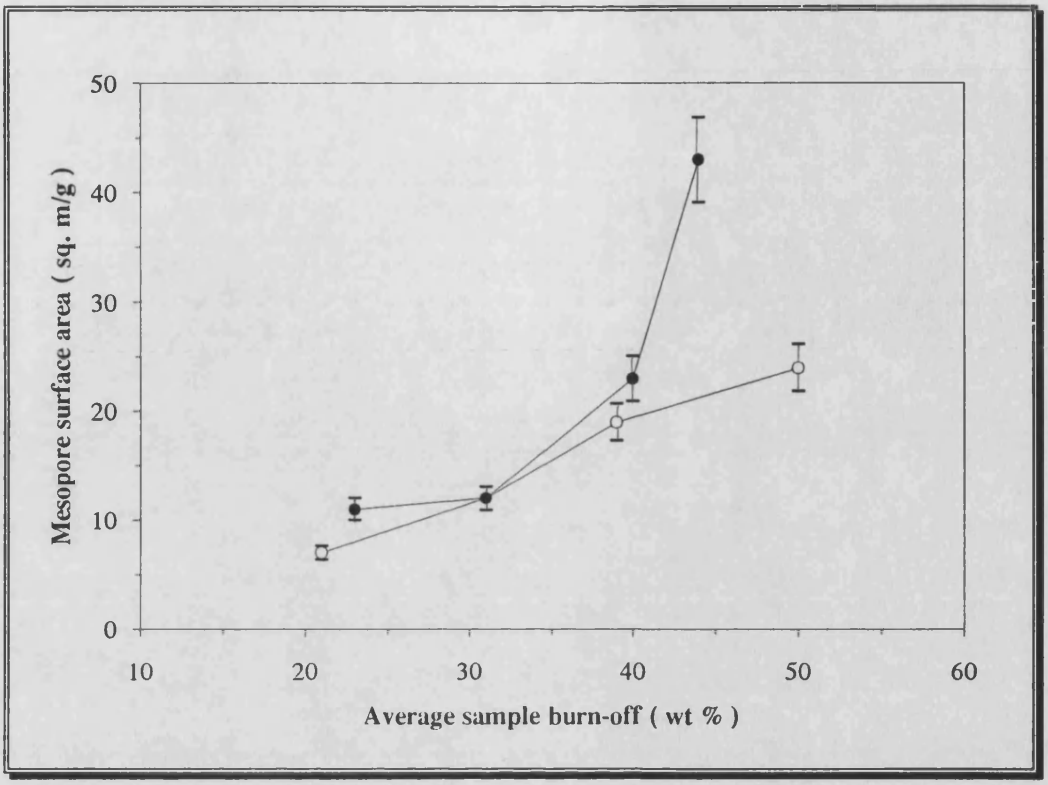

Figure 5.19 : Development of mesopore surface area in BCC activated carbons
(o CO_2 activation • Steam activation)

Figure 5.19 shows that steam activation can be used successfully to produce a higher degree of mesoporosity in the samples. The development of mesoporosity for high sample burn-off (> 40 %) occurs mainly by enlarging existing micropores, and not by the development of new pores, as the micropore surface area for the sample decreased with increases in S'_{BET}. Similar trends were found for the BROM activated carbons, showing that steam activation will produce carbons with substantial mesopore and micropore surface areas. Predominantly microporous carbons can be synthesized by CO_2 activation for sample burn-offs higher than 40 %.

5.6.6. Influence of acid washing on BCC activated carbons

The porosity values for the BCC samples subjected to the mild HCl-wash before and after the acid washing are compared in Table 5.11.

Table 5.11 : Influence of acid washing on BCC activated carbons.

Sample no.	Ash in carbon	Parameters from N_2 adsorption						Parameters from Hg porosimetry	
		BET surface area	BET surface area ash free	Micro-pore surface area	Meso-pore surface area	Micro-pore volume	Charac-teristic energy	Macro-pore volume	Meso-pore volume
	%	S_{BET} m^2/g	S_{MAX} m^2/g	S_{micro} m^2/g	S'_{BET} m^2/g	V_0 cm^3/g	E_0 kJ/mol	V_{macro} cm^3/g	V_{meso} cm^3/g
A50	22	530	670	520	10	0.19	14.3	0.65	0.05
A50HCl	14	630	710	612	18	0.24	10.5	0.72	0.04
% Difference	*- 36*	*+ 19*		*+ 18*	*+ 80*	*+ 26*	*- 27*	*+ 11*	*- 20*
A42	27	680	930	662	18	0.25	11.3	0.87	0.05
A42HCl	15	720	850	696	24	0.26	10.4	0.80	0.05
% Difference	*- 44*	*+ 6*		*+ 5*	*+ 33*	*+ 4*	*- 8*	*- 8*	*0*
A65	22	560	710	546	14	0.22	8.8	0.78	0.04
A65HCl	13	390	450	375	15	0.15	8.3	0.21	0.02
% Difference	*- 41*	*- 29*		*- 27*	*+ 7*	*- 32*	*- 6*	*- 63*	*- 50*
A68	19	480	600	468	12	0.18	11.6	0.68	0.02
A68HCl	12	580	660	560	20	0.22	8.9	0.70	0.04
% Difference	*- 37*	*+ 20*		*+ 18*	*+ 66*	*+ 22*	*- 23*	*+ 3*	*+ 50*
A69	24	580	760	557	23	0.23	8.0	0.80	0.04
A69HCl	12	670	760	638	32	0.26	7.1	0.80	0.07
% Difference	*- 50*	*+ 14*		*+ 13*	*+ 48*	*+ 13*	*- 11*	*0*	*+ 75*
A71	23	600	780	581	19	0.23	8.7	0.77	0.03
A71HCl	12	700	780	661	39	0.27	7.5	0.81	0.07
% Difference	*- 48*	*+ 16*		*+ 13*	*+ 105*	*+ 17*	*- 14*	*+ 5*	*+ 133*

Sample A50, and A42 prepared by CO_2 activation
Sample A65, A68, A69 and A71 prepared by steam activation

The ash contents of the BCC activated carbons (ranging from 20 - 30 %) were lower than the ash contents for the BROM carbons with the highest surface areas (ranging from 30 - 50 %). It is therefore to be expected that the BCC carbons after the acid washing will yield final products with lower ash contents than the results found for the BROM carbons. It is interesting to note that the final ash content of all the BCC carbons after the acid washing was in the range of 12 - 15 %. The ash content of the final product is also independent of the activation conditions and method. This suggests that the ash value in the final product is inherent to the carbon structure and is the minimum value to be expected for the BCC carbons.

Although high percentages of ash removal were obtained with the acid wash, most of the samples showed only a small increase in microporous surface area, with the highest S_{BET} of 720 m^2/g for sample A42HCl. A comparison of the N_2 and porosimetry data shows that most of the ash was concentrated in the mesopores, with sample A71HCl doubling its mesopore surface area after acid washing, while showing only a 16 % increase in S_{BET}. The macropore volumes V_{macro} of the samples showed small increases after the ash removal, or in the case of sample A69, no increase at all. This is in contrast to the values found for the BROM carbons in Table 5.6, page 100, which showed either large increases or large decreases in V_{macro}. Thus the ash in the BROM carbons was concentrated in the macropores and mesopores, while in the BCC carbons, the ash was concentrated predominantly in the mesopore range. This shows that the column cleaning process mainly removes mineral matter in the macropore size range.

5.6.7. Summary of the activation results for BCC chars

The main findings for the activation of the BCC chars are summarized below :

⌘ The maximum BET surface area that could be produced from the BCC chars for a burn-off less than 50 % was 680 m^2/g, using CO_2 as activating gas. This carbon had a micropore volume of 0.25 cm^3/g.

⌘ Similar to the BROM carbons, the BCC carbons were found to be predominantly microporous with the mesopores constituting less than 10 % of the total surface area.

⌘ For burn-off values less than 40 %, steam activation will produce the maximum values of both meso- and microporosity. For burn-off values higher than 40 %, CO_2 activation will produce predominantly microporous carbons, while steam activation will produce higher mesoporosity by burn-out of existing micropores.

⌘ The BCC carbons showed a lower ash content when compared to the BROM carbons, varying in the range 20 - 30 % for burn-offs less than 50 %. The ash is concentrated mainly in the mesopores of the carbons.

⌘ Some of the ash can be successfully removed by washing the carbons with a 0.5M HCl solution. Although high percentages of ash removal was obtained, little increases in microporosity were found with big gains only in mesoporosity. Single parameter estimates of the micropore width showed that the acid washing also led to a widening of the micropores. There is evidence that all the BCC carbons have an inherent ash content of 12 - 15 %.

5.7. Activation of Waterberg column cleaned (WCC) chars

5.7.1. CO_2 activation of WCC chars

The development of BET surface area for different extents of burn-off for the CO_2 activation of the WCC chars is shown in Figure 5.20.

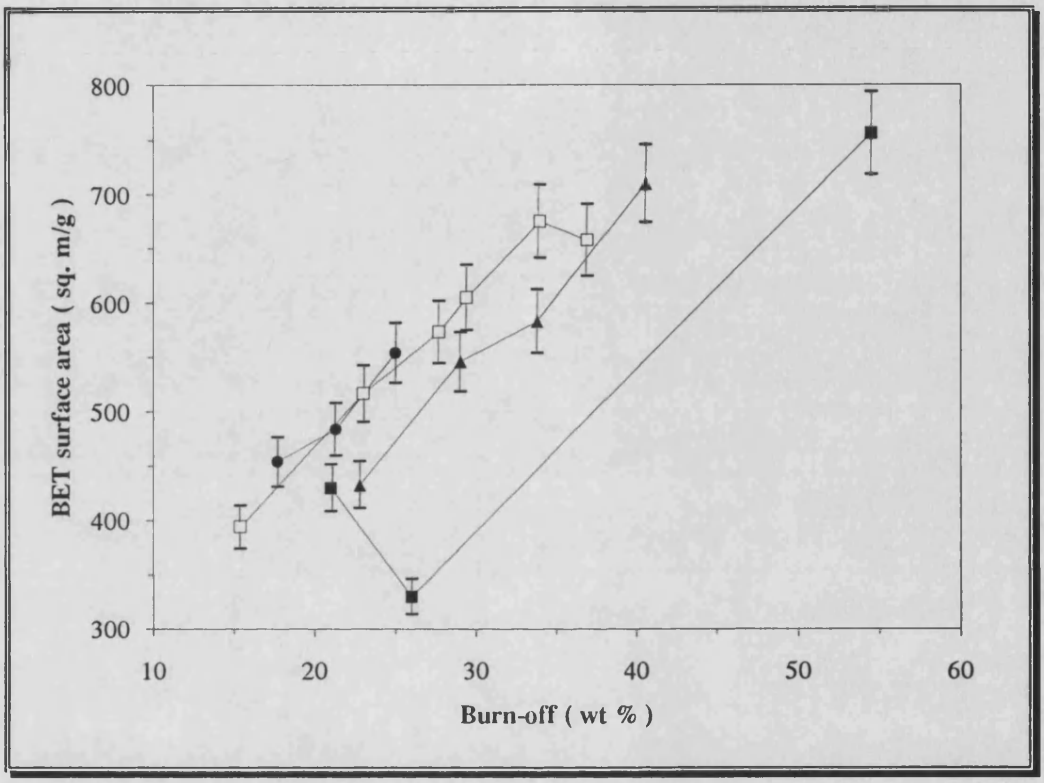

Figure 5.20 : Development of BET surface area for CO_2 activation of WCC chars.
(Activation temperatures : ● 850 °C □ 875 °C ▲ 900 °C ■ 950 °C)

Figure 5.20 shows that surface area in the WCC chars was developed in a narrow range, with a marginal shift to higher surface areas for a given burn-off value when using lower activation temperatures, which suggests that the activation process is more efficient at lower temperatures. The surface areas and pore volumes calculated from the nitrogen data are given in Table 5.12, page 119. The difference between the S_{BET} values for samples A96 and A104 at 875 °C is within the 5 % experimental

variance allowed for the BET equation, showing that the surface areas in these samples are similar. This is also reflected in the similar values obtained for micropore volume and mesopore surface area S'_{BET}. The surface area at 900 °C showed a progressive increase in S_{BET} for burn-offs up to 40 %. Micropore volumes and S'_{BET} also showed an increase with activation reaching values of 0.29 cm^3/g and 30 m^2/g respectively.

Table 5.12 : Pore structure analysis from N_2 adsorption data for CO_2 activated WCC carbons.

Sample no.	Activation conditions		Burn-off	BET N_2 surface area, S_{BET}	Notional micropore surface area, S_{micro}	Micropore volume, V_o	Mesopore surface area, S'_{BET}	Charac-teristic energy E_o	Ash
	Temp °C	Time h	%	m^2/g	m^2/g	cm^3/g	m^2/g	kJ/mol	%
A90	850	2	18	450	446	0.17	4	21.5	21
A91		3	21	480	476	0.18	4	19.9	20
A92		4	25	550	545	0.21	5	18.9	21
A93	875	1	15	390	386	0.15	4	19.6	19
A94		2	23	520	515	0.19	5	18.9	21
A97		3	28	570	564	0.22	6	18.4	22
A95		4	30	600	593	0.23	7	15.3	23
A96		5	37	680	668	0.27	12	10.9	25
A104		6	40	660	649	0.26	11	11.3	23
A99	900	1	23	430	427	0.17	3	17.1	19
A98		2	29	550	544	0.21	6	15.7	21
A100		3	34	580	564	0.23	16	8.8	22
A105		5	41	710	680	0.29	30	7.2	26
A101	950	1	21	430	424	0.16	6	15.4	19
A102		2	28	330	318	0.13	12	9.3	20
A103		4	55	760	622	0.28	140	4.5	30

The development of S_{BET} at 950 °C showed a particularly interesting trend, and the sorption isotherms for samples A101, A102 and A103 are given in Figure 5.21.

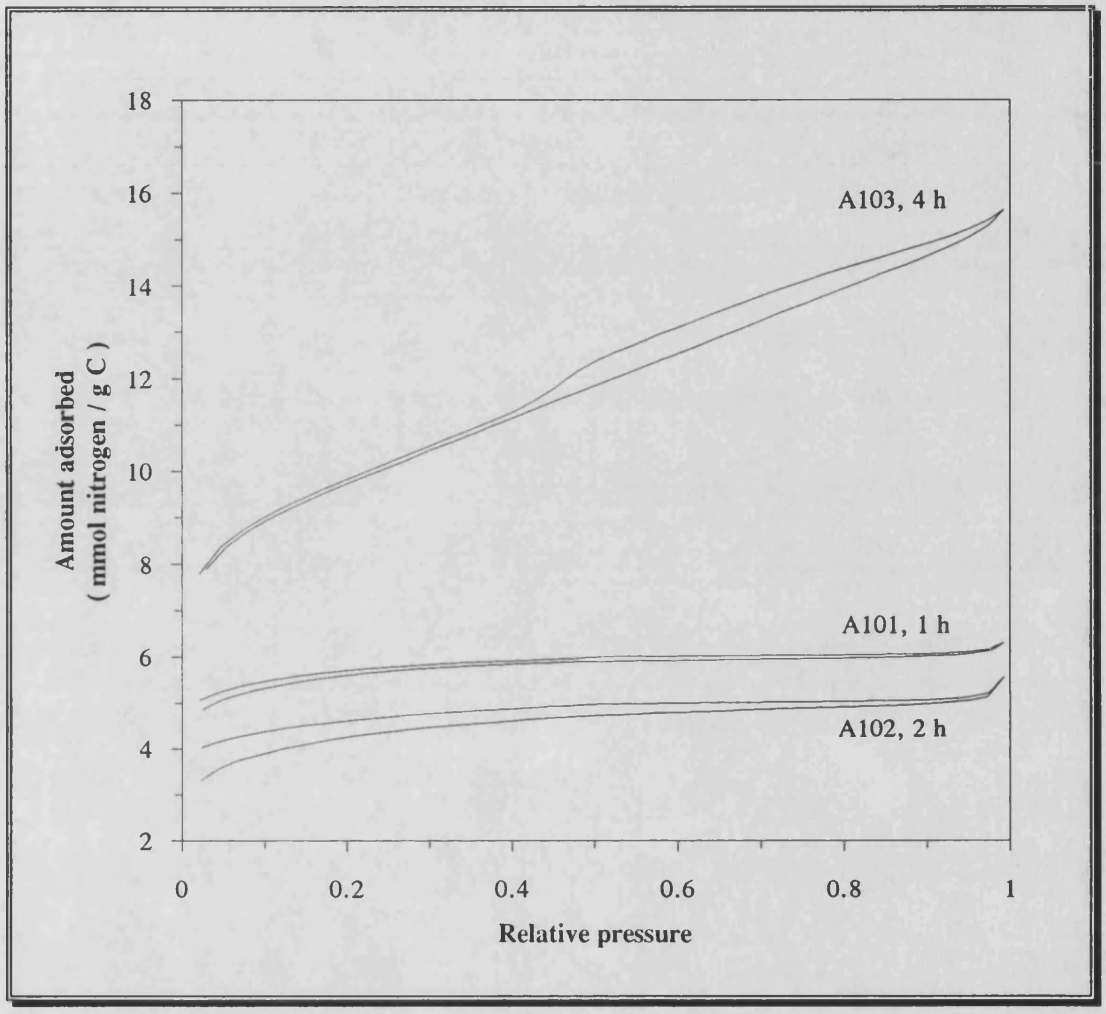

Figure 5.21 : Nitrogen sorption isotherms at 77 K for WCC carbons activated using CO_2 at 950 °C .

Increasing the sample burn-off from 21 to 28 % led to a decrease in S_{BET} from 430 to 330 m^2/g, while showing an increase in S'_{BET} from 6 to 12 m^2/g. The difference between the two S_{BET} values is more than the variance allowed for the BET equation, and thus cannot be ascribed to experimental error. The shape of the adsorption

branch of the isotherms for 1 h and 2 h activation time was similar, but the 2 h isotherm showed a lower uptake of nitrogen, and also exhibited a higher degree of open loop hysteresis at low relative pressures, which is indicative of activated diffusion. This suggests that some of the micropores may have collapsed after the longer activation time. For an activation time of four hours, a sample burn-off of 55 % was obtained, but S'_{BET} had a value of 140 m^2/g calculated by the α_s - method. This value of S'_{BET} is the highest of all the prepared samples and shows that the reaction of CO_2 with the WCC char develops a high degree of mesoporosity in the carbon. The high mesoporosity of the sample is confirmed by the slope of the isotherm, which showed a sharp increase in the higher relative pressure range. The open loop hysteresis at low relative pressures was also reduced in this sample, showing a widening of the micropores and reduced activated diffusion.

The mercury porosimetry results for the CO_2 activated chars are given in Table 5.13, page 121. All samples have small macroporous surface areas, which are negligible when compared to S_{BET}. The macropore volumes of the samples at 900 and 950 °C increased with increasing activation while V_{macro} at the lower temperatures varied between 0.49 and 0.55 cm^3/g. Sample A103, which showed a S'_{BET} value of 140 m^2/g, had a macropore volume of 0.69 cm^3/g. This is comparable to the macropore volume of 0.65 cm^3/g of sample A105, prepared at 900 °C for five hours activation time.

Sample A105, however, only had a S'_{BET} of 30 m^2/g, and since this carbon has a comparable S_{BET} value to sample A103, it shows that the development of mesoporosity in sample A103 is not due to excessive burn-out of micropores, even though the sample had a higher burn-off value. Mercury porosimetry at 50 kpsig overestimated the mesopore surface area of the samples; better agreement was found

at 40 kpsig. This is in contrast to the porosimetry results for the BCC carbons at 50 kpsig, which showed good agreement between the nitrogen and mercury S'_{BET} values.

Table 5.13 : Pore structure analysis from mercury porosimetry data for CO_2 activated WCC carbons.

Sample no.	Activation conditions		Mercury porosimetry data (50 kpsig max)				40 kpsig	N_2 data
	Temp °C	Time h	Macropore volume cm^3/g	Mesopore volume cm^3/g	Macropore surface area m^2/g	Mesopore surface area m^2/g	Mesopore surface area m^2/g	Mesopore surface area m^2/g
A90	850	2	0.55	0.02	1	12	7	4
A91		3	0.51	0.01	1	9	7	4
A92		4	0.50	0.02	2	11	7	5
A93	875	1	0.52	0.01	1	9	6	4
A94		2	0.49	0.02	1	12	8	5
A97		3	0.52	0.03	1	16	12	6
A95		4	0.55	0.04	2	18	12	7
A96		5	0.50	0.05	2	19	14	12
A104		6	0.54	0.04	2	25	16	11
A99	900	1	0.47	0.03	1	12	7	3
A98		2	0.51	0.03	2	18	10	6
A100		3	0.54	0.03	2	21	12	16
A105		5	0.65	0.06	2	38	26	30
A101	950	1	0.41	0.02	1	14	10	6
A102		2	0.53	0.02	2	14	9	12
A103		4	0.69	0.10	2	70	43	138

These results show that the pore structure in the WCC carbons is more fragile than the structure in the BROM or BCC carbons. Porosimetry at 50 kpsig, however, underestimated the S'_{BET} value of sample A103 by 70 m^2/g. Since a pressure of 50 kpsig corresponds to a pore diameter of 5.3 nm, it shows that ~ 50 % of the mesoporosity of sample A103 is in pores having a diameter of less than 5 nm.

5.7.2. Characteristic energy of CO_2 activated WCC carbons

The characteristic energy plots of the CO_2 activated WCC carbons are represented in Figure 5.22.

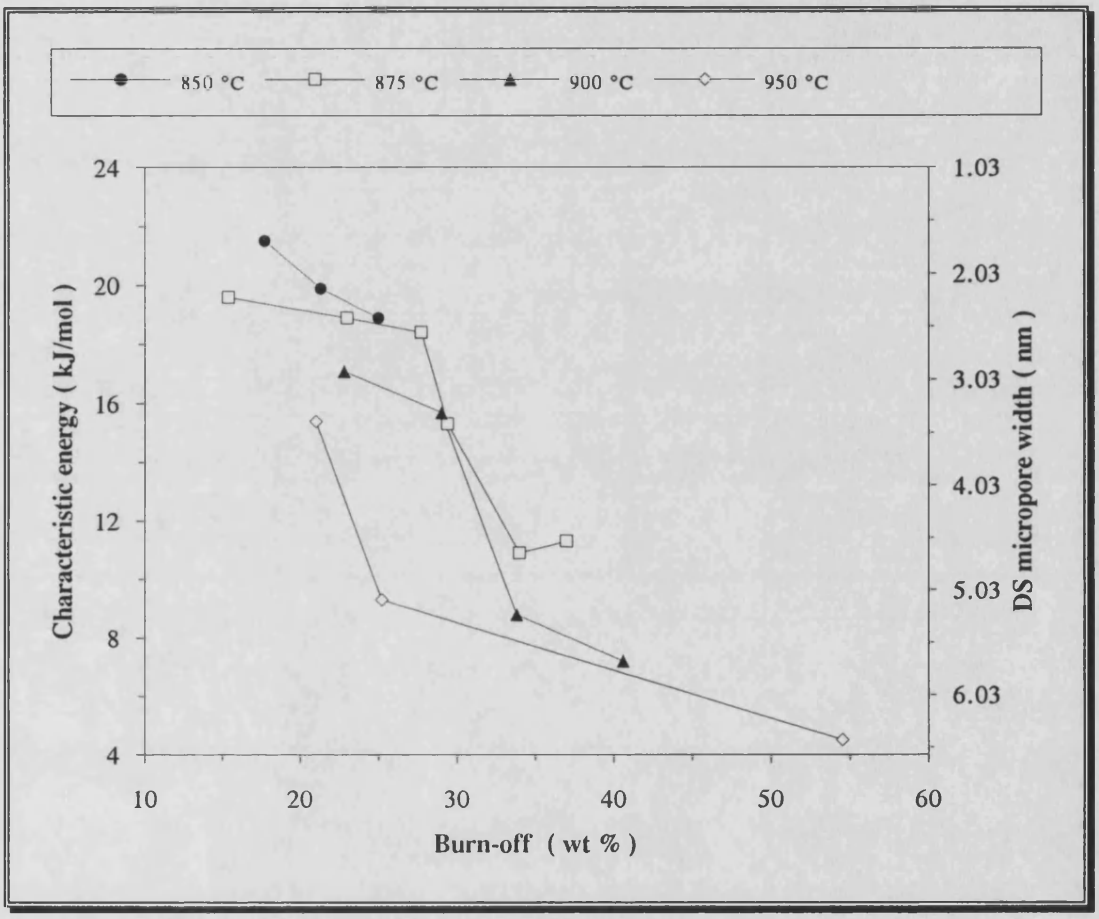

Figure 5.22 : Characteristic energy plots for CO_2 activated WCC carbons.

The plots were similar to the E_o plots found for the CO_2 activated BROM and BCC carbons, showing a shift towards lower energy values for a fixed burn-off as the temperature increased. This shows that for a given burn-off, higher temperatures produced pores with larger diameters. For burn-offs below 35 %, the widening of the pores was especially marked at 950 °C. The E_o values and BET surface areas of

the column cleaned coals with similar burn-off values are given in Table 5.14 for two activation temperatures of 875 and 900 °C. It was found for sample burn-offs below 30 %, that the energy values for the WCC carbons are higher than the corresponding values found for the BCC carbons, showing that the activated WCC carbons have smaller pore widths. This suggests that the activation process in the WCC carbons is more effective than for the BCC carbons, even though the two precursors had similar mineral matter contents. For sample burn-off values higher than 30 %, the WCC carbons had energy values lower than corresponding BCC carbons, showing that the WCC samples had larger pore widths, due to the burn-out of the micropores.

Table 5.14 : Comparison of characteristic energy values for the carbons prepared from the column cleaned coals by CO_2 activation.

Average sample burn-off	Samples activated at 875 °C				Samples activated at 900 °C			
	BCC carbon		WCC carbon		BCC carbon		WCC carbon	
	S_{BET} m^2/g	E_o kJ/mol	S_{BET} m^2/g	E_o kJ/mol	S_{BET} m^2/g	E_o kJ/mol	S_{BET} m^2/g	E_o kJ/mol
22	379	15.1	517	18.9				
30	469	13.5	605	15.3	445	11.7	546	15.7
41	586	11.6	658	11.3	537	10.4	710	7.2

5.7.3. Steam activation of WCC carbons

Figure 5.23 shows the development of surface area vs burn-off for the steam activation of the WCC chars.

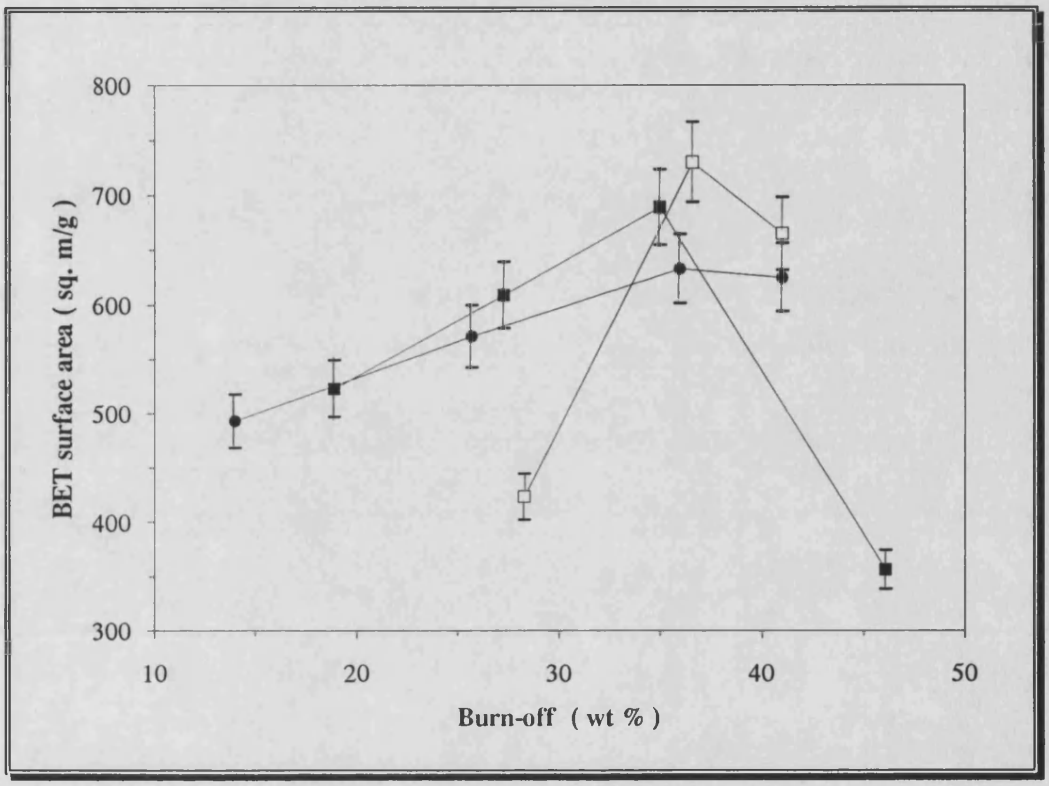

Figure 5.23 : Development of BET surface area for steam activated WCC carbons.
(Activation temperatures : ● 750 °C ■ 775 °C □ 800 °C)

The influence of activation temperature on surface areas development were little affected at lower activation temperatures, although S_{BET} seemed to be sensitive to the higher activation temperature of 800 °C for burn-off values lower than 40 %. S_{BET} reached a maximum value when using 775 °C as activation temperature, but this occurred at a lower burn-off value than a similar maxima observed at 800 °C for the steam activated BCC carbons. These observations suggest that the activation process

for the WCC chars is more efficient than for the BCC chars. The surface areas and pore volumes of the steam activated WCC samples are given in Table 5.15.

Table 5.15 : Pore structure analysis for steam activated WCC carbons from N_2 adsorption data.

Sample no.	Activation conditions								
	Temp °C	Time h	Burn-off %	BET N_2 surface area, S_{BET} m^2/g	Notional micropore surface area, S_{micro} m^2/g	Micropore volume, V_o cm^3/g	Mesopore surface area, S'_{BET} m^2/g	Characteristic energy E_o kJ/mol	Ash %
A85	750	2	14	490	484	0.18	6	17.7	19
A80		3	26	570	563	0.21	7	16.0	21
A82		4	36	630	622	0.24	8	13.2	24
A83		5	41	630	622	0.23	8	13.2	24
A75	775	2	19	520	514	0.19	6	16.2	20
A76		3	27	610	602	0.23	8	13.4	21
A77		4	35	690	679	0.26	11	11.6	23
A74		5	46	360	353	0.13	7	10.2	29
A79	800	1	28	420	415	0.16	5	16.9	21
A78		2	37	730	720	0.28	10	12.7	24
A81		3	41	670	656	0.25	14	10.0	26

S_{BET} at 750 °C reached a maximum value which did not increase with extended burn-off, suggesting that a maximum surface area of ~ 630 m^2/g can be produced at 750 °C. Little mesoporosity was developed in the samples, showing that the samples were predominantly microporous. S_{BET} at 750 °C also reached a maximum for the BROM and BCC steam activated carbons, although the S_{BET} values were lower than for the WCC carbons.

Table 5.16 : Pore structure analysis from mercury porosimetry data for steam activated WCC carbons.

Sample no.	Activation conditions		Mercury porosimetry data (50 kpsig max)				40 kpsig	N_2 data
	Temp °C	Time h	Macropore volume, V_{macro} cm^3/g	Mesopore volume, V_{meso} cm^3/g	Macropore surface area, S_{macro} m^2/g	Mesopore surface area, S'_{BET} m^2/g	Mesopore surface area, S'_{BET} m^2/g	Mesopore surface area, S'_{BET} m^2/g
A85	750	2	0.35	0.02	1	14	9	6
A80		3	0.40	0.03	1	15	10	7
A82		4	0.56	0.04	2	21	14	8
A83		5	0.56	0.04	2	21	15	8
A75	775	2	0.48	0.04	1	15	10	6
A76		3	0.51	0.03	2	17	12	8
A77		4	0.51	0.06	2	21	15	11
A74		5	0.70	0.06	2	38	25	7
A79	800	1	0.51	0.02	1	16	10	5
A78		2	0.60	0.04	2	21	14	10
A81		3	0.60	0.05	2	26	17	14

Table 5.16 gives the mercury intrusion data for the steam activated WCC carbons. All samples showed little macroporous surface area. The samples prepared at 750 °C reached constant values of both macro- and mesopore volumes, and this shows that development of porosity in the samples are limited at this temperature. Samples activated at 775 °C showed a progressive increase of V_{macro} and V_{meso} for increased activation. V_{macro} reached a value of 0.70 cm^3/g for sample A74, even though S_{BET} for the sample decreased from 690 to 370 m^2/g. This suggests that the increase in V_{macro} was by burn-out of the existing pore structure. Sample A81 showed a constant V_{macro} although the S_{BET} of the sample decreased. The decrease in S_{micro} in this sample is thus entirely due to the formation of mesopores, in contrast to sample A74

discussed above, where the decrease in S_{micro} was partially due to the formation of macropores.

Porosimetry data at both 50 kpsig and 40 kpsig overestimated the mesopore surface area when compared to the surface area obtained from N_2 data, showing that the mercury could easily damage the pore structure. This suggests that the pore system produced by steam activation is more fragile than the CO_2 activated carbons, since a good agreement was found between the nitrogen and 40 kpsig mercury intrusion data for the CO_2 activated carbons.

5.7.4. Characteristic energy of steam activated WCC carbons

The characteristic energy values for the steam activated WCC carbons are given in Figure 5.24. For burn-off values below ~ 35 %, higher activation temperatures led to samples having higher E_o values, or smaller pore widths. This suggests that the higher temperatures are more efficient in creating narrow micropores for burn-off values below 35 %. For burn-off values higher than 35 %, higher temperatures leads to samples with wider pores, which is also evident in the increase in mesoporosity of the samples when using higher activation temperatures. This is in contrast to the E_o plots for the BCC activated samples, which showed higher E_o values for increasing temperatures for all burn-offs over the range 20 - 50 %. Similar plots for the steam activation of the BROM carbons showed that the E_o values were little affected by temperature shifts for burn-offs larger than 35 %. When comparing similar burn-off values for the steam activated BCC carbons and the steam activated WCC carbons, it was also found that the WCC carbons had higher E_o values, or smaller micropore widths. All these results show that the pore width is not only influenced by the activation temperature, but also by the nature of the coal precursor and the inherent mineral matter content.

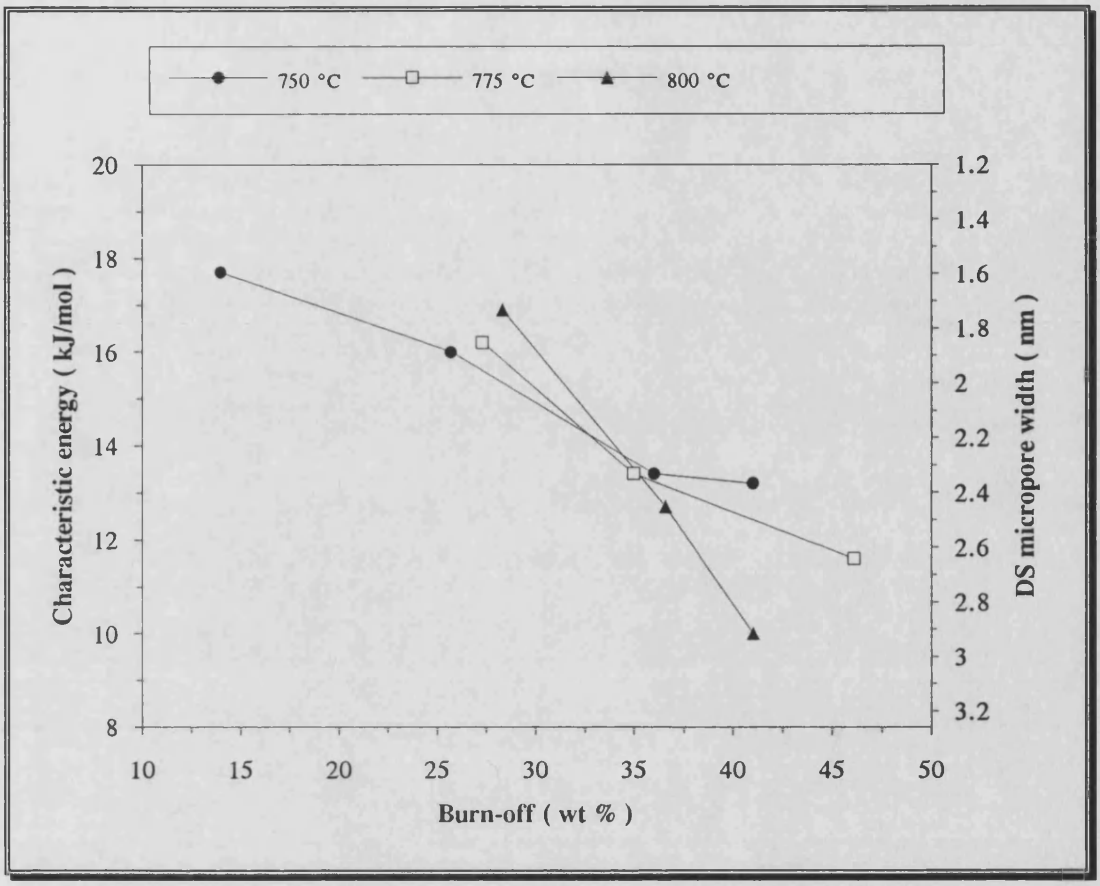

Figure 5.24 : Characteristic energy plots for steam activated WCC carbons.

5.7.5. Comparison between CO_2 and steam activation of WCC chars

The micropore - and mesopore surface areas of the WCC carbons prepared by CO_2 and steam activation are compared in Figures 5.25 and 5.26 respectively. For burn-off values lower than 25 %, steam activation will produce a more microporous carbon with a higher dgree of mesoporosity, as is shown in Figure 5.26. Similar results were found for the BROM and BCC carbons. For burn-off values higher than 25 %, both activating agents produce similar microporous carbons, but CO_2 activation will produce carbons with a higher degree of mesoporosity if the sample burn-off is higher than ~ 40 %. This is in contrast to the BCC and BROM carbons,

where steam activation at burn-offs higher than 40 % produced substantial mesoporosity in the sample.

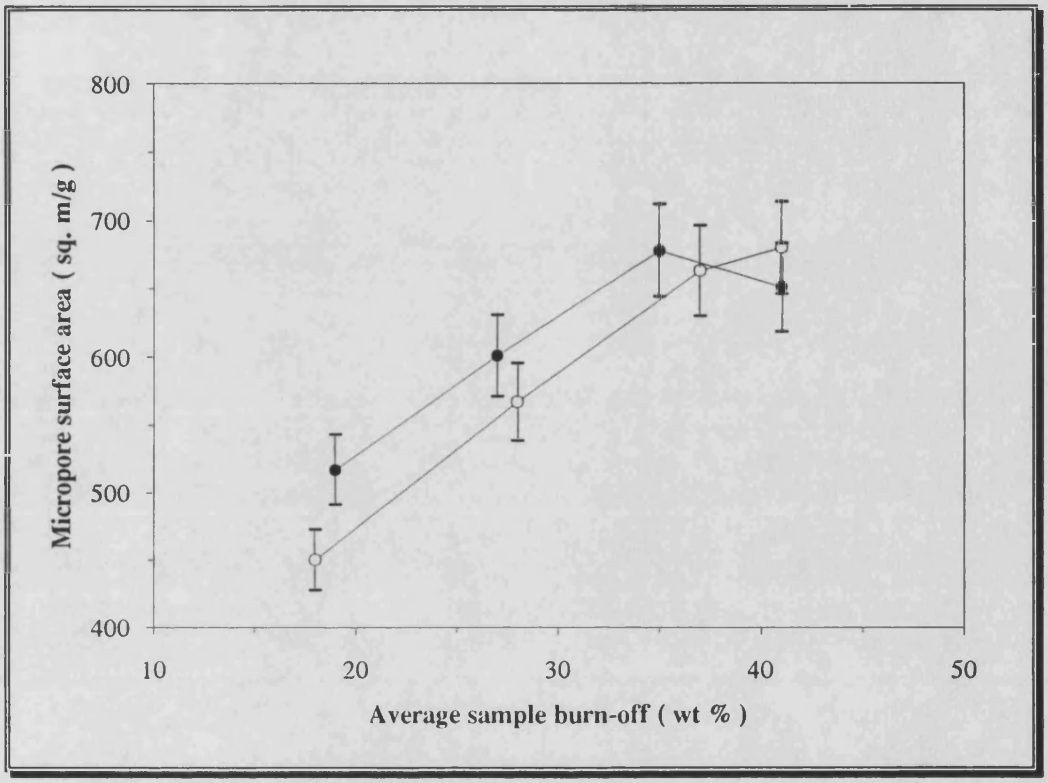

Figure 5.25 : Development of micropore surface area in WCC activated carbons.

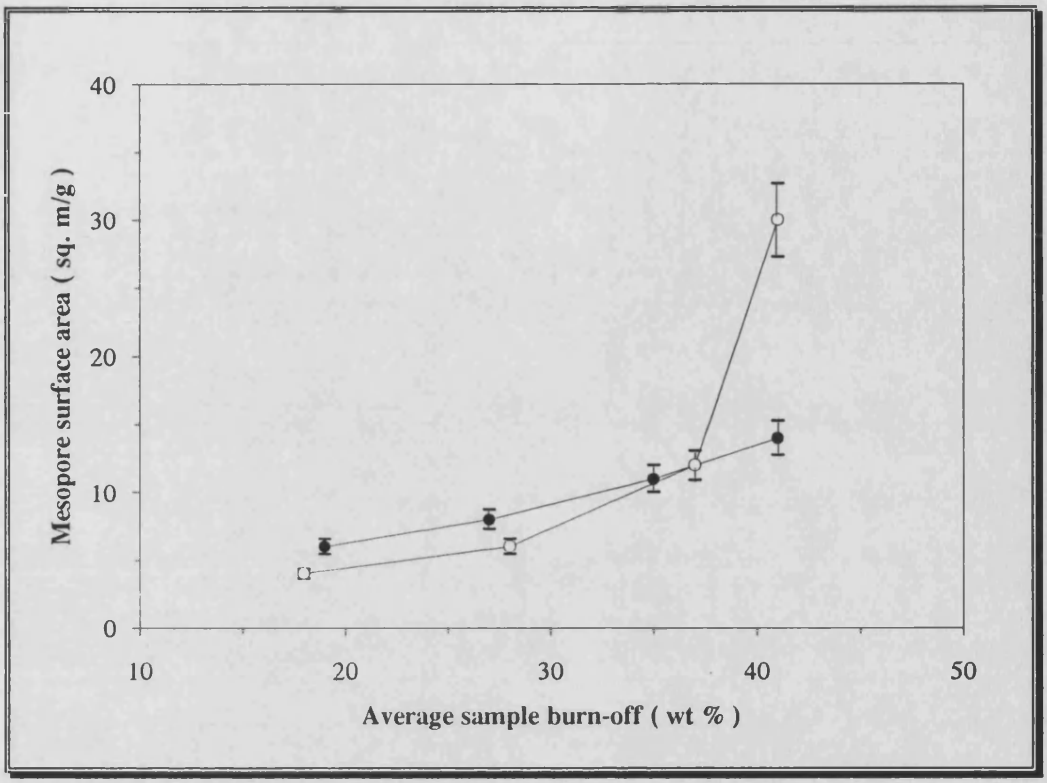

Figure 5.26 : Development of mesopore surface area in WCC activated carbons.
(○ CO_2 activation ● Steam activation)

5.7.6. Influence of acid washing on WCC activated carbons

Selected samples of the WCC carbons were subjected to the mild acid wash to reduce the ash contents of the carbons. The porosity values for these carbons before and after the acid washing are given in Table 5.17. Sample A77, prepared by steam activation, showed a 13 % decrease in its ash content, and a proportional increase in S_{micro} of 13 % and an increase in S'_{BET} of 18 %, showing that the ash blocked the meso- and micro-pores to a similar extent. A large increase in macropore volume was also observed. Although the ash content for sample A80 decreased by 19 %, an increase of only 12 % was obtained for both the mesopore and micropore surface area. A high increase in V_{meso} of 200 % was observed, showing that ash blocked the entrances to the mesopores. The ash content of sample A96, prepared by CO_2

activation, could be reduced by 32 %, but most of the ash was concentrated in the larger meso- and macropores. Smaller values for V_{macro} and V_{meso} were also found, showing that pores may have collapsed after the removal of the ash.

Table 5.17 : Influence of acid washing on WCC activated carbons.

Sample no.	Ash in carbon	Parameters from N_2 adsorption						Parameters from Hg porosimetry	
		BET surface area	BET surface area ash free	Micro-pore surface area	Meso-pore surface area	Micro-pore volume	Charac-teristic energy	Macro-pore volume	Meso-pore volume
	%	S_{BET} m^2/g	S_{MAX} m^2/g	S_{micro} m^2/g	S'_{BET} m^2/g	V_0 cm^3/g	E_0 kJ/mol	V_{macro} cm^3/g	V_{meso} cm^3/g
A80	21	570	720	563	7	0.21	16.0	0.40	0.03
A80HCl	17	640	760	632	8	0.24	15.1	0.50	0.09
% Difference	*- 19*	*+ 12*		*+ 12*	*+ 14*	*+ 14*	*- 6*	*+ 25*	*+ 200*
A77	23	690	890	679	11	0.26	11.6	0.51	0.06
A77HCl	20	780	970	767	13	0.29	11.5	0.70	0.06
% Difference	*- 13*	*+ 13*		*+ 13*	*+ 18*	*+ 12*	*- 1*	*+ 37*	*0*
A96	25	680	900	668	12	0.27	10.9	0.50	0.05
A96HCl	17	700	840	685	15	0.28	10.7	0.36	0.03
% Difference	*- 32*	*+ 3*		*+ 3*	*+ 25*	*+ 4*	*- 2*	*- 28*	*- 40*
A103	30	760	1090	620	140	0.28	4.5	0.69	0.10
A103HCl	29	760	1070	620	140	0.28	4.4	0.70	0.12
% Difference	*- 3*	*0*		*0*	*0*	*0*	*- 2*	*+ 1*	*+ 20*

Samples A96 and A103 prepared by CO_2 activation
Samples A80 and A77 prepared by steam activation

Sample A103 was the sample with the highest mesoporosity. The acid washing seemed to be unsuccessful in removing ash from this sample, except for an increase of 20 % for V_{meso} . This suggests that the ash may either be trapped in the sample, or that the activation temperature of 950 °C altered the ash to an HCl - insoluble

form. It is also interesting to note that the removal of the ash for the CO_2 - activated carbons had little effect on the value of S_{micro} , showing that the distribution of the ash in the carbon is also influenced by the activation method. The S_{BET} values for samples A77HCl, A80HCl and A96HCl varied between 20 - 25 % of their corresponding S_{MAX} values, while S_{BET} for sample A103HCl was 40 % less than its S_{MAX} value, showing that the ash content limit the maximum surface area that can be obtained.

5.7.7. Summary of the activation results for WCC chars

The main findings for the activation of the WCC chars are summarized below :

⌘ The maximum BET surface area that can be obtained from the WCC chars for a burn-off value less than 50 % is 710 m^2/g, (Sample A105, CO_2 activation); this sample had a micropore volume of 0.29 cm^3/g.

⌘ The carbons are predominantly microporous with the mesopores constituting less than 10 % of the total surface area. Sample A103, prepared by CO_2 activation at 950 °C for 4 h activation time, had a mesopore surface area constituting 18 % of the total surface area for a sample burn-off of 55 %.

⌘ Single parameter estimates of the micropore width showed that the WCC carbons had a narrower pore width than the BCC and BROM carbons for burn-off values less than 35 %. For burn-off values larger than 35 % the WCC carbons showed larger pore widths when compared to the BCC carbons. Mercury porosimetry results indicated that the WCC carbon structure is more susceptible to be damaged by mercury intrusion than the BROM or BCC carbons.

⌘ For burn-off values less than 35 %, steam activation will produce the maximum values of both meso- and microporosity. At burn-off values higher than 35 % however, CO_2 activation will produce microporous carbons with higher mesoporosity.

⌘ The ash content of the WCC carbons varied in the range 19 - 30 %. Some of the ash can be successfully removed by washing the carbons with a 0.5M HCl solution. The steam activated carbons showed gains in both meso- and micro-porosity after the acid wash, and there is evidence that the ash blocked both types of pores to similar

extents. The CO_2 activated carbons showed increases mainly in the mesopores, with very small increases in microporosity.

CHAPTER 6

RESULTS AND DISCUSSION
Chemical activation

Summary

This chapter summarizes the results for the chemical activation of the column cleaned coals (BCC and WCC) using H_3PO_4 acid as activating agent. First, the development of surface area in the samples are discussed from the N_2 adsorption data and mercury intrusion results. Samples from each of the coal precursors are subjected to the mild acid wash to remove the ash in the carbon before the porosity of the carbons are compared to the commercially-available carbons.

6.1. H_3PO_4 activation of Bosjesspruit column cleaned (BCC) coal

6.1.1. Development of porosity in the BCC chars

The phosphorus content of all the samples increased after activation, showing that phosphorus was retained in the carbon structure and could not be removed by the washing procedure discussed in section 3.3.1. This made the determination of weight loss for the samples after activation difficult and unreliable, and therefore the development of surface area will be compared at the different activation temperatures, rather than burn-off, as was the case for physical activation. The development of BET surface area for the H_3PO_4 activation of the BCC chars are given in Figure 6.1 for 1 and 2 hours activation time respectively.

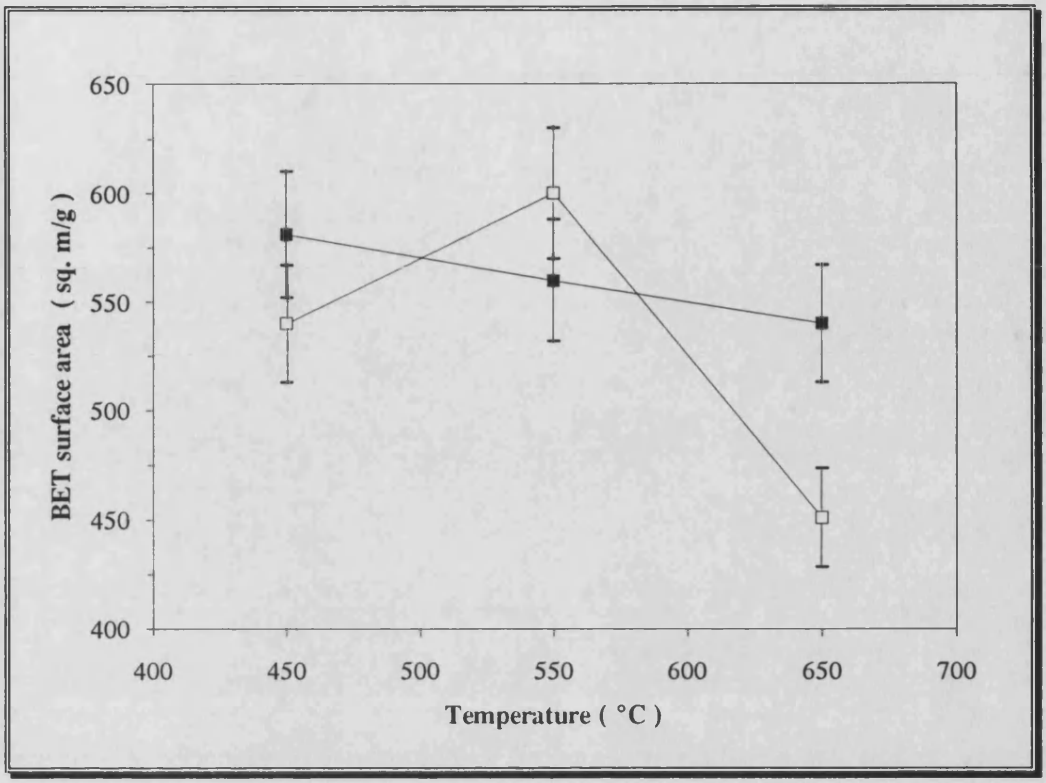

Figure 6.1 : Development of BET surface area for the chemical activation of BCC coal. (Activation times : □ 1 h ■ 2 h)

For 1 hour activation time, S_{BET} increased with temperature up to 550 °C reaching a maximum value of 600 m^2/g before declining. When taking the 5 % error on the BET equation into account, similar surface areas were developed for a 2 h activation time at the three temperatures investigated. Analysis of the nitrogen adsorption data for the samples are shown in Table 6.1.

Table 6.1 : Pore structure analysis from N_2 adsorption data for H_3PO_4 activated BCC coal.

Sample no.	Activation conditions		BET N_2 surface area, S_{BET} m^2/g	Notional micropore surface area, S_{micro} m^2/g	Micropore volume, V_o cm^3/g	Mesopore surface area, S'_{BET} m^2/g	Characteristic energy E_o kJ/mol	Ash in product %
	Temp °C	Time h						
P1	450	2	540	519	0.20	21	9.4	28
P2		3	580	559	0.21	21	9.7	28
P3	550	1	600	583	0.22	17	11.3	29
P4		2	560	544	0.21	16	11.6	29
P5	650	1	450	439	0.16	11	12.8	30
P6		2	540	527	0.20	13	12.3	32

The sorption isotherms for the carbons activated for one hour activation time are given in Figure 6.2, page 139. Increasing the activation temperature from 450 to 550 °C led to the development of microporosity, which is evident by the increased uptake of nitrogen of the sample at low relative pressures, and a decrease in mesoporosity, shown by the decrease in the slope of the adsorption branch at higher relative pressures. Type IV hysteresis in the sample activated at 550 °C are indicative of slit-shaped pores. Open loop hysteresis at low relative pressures, indicative of activated diffusion, was also reduced at 550 °C, showing that a widening of the micropores occurred. Increasing the temperature to 650 °C caused a lower initial uptake of N_2, showing that some of the microporosity was destroyed at the higher activation temperature. The shape of the isotherm at higher relative pressures show that little mesoporosity was developed. If the reaction of H_3PO_4 with the carbons did not convert the micropores to mesopores at 650 °C, but rather caused a burn-out of the micropores to macropores, a higher macropore volume

should be seen for sample P5. The mercury intrusion results given in Table 6.2 showed that there was no increase in the macropore volume for sample P5, thus the higher temperature of 650 °C caused a partial collapse of the micropore system.

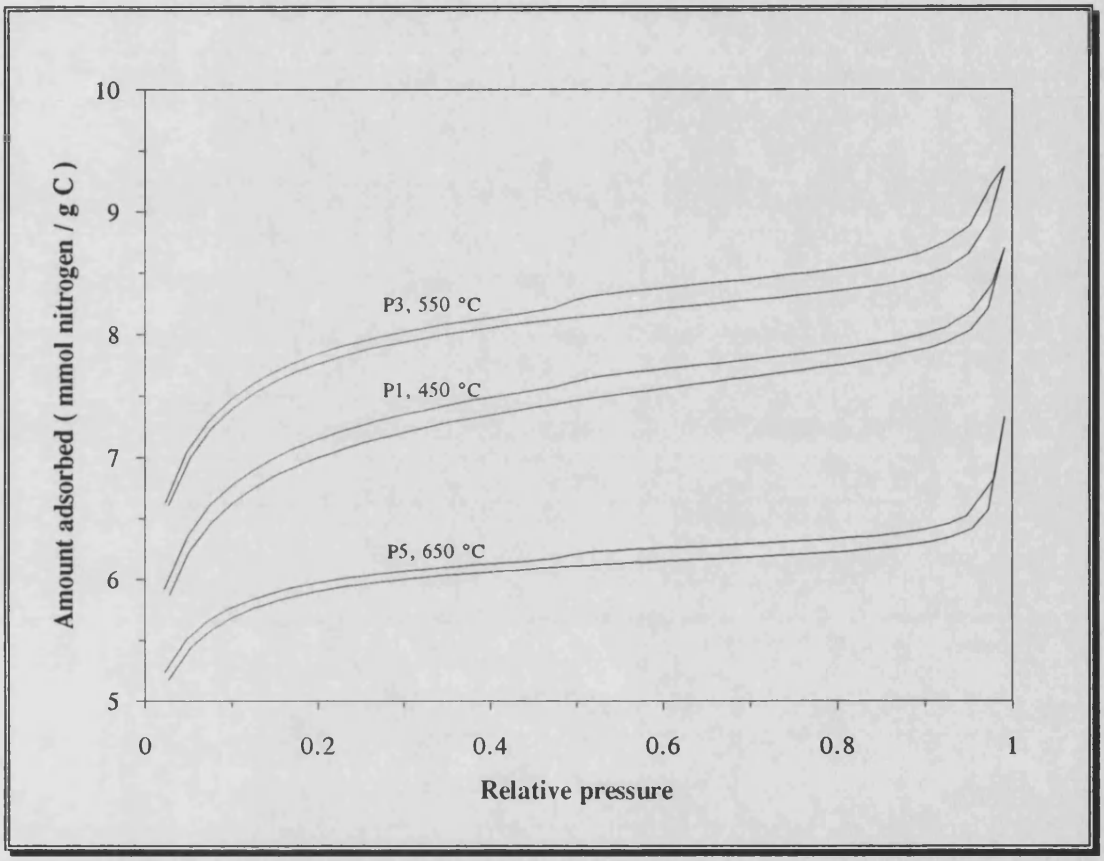

Figure 6.2 : Sorption isotherms of N_2 at 77 K for 1 hour H_3PO_4 activated BCC carbons.

The mercury porosimetry results, Table 6.2, page 140, showed that the chemically activated samples had macropore surface areas similar to those produced by the physical activation of the chars. The porosimetry results confirmed the N_2 adsorption observations that an increase in temperature leads to a decrease in mesoporosity, seen from the table in the decreasing values of mesopore volume and S'_{BET} . Porosimetry also overestimated the value of S'_{BET} when compared to the surface area

obtained from N_2 data, suggesting a more fragile pore structure than the carbons prepared by physical activation.

Table 6.2 : Pore structure analysis from mercury porosimetry data for H_3PO_4 activated BCC carbons.

Sample no.	Activation conditions		Mercury porosimetry data (50 kpsig max)				40 kpsig	N_2 data
	Temp °C	Time h	Macropore volume cm^3/g	Mesopore volume cm^3/g	Macropore surface area m^2/g	Mesopore surface area m^2/g	Mesopore surface area m^2/g	Mesopore surface area m^2/g
P1	450	1	0.84	0.10	3	51	38	21
P2		2	0.85	0.09	3	47	35	21
P3	550	1	0.76	0.07	3	39	26	17
P4		2	0.83	0.06	2	40	27	16
P5	650	1	0.76	0.03	2	20	14	10
P6		2	0.77	0.05	2	27	19	11

6.1.2. Characteristic energy of the H_3PO_4 activated BCC carbons

The E_o values for the H_3PO_4 activated BCC carbons are given in Figure 6.3, page 141. In contrast to the E_o results for the physically activated carbons, an increase in E_o was found for an increase in activation temperature for both activation times under study; this means that higher activation temperatures and times leads to narrower pores. These results suggests that chemical activation creates narrower pores at higher activation temperatures and times, which seems to be dubious since an increase in surface area was found for samples P2 and P4. A more feasible explanation is that the activation process causes the pore structure to collapse, leading not only to narrower pores, but also to lower surface areas as was seen for samples P5 and P6.

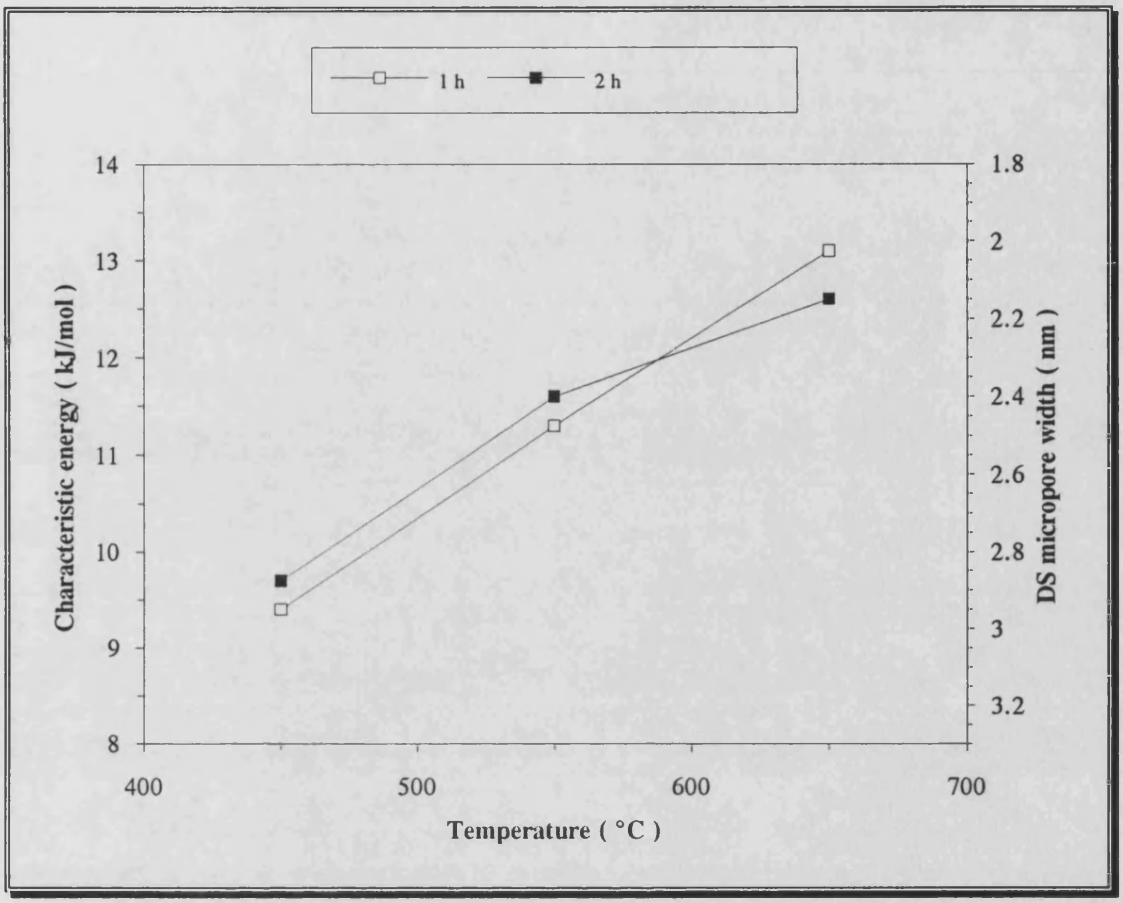

Figure 6.3 : Characteristic energy plots for H_3PO_4 activated BCC carbons.

6.1.3. Elemental analysis of the activated BCC carbons

Elemental analysis of the carbons (Table 6.3) showed significant increases in the phosphorus content of the samples, even after the extensive washing procedures of the samples after activation.

Table 6.3 : Phosphorus content for H_3PO_4 activated BCC carbons.

	1 h activation time			2 h activation time		
Activation temperature	**450 °C**	**550 °C**	**650 °C**	**450 °C**	**550 °C**	**650 °C**
Sample	P1	P3	P5	P2	P4	P6
Phosphorus (wt %)	7.9	8.0	6.4	7.1	7.6	6.0
Ash (wt %)	28	29	30	28	29	32

The phosphorus content reached a maximum value at 550 °C for both activation times, varying between 6 - 8 %, compared to 0.3 % of the coal precursor. No definite trend was observed for the influence of phosphorus content on the S_{BET} value or the ash content of the carbons. The sulphur content of the carbons decreased with an increase in activation for both activation temperatures and times used in this study. H/C and O/C atomic ratios decreased with an increase in activation temperature for both activation times. The ratios are graphically represented for 1 h activation time in Figure 6.4. The N/C atomic ratios showed little variance over the temperature range investigated, while a decrease in the sulphur content of the carbons at higher temperatures was found.

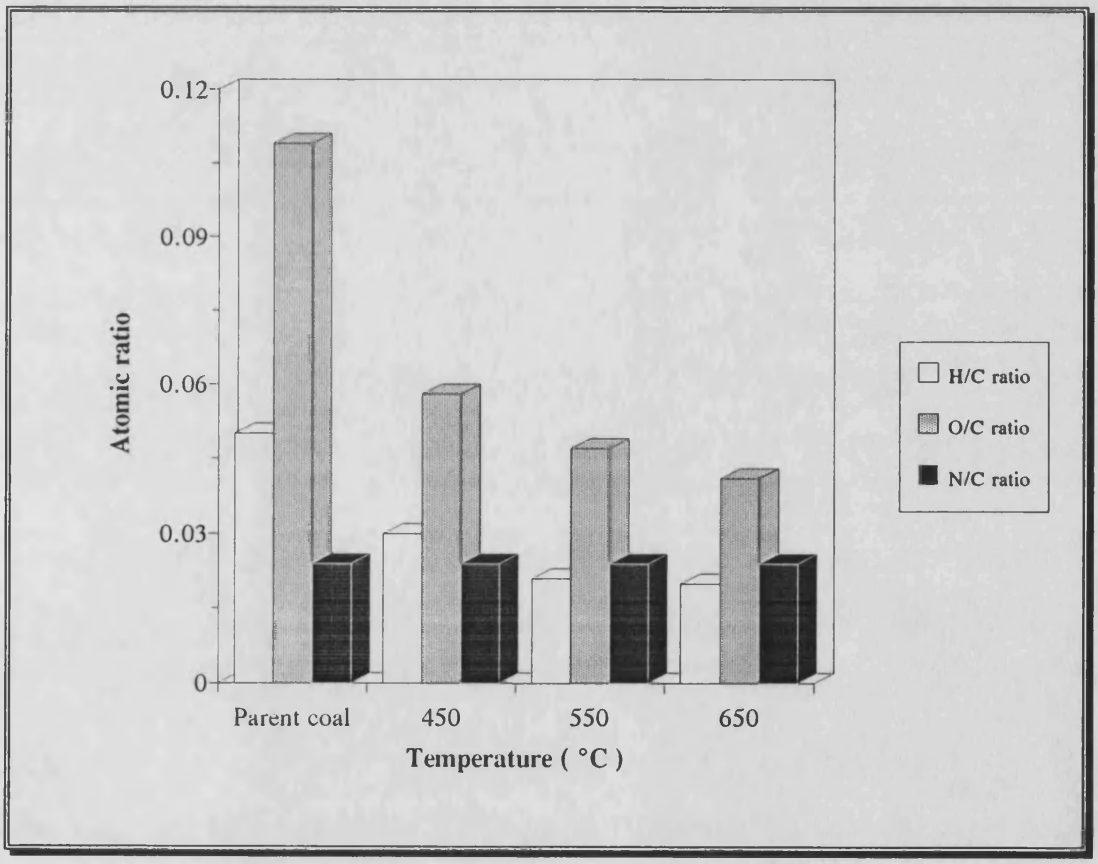

Figure 6.4 : Atomic ratios of H_3PO_4 activated BCC carbons after 1 h activation time.

6.2. H_3PO_4 activation of Waterberg column cleaned (WCC) coal

6.2.1. Development of porosity in the WCC chars

The development of BET surface area for the H_3PO_4 acid activation of the WCC coal is shown in Figure 6.5.

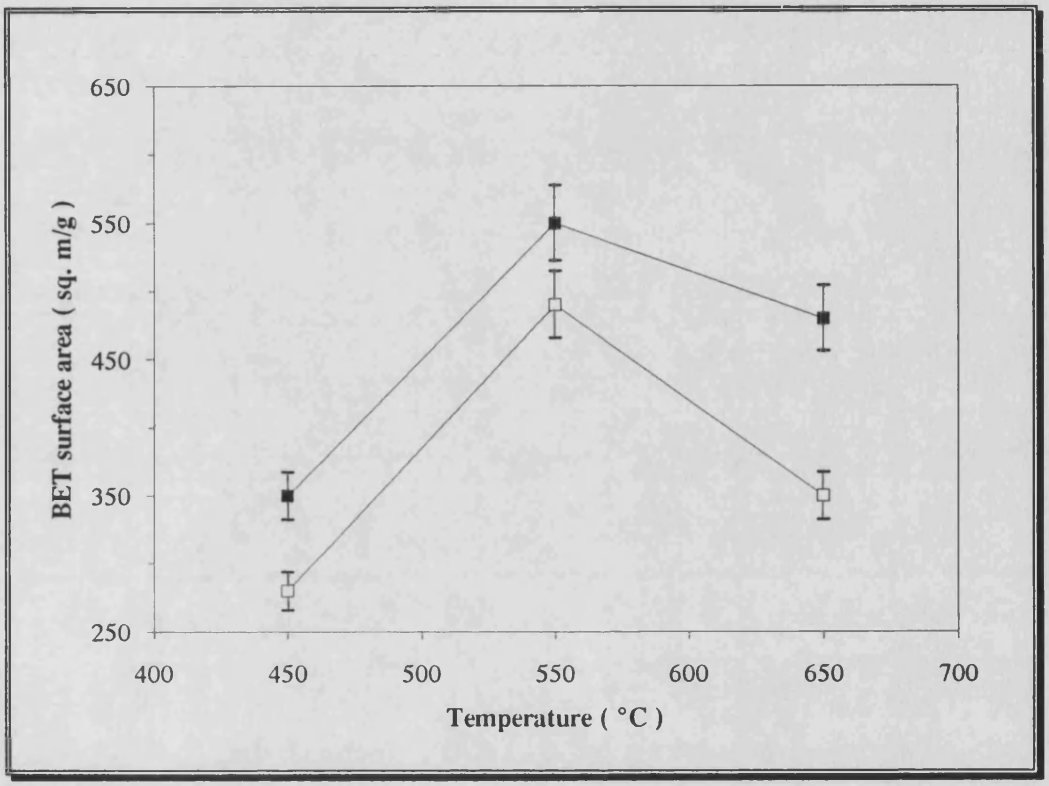

Figure 6.5 : Development of BET surface area for the chemical activation of WCC coal. (Activation times : □ 1 h ■ 2 h)

For both activation times S_{BET} reached a maximum at 550 °C before declining, similar to the results found for 1 h activation time of the BCC coal. At 2 h activation time the surface areas of the WCC and BCC carbons were similar, but the surface area for the WCC carbons prepared at a 1 h activation time however was lower than for the BCC carbons, showing that the H_3PO_4 reaction is more successful in generating surface area in the BCC coal precursor. The porosity values calculated from the nitrogen adsorption data for the carbons are given in Table 6.4. The

development of micropore volume followed the trend seen for S_{BET} and reached a maximum value of 0.21 cm^3/g for sample P10. For 1 h activation time S'_{BET} reached a value of 21 m^2/g before declining, while S'_{BET} at 2 h activation time showed a progressive increase to reach a value of 28 m^2/g at 650 °C.

Table 6.4 : Pore structure analysis from N_2 adsorption data for H_3PO_4 activated WCC coal.

Sample no.	Activation conditions		BET N_2 surface area S_{BET} m^2/g	Notional micropore surface area S_{micro} m^2/g	Micropore volume V_o cm^3/g	Mesopore surface area S'_{BET} m^2/g	Charac-teristic energy E_o kJ/mol	Ash in product %
	Temp °C	Time h						
P7	450	2	280	267	0.11	13	8.3	28
P8		3	350	333	0.13	17	8.5	30
P9	550	1	490	469	0.19	21	8.4	29
P10		2	550	524	0.21	26	7.9	31
P11	650	1	350	332	0.13	18	8.2	32
P12		2	480	452	0.17	28	7.8	36

Mercury porosimetry data, given in Table 6.5, page 145, revealed little macropore surface area in the samples, while the macropore volume reached a maximum value at 550 °C for each of the activation times. The value of V_{macro} changed little with HTT; similar results were found by Derbyshire *et al.* [1991b]. The lower macropore and mesopore volumes and decrease in S_{BET} for sample P12 suggests that the pore structure collapsed, leading to lower values. Mercury porosimetry at both 50 kpsig and 40 kpsig overestimated the S'_{BET} value as calculated from the N_2 data, except for

samples P11 and P12. This shows that porosimetry is not reliable for the determination of mesoporosity in H_3PO_4 activated carbons.

Table 6.5 : Pore structure analysis from mercury porosimetry data for H_3PO_4 activated WCC carbons.

Sample no.	Activation conditions		Mercury porosimetry data (50 kpsig max)				40 kpsig	N_2 data
	Temp	Time	Macropore volume	Mesopore volume	Macropore surface area	Mesopore surface area	Mesopore surface area	Mesopore surface area
	°C	h	cm^3/g	cm^3/g	m^2/g	m^2/g	m^2/g	m^2/g
P7	450	1	0.25	0.12	2	46	35	13
P8		2	0.27	0.09	2	48	38	17
P9	550	1	0.27	0.11	2	60	46	21
P10		2	0.31	0.10	2	55	40	26
P11	650	1	0.25	0.06	2	30	21	18
P12		2	0.21	0.08	2	42	29	28

6.2.2. Characteristic energy of the H_3PO_4 activated WCC carbons

The E_o values for the chemically activated WCC carbons are given in Figure 6.6, page 146. For a 2 h activation time the E_o values showed a progressive decrease, indicating a widening of the micropores. Although the sample activated at 650 °C for 2 h (sample P12) showed a decrease in S_{BET} , the E_o value of this sample suggests that the pores in this sample are wider than for sample P10, prepared at 550 °C for the same activation time. The E_o values for a 1 h activation time suggests that the pores in sample P9, produced at 550 °C, are narrower than the pores produced in sample P7 at 450 °C. The increase in S_{BET} for sample P9 (550 °C, 1 h) showed that substantial activation of the sample occurred. These results all suggest that there is a partial collapse of the pore walls at higher HTT.

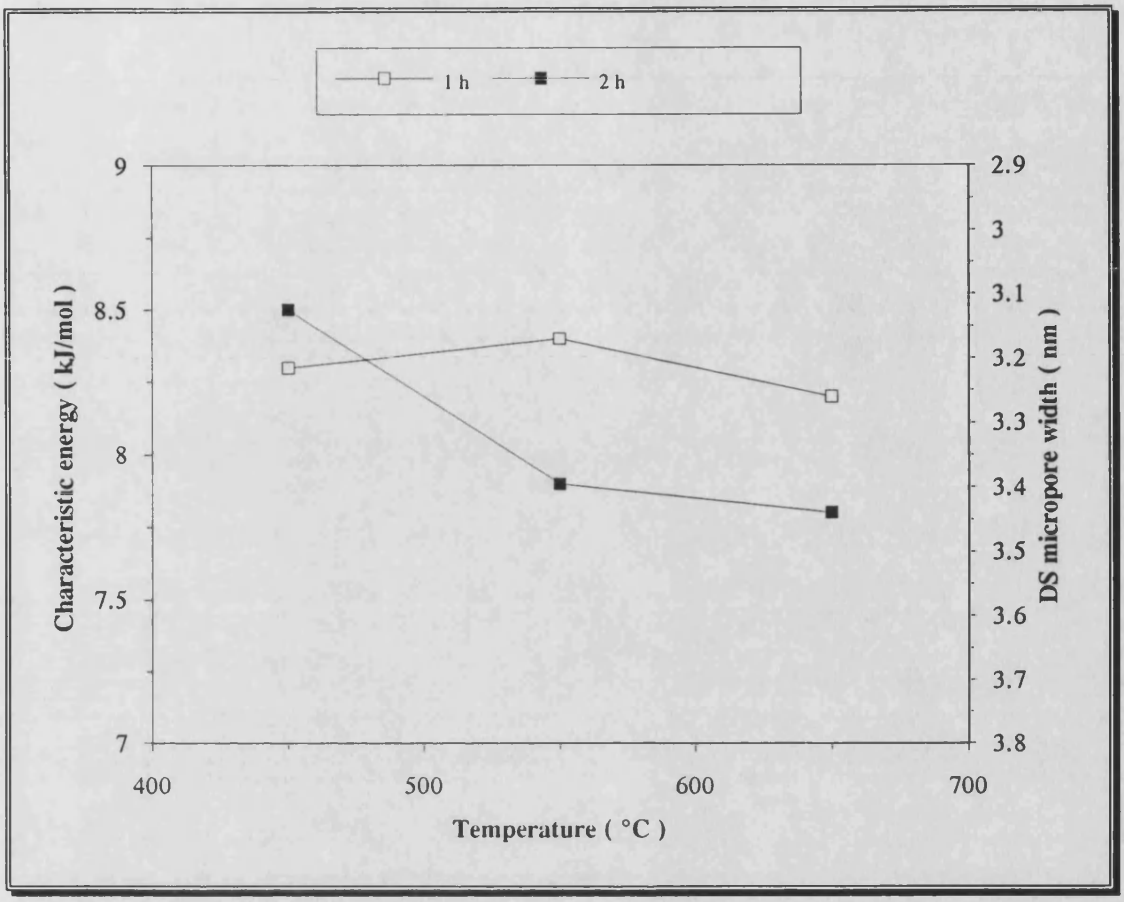

Figure 6.6 : Characteristic energy plots for H_3PO_4 activated WCC carbons.

6.2.3. Elemental analysis of the activated WCC carbons

Elemental analysis of the samples showed significant increases in the phosphorus content of the samples; the values are given in Table 6.6.

Table 6.6 : Phosphorus content for H_3PO_4 activated WCC carbons.

	1 h activation time			2 h activation time		
Activation temperature	**450 °C**	**550 °C**	**650 °C**	**450 °C**	**550 °C**	**650 °C**
Sample	P7	P9	P11	P8	P10	P12
Phosphorus (wt %)	7.5	8.2	7.9	6.2	8.0	7.4
Ash (wt %)	28	29	32	30	31	36

The phosphorus content reached a maximum value in the samples produced at 550 °C, and varied between 6 - 8 %, which is similar to the results found for the BCC carbons. For both the BCC and WCC carbons the results for the phosphorus - ash relationship are scattered, contrary to the positive linear trend found by Derbyshire *et al.* [1991b] for the H_3PO_4 activation of a column cleaned Illinois basin coal (IBC 101). This is shown in Figure 6.7.

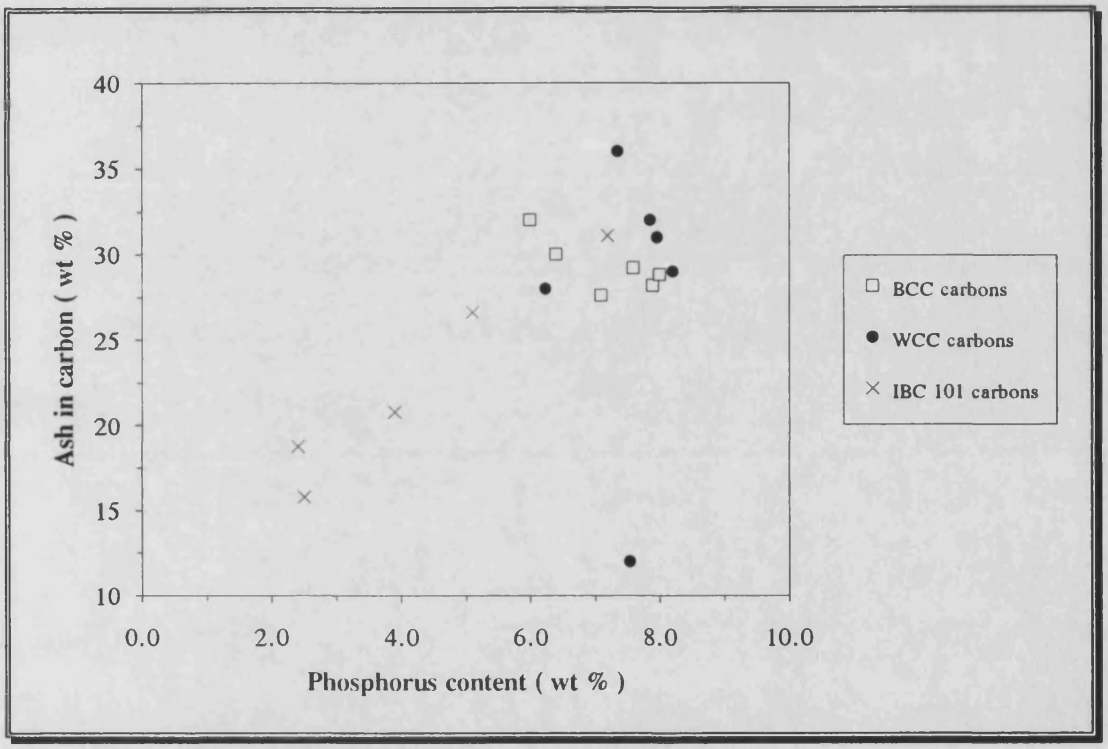

Figure 6.7 : The relationship between the phosphorus and ash contents of H_3PO_4 activated coals. (IBC 101 data from Derbyshire *et al.* [1991b])

H/C and O/C atomic ratios decreased with an increase in activation temperature for both activation times. Little variance was observed for the N/C atomic ratio, similar to the results for the BCC carbons. The sulphur content of the carbons decreased with an increase in activation for both activation temperatures, similar to the results found for the BCC carbons. Derbyshire *et al.* [1991b] found that the acid treatment

enhanced the liberation of sulphur, which is released mainly as hydrogen sulphide (H_2S) gas.

6.3. Influence of acid washing on chemically activated carbons

Sample P3, prepared from BCC coal, and sample P10, prepared from WCC coal, which exhibited the largest S_{BET} values were subsequently subjected to the HCl washing to remove some of the ash in the carbon. The influence of the acid washing on the porosity parameters of the carbons are shown in Table 6.7.

Table 6.7 : Influence of acid washing on chemically activated carbons.

Sample no.	Ash in carbon	Parameters from N_2 adsorption						Parameters from Hg porosimetry	
		BET N_2 surface area	BET N_2 surface area ash free	Micro-pore surface area	Meso-pore surface area	Micro-pore volume	Charac-teristic energy	Macro-pore volume	Meso-pore volume
		S_{BET}	S_{MAX}	S_{micro}	S'_{BET}	V_o	E_o	V_{macro}	V_{meso}
	%	m^2/g	m^2/g	m^2/g	m^2/g	cm^3/g	kJ/mol	cm^3/g	cm^3/g
P3	29	600	840	583	17	0.22	11.3	0.76	0.07
P3HCl	25	590	790	574	16	0.22	11.5	0.84	0.07
% Difference	*- 14*	*- 2*		*- 2*	*+ 6*	*0*	*+ 2*	*+ 8*	*0*
P10	31	550	790	529	21	0.21	7.9	0.31	0.10
P10HCl	31	530	770	509	21	0.21	8.9	0.54	0.10
% Difference	*0*	*- 4*		*- 4*	*0*	*0*	*+ 13*	*+ 74*	*0*

Sample P3 prepared from BCC coal
Samples P10 prepared from WCC coal

Acid washing was not as successful in removing the ash in the carbons as was observed in the physically activated samples. Although the ash in the BCC carbon was reduced by 14 %, no increase in S_{BET} was found while S'_{BET} increased by only 6

%. Since an increase of 8 % in V_{macro} was also found, it suggests that most of the ash was concentrated in the macro- and meso-pores. Acid washing of the WCC carbon did not reduce the ash content, showing that the ash is either trapped in the carbon structure, or has been altered into a HCl - insoluble form by the H_3PO_4 acid. The reason for an increase in V_{macro} without a reduction in the ash content is unknown. An increase in the E_o values indicates that the pores in the acid - washed carbons are narrower, suggesting that the acid washing caused a reduction in the width of the pores. These observations confirm that the pore structure in the H_3PO_4 activated carbons is fragile and easily susceptible to pore collapse.

6.4. Summary of the activation results for BCC and WCC chars

The main findings for the H_3PO_4 activation of the BCC and WCC chars are summarized below :

- The maximum BET surface area that was obtained for the BCC carbons was 600 m^2/g, (Sample P3, 1 h activation time); the sample had a micropore volume of 0.22 cm^3/g. The maximum S_{BET} obtained for the WCC carbons was 550 m^2/g, (Sample P10, 2 h activation time); this sample had a micropore volume of 0.21 cm^3/g.

- For both the BCC and WCC carbons S_{BET} and S'_{BET} passed through a maximum at 550 °C; similar results were found by Derbyshire *et al.* [1991b] and Laine *et al.* [1989]. The carbons are predominantly microporous with the mesopores constituting less than 10 % of the total surface area.

- Mercury porosimetry results indicated that the carbon structure in the chemically-activated carbons is fragile, easily damaged by mercury intrusion and susceptible to collapsing of the pore structure .

- The ash content of the carbons varied in the range 28 - 36 %. The removal of the ash in the carbons by an acid washing with a 0.5M HCl solution was not as successful as for the thermally-activated carbons. Phosphorus is incorporated into the carbon structure, and the phosphorus content of the carbons varied between 5.5 - 8.5 %, compared to the phosphorus content of < 1 % of the parent coals. The acid washing results suggest that the mineral matter in the coal may react with the H_3PO_4 acid to form a HCl - insoluble species.

CHAPTER 7

RESULTS AND DISCUSSION
Gold adsorption

Summary

This section starts by discussing the adsorption of gold cyanide ($Au(CN)_2^-$) onto granular activated carbons, since this is the method currently used in the gold industry. The adsorption of $Au(CN)_2^-$ onto selected powdered carbons prepared in this study is then compared to each other and to the results found for the granular carbons. Finally, the structural and chemical factors influencing adsorption of $Au(CN)_2^-$ onto the powdered carbons are investigated.

7.1. Adsorption of gold cyanide onto granular activated carbons

7.1.1. Adsorption curves

The adsorption of $Au(CN)_2^-$ onto two commercial carbons G210 and 207A are graphically represented in Figure 7.1, page 152. In this figure the amount of gold loaded onto the carbon Q is plotted against time for the first 60 minutes of $Au(CN)_2^-$ adsorption. Carbon G210 is prepared from a coconut shell precursor, and is used widely in the gold industry in South Africa, while 207A is a coal based carbon which is included for reference purposes. The structural parameters of the granular carbons are given in Table 7.1, page 152.

Although the carbons were of similar particle size and displayed similar BET surface areas (see Table 7.1), the coconut shell carbon not only showed a faster uptake of $Au(CN)_2^-$, but also displayed a higher gold loading value after 60 minutes. Since the porosity values of the carbons are similar, it would seem that there are other factors that affects the adsorption of $Au(CN)_2^-$ onto activated carbon, e.g. the nature of the precursor.

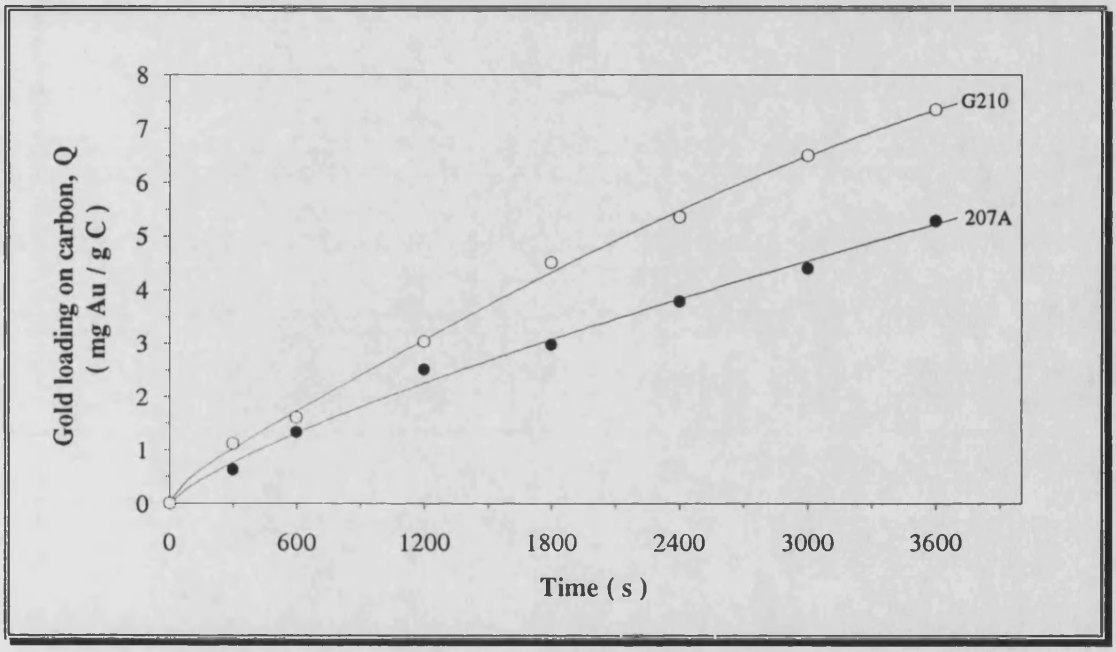

Figure 7.1 : Adsorption curves of $Au(CN)_2^-$ onto two commercial granular (1.2 - 2.4 mm) activated carbons at 25 °C and pH = 10.

Table 7.1 : Structural parameters for granular commercial carbons.

Sample	Precursor	BET surface area m^2/g	Micropore surface area m^2/g	Mesopore surface area m^2/g	Micropore volume cm^3/g	Macropore volume cm^3/g	Q mg Au.g C^{-1}
207A	Coal	1060	1025	35	0.38	0.21	5.3
G210	Coconut shell	1190	1175	15	0.44	0.28	7.4

How much surface area is covered at this time

7.1.2. Calculation of the film transfer coefficient

The rate of $Au(CN)_2^-$ adsorption onto activated carbon can be modeled by a first order rate equation : $\ln C/C_o = -kt$ (see section 2.7.6, equation 2.23), with k the observed rate constant. The rate constant is then calculated from the slope of the linear equation when plotting $\ln C/C_o$ vs t. The plots for the two granular carbons are given in Figure 7.2.

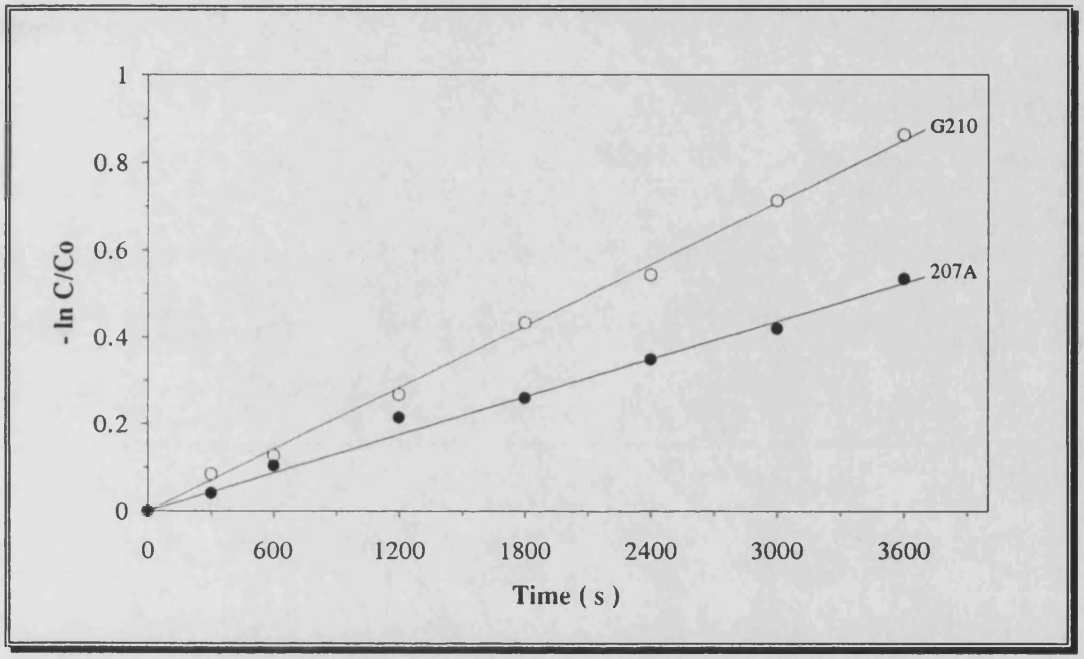

Figure 7.2 : Reaction kinetics plots for the adsorption of $Au(CN)_2^-$ onto granular activated carbon at 25 °C and pH = 10.

The rate constants calculated for the two carbons are :

G210 : 2.2×10^{-4} s^{-1}

207A : 1.8×10^{-4} s^{-1}

These results show that the coconut shell carbon G210 loads $Au(CN)_2^-$ almost 20 % faster than the coal based 207A carbon, even though the carbons have similar S_{BET}

values. The reason for the faster uptake in G210 may be the way the pores are interlinked in the three dimensional pore network, although the nature of the precursor may also influence the adsorption of $Au(CN)_2^-$ onto the carbon. The influence of structural factors on the $Au(CN)_2^-$ adsorption process will be investigated in the following sections.

Equation 2.7.4, page 54, can be used to calculate the film transfer coefficient k_f of the carbons :

$$k_f = \frac{k \cdot d' \cdot \rho \cdot V'}{6 \cdot M \cdot \psi}$$

The experimental values of V' and M are given in section 3.6, page 60, and the following assumptions are made for the granular carbons in the calculation :

spherical particles $\psi = 1$

average particle diameter $d' = 1.77$ mm

carbon particle density $\rho = 1.2$ g/cm^3

Substituting these values into the equation gives (for granular carbons in this study) :

$$k_f = 0.354\ k \quad (\text{m/s}) \qquad 7.1$$

The film transfer coefficients for the two commercial carbons were calculated from the observed rate constants as :

G210 : $k_f = 7.7 \times 10^{-5}$ m/s

207A : $k_f = 5.4 \times 10^{-5}$ m/s

The k_f value for carbon G210 is higher than the k_f value than carbon 207A, showing faster loading of $Au(CN)_2^-$ onto this carbon. A low value of k_f indicates a higher degree of film diffusional resistance [Van Deventer 1983], and for carbon 207A this may be due to the surface chemistry of the coal based precursor. The k_f value for G210 of 7.7 x 10^{-5} m/s correlates well with the value of k_f = 5.4 x 10^{-5} m/s calculated for G210 by Van Deventer [1983] in a study of $Au(CN)_2^-$ adsorption onto various granular carbons.

7.2. Adsorption of gold cyanide onto powdered activated carbons

7.2.1. Comparison of the adsorption curves between granular and powdered carbons

The gold cyanide adsorption curves for the first 60 minutes of adsorption at 25 °C and pH = 10 are compared for the powdered and granular G210 activated carbon in Figure 7.3, page 157. The powdered carbon showed a fast initial uptake typical for adsorption without diffusion limitations and approached a pseudo-equilibrium value after ~ 20 minutes of contact with the solution. The granular carbon showed a slower uptake due to diffusion limitations in the pore structure and also exhibited a steady increase in gold loading. The amount of gold loaded onto each of the carbons after 60 minutes are 81 and 7 mg Au/g C for the powdered and granular carbon respectively. These values show that the powdered activated carbon adsorbed almost 12 times more gold per gram of carbon, due to the smaller particles which allows the gold to be adsorbed very fast onto all the available surface sites and the graphitic planes. In the case of the granular carbon the molecules are subjected to diffusion through the pore system of the carbon.

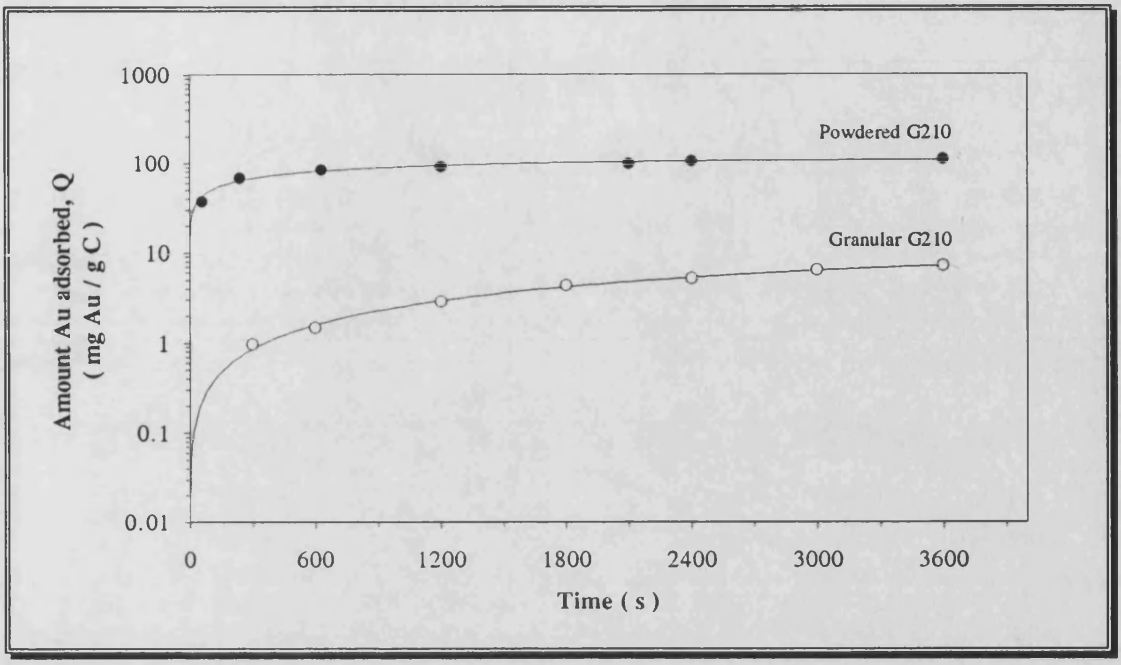

Figure 7.3 : Adsorption curves of gold cyanide onto powdered (75 -150 μm) and granular (1.2 - 2.4 mm) activated carbon G210 at 25 °C and pH=10.

7.2.2. Comparison of the reaction kinetics between granular and powdered carbons

The reaction kinetics plots for the granular and powdered carbon G210 are compared in Figure 7.4, page 155. From Figure 7.4 it can be seen that the plot for the powdered carbon was found to be non-linear, contrary to the plot found for granular carbon. This discrepancy is due to the small particle size, which enhances every stage of the adsorption model discussed in Chapter 2, section 2.7.4. In this study the reaction rate plot for the powdered carbons will be approached by linear equations in two distinct regions. The fast initial uptake will be calculated for the first 5 minutes of adsorption, and will be labeled k_1. The value of k_1 gives the fast mass transfer of gold molecules to the carbon particles and the adsorption of the molecules onto the available surface sites. The uptake of $Au(CN)_2^-$ for the time period 20 - 60 minutes

will be labeled k_2, and represents the slower adsorption rate due to the mass transfer of $Au(CN)_2^-$ in the pore network of the carbon. The adsorption of $Au(CN)_2^-$ for the period 5 - 20 minutes is a combination of mass transport of $Au(CN)_2^-$ to the surface of the carbon, and the transport of $Au(CN)_2^-$ in the pores of the carbon. No calculations will be done in this region.

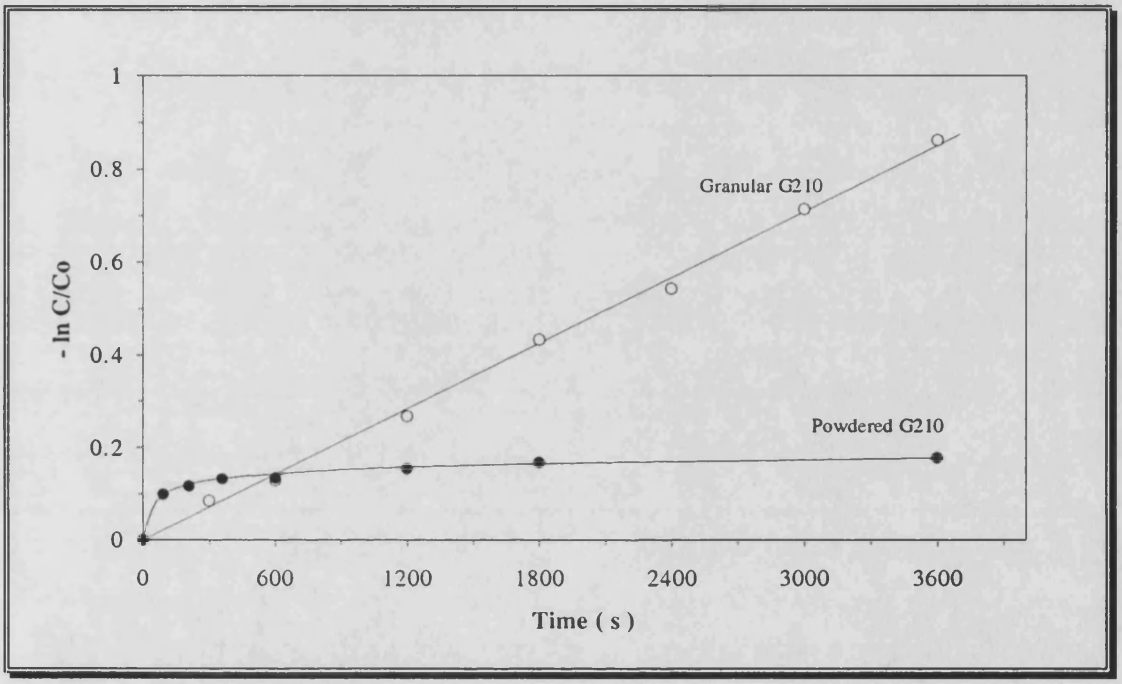

Figure 7.4 : Reaction kinetics plots for powdered (75 -150 μm) and granular (1.2 - 2.4 mm) activated carbon G210 at 25 °C and pH=10.

7.2.3. Adsorption curves for the powdered carbons prepared in this study

Representative plots for the adsorption of gold cyanide onto the powdered activated carbons prepared in this study are given in Figure 7.5.

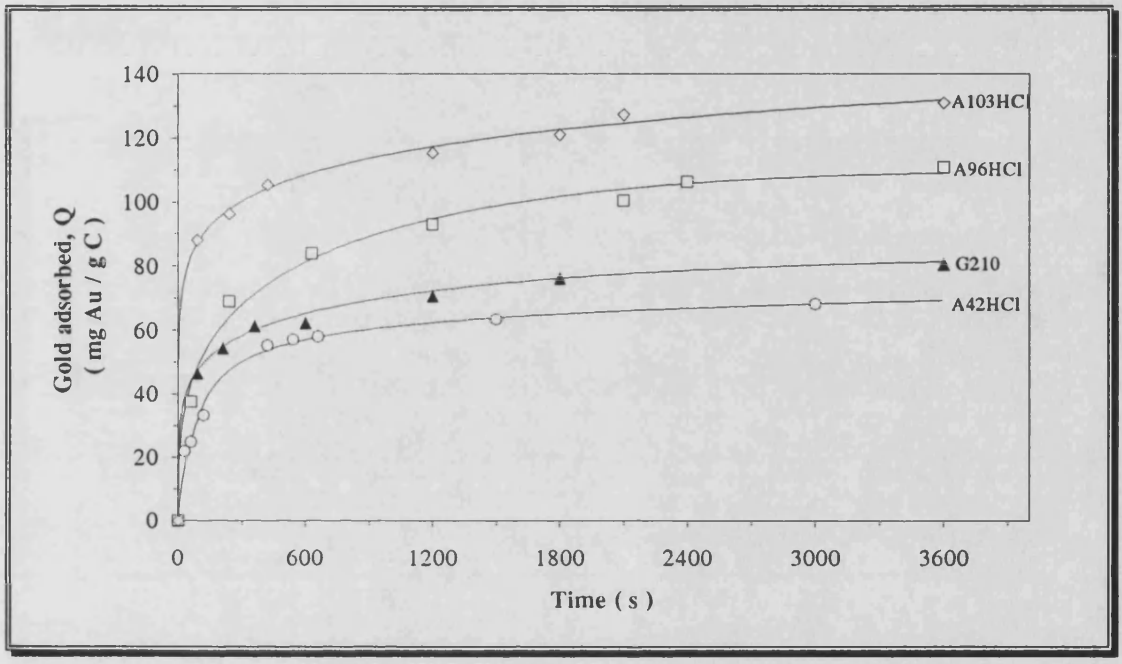

Figure 7.5 : Adsorption curves of $Au(CN)_2^-$ onto powdered activated carbons (75 -150 μm) at 25 °C and pH = 10.

The adsorption curve for carbon A42HCl is representative for the carbons prepared from Bosjesspruit coal; these curves are characterized by slow kinetics and low gold loadings onto the carbon when compared to carbon G210. The adsorption curve for carbon A96HCl is typical of the curves found for the carbons prepared from Waterberg coal, and is characterized by faster kinetics and higher gold loading values than the other carbons. The adsorption curve for carbon A103HCl is included since this was the carbon that showed the highest gold loading. From Figure 7.5 it can be seen that although the initial adsorption of gold cyanide vary for each carbon, the adsorption curves show similar adsorption kinetics after 10 minutes of contact

with the solution. The amount of $Au(CN)_2^-$ adsorbed onto the carbon after 60 minutes will be called Q_s. Although Q_s is not the equilibrium value, it will be used as a measure of the adsorptive capacity of the carbons in the following discussions.

7.2.4. Reaction kinetics and Q_s values for powdered carbons

Typical reaction kinetic plots for the powdered carbons are shown in Figure 7.6.

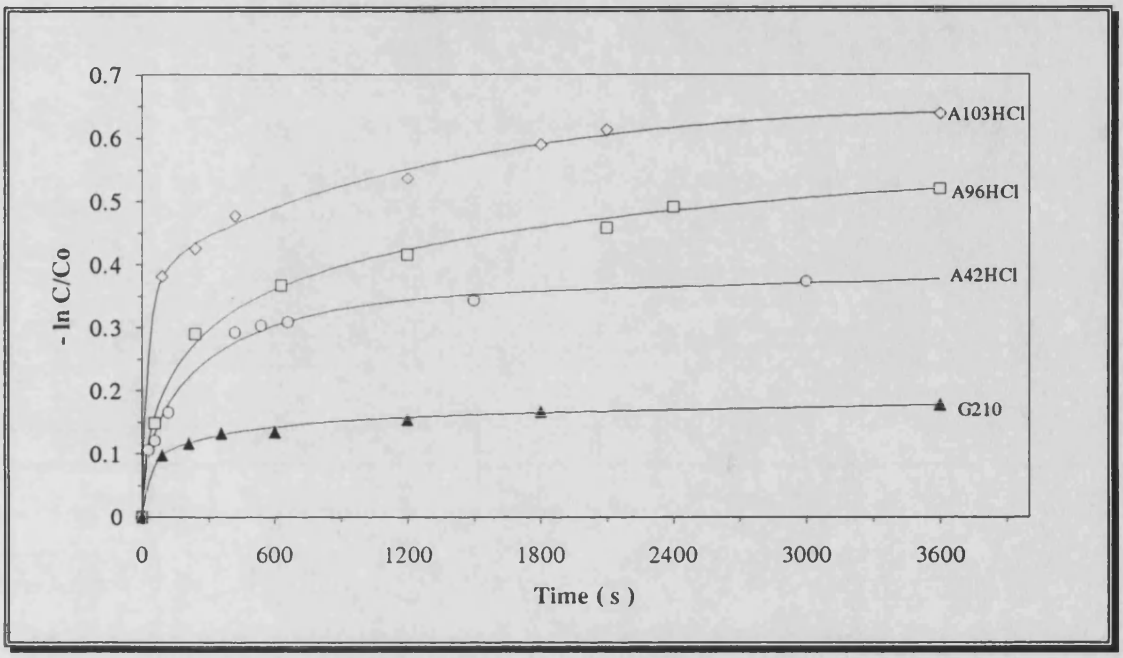

Figure 7.6 : Reaction rate plots for the adsorption of $Au(CN)_2^-$ onto powdered activated carbons (75 -150 μm) at 25 °C and pH = 10.

The porosity parameters of the carbons selected for the gold adsorption tests as well as the two observed rate constants k_1 and k_2 (calculated from the reaction kinetic plots) and the value of Q_s (calculated from the adsorption curves) are given in Table 7.2. The commercial carbons G210 and Supra are included as reference carbons.

Table 7.2 : Rate constants and Q_s values for the prepared powdered (75 - 150 μm) activated carbons.

Sample	Precursor	Activation method	BET surface area m^2/g	Micropore surface area m^2/g	Mesopore surface area m^2/g	Micropore volume cm^3/g	Macropore volume cm^3/g	Q_S mg Au·g C^{-1}	k_1 s^{-1}	k_2 s^{-1}
Supra	Peat	☹	940	855	85	0.32	0.46	111	$2.2x10^{-3}$	$9.6x10^{-6}$
G210	Coconut shell	☹	990	976	14	0.37	0.28	81	$1.1x10^{-3}$	$8.9x10^{-6}$
A65HCl	BCC	H_2O	390	375	15	0.15	0.21	49	$5.6x10^{-4}$	$2.7x10^{-5}$
A68HCl	BCC	H_2O	580	560	20	0.22	0.70	62	$3.4x10^{-4}$	$4.3x10^{-5}$
A69HCl	BCC	H_2O	670	638	32	0.26	0.80	53	$2.1x10^{-3}$	$5.0x10^{-5}$
A50HCl	BCC	CO_2	630	612	18	0.24	0.72	74	$6.5x10^{-4}$	$1.7x10^{-6}$
A42HCl	BCC	CO_2	720	696	24	0.26	0.80	69	$1.4x10^{-3}$	$2.1x10^{-5}$
A77HCl	WCC	H_2O	780	767	13	0.29	0.70	64	$9.1x10^{-4}$	$1.9x10^{-5}$
A80HCl	WCC	H_2O	640	632	8	0.24	0.05	87	$1.9x10^{-3}$	$9.1x10^{-6}$
A96HCl	WCC	CO_2	700	685	15	0.28	0.36	109	$2.5x10^{-3}$	$4.4x10^{-5}$
A103HCl	WCC	CO_2	760	620	140	0.28	0.70	132	$4.2x10^{-3}$	$4.2x10^{-5}$

☹ Activation method unknown

The carbons prepared from Bosjesspruit coal all showed lower Q_s values than the commercial carbon G210, while three of the Waterberg carbons showed superior gold loadings when compared to carbon G210. The observed rate constant k_1 varied in the range between 0.3 - 4.2 x 10^{-3} s^{-1}, with carbon A103HCl showing the highest value of 4.2 x 10^{-3} s^{-1}. Many of the prepared carbons showed higher k_1 values than G210, showing that the carbons have faster adsorption rates than the commercial carbon. The value of k_2 varied in the range of 0.17 - 5 x 10^{-5} s^{-1}, which is about 106 times lower than the values found for k_1. Some of the carbons, like A69HCl and A96HCl (Table 7.2), showed higher gold adsorption rates after 20 minutes

compared to G210, which showed little adsorption of $Au(CN)_2^-$ during the same time period.

The results from Table 7.4 are scattered, making it difficult to predict a correlation between the value of Q_s and the micropore and mesopore surface areas of the carbons. There is evidence that other factors may be influencing the adsorption of $Au(CN)_2^-$ onto the powdered carbons, and this will be discussed in detail in the following sections.

7.2.5. Calculation of the film transfer coefficient for powdered activated carbons

The film transfer coefficient k_f for the powdered carbons were calculated from the value of the observed rate constant k_1. In calculating k_f the following assumptions were made :

spherical particles $\psi = 1$

average particle diameter $d' = 100\ \mu m$

carbon particle density $\rho = 1.2\ g/cm^3$

The calculated values of k_f are given in Table 7.3, page 162.

The calculated values of k_f varied in the range of 0.4 - 4.0 x 10^{-4} m/s, with carbon A103HCl showing the largest value. The average k_f value of the powdered activated carbons are ~ 1.8 x 10^{-4} m/s, which is about 2.7 times higher than the average k_f value (6.5 x 10^{-5} m/s) calculated for the two granular carbons. This shows that the powdered carbons display less film diffusional resistance to the adsorption of $Au(CN)_2^-$ due to their smaller particle size. Low values of k_f indicates a high degree of film diffusional resistance to the adsorption of $Au(CN)_2^-$, as observed for carbons A65HCl and A68HCl. These two carbons displayed k_f values that were

similar to the k_f values of the granular activated carbons. Higher S'_{BET} values in samples A103HCl and Supra resulted in higher k_f values, but the commercial carbon G210 showed a low k_f value of 1.1 x 10^{-4} m/s, which is surprisingly low when the BET surface area of the carbon is taken into account. This suggests that in the case of the powdered activated carbons the rate of gold loading, and the final amount of gold adsorbed onto the carbon from the $Au(CN)_2^-$ solution, is not solely a factor of the available surface area. This was investigated further and is the subject of the following sections.

Table 7.3 : Film transfer coefficients k_f for the powdered (75 - 150 μm) activated carbons.

Sample	Precursor	Activation method	BET surface area m^2/g	Micro-pore surface area m^2/g	Meso-pore surface area m^2/g	Micro-pore volume cm^3/g	Macro-pore volume cm^3/g	k_1 s^{-1}	k_f m/s
Supra	Peat	☹	938	853	85	0.32	0.46	$2.2x10^{-3}$	$2.9x10^{-4}$
G210	Coconut shell	☹	988	974	14	0.37	0.28	$1.1x10^{-3}$	$1.1x10^{-4}$
A65HCl	BCC	H_2O	394	379	15	0.15	0.21	$5.6x10^{-4}$	$6.3x10^{-5}$
A68HCl	BCC	H_2O	578	558	20	0.22	0.70	$3.4x10^{-4}$	$3.9x10^{-5}$
A69HCl	BCC	H_2O	666	634	32	0.26	0.80	$2.1x10^{-3}$	$2.0x10^{-4}$
A50HCl	BCC	CO_2	626	608	18	0.24	0.72	$6.5x10^{-4}$	$1.4x10^{-4}$
A42HCl	BCC	CO_2	721	697	24	0.26	0.80	$1.4x10^{-3}$	$2.0x10^{-4}$
A77HCl	WCC	H_2O	776	763	13	0.29	0.70	$9.1x10^{-4}$	$1.1x10^{-4}$
A80HCl	WCC	H_2O	637	629	8	0.24	0.05	$1.9x10^{-3}$	$1.9x10^{-4}$
A96HCl	WCC	CO_2	695	680	15	0.28	0.36	$2.5x10^{-3}$	$2.3x10^{-4}$
A103HCl	WCC	CO_2	760	623	137	0.28	0.70	$4.2x10^{-3}$	$4.0x10^{-4}$

☹ Activation method unknown

7.3. Correlation between Q_s and the rate constants k_1 and k_2

Figure 7.7 shows the graph for the data of Q_s *vs* k_1. In the graph a linear fit to the data was performed with all the data points carrying the same weight. The prediction limits for a 95 % confidence interval is included in the graph. These limits are based on predicting the ordinate value for a random abscissa value, and is calculated from the standard errors of the data. Smaller prediction bands will be due to smaller standard errors and means a better fit of the linear equation to the data. A linear fit for the data of Q_s *vs* k_1 resulted in a correlation coefficient of 0.87, showing that higher gold loadings is due to faster initial rate constants.

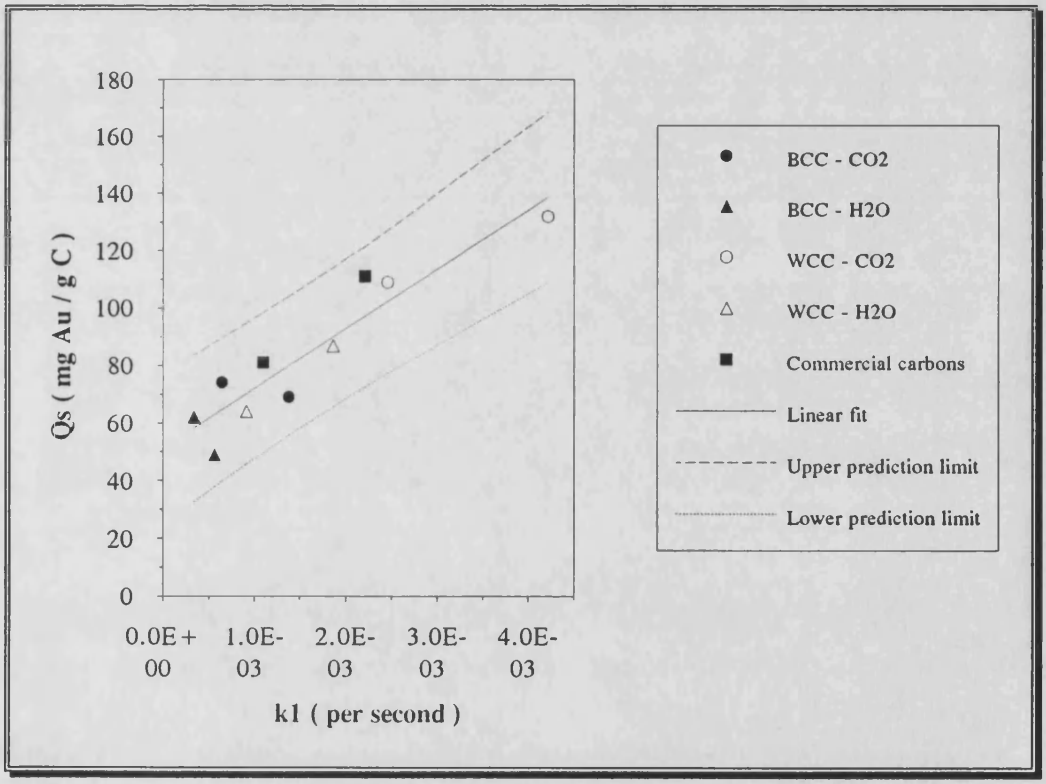

Figure 7.7 : Graph of Q_s *vs* k_1 for powdered activated carbons.
(r^2 for linear fit = 0.87)

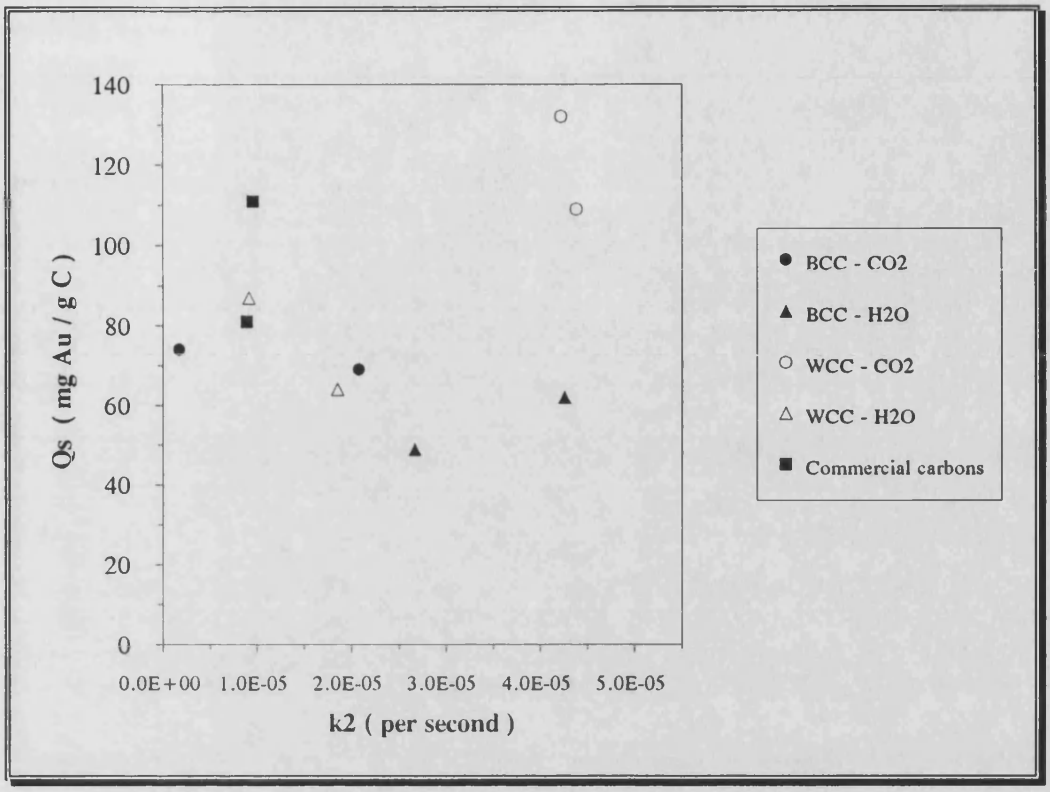

Figure 7.8 : Graph of Q_s *vs* k_2 for powdered activated carbons.

Figure 7.8 shows the graph for the data of Q_s *vs* k_2. This data was scattered, suggesting that the rate constant after 20 minutes of adsorption is little influenced by the value of Q_s.

7.4. Influence of the structural parameters of the carbons on Q_s

The influence of the micropore surface areas of the powdered carbons on the value of Q_s are represented graphically in Figure 7.9. The data suggests a positive correlation for the BCC carbons, showing that the amount of gold loaded is influenced by the available S_{micro}. There is evidence for a negative correlation for the WCC carbons, showing that the higher Q_s values in these carbons are strongly influenced by other factors than the available S_{micro}. The data for the graph of Q_s *vs* mesopore surface area, Figure 7.10, show that the Q_s value is little influenced by

S'_{BET} values < 30 m^2/g, although S'_{BET} values > 80 m^2/g seemed to produce higher Q_s values.

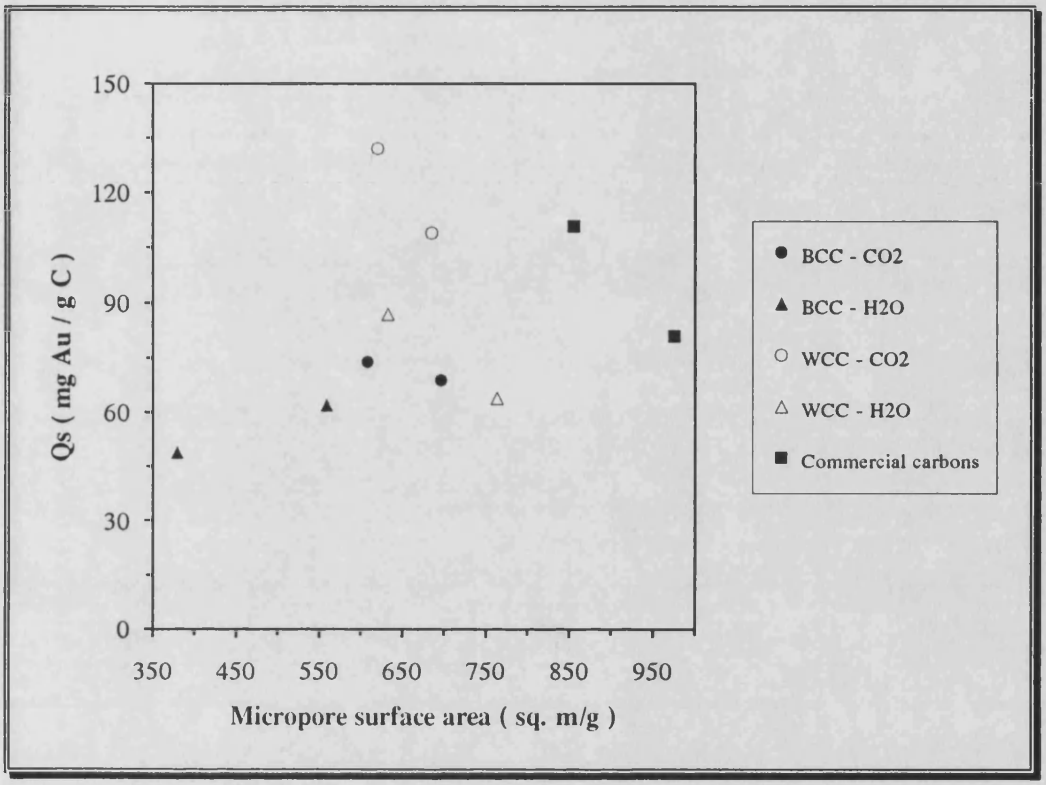

Figure 7.9 : Graph of Q_s *vs* S_{micro} for powdered activated carbons.

No correlation.

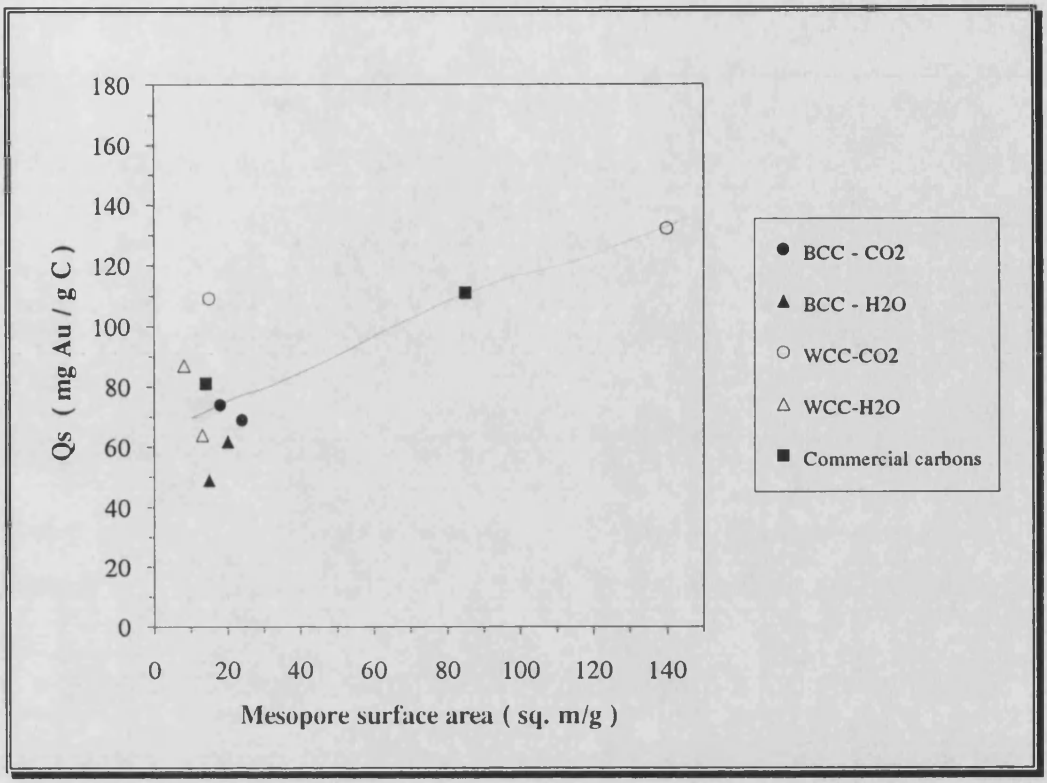

Figure 7.10 : Graph of Q_S *vs* S'_{BET} for powdered activated carbons.

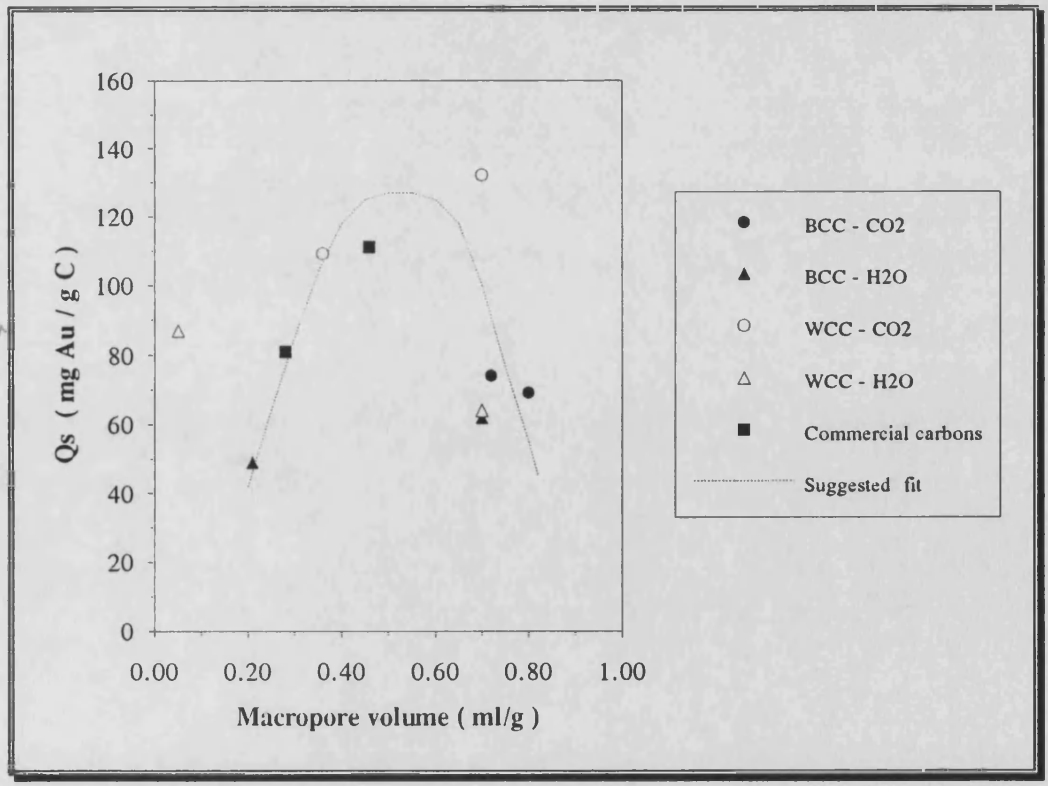

Figure 7.11 : Graph of Q_S *vs* V_{macro} for powdered activated carbons.

There is evidence that the Q_s - V_{macro} relationship reaches a maximum value before declining. This suggested fit is indicated by the dotted curve in Figure 7.11. Large macropore volumes will prevent any adsorption of $Au(CN)_2^-$ onto the carbon, but a well developed macropore system can ensure fast transport of the gold molecules through the pore network of the carbon. This suggests that the process of adsorption of gold cyanide has reached the intermediate stage in the model of Fuerstenau *et al.* [1987] in which gold adsorption is controlled by diffusion through transport pores. These observations all suggest that for powdered activated carbon the adsorption of gold cyanide is enhanced by a well developed macro-mesopore system. A substantial microporosity can give access to the basal planes for adsorption of $Au(CN)_2^-$ as suggested by Jones *et al.* [1989] (section 2.7.4), thus acting as a sink for the adsorbed species, but the microporosity of the sample does not appear to be important in controlling the rate of adsorption. This observation is supported by the fact that the commercial carbon G210 had the largest micropore surface area, but did not exhibit the largest Q_s value.

7.5. Influence of the chemical structure of the carbons on Q_s

7.5.1. Influence of C,H,N and O content of the carbons on Q_s

Figures 7.12 - 7.20 represents the plots of Q_s against the dry, ash free elemental content of the carbons. An average linear plot has been fitted to the data as before, and includes 95 % prediction limits for the correlation. Figure 7.11 gives the correlation of Q_s *vs* the carbon content of the activated carbons.

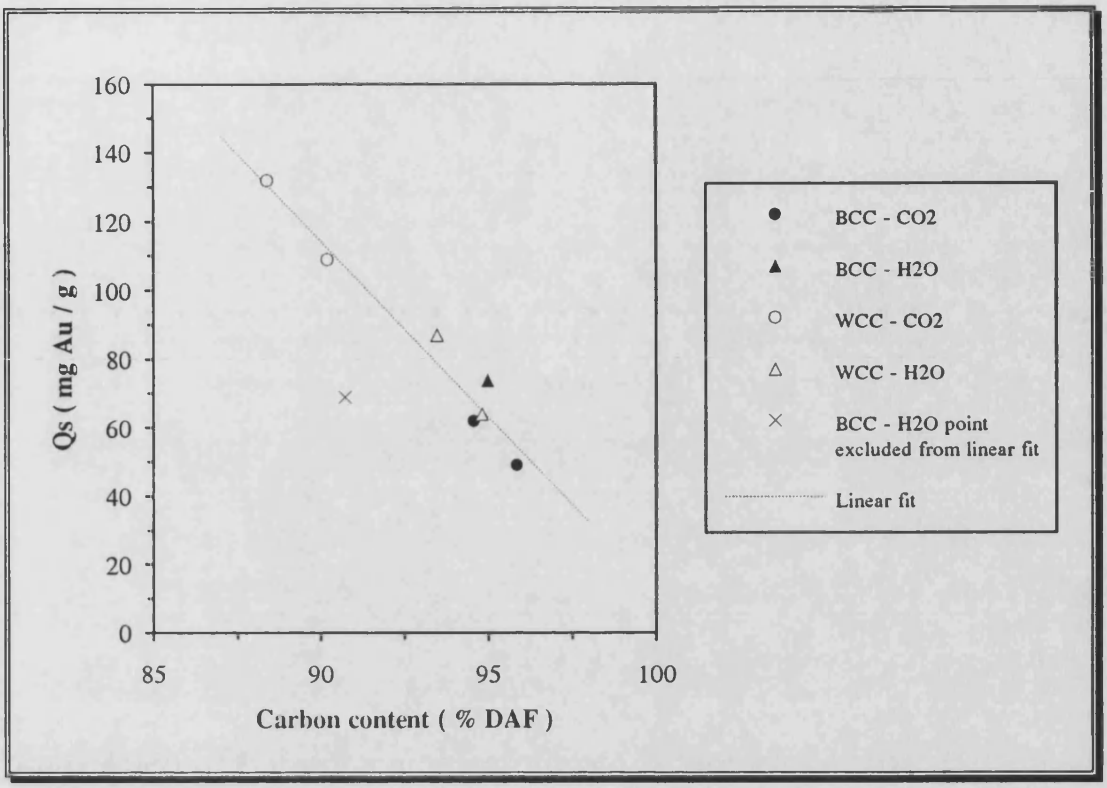

Figure 7.12 : Correlation between Q_s and the carbon content of powdered activated carbons. (r^2 for linear fit = 0.95)

The trend of the data suggests that a lower carbon content can lead to higher values of Q_s. Increased activation of the activated carbon leads to an increase in carbon content, due to the removal of hetero-elements during the activation process. These elements may be oxygen functional groups, which, if removed, would lead to a decrease in Q_s values. These results also suggest that good adsorption results can be obtained with moderately activated carbons, eliminating the need for the resources to produce a highly activated carbon.

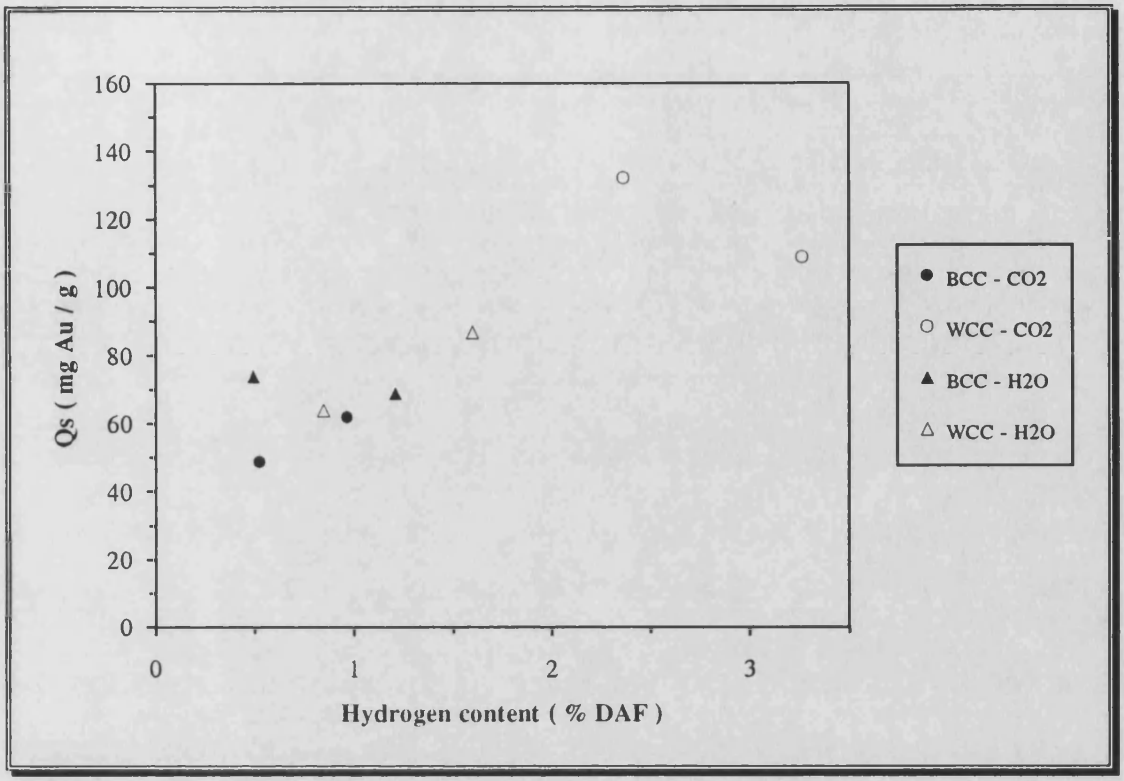

Figure 7.13 : Graph of Q_s *vs* the hydrogen content of powdered activated carbons.

The graph of Q_s *vs* the hydrogen content of the carbons in Figure 7.12 suggest that a higher hydrogen content can lead to an increase in the amount of $Au(CN)_2^-$ that can be adsorbed onto the carbon. The reason for this may be that the hydrogen is associated with the oxygen functional groups such as - OH and - COOH.

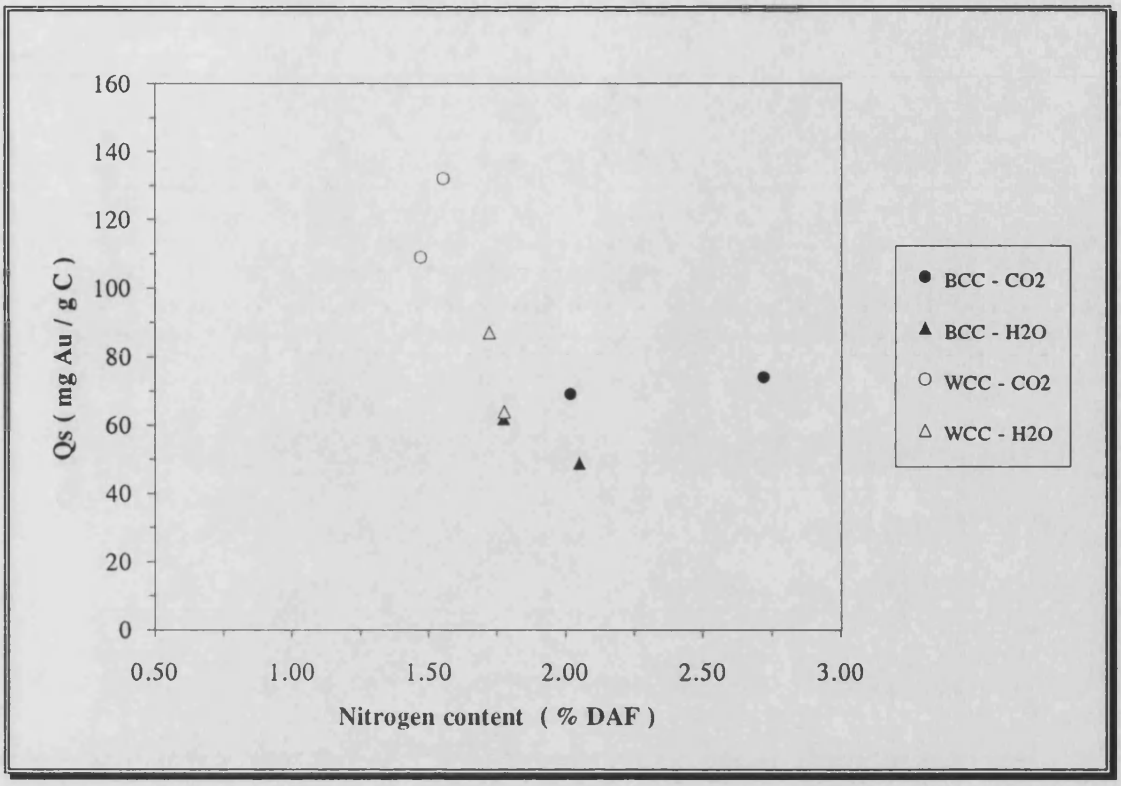

Figure 7.14 : Graph of Q_s *vs* the nitrogen content of powdered activated carbons.

Figure 7.13 is the graph of Q_s *vs* nitrogen content of the carbons. Although the range of the nitrogen content is small, there is evidence that nitrogen functionality in the WCC carbons negatively influences the adsorption of $Au(CN)_2^-$ onto the carbon. The results for the BCC carbons are scattered, making a prediction difficult.

A linear correlation ($r^2 = 0.88$) can be established for the relationship between Q_s and the amount of oxygen present in the carbons, shown in Figure 7.14, page 171. The importance of oxygen containing functional groups in the adsorption of gold cyanide has been shown in Chapter 2, section 2.7.5. The positive trend observed in this study confirms the results found by Tshuchida and Muir [1986] that a decrease in surface functional groups on the surface of the carbon leads to a decrease in the amount of $Au(CN)_2^-$ that can be adsorbed onto the carbon.

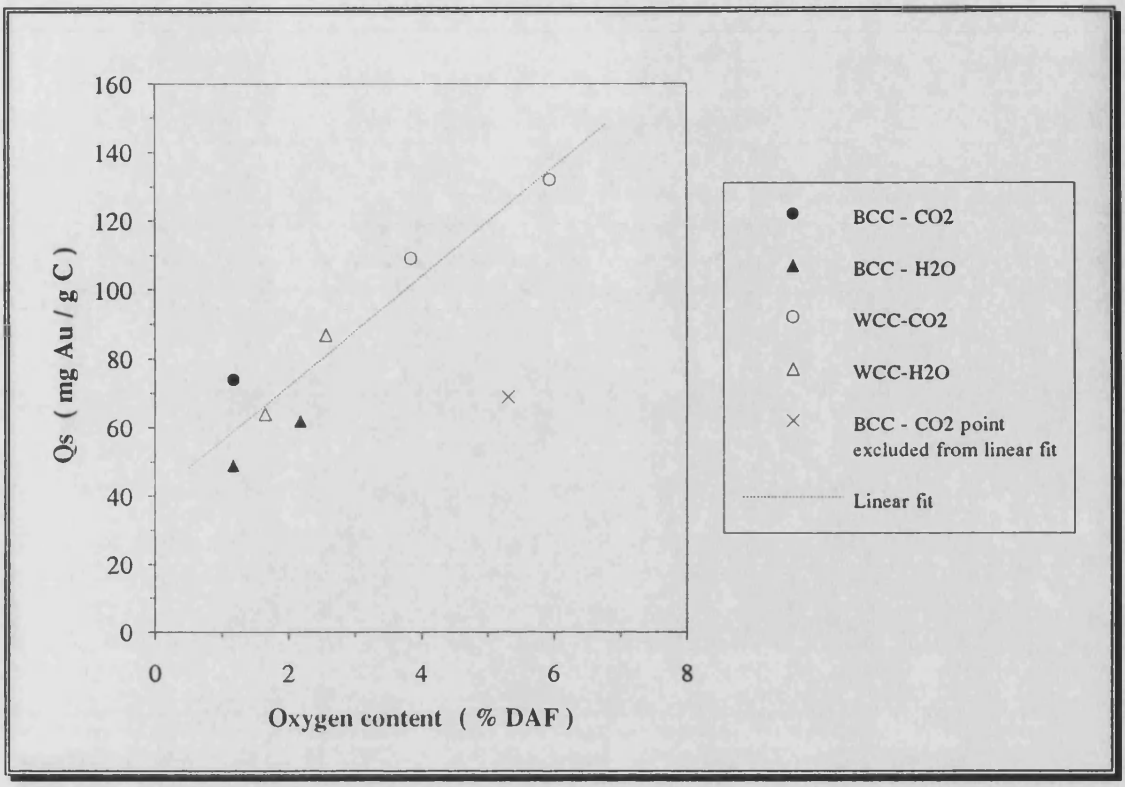

Figure 7.15 : Correlation between Q_s and the oxygen content of powdered activated carbons. (r^2 for linear fit = 0.88)

7.5.2. Influence of sulphur and ash content of the carbons on Q_s

The plot of Q_S vs the sulphur content of the carbons is given in Figure 7.15, page 172. Contrary to expectations the powdered activated carbon samples showed an increase in the value of Q_s as the sulphur content of the samples increased. Little is known about the reaction of sulphur-containing species with gold cyanide. Grabovskii *et al.* [1977] in conducting gold elution experiments from an activated carbon prepared from a phenol-formaldehyde polymer, found that the gold could only be desorbed if strong ligands such as SCN^- were present in the eluant. They concluded that a complex was formed during the elution between the gold cyanide and the ligand. There has also been investigations into using thiourea and thiosulphate as lixiviants during the leaching process [Prasad *et al.* 1991].

Why should a relatively small amount of sulphur influence the capacity by a factor of 2

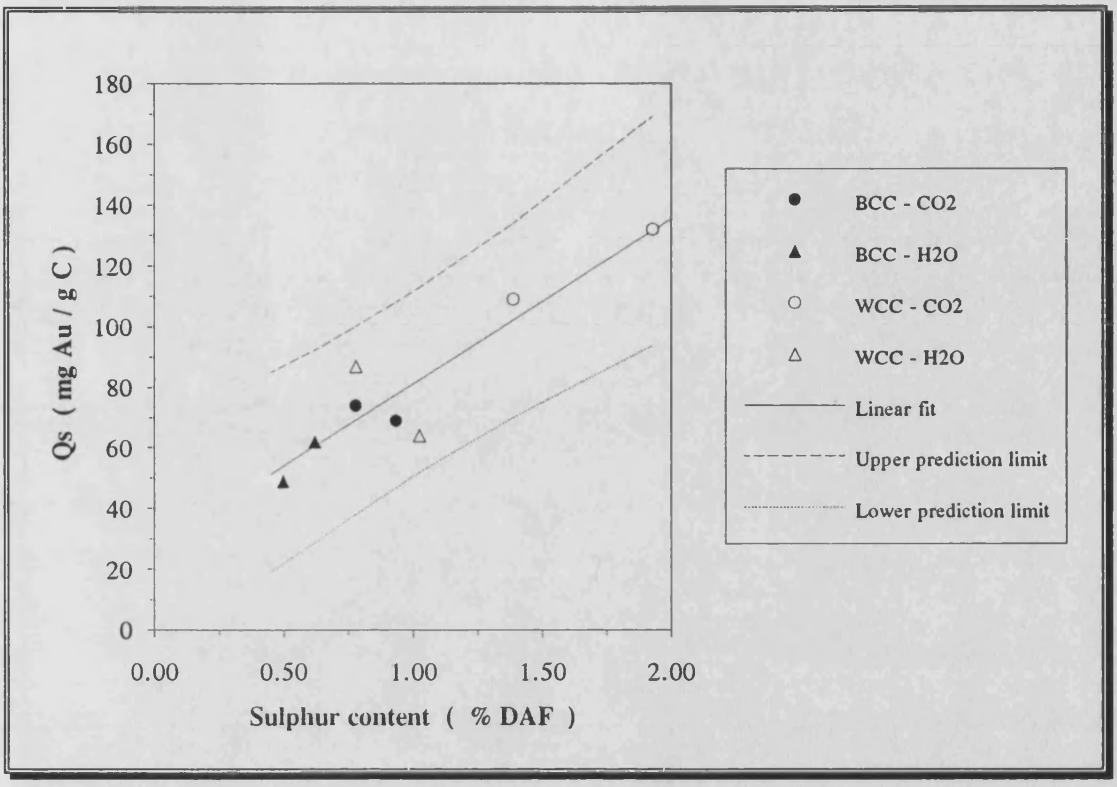

Figure 7.16 : Correlation between Q_s and the sulphur content of powdered activated carbons. (r^2 for linear fit = 0.87)

The plot for Q_s *vs* the ash content of the carbons also showed a positive trend, as is shown in Figure 7.16, page 173. Carbonaceous matter in the minerals in the form of kerogen is known to have an affinity for gold while clays and pyrite have been suspected, but not confirmed. [Hausen and Bucknam 1984] This observation, taken with the positive trend found for the Q_s - sulphur content relationship, suggest that gold cyanide may have affinities with certain S - containing species in the mineral matter in the activated carbon powders. Sulphur in coal is usually in the form of mineral matter e.g. sulphides and sulphates, and as organic S, e.g. thioeters and thiophens. The chemical nature of the thermally transformed S species in the activated carbons is unknown; but the carbons were analyzed for pyritic, organic and

sulphate forms. The relationships between Q_s each of these species are represented in Figures 7.17 - 7.18 respectively.

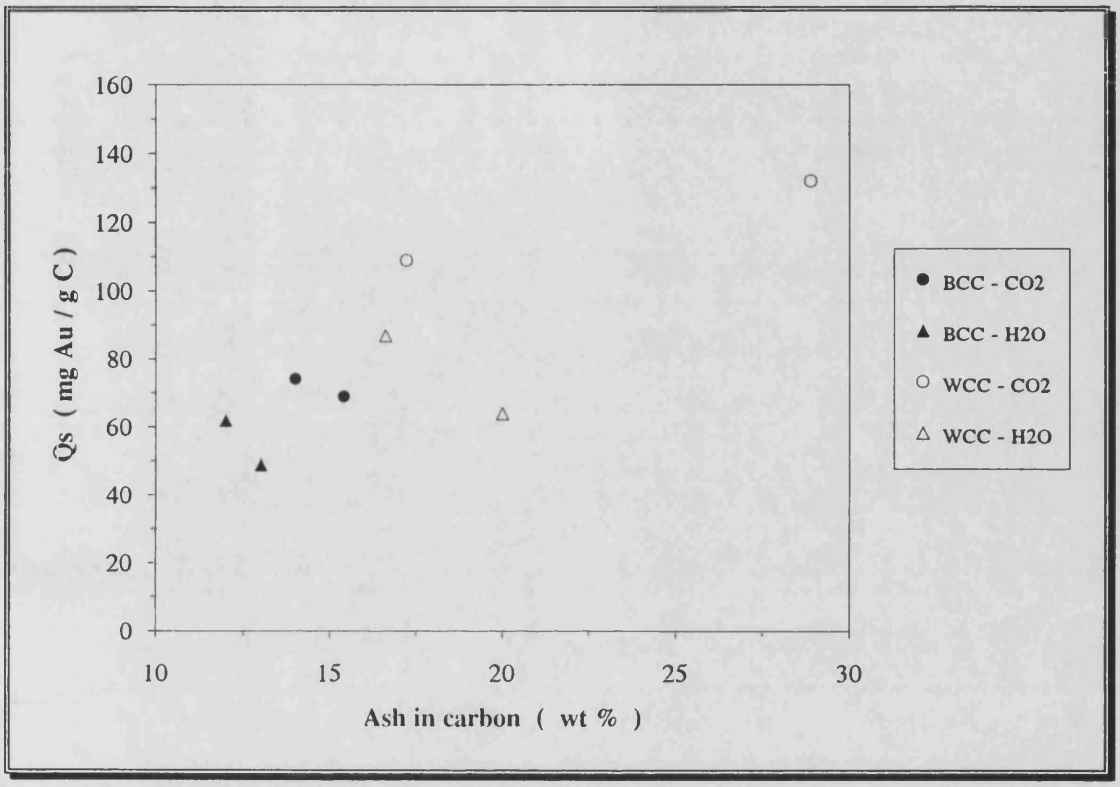

Figure 7.17 : Graph of Q_s *vs* the ash content of powdered activated carbons.

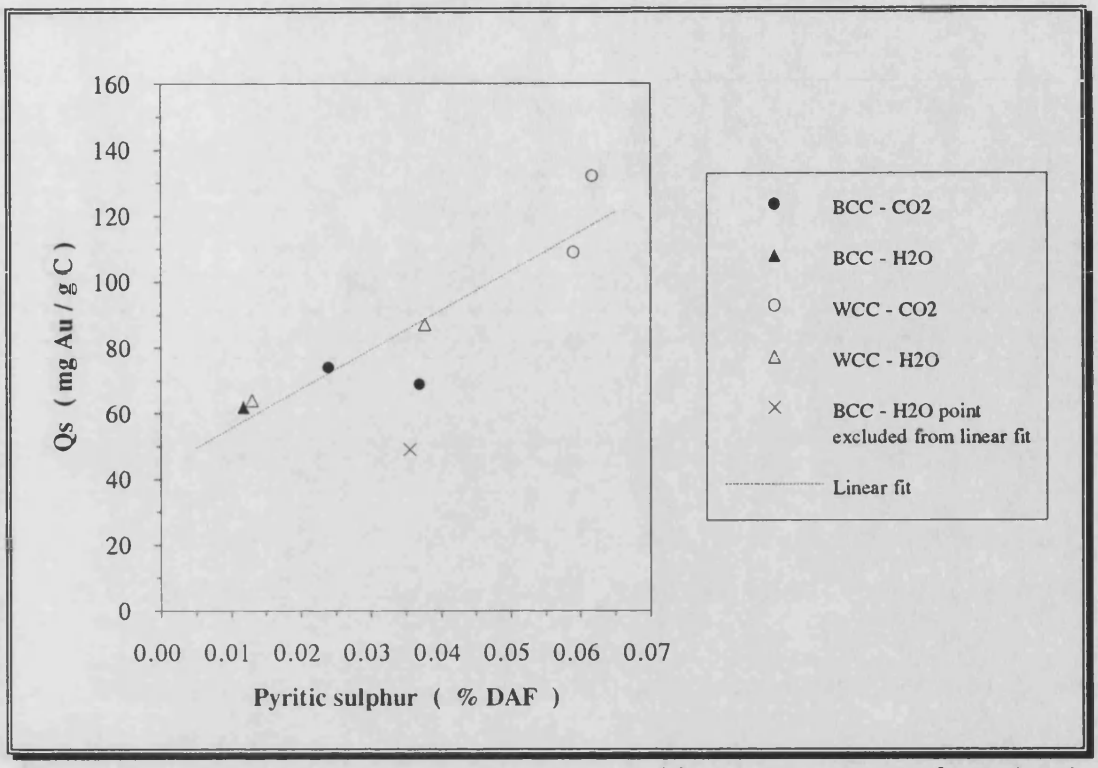

Figure 7.18 : Correlation between Q_s and the pyritic sulphur content of powdered activated carbons. (r^2 for linear fit = 0.85)

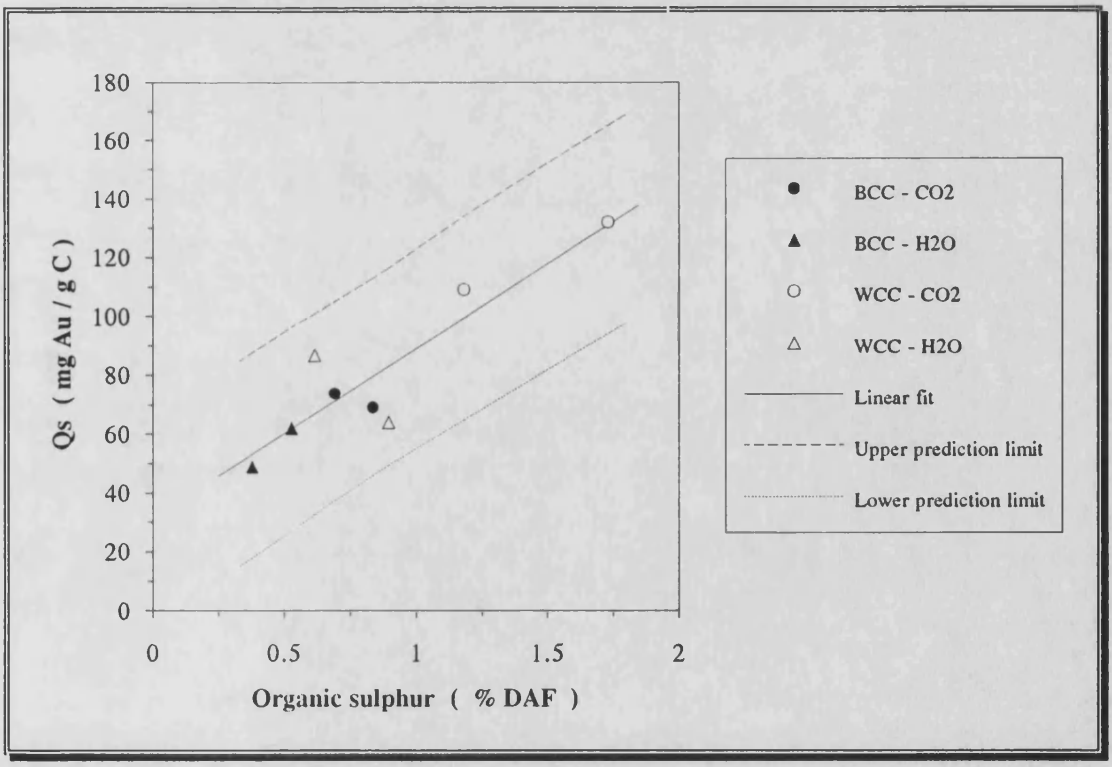

Figure 7.19 : Correlation between Q_s and the organic sulphur content of powdered activated carbons. (r^2 for linear fit = 0.83)

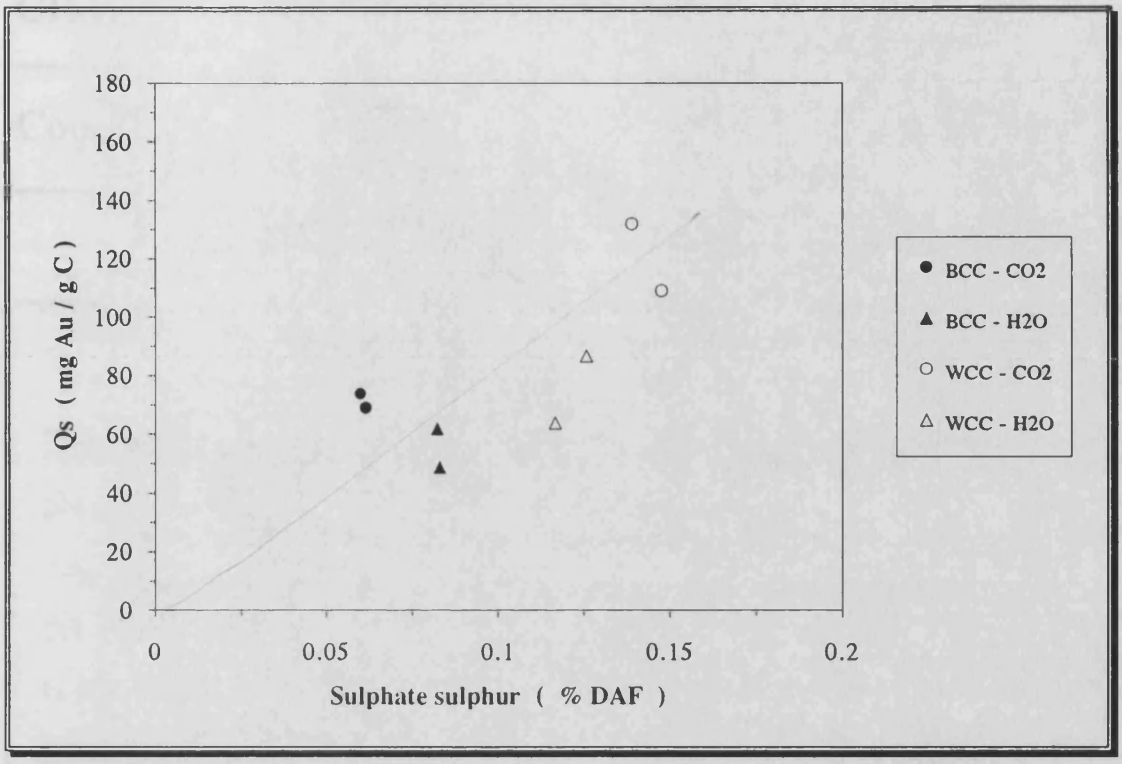

Figure 7.20 : Graph of Q_s *vs* the sulphate content of powdered activated carbons.

Although the data for the sulphate form of sulphur is scattered, there is evidence that an increase in sulphate sulphur leads to higher Q_s values in the WCC carbons, but leads to a decrease in the BCC carbons. The pyritic and organic forms of sulphur showed a positive correlation, similar to the plot of Q_s *vs* elemental sulphur in Figure 7.16 on page In a study of the adsorption of $Au(CN)_2^-$ onto components of gold bearing ore Hausen and Bucknam [1984] found that a pyrite sample from Colorado, U.S.A. showed evidence of gold adsorption if the pyrite concentration was high (> 40 %). Although the pyritic forms of sulphur differs in the ore and the activated carbon, the results of this study prove that the thermally transformed pyrite has an affinity for gold cyanide.

CHAPTER 8

Concluding remarks and future research

Summary

This chapter summarizes the beneficiation and activation results for the physical and chemical activation of the South African coals used in this study before commenting on the results of the gold cyanide adsorption tests. Finally, the porosity of the final activated carbon products after the acid washing is compared to two commercially - available carbons. Suggestions for further research concludes this chapter.

8.1. Preparation of the coal

A characteristic of the South African coals used in this study to prepare activated carbon is their high mineral matter content. Some of the minerals are inherent to the coal structure and are difficult or impossible to remove by conventional cleaning techniques. A high mineral matter content in the precursor coal will be thermally transformed to ash during the activation process, leading to reduced mechanical strength in the activated carbon product and may also block entrances to some of the pores.

This research has shown that the column flotation technique is successful in reducing the mineral matter content of the coals. The mineral matter content of the

Bosjesspruit coal decreased from 24 to 12 wt. % with an overall product yield of 76 wt. % after the second flotation step. It was found that the vitrinite and exinite macerals were removed in the tailings, leading to a coal product with an inertinite content of 89 vol. %.

In the case of the Waterberg coal, the mineral matter content was reduced from 60 to 11 wt. % using a two-step flotation, but the product yield was only 22 wt. %. In contrast to the Bosjesspruit coal, the Waterberg coal did not exhibit selective flotation of macerals.

Carbonization of the coals at a heat treatment temperature 600 °C for a soak time of 40 minutes showed a faster devolatilization rate for the Waterberg coal, also leading to a larger final weight loss in the char. Little porosity was developed in the carbonized chars.

8.2. Physical activation

The WCC activated carbons exhibited the highest BET surface area, followed by the BCC and the BROM carbons. The difference in the behaviour of the BCC and WCC chars to the activation process is not only a function of the mineral matter content, which is known to act as a catalyst during the activation process, but can also be ascribed to the maceral contents of the coal precursors. [Crelling *et al.* 1988; Ehrburger *et al.* 1988; Hunt *et al.* 1986; Jones *et al.* 1985; Serio *et al.* 1989]

For all three coal precursors (BROM, BCC and WCC) steam activation of the carbonized chars developed the highest degree of micro- and meso-porosity for a char burn-off of less than 40 wt. %. Similar results were found by Tomków *et al.* [1977] in the steam activation of brown coal chars. For sample burn-offs higher than

40 wt. % in the BCC and BROM carbons, the steam activation process creates mesopores by the burn-out of existing micropores, resulting in a carbon with a higher degree of mesoporosity. There is evidence that these results are reversed for the WCC carbons, which showed higher mesoporosity by CO_2 activation for sample burn-offs larger than 40 wt. %. Except for one sample prepared from the WCC chars at 950 °C by CO_2 activation for 4 h activation time, all the samples showed a mesoporous surface area constituting less than 10 % of the total BET surface area. Single parameter estimates of the micropore width showed an increase in micropore width with increased activation. The WCC carbons displayed narrower pore widths than the BCC or BROM carbons for sample burn-offs less than 40 wt. %, but the pore widths were wider in the WCC carbons for burn-offs higher than 40 wt. %.

Czechowski and Kidawa [1991], in a reactivity study of steam and CO_2 gasification of coal macerals, found that the reactions of steam proceeds preferentially at the internal surface of the pore char surface, within pores of a radius smaller than 7.5 μm. The CO_2 reactions on the other hand occur mainly at the external char surface. Their results suggested that the steam molecules have a greater ability to penetrate the char pore system, and would thus lead to a better development of microporosity, which is also seen in this study. This is contrary to expectations, because the reaction rate of CO_2 is lower than for steam, and thus higher penetration is expected for the CO_2 molecules.

Czechowski and Kidawa also found that the porosity of the maceral gasification products differed, with the fusinite char exhibiting the highest microporosity, while the vitrinite char displayed a high degree of mesoporosity. These results support the observations obtained in this study of high mesoporosity in the CO_2 activation of the vitrinite rich WCC chars, but this study also found the highest microporosity in the WCC chars. This discrepancy may be due to the inherent mineral matter associated

with the macerals. They also found that the total pore volume of micro- and meso-pores in the gasification products decreased in the order vitrinite > fusinite > exinite; in this study the pore volumes decreased (for a given burn-off) WCC carbons (vitrinite rich) > BCC carbons (inertinite rich) > BROM carbons (inertinite rich, high in ash).

The ash in the BROM activated carbons was found to be concentrated mainly in the macro- and mesopores, while the ash was predominantly concentrated in the mesopores for the BCC and WCC activated carbons. Removal of the ash by a mild acid washing gave access to micropores previously blocked by the ash. In some cases a decrease in the surface areas and pore volumes were found - this may be due to the collapse of the pore structure when the ash is removed, or a displacement of the ash from cavities to the entrances of apertures, as suggested by Mahajan and Walker [1979]. There is evidence that the chemical activation of the chars renders the ash into a HCl - insoluble form.

8.3. Chemical activation

The BET surface areas of the WCC and BCC carbons prepared by chemical activation using H_3PO_4 as activating agent were much lower than the maximum surface areas obtained by physical activation of the coal chars. The values of the surface areas went through a maximum at a heat treatment temperatures of 550 °C and phosphorus was found incorporated into the carbon structure during the activation process. Similar results were found by Derbyshire *et al.* [1991b] and Laine *et al.* [1989]. The results of Derbyshire *et al.* suggest that there is a condensation reaction of phosphates to polyphosphates; evidence was also found for the presence of inorganic hydrophosphate groups and P_2O_5. The decrease in surface area at heat treatment temperatures higher than 550 °C was ascribed to a major structural rearrangement that occurs in the carbon. Although Derbyshire and his

group found a positive linear correlation for the phosphorus - ash content of the carbons, the results for this study were scattered.

8.4. Comparison between carbons prepared in this study and commercially - available activated carbons

The surface areas and pore volumes of the acid washed carbons are compared to the two commercial carbons Supra and G210 in Figures 8.1 - 8.8. In the figures the postscript C denotes samples activated by CO_2 while the postscript S denotes samples activated using steam as the activating agent. The BROM carbons had insufficient porosity when compared to the commercial samples, but the carbons prepared from the column cleaned coals, and especially the WCC carbons, showed porosities approaching the values found for the commercial carbons. All the prepared samples however displayed high macropore volumes, due to the high ash content of the coal precursors. Although the H_3PO_4 activation produced samples with substantial porosity, it can be seen from the figures that the samples compare unfavourably to the commercial carbons, especially exhibiting excessive macroporosity.

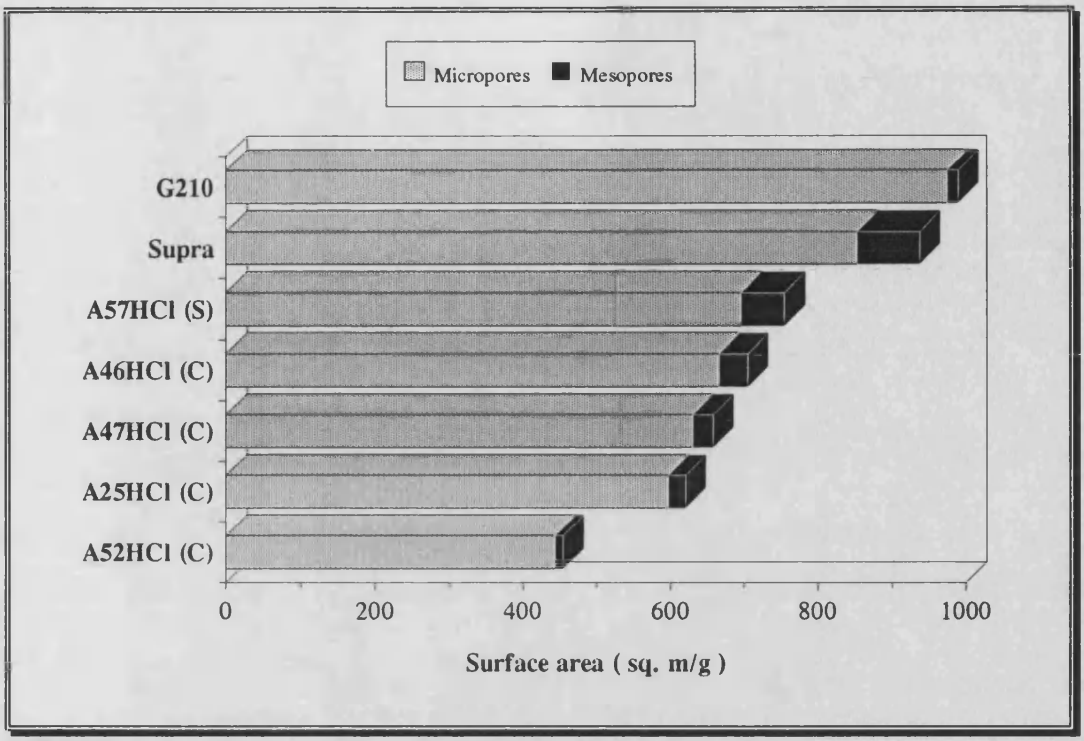

Figure 8.1 : Comparison between the surface areas of commercial and BROM activated carbons.

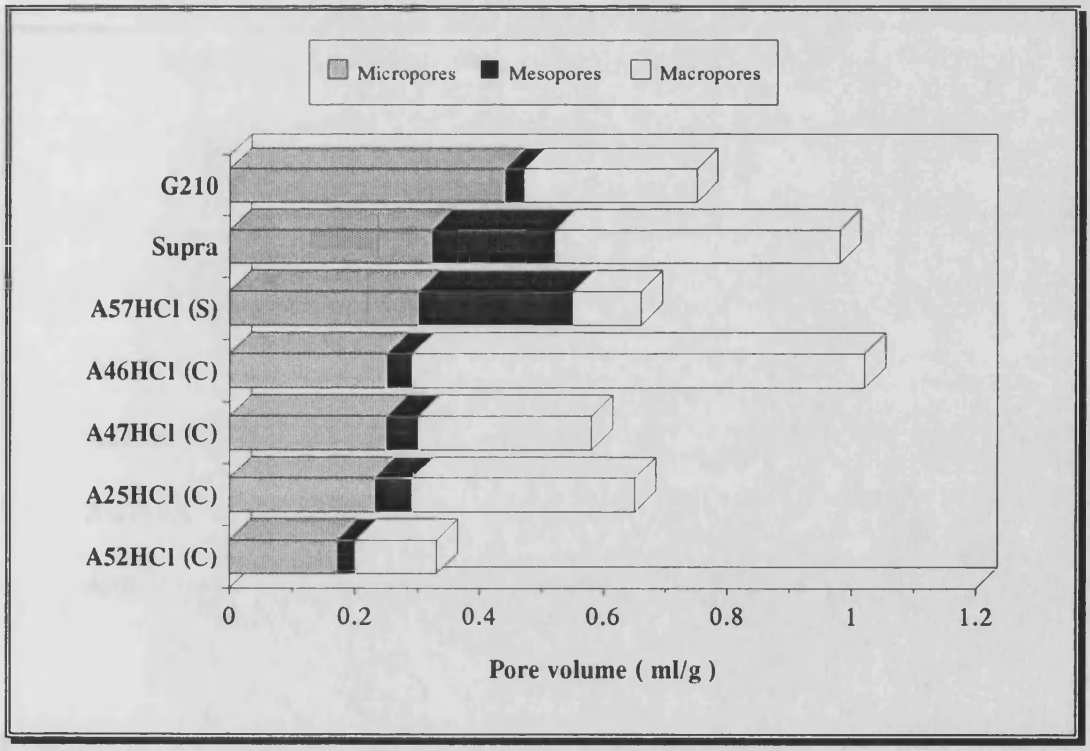

Figure 8.2 : Comparison between the pore volumes of commercial and BROM activated carbons.

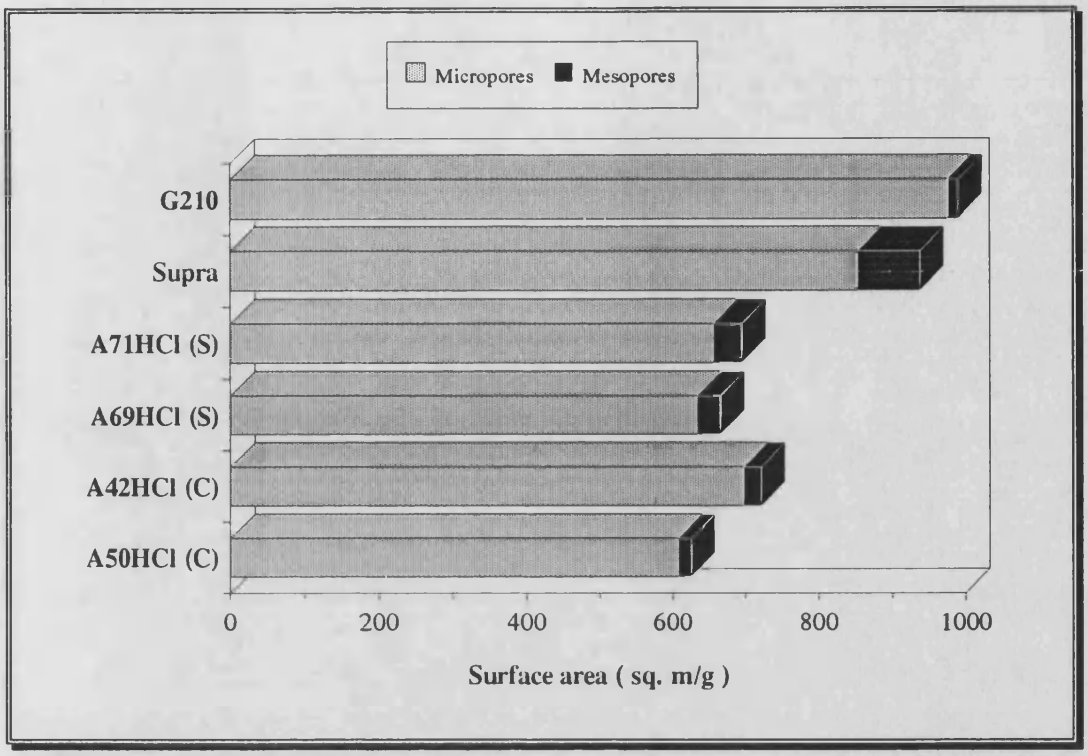

Figure 8.3 : Comparison between the surface areas of commercial and BCC activated carbons.

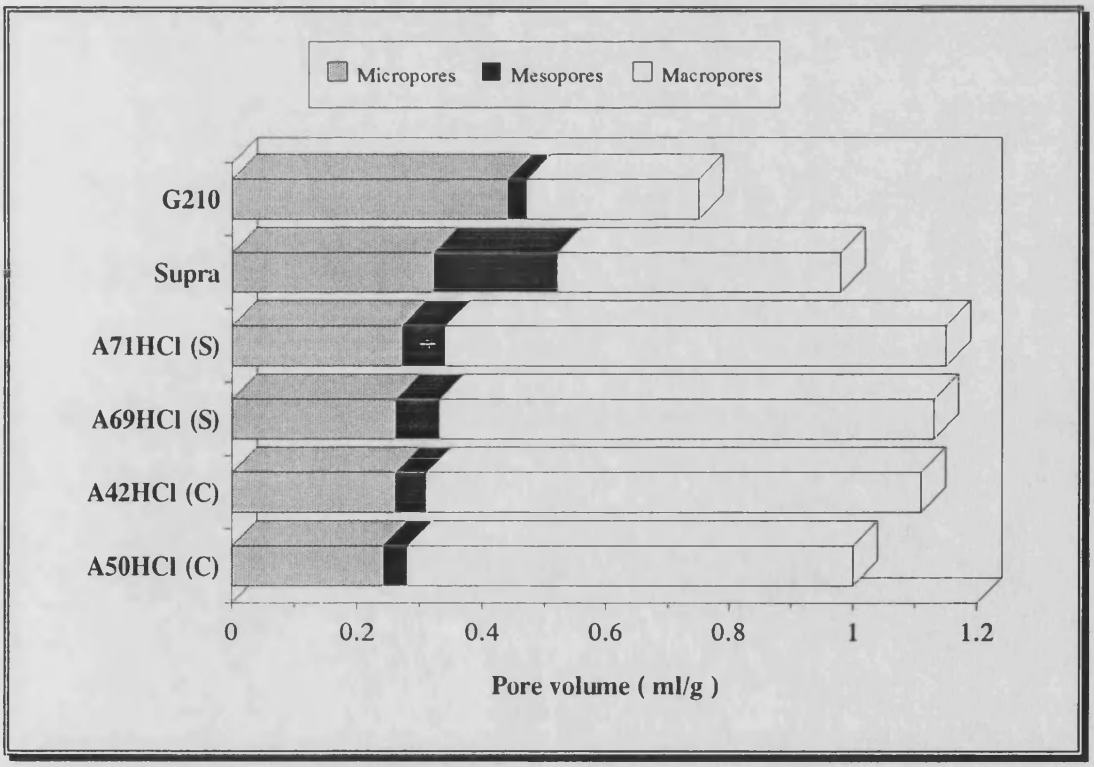

Figure 8.4 : Comparison between the pore volumes of commercial and BCC activated carbons.

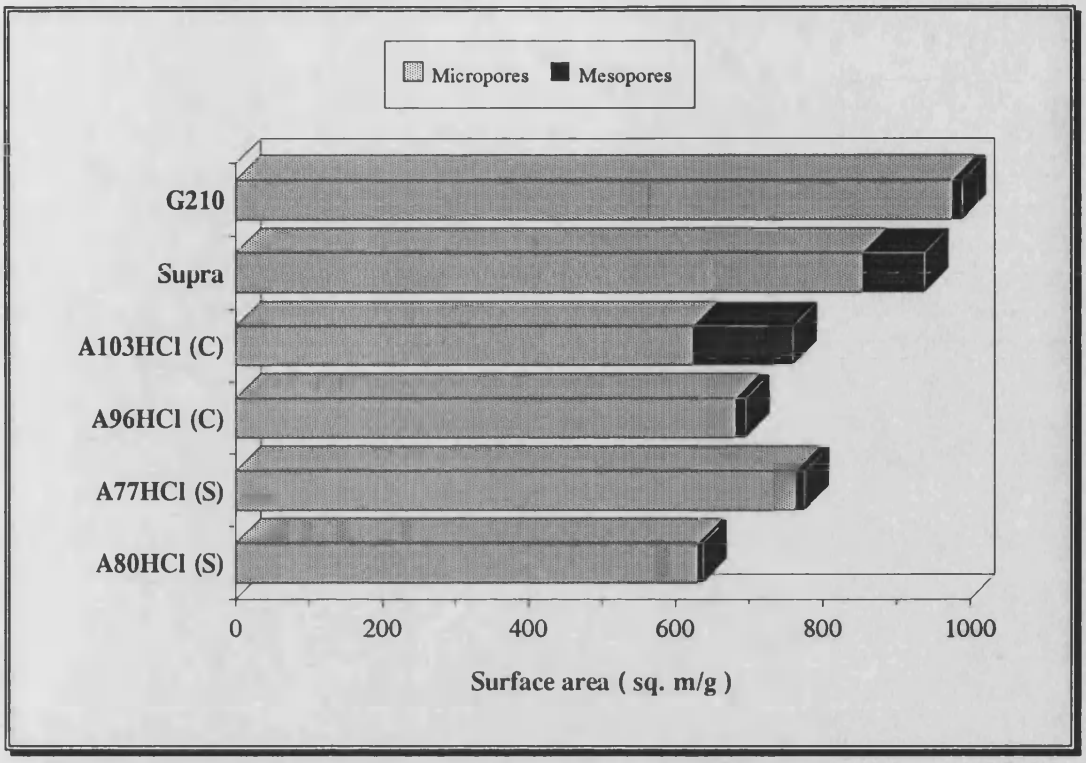

Figure 8.5 : Comparison between the surface areas of commercial and WCC activated carbons.

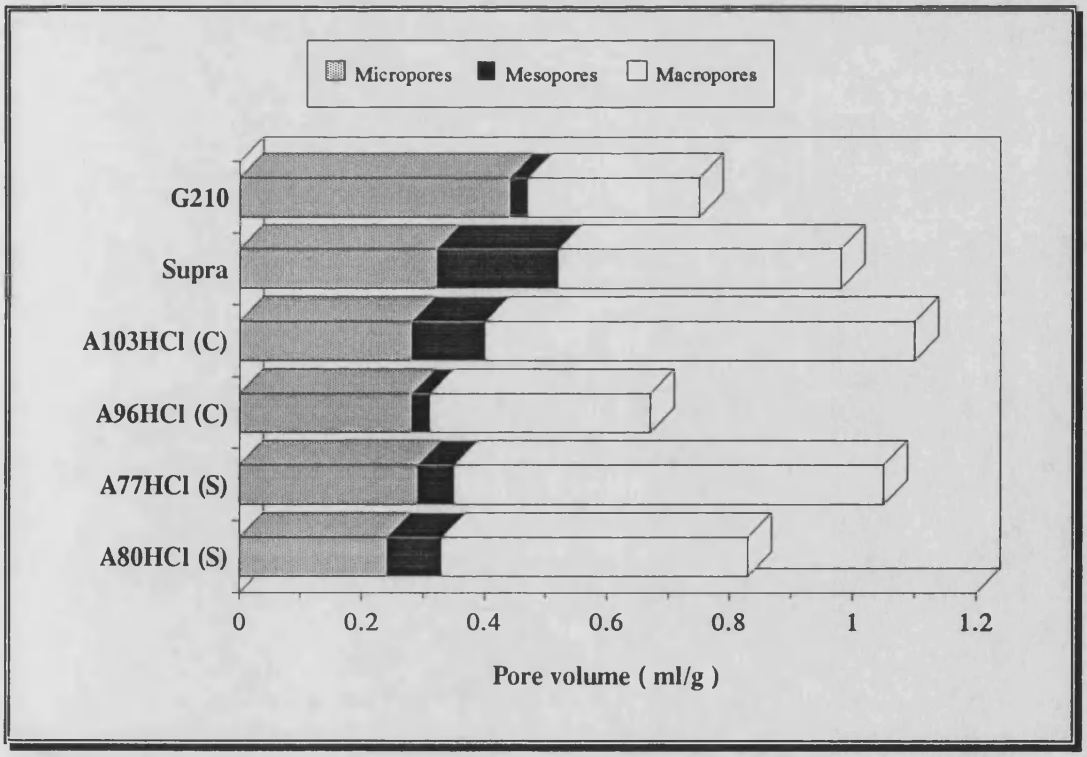

Figure 8.6 : Comparison between the pore volumes of commercial and WCC activated carbons.

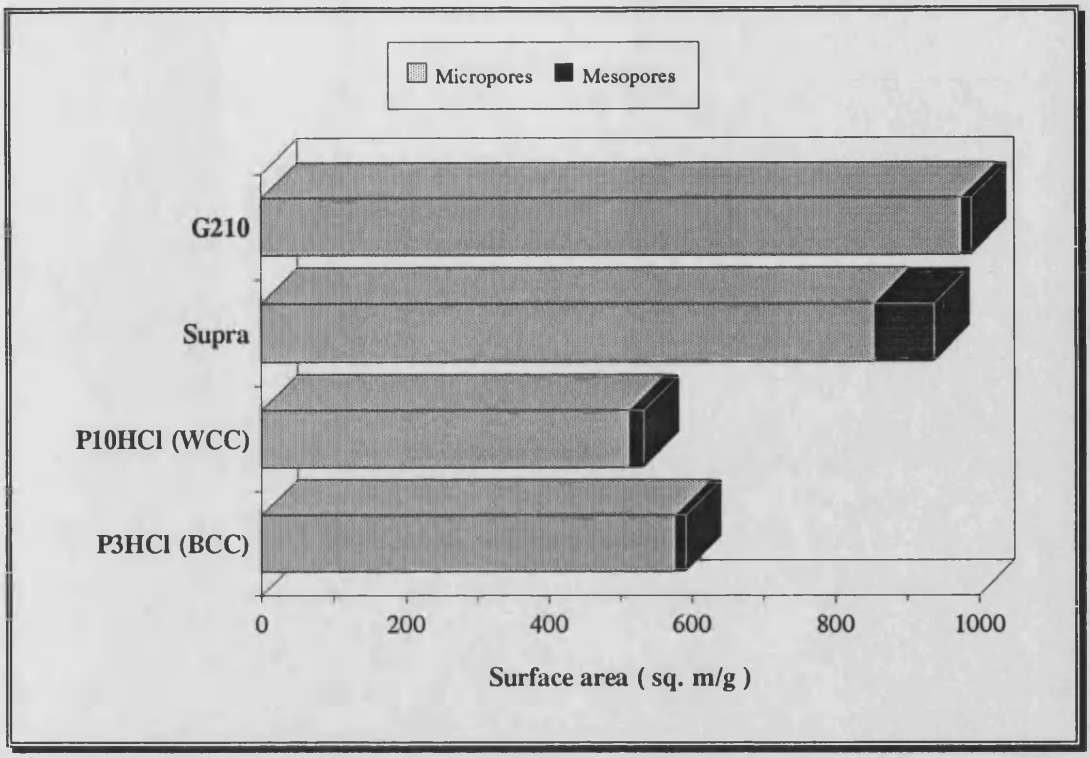

Figure 8.7 : Comparison between the surface areas of commercial and H_3PO_4 activated carbons.

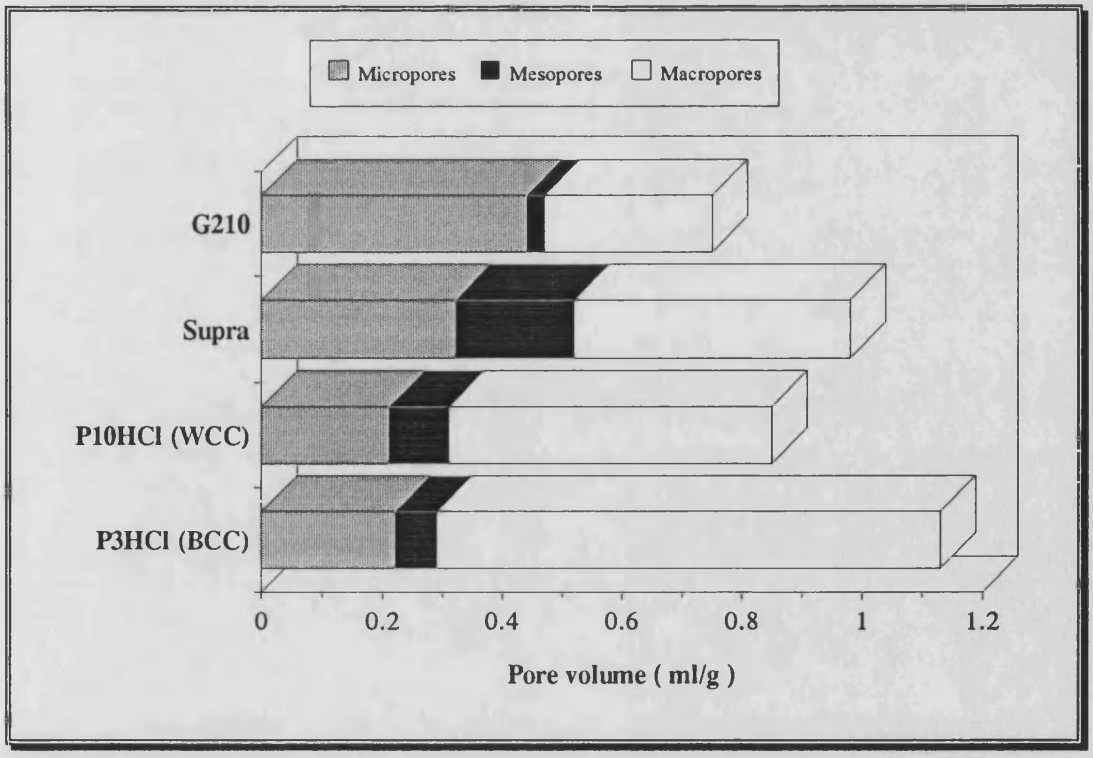

Figure 8.8 : Comparison between the pore volumes of commercial and H_3PO_4 activated carbons.

8.5. Gold cyanide adsorption

The adsorption of gold cyanide, as given by the Q_s value, onto powdered activated carbons is influenced by diffusion through the transport pore network (macro- and meso-pores) rather than the total adsorptive capacity of the carbon, e.g. as measured by the BET surface area. The Q_s values appear to be influenced more by the transport pore network than by micropore capacity, since the commercial carbon G210 had the largest micropore surface area, but showed lower Q_s values when compared to some of the WCC samples. This suggests that the process of adsorption of gold cyanide has reached the intermediate stage in the model of Fuerstenau *et al.* [1987] in which gold adsorption is controlled by diffusion through transport pores. These observations suggest that for powdered activated carbon the adsorption of gold cyanide is enhanced by a well developed macro - mesopore system; a substantial microporosity will give access to the basal planes of the carbon for adsorption of $Au(CN)_2^-$ as suggested by Jones et al. [1989], but microporosity does not appear to be important in controlling the rate of adsorption.

All the BCC carbons showed lower Q_s values when compared to the WCC carbons, although many of the samples had similar porosity values, suggesting that the adsorption of gold cyanide onto the powdered carbons is also influenced by other factors, e.g. the nature of the coal precursor and the chemical composition of the carbon surface. The oxygen content of the carbon influenced the adsorption process, with a higher oxygen content leading to higher gold loadings. Similar results were found by Tshuchida and Muir [1986].

Evidence was found for correlations between Q_s values and the sulphur and ash content of the carbon. The nature of the thermally transformed S - species or the mineral matter is unknown, therefore it is possible to have an interaction between the gold cyanide and mineral matter during the adsorption process. A reaction

between sulphur and gold cyanide could explain the increase in Q_s values for an increase in ash content of the carbons since sulfur is usually associated with mineral matter content.

8.6. Suggestions for future research

The following aspects addressed in this study will benefit from further research :

- The optimization of the column flotation parameters can possibly lead to higher product yields and lower mineral matter content coal products. It is especially important to try and increase the low product yield for the Waterberg coal, since the carbons from this coal precursor showed superior gold loadings.

- This research showed that high surface area carbons can be prepared from high mineral matter coal precursors. The activation parameters however need to be optimized, and may lead to an even better developed porosity distribution in the carbons.

- Although the activated carbons can find many uses in its powdered form, many applications still prefer to use activated carbon in granular form. The formation of pelleted activated carbon from the powdered carbons should receive extensive investigation.

- This study showed that the nature of the carbon surface is an important factor in the adsorption of $Au(CN)_2^-$ onto powdered activated carbons. A qualitative characterization of the activated carbon surface will answer many of the questions that arose during this study.

⌘ The influence of sulphur on the adsorption of $Au(CN)_2^-$ onto powdered activated carbon needs to be investigated. The positive correlation between Q_s and sulphur found in this research needs to be broadened to include high sulphur content carbons. The nature of the S - species, and their interaction with the $Au(CN)_2^-$ anion also needs to be clarified.

LITERATURE REFERENCES

Adams M.D., Fleming C.A. [1989]
Metall. Trans. B **20B** 315

Allum J.A., Whelan P.F. [1954]
J. Inst. Energy **27** 142

Androutsopoulos G.P., Mann R. [1979]
Chem. Eng. Sci. **34** 1203

Anglo American Research Laboratories Reference No. CA/75
Issued by A.A.R.L., Johannesburg, South Africa.

Anon [1990]
"New zip in Activated Carbon"
Chem. Eng. **2** 43

Aplan F.F. [1976]
Coal flotation. A.M. Gaudin Memorial Volume III. New York : AIME. Ed. by M.C. Fuerstenau.

Bailey A., Maggs F.A.P. [1971]
British Patent 1 310 101

Bansal R.C., Donnet J., Stoeckli H.F. [1988]
in *Active Carbon.* Published by Marcel Dekker Inc., New York-Basel

Barton S.S., Evans M.J.B., Harrison B.H. [1974]
J. Colloid Interface Sci. **49** 462

Beafore F.J., Cawiezel K.E., Montgomery C.T. [1979]
Oxidized coal - What it is and how it affects your preparation plant performance. Paper delivered at the Symposium for Coal Preparation and Utilization, April 1 - 9, Sydney, Australia.

Boehm H.P., Voll M. [1970]
Carbon **7** 227

Boehm H.P., Voll M. [1971]
Carbon **8** 481

Brunauer S., Deming L.S., Deming W.S., Teller E. [1940]
J. Am. Chem. Soc. **62** 1723

Brunauer S., Emmett P.H., Teller E. [1938]
J. Am. Chem. Soc. **60** 309

Bujnowska B. [1985]
Coal Prep. **1** 169

Carrott P.J.M., Raistrick J.H., Sing K.S.W. [1986]
Colloid Surfaces **21** 9

Cook R., Crathorne E.A., Monhemius A.J., Perry D.L. [1989]
J. Hydrometallurgy **22** 171

Cookson J.T. (Jr.) [1978]
in *Carbon Adsorption Handbook.* Edited by P.N. Cherimisinoff and F. Ellerbusch, published by Ann Arbor Science Inc., Michigan

Cormack B.,Freeman J.J., Sing K.S.W. [1980]
J. Chem. Tech. Biotechnol. **31** 367

Crelling J.C., Skorupska N.M., Marsh H. [1988]
Fuel **67** 781

Czechowski F., Kidawa H. [1991]
Fuel Proc. Technol. **29** 57

Dacey J.R., Evans M.J.B. [1971]
Carbon **9** 579

Davidson R.J., Duncanson D. [1977]
J. S. Afr. Inst. Min. Metall. **77(12)** 254

Davis W.N. [1880]
U.S. Patent 227 963

Davidson R.J. [1974]
J. S. Afr. Inst. Min. Metall. **75(4)** 67

Derbyshire F.J., Jagtoyen M, McEnaney B., Stencel J.M. [1991]
Synthesis of adsorbent carbons from Illinois coals. CRSC Technical Report September 1 - November 30

Derbyshire F.J., Jagtoyen M, McEnaney B., Stencel J.M., Thwaites M.W. [1991b]
An investigation of the conversion of Illinois coals to activated carbons. CRSC Final Technical Report September 1, 1990 - September 3, 1991

Dickinson J.M., Shore J.W. [1968]
Carbon **6** 937

Dixon S., Cho E., Pitt C.H. [1978]
A. I. Ch. E Symposium Series **147(173)** 75

Doying E.G. [1965]
U.S. Patent 3 256 206

Dubinin M.M. [1965]
Zh. Fiz. Khimii **1965** 1305

Dubinin M.M. [1966]
in *Chemistry and Physics of Carbon.* Edited by P.L. Walker, Jr. Volume 2, pp. 51 - 120. Published by Marcel Dekker Inc., New York

Dubinin M.M. [1975]
in *Progress in Surface and Membrane Science.* Edited by D.A. Cadenhead. Volume 9, pp. 1 - 70. Published by Academic Press, New York

Dubinin M.M. [1988]
Carbon **26** 97

Dubinin M.M., Radushkevich L.V. [1947]
Proc. Acad. Sci. USSR. **55** 331

Dubinin M.M., Stoeckli H.F. [1980]
J. Colloid Interface Sci. **75** 34

Dubinin M.M., Zaverina E.D. [1949]
Dokl. Akad. Nauk. SSSR **65** 295

Du Plessis H.G. [1985]
Oil agglomeration as a maceral seperation technique of coal. D.Sc thesis, Potchefstroom University for CHE, Potchefstroom, South Africa. (in Afrikaans)

Dyrkacz G.R., Horwitz E.P. [1982]
Fuel **61** 3

Dyrkacz G.R., Bloomquist C.A.A., Ruscic L. [1984]
Fuel **63** 1166

Ehrburger P., Addoun F., Donnet J-B. [1988]
Fuel **67** 1228

Elasivich M.G., Konovalova T.F. [1969]
Coke and Chem. USSR **11** 5

Falcon R.M.S., Snyman C.P. [1986]
in *An Introduction to Coal Petrography*. Review Paper no. 2, The Geological Society of South Africa, Johannesburg, South Africa, February 1986

Faust S.D., Aly O.M. [1983]
in *Chemistry of Water Treatment*. Published by Butterworth & Company, Woburn, Massachusetts

Fryer J.R. [1981]
Carbon **19** 431

Fuerstenau D.W. [1982]
Flotation and Selective Agglomeration of Western Coals. California Mining and Mineral Resources Research Institute - University of California at Berkeley, August

Fuerstenau M.C., Nebo C.O., Kelso J.R., Zaragoza M. [1987]
Mining Metals. Proc. **11** 177

Fullard A.F. [1986]
An Industrial study in Coal Beneficiation. M.Sc thesis, Potchefstroom University for CHE, Potchefstroom, South Africa. (in Afrikaans)

Garten V.A., Weiss D.E. [1957]
Rev. Pure Appl. Chem. 7 69

Given P.H., Peover M.E., Wyss W.F. [1960]
Fuel **39** 323

Gregg S.J., Sing K.S.W. [1982]
in *Adsorption, Surface Area and Porosity*. Second edition. Published by Academic Press Inc., London

Hall K.B. [1974]
World Mining **27** 44

Harris L.A., Yust C.S. [1976]
Fuel **55** 233

Hausen D.M., Bucknam C.H. [1984]
Appl. Mineral. Proc. Int. Congr. Appl. Mineral. Miner. Ind., Edited by W.C. Park, D.M. Hausen, R.D. Hagni. Published by Metall. Soc. AIME, Warrendale, Pennsylvania, pp. 833 -856

Hower J.C., Frankie K.A., Wild G.D., Trinkle E.J. [1984]
Fuel Proc. Tech. **9** 1

Hunt R.H., Longwell J.P., Sarofin A.F. [1988]
Fuel 65 451

Hyde G.R., Stojsic A. [1987]
Mining Eng. **7** 481

Jaroniec M., Lu X., Madey R., Choma J., Klinik J. [1990]
Fuel **69** 516

Johnson W.D. [1894]
U.S. Patent 522 260

Jones R.B., McCourt C.B., Morley C., King K. [1985]
Fuel **64** 1460

Jones W.G., Klauber C., Linge H.G. [1989]
Proc. Carbon '89. 19th Biennial Conference on Carbon, June 25-30, 1989 pp 38 - 39

Kadlec O., Varhanikova A., Zukal A. [1970]
Carbon **8** 321

Kessler M.F. [1973]
Fuel **52** 191

Laine J., Calafat A., Labady M. [1989]
Carbon **27** 191

Landais P., Muller J., Michels R., Oudin J., Zaugg P. [1989]
Fuel **68** 1616

Lee T.V., Madey R., Rothstein D., Jaroniec M. [1987]
Mat. Chem. Phys. **15** 583

Leja J. [1982]
in *Surface Chemistry of Froth Floation.* Published by Plenum, New York. 450 pp

Loison R., Foch P., Boyer A. [1989]
in *Coke Quality and Production*, Chapter 2. Second Edition. Published by Butterworth & Co Ltd, London

Mahajan O.P., Walker P.L. (Jr) [1979]
Fuel **58** 333

Mahle J.J., Friday D.K. [1989]
Carbon **27** 835

Mastral A.M., Rubio B., Membrado L., Fananas F.J. [1990]
Carbon **28** 65

Mattson J.S., Mark H.B. (Jr), Malbin M.P., Weber W.J., Crittenden J.C. [1969]
J. Colloid Interface Sci. **31(1)** 116

McDougall G.J., Fleming C.A. [1987]
in *Ion Exchange and Sorption Processes in Hydrometallurgy.* Edited by M. Streat and D. Naden. Published by the Society of Chemistry and Industry, Wiley, Chichester pp. 56-126

McDougall G.J., Hancock R.D. [1981]
Gold Bullion **14(4)** 138

McDougall G.J., Hancock R.D., Nicol M.J., Wellington O.L., Copperthwaite R.G. [1980]
J. S. Afr. Inst. Min. Metall. **80(9)** 344

McEnaney B. [1987]
Carbon **25** 69

McEnaney B. [1988]
Carbon **26** 267

Mikhail R.S., Brunauer S. [1975]
J. Colloid Interface Sci. **52** 572

Milburn D.R., Adkins B.D., Davis B.H. [1991]
in *Characterization of Porous Solids II.* Edited by F. Rodriguez-Reinoso, J. Rouquerol, K.S.W. Sing and K.K. Unger. Published by Elsevier, Amsterdam, pp. 543 - 551

Muir D.M. [1982]
The Australian Institute of Mining Metallurgy Perth and Kalgoorlie Branches and Murdoch University, Carbon-in-pulp seminar, July 1982 pp 7-22

Nieuwoudt I. [1989]
Dynamic model for the competitive adsorption of metal cyanides on activated carbon in batch reactors. M.Eng thesis, University of Stellenbosch, South Africa, 289 pp.

Oberlin A., Villey M., Combaz A. [1980]
Carbon **18** 347

Pandolfo A.G., Johns R.B., Dyrkacz G.R., Buchanan A.S. [1988]
Energy and Fuels **2** 657

Peters E.M. [1966]
U.S. Patent 3 235 323

Pinote R.S., Cournnault P., Du Chaffant F. [1968]
J. Chem. Phys. **65** 1188

Prasad M.S., Mensah-Biney R., Pizarro R.S. [1991]
Min. Eng. **4** 1257

Rand B., Marsh H. [1971]
Carbon **9** 79

Reinecke C.F. [1987]
A correlation between oil - agglomeration and surface functional groups of typical South African coals. D.Sc thesis, Potchefstroom University for CHE, Potchefstroom, South Africa. (in Afrikaans)

Reinecke C.F. [1987b]
The flotation behaviour of Grootegeluk. Paper given at the Grootegeluk coal mine, Ellisras, South Africa. 30 July 1987.

Ritter H.L., Drake L.C. [1945]
Ind. Eng. Chem. Analyt. Ed. **17** 782

Robinson J.W. [1966]
in *Atomic Absorption Spectroscopy*, pp 91-127. Published by Edward Arnold Ltd., London and Marcel Dekker Inc., New York

Rodriguez-Reinoso F., Martin-Martinez J.M., McEnaney B. [1989]
Carbon **27** 297

Rodriguez-Reinoso F., Martin-Martinez J.M., Prado-Burguette C., McEnaney B. [1987]
J. Phys. Chem. **91** 515

Rootare H.M., Prenzlow C.F. [1967]
J. Phys. Chem. **71** 2733

Salinas-Martinez de Lecea C., Almela-Alarcon M., Linares-Solano A. [1990]
Fuel **69** 21

Sarkar G.G., Ghose S., Chaudhuri S.G.,Sarka S., Dasclowdhury K.P. [1984]
Coal Prep. **1** 39

Schofield R.K. [1948]
Disc. Faraday Soc. **3** 105

Seaton N.A., Walton J.P.R.B., Quirke N. [1989]
Carbon **27** 853

Serio M.A., Solomon P.R., Bassilakis R. [1989]
Fuel **68** 9

Sing K.S.W. [1970]
in *Surface Area Determination.* Edited by D.H. Everett. Published by Butterworths and Company, London.

Sing K.S.W., Everett D.H., Haul R.A.W., Moscou L., Pierotti R.A., Rouquerol J., Siemieniewska T. [1985]
Pure and Appl. Chem. **57** 603

Smisek M., Cerny S. [1970]
in *Active Carbon.* Published by Elsevier Scientific Publishing Company, Amsterdam

Solomon P.R., Hamblen D.G. [1985]
in *Chemistry of Coal Conversion*, Chapter 5. Edited by R.H. Schlosberg, published by Plenum Press, New York

Stach E., Mackowsky M.TH., Teichmüller M., Taylor G.H., Chandra D., Teichmüller R. [1982]
in *Stach's Textbook of Coal Petrology.* Third edition. Published by Berlin Gebrüder Borntraeger, 206 pp.

Stoeckli H.F. [1990]
Carbon **28** 1

Stoeckli H.F., Ballerini L. [1991]
Fuel **70** 557

Strelow F.W.E., Feast E.C., Mathews P.M., Bothma C.J.C., Van Zyl C.R. [1966]
Anal. Chem. **38** 115

Sun S.C. [1954]
Mining Eng. **4** 396

Tomków K., Siemieniewska T., Czechowski F., Jankowska A. [1977]
Fuel **56** 121

Tsai S.C. [1982]
in *Fundamentals of Coal Beneficiation and Utilization.* Edited by L.L. Anderson, published by Elsevier Scientific Publishing Company, Amsterdam

Tsuchida N., Muir D.M. [1986]
Metall. Trans. B **17B** 523

Tsuchida N., Muir D.M. [1986b]
Metall. Trans. B **17B** 529

Van der Merwe P.F., Van Deventer J.S.J. [1988]
Chem. Eng. Comm. **65** 121

Van Deventer J.S.J. [1983]
Reagents in the Minerals Industry. Institution of Mining and Metallurgy, London. Editor : M.J. Jones, pp 155-160

Van Krevelen D.W., Schuyer J. [1957]
in *Coal Science.* Published by Elsevier Publishing Company, Amsterdam

Van Nierop P. [1986]
The relationship between flotation selectivity, surface functional groups and surface conditioning of coal. M.Sc thesis, Potchefstroom University for CHE, Potchefstroom, South Africa. (in Afrikaans)

Van Nierop P. [1988]
The influence of surface functional groups of coal on froth flotation. D.Sc thesis, Potchefstroom University for CHE, Potchefstroom, South Africa. (in Afrikaans)

Washburn E.W. [1921]
Proc. Nat. Acad. Sci. U.S.A. 7 115

Wills B.A. [1981]
in *Minerals Processing Technology.* Second edition. Published by Wiley, London.

Wilson J. [1981]
Fuel **60** 823

Winans R.E., Scott R.G., Neill P.H., Dyrkacz G.R., Hayatsu R. [1986]
Fuel Proc. Technol. **12** 77

Zadra J.B. [1950]
U.S. Bureau of Mines Report of Investigations 11672

Zadra J.B., Angel A.K., Heinen H.J. [1952]
U.S. Bureau of Mines Report of Investigations 4843

Zaragoza R.M. [1982]
M.Sc Thesis, South Dakota School of Mines and Technology

Zimmerman R.E. [1964]
Mining Congress J. **5** 26

Zsigmondy A [1911]
Z. Anorg. Chem. **71** 356

APPENDIX

Anglo American Research Laboratories guidelines for gold cyanide adsorption experiments.

THE DETERMINATION OF GOLD ADSORPTION RATE (R-VALUE) OF ACTIVATED CARBON, MESH NUMBER 8 X 16 AND 6 X 12

1.0 PRINCIPLE

The activated carbon, after acid wash, is contacted with 10 mg/ℓ gold solution at 25°C, in the presence of potassium cyanide.

At periodic intervals, small aliquot portions of the solution are taken, and gold content is determined.

The rate of gold adsorption is obtained from a calibration graph, of per cent gold adsorbed on the carbon plotted against time.

The quantity of gold (%), adsorbed after 60 minutes, is known as "R-value".

2.0 APPARATUS

2.1 A set of sives.

2.1.1 For virgin activated carbon, of mesh number 6 x 12 : 2,0 and 2,38 mm.

2.1.2 For virgin activated carbon, of mesh number 8 x 16 : 1,41 and 1,68 mm.

2.2 An ultrasonic bath.

Brauson ultrasonic cleaner was found to be suitable.

2.3 An analytical balance, capable of measuring to 0,1 mg.

2.4 A drying oven.

2.5 A linear shaker-incubator with timer, adjusted to 130 oscillation/min.

The Labotec scientific linear shaker was found to be suitable.

2.6 An oblong plastic container: 95 x 130 x 210 mm or 150 x 150 x 140 mm.

The volume of the container must be 2-3 ℓ (Note 6.1).

2.7 A desiccator.

2.8 An AA spectrophotometer.

3.0 REAGENTS

All reagents are of analytical grade or equivalent. When water is mentioned, deionized water is understood.

3.1 Sodium hydroxide solution: 1 M NaOH

Dissolve 40,0 g of sodium hydroxide in 700 mℓ of water. Cool and dilute to 1 ℓ.

3.2 Borate buffer solution

Dissolve 3,09 g of H_3BO_3 and 3,73 of KCl in approximately 500 mℓ of water. Adjust the pH of the solution, using 1 M NaOH, to a pH value of 10. Dilute to 1 ℓ.

3.3 Gold solution: 10 mg/ℓ Au

Dissolve 0,074 g K Au $(CN)_2$ in 4 ℓ of water. Add 1,834 g of $CaCl_2.2H_2O$ or 1,384 g $CaCl_2$ (Note 6.2). To the solution add 1,251 g of KCN. Mix and dilute to 5 ℓ.

The concentration of the solution is: 10 mg/ℓ Au, 100 mg/ℓ Ca and 100 mg/ℓ CN^-.

3.4 Hydrochloric acid solution: 3% (v/v) HCl

Measure 30 mℓ of concentrated HCl into a 1 ℓ volumetric flask. Dilute to volume with water.

3.5 Lanthanum nitrate solution: 20 g/ℓ La

Dissolve 62,3 g of $La(NO_3)_3.6H_2O$ in water. Adjust the pH value to 10,0. Dilute to 1 ℓ with water.
1 mℓ = 20 mg La.

4.0 PROCEDURE

4.1 Using the rotary sample splitter, select mass of about 50 g of the activated carbon.

4.2 Screen the sample through the 1,68 mm (Note 6.3) and collect on 1,41 mm sieve (Note 6.4).

4.3 Transfer the carbon, collected on top of the 1,41 mm sieve, to a 100 mℓ beaker. Add 50 mℓ of the acid solution. Boil for 10 minutes. Decant and wash the carbon three times with water.

4.4 Cover the carbon with 50 mℓ of water. Position the beaker in the ultrasonic bath. After 2 minutes, decant the water and wash the carbon twice. Repeat the procedure four times (Note 6.5).

4.5 Transfer the carbon to the oven and dry at 105°C to constant mass. Cool in a desiccator (Note 6.6).

4.6 Measure, accurately, 1,000 g of the dried carbon sample (Note 6.7). Moisten the sample with 1 mℓ of the buffer solution, and allow to stand for ½ hour (Note 6.8).

4.7 Allow the flask, containing the gold solution, to stand for ½ hour in the incubator at 25°C, to adjust the temperature of the solution.

4.8 Measure 1 ℓ of the gold solution, using a measuring cylinder, into the oblong plastic container, and add the prepared carbon sample.

4.9 Position the container on the linear shaker-incubator, the temperature (25°C) and speed (130 oscillation/min) of which should have been adjusted previously. Commence shaking immediately.

4.10 Withdraw 5 mℓ aliquots after 0, 15, 30, 45, 60, 75 and 90 minutes (Note 6.9).

4.11 Proceed with the determination of gold, using drect atomic absorption measurement. Application of background correction and addition of $La(NO_3)_3$ solution, as interference suppresing agent, is essential (Note 6.10).

5.0 CALCULATION

5.1 The results from the atomic absorption measurement will give the residual gold in the solution (mg/ℓ Au) at the time of aliquot withdrawal (0, 15, 30, 45, 60, 70 and 90 min): Value B.

5.2 Subtract the residual gold concentration from the original gold content (10 mg/ℓ Au). Calculate, in percent, the quantity of gold adsorbed on the carbon at any given time:

$$\text{R Value (\%)} = \frac{(A - B)}{A} \times 100$$

where: A is the Au concentration (mg/ℓ) of the solution (10 mℓ/ℓ).

and B is the residual Au concentration (mg/ℓ) at the time of aliquot withdrawal

5.3 Plot a calibration curve of percentage gold adsorbed, against time, to obtain the mean percentage of gold adsorbed onto the carbon after 60 min. The statistical data for the test are: SD = 1,7% and RSD = 3,4%.

6.0 NOTES

6.1 The 2-3 ℓ volume of the plastic container was found to ensure sufficient sample agitation during the test.

6.2 The addition of $CaCl_2$ is to simulate the plant conditions; it also accelerates the gold adsorption rate.

6.3 A sieve of mesh size 2,38 mm should be used when 6 x 12 mesh activated carbon is tested.

6.4 A sieve of mesh size 2,00 mm should be used when 8 x 16 mesh carbon is tested.

6.5 Four washings were found to be sufficient for complete removal of dust and small particles.

6.6 Before starting the test, ensure that the desiccator and its drying material are in good condition.

6.7 Dry carbon is very hydroscopic; allow the minimum time for sample measurement.

6.8 The sample is wetted ½ hour prior to the test, to displace the air, entrapped in the carbon.

Buffer solution is used, so that, simultaneously with the air displacement, appropriate neutralisation of the acid washed carbon is ensured.

6.9 The original gold concentration is maintained, when small aliquot portions are withdrawn from the solution.

6.10 The final concentration of La in the solution should be 2 g/ℓ.